UNCERTAINTY QUANTIFICATION OF BUILDING ENERGY MODELS THAT ASSUME IDEAL TEMPERATURE CONTROL

A Dissertation
Presented to
The Academic Faculty

by

Yifu Shi

In Partial Fulfillment
of the Requirements for the Degree
Doctor of Philosophy in the
School of Architecture

Georgia Institute of Technology
December 2020

COPYRIGHT © 2020 BY YIFU SHI

UNCERTAINTY QUANTIFICATION OF BUILDING ENERGY MODELS THAT ASSUME IDEAL TEMPERATURE CONTROL

Approved by:

Prof. Godfried Augenbroe, Advisor
School of Architecture
Georgia Institute of Technology

Dr. Sheldon Jeter
Woodruff School of Mechanical Engineering
Georgia Institute of Technology

Dr. Cheol-Soo Park
School of Architecture & Architectural Engineering
Seoul National University, Korea

Dr. Jason Brown
School of Architecture
Georgia Institute of Technology

Dr. Tianzhen Hong
Building Technology & Urban Systems Division
Lawrence Berkeley National Laboratory

Date Approved: July 29, 2020

To my parents and families who have always supported me

ACKNOWLEDGEMENTS

I would like to express my deepest appreciation to my advisor Professor Godfried Augenbroe. His vision on the research frontier, profound knowledge, sharp insight, constructive criticism, and more importantly, his optimistic attitude towards life, witty humor, encourage, patience nurtured me throughout my study and guide me out of the trough of life. It has been a great honor for me to be his Ph.D. student. I would also like to extend my deepest gratitude to my committee members: Dr. Cheol-Soo Park, Dr. Sheldon Jeter, Dr. Jason Brown, for their kind support and invaluable advice. I'm extremely grateful to Dr. Tianzhen Hong who provided me the insightful knowledge and valuable advice during my internship at Lawrence Berkeley National Lab.

I would like to extend my sincere thanks to Yuna Zhang, Di Lu, Qinpeng Wang, and Qi Li, who provided me with insightful suggestions and constructive discussions that shaped this dissertation. Many thanks to my colleague Alya, Mohanned, Zhaoyun, Jianli, Yun Joon, Mayuri, Qiong, Gustavo, Yiwen, Tianyu, Mansour for their support and company in the lab. I would like to thank my friends Fei, Te, Yixing, Kaiyu, Xuan, Sang Hoon for their moral support and encouragement.

A heartfelt gratitude goes to my beloved Junran, with her continuous encouragement and unreserved support, I have the belief in the future and never feel alone. Lastly, I would like to express my deepest appreciation to my parents, I would never be able to accomplish all this without their full support and unconditional love.

TABLE OF CONTENTS

LIST OF TABLES

LIST OF FIGURES

SUMMARY

An increasing number of studies conduct uncertainty analyses to investigate discrepancies between predicted energy performance of buildings and their actual measured energy use. Based on prior uncertainty quantification studies, there is evidence that there remain unquantified uncertainties related to the HVAC system. Most current studies of HVAC system uncertainties focus on investigating the probabilistic nature of building thermal loads and assume this nature to be the key factor to impact the accuracy of performance predictions of the HVAC system. To verify this one has to acknowledge that instead of reacting ideally to the "thermal load", HVAC systems sense space temperature and use it as the control state in HVAC control loops, thus deciding on the heating or cooling requirement of a space based on sensed space temperature. For a VAV terminal box which serves multiple spaces, temperature controllability only applies to the space where a thermostat is installed. The temperature in other spaces may consequently not be maintained and the delivered cooling/heating from the terminal box will typically not (fully) satisfy the removal or supply of the room cooling and heating load.

Commonly used EnergyPlus simulations introduce an idealization on the space temperature controllability by matching building zone partition with the HVAC supply network topology and using thermal zone as the atomic control object. This thesis targets an uncertainty quantification approach to identify model form uncertainties in EnergyPlus stemming from such idealized space temperature controllability. A high-fidelity co-simulation model which integrates an EnergyPlus building energy model with a Modelica HVAC system model is developed as the high-fidelity reference model. The differences

between outcomes of the EnergyPlus simulation and outcomes of the reference model are then established. Two new characteristic parameters, “spatial-HVAC mismatch” and “occupant load diversity”, are introduced in this thesis. The first defines the area of non-sensed spaces in relation to directly controlled areas where the space temperature is sensed. Occupant load diversity expresses the variabilities of occupancy related load profiles in each space.

The uncertainty analysis of the impact of the idealized temperature control of the EnergyPlus representation of VAV system considering the stochastic usage pattern of occupants in two space functions with five alignment configurations in three boundary situations focusing on the risk of underestimating energy consumption and over estimating occupant comfort (unmet hours in particular).

The thesis quantifies the differences between low and high fidelity predictions in the outcomes of space air temperature, cooling energy in different time interval (hourly, daily, and monthly), fan power, and unmet hours as a result of the idealizations used in routine EnergyPlus simulations. It then correlates them with the mismatch and load diversity factors introduced above. Based upon the uncertainty analysis, this study explores the characterizations of the results from the case studies and discuss the methodologies and steps for “post corrections” or MFU inclusion in the low fidelity model by using fan power as an example.

The research outcomes generate significant knowledge to the understanding of the origins of building energy model deficiency generated by idealization assumptions about temperature control and how it contributes to the performance gap.

INTRODUCTION

In 2017, about 39% (or about 38 quadrillion British thermal units) of total U.S. energy consumption was consumed by the residential and commercial sectors. (EIA, 2018). The energy consumption from buildings and activities in buildings is projected to increase by an average of 1.5% per year for the period of 2012–2040 under a business as usual scenario (Zhang, Bai, Mills, & Pezzey, 2018) (EIA, 2017). Based on the prediction by the International Energy Agency, the global building floor area will keep a rapid growth at nearly 3% per year (IEA, 2019). With the growing concerns to reduce the energy consumption in building, more attention has been paid to how to design, construct and operate high-performance buildings. Many buildings are labeled as energy efficient based on certification by third party rating systems, such as the U.S. Green Building Council's (USGBC's) Leadership in Energy and Environmental Design (LEED) system, Three Star in China, the Comprehensive Assessment System for Built Environment Efficiency (CASBEE) in Japan, Deutsche Gesellschaft für Nachhaltiges Bauen (DGNB) in Germany, and the Building Research Establishment Environmental Assessment Methodology (BREEAM) in the UK. The green building market experiences a rapid growth over the last few years. Taking LEED certification as an example, the number of LEED-certified projects in the United States rose from 296 certifications in 2006 up to over 65,000 in 2017. Based on the data released by USGBC, there are more than 39,000 certified commercial projects as of October 2017 while this number is only 29,000 in 2015.

Building energy simulation is adopted as the widely accepted method to predict building energy performance based on the supplied documentation of a proposed design.

In this thesis, building energy refers to the energy that is delivered through supply networks in the operation stage, i.e. the energy that maintains the building internal environment e.g., by fresh air supply, lighting, supply of heating, and cooling to maintain comfort and various types of building activities (e.g., working on IT devices, cooking and entertainment) (Zou, Xu, Sanjayan, & Wang, 2018).

Building energy simulation has been introduced into the design and engineering of buildings in the 1960s and many tools have been developed and matured over the decades since. However, it has been identified in existing literature that the actual measured energy consumption deviates from predicted consumption even after we compensate for actual weather and usage. This discrepancy between prediction and actual is typically referred to as the "performance gap" (de Wilde, 2014) (Zou, Xu, Sanjayan, & Wang, 2018). The performance gap has been shown to become more pronounced if we consider hourly or even sub-hourly interval data rather than aggregated energy consumption. In 2008, the New Buildings Institute (NBI) analyzed utility billing data and simulated predictions for 121 LEED new construction commercial buildings. It is apparent that the ratio of actual to predicted energy use varies widely, Figure 0.1 shows the ratio of measured to predicted Energy Use Intensity (EUI) ranging from less than 0.5 to more than 2.75 (Turner & Franke, 2008).

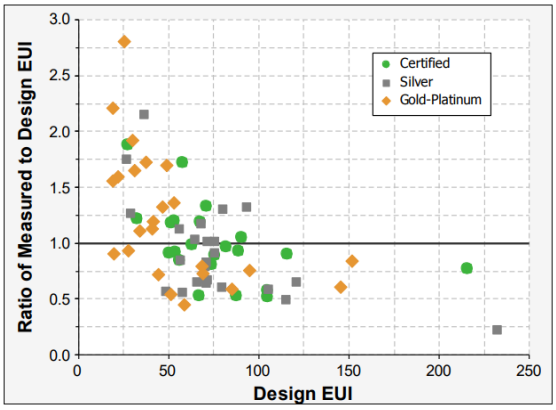

Figure 0.1 Predicted and measured EUI of LEED buildings (Turner & Franke, 2008)

We see that there are large gaps between the actual energy consumption from buildings in-use and the energy consumption predicted by building energy simulation before the buildings are built. Obviously, there are many reasons why this is the case, such as the deviation between assumed and actual weather and the fact that building usage, in particular occupancy, cannot be accurately predicted in the design stage. Recent studies have shown that this contributes to the gaps but does not fully explain it. (Sun Y. , 2014). The remaining performance gap is a concern for practitioners and researchers alike. For the first group, it undermines the credibility of the profession, while the second group sees this as a challenge to unearth different causes of the discrepancy and rank them in order of importance. It should be noted that the absolute discrepancies between predicted and actual performance are of less importance than many authors claim. For instance, in performance based energy standards the predicted consumption is only used as a normative reference without a claim of correctness (ISO, 2008) (Kim, Augenbroe, & Suh, 2013). In design support environments there is typically no need to predict the actual energy consumption, as design decisions are well informed by comparative analysis, without the need for absolute correctness (Kim, Augenbroe, & Suh, 2013). The latter is also based on the

recognition that weather and usage scenarios can never be predicted with great accuracy. In this thesis we take the view that an inspection of the underlying reasons of the performance gap is nevertheless relevant in order to understand the effect and magnitude of the different causes and thereby further a deeper understanding of the core of building simulation methods and tools and thereby strengthen the building energy modeling discipline. In that vein, quantifying the causes of the discrepancy between the prediction and the measurement is the overall theme of this thesis, following on earlier work performed in the NSF-EFRI project conducted in the HPB lab at Georgia Tech. This previous work is briefly introduced below.

Besides the numerical errors in simulation, and the experimental variation in observations (Oberkampf & Roy, 2010), we can link the discrepancies to several root causes: (1) missing information about the actual building usage, operation conditions, and the physics of the building and mechanical systems. Most of these are only known by approximation, not in the least affected by the uncertainty on the realization from the design documentation stage to the actual operation stage. The sources of uncertain include weather condition, randomness in building envelope and HVAC system parameters, and occupancy behavior; (2) model discrepancies resulting from model simplification and idealization that are mostly intrinsic to the simulation models used in the prediction.

In the traditional approach of building energy simulation, the prediction is based on deterministic analysis, which compares the one-point estimation with the measurement of the same building. However, a specific building realization will typically not fully comply with the proposed design and the simulation model derived from the design documentation. This has given rise to an alternative approach based on uncertainty analysis which has

received increasing interest from the building research community (De Wit, 2001) (Macdonald & Strachan, 2001) (de Wit & Augenbroe, 2002) (Hopfe & Hensen, 2011). An uncertainty analysis can help us to understand how wrong the prediction is by modeling all sources of uncertainty and embedding them in the building simulation. The latter is achieved by stochastic simulation for which well consolidated techniques exist, usually with the Monte Carlo technique at its core. This puts the emphasis on characterizing and statistical modeling of the sources of uncertainty, a domain that is referred to as uncertainty quantification (UQ). Moreover, the research on uncertainty sources and their effects lifts our understanding of the characteristic behavior modes of buildings and their impacts on the energy consumption while the stochastic simulation methods quantifying the uncertainty in simulation outcomes. In practice, these uncertainty distributions have limited significance of their own, but can be the prime inputs and determinants in risk conscious building design decisions.

Walker et al. (2003) defined uncertainty as "being any deviation from the unachievable ideal of completely deterministic knowledge of the relevant system", which became the widely accepted definition of uncertainty. Theoretically, the uncertainty can be divided into two types: aleatory and epistemic. However, Morgan (2009) suggested to distinguish the uncertainty as (1) uncertainty about the value of empirical quantities that appear as parameters in modeling systems, and (2) uncertainty about the model functional form itself. Uncertainties are typically a combination of the effect of aleatory and epistemic uncertainty. Developing from the categorization of uncertainty by Morgan, the High Performance Building (HPB) group at Georgia Tech suggested to categorize uncertainties in building thermal models into model form uncertainty, parameter uncertainty, and

scenario uncertainty. If we represent a building energy model as $y = f(X, \beta)$, in which the input set $X = (x_1, x_2, \dots, x_n)$ defines the variables related to the building operation and climate conditions, $\beta = (\beta_1, \beta_2, \dots, \beta_n)$ indicates the parameters reflecting the physical characteristics of the building as well as the parameters describing the physical processes in the building. It is important to note that all β can be random variables representing a level of uncertainty. Uncertainties in the function $f()$ itself are referred to as model form uncertainty which reflects the model inadequacy resulting from ignored physical phenomena, simplified conceptualization, numerical approximation, i.e. all issues related to translating a physical reality in a virtual (computer) simulation. Uncertainties in X are categorized as scenario uncertainty that indicates the uncertainties reflecting the stochastic nature of building external and internal environment during the building energy simulation, which mainly considers the uncertainties caused by occupant, weather as well as system control and operation. Uncertainties in β should cover the range of plausible values of the parameters that appear in building energy simulation models (Tian, et al., 2018). Model form uncertainty and parameter uncertainty are associated with a specific system model, or the software that executes the model. The resolution and fidelity of embedded physical equations vary greatly across models and their software implementations. This is the reason why model form uncertainty in one energy model could be looked at as parameter uncertainty in another model or vice versa.

The HPB team quantified and documented uncertainty in an uncertainty quantification (UQ) repository as part of the EFRI-SEED project (Lee, Sun, Augenbroe, & Paredis, 2013). The UQ repository organizes the source of uncertainty according to four

scales ranging from large to small, i.e. meso-scale, building level scale, HVAC system scale, down to occupant and process scale.

Wang (2016) conducted a study to verify the result of an uncertainty analysis based on the UQ repository for six university campus building with EnergyPlus. He proved that a systematic bias (in the statistical sense) exists between predicted (probabilistic) and measured outcomes. The result illustrates that a part of the discrepancy between measurement and prediction cannot be fully explained by an uncertainty analysis based on the quantified parameter, scenario or model form uncertainty in the UQ repository as introduced above.

One of the obvious reasons for the unexplained discrepancy is that the current UQ repository lacks a thorough quantification of uncertainty at the HVAC system scale. It is in fact limited to quantifying the uncertainty due to manufacturing tolerances in the COP part load curve of the designed HVAC system (Augenbroe, et al., 2013). Therefore, Wang (2016) utilized a top-down approach to speculatively identify any additional uncertainties related to the HVAC system which could result from faults and defects and of course model simplifications. His work does not separate these individual sources, but instead coins an overall HVAC "operation uncertainty (OU)" factor. This OU factor is not just determined by HVAC internal attributes but is strongly related to the other building components since the behavior and operation of the HVAC system is based on the interaction with components such as zones, sensors, controllers, and the behavior of the integrated building-HVAC system as a whole.

OU reflects the combined effect of all HVAC related parameters and model uncertainties, including the impact of faults and defects as well as the deviation of actual operation from the designated (ideally controlled) operation of the HVAC system. The latter is linked to the fact that the specified temperature and humidity setpoints are assumed in most current prediction models to be perfectly matched. In reality, this is not the case and there are many case studies in existing buildings where the mismatch between setpoints and actual occurring temperatures is discussed. To estimate the magnitude of the OU, Wang performed afore mentioned study and reported the estimates for the OU factor based on his study of six campus buildings.

He introduced the HVAC OU factor for heating η_{heat} and η_{cool} as post-multipliers of HVAC monthly energy consumption and assumed that both factors follow a normal distribution with mean μ and standard deviation σ. In his definition the OU factor is a stand-in macro uncertainty that combines all primary sources of uncertainty in one blended factor. Based on the K-S test for PIT analysis on the six campus buildings, Wang obtained that: $\eta_{heat} \sim N(0.996, 0.19^2)$ and $\eta_{cool} \sim N(1.157, 0.0754^2)$. The distributions are shown in Figure 0.2 and Figure 0.3.

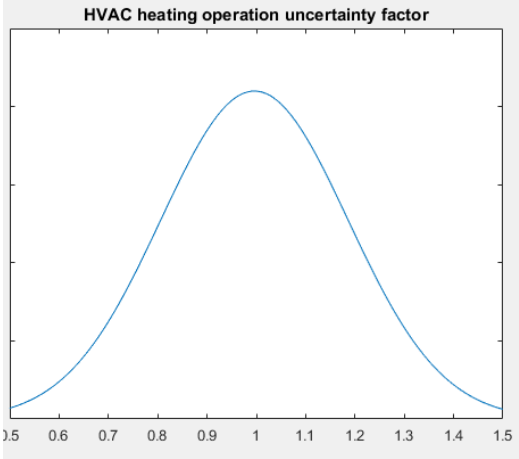

Figure 0.2 Heating operation uncertainty factor

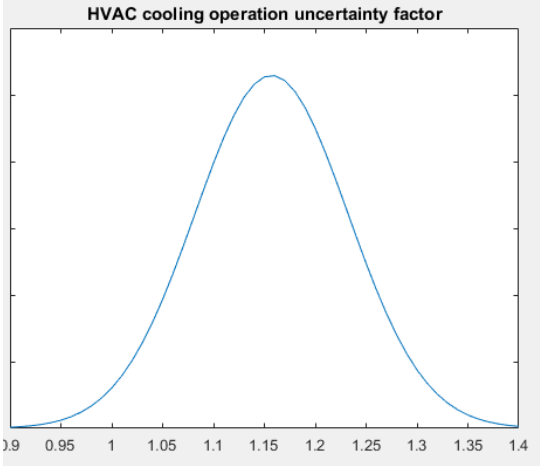

Figure 0.3 Cooling operation uncertainty factor

Note that the η_{heat} and η_{cool} can take values smaller than 1, which indicates that the actual energy consumption could be less than predicted. This seems illogical as we expect that the idealization that underlies our HVAC model usually leads to an underestimate of the real energy use. One plausible reason for this counter-intuitive result is that the HVAC system operation may not maintain the indoor set point temperature or supply the required fresh air amount whereas the prediction model always assumes the space air temperature setpoints and fresh air supply to be satisfied. In certain cases, the actual building can thus be more "efficient" than predicted when the required setpoint is not adequately maintained. From the OU factor distributions above we note that although this situation cannot be excluded, it is relatively rare.

It is important to note that this is based on a macro assessment without trying to find the actual causes of the established, rather wide OU distributions. There are in fact many anecdotal causes that contribute to performance gaps of the six test buildings used in the study, but this will not be further pursued in this thesis.

Indeed, once the building starts operating, various scenarios do not conform to the designed ones. The model simplification/idealization, parameter impreciseness, maintenance practice, occupant behavior, system fault and malfunctions, all of these lead to the performance of the HVAC system drifting away from the predictions generated by the simulation model (Sun, Hong, & Kim, 2017) (Yu, Woradechjumroen, & Yu, 2014). Considering the existence of many unknowns during the building operation stages, the HVAC operation uncertainty factor above is a compounded mix of many unknowns and thus provides insufficient understanding to explain the causal relationship between the HVAC model idealization and the performance gap as well as how to improve our model to reflect the actual HVAC system in the real building. In this thesis we will not attempt to find all underlying causes of the OU factor distribution. But the mean and variance of the OU distribution as found by Wang demands a deeper study into what may cause the additional performance gap driven by HVAC related uncertainties. This thesis will in particular zoom in on one particular contribution, i.e. the one that results from the operation mismatch between idealized model and actual building.

This study uses a bottom-up approach to investigate the uncertainty associated with the HVAC system model as caused by the idealization and simplification of the HVAC system itself and its interaction with dynamic occupancy patterns and other physical components in the building. It focuses in particular on the deviations between idealized and actual temperature control in building zones.

1.1 Literature review

In the uncertainty analysis area of building performance, studies conducted in the early 2000s. Macdonald (2002) develops external and internal approaches to quantify the effect of uncertainty on the predictions of a building simulation. Thermophysical properties, causal heat gains and infiltration rates as the key uncertainty parameters are quantified. de Wit (2001) conducts crude uncertainty analysis and quantifies uncertainties which cannot be derived by straightforward statistics including wind pressure coefficients and indoor air temperature distributions. Macdonald and Strachan (2001) review popular uncertainty analysis methods and apply these methods to buildings via the thermal simulation program ESP-r. They also investigate the sources of uncertainty in the predictions from thermal simulation programs and incorporate uncertainty analysis into ESP-r. de Wit and Augenbroe (2002) address uncertainties in building performance evaluations by integrating an expert judgement and discuss the potential impact of uncertainties on design decisions.

Following the initial studies, more effort has been spent on uncertainty quantification in the building simulation field. Hopfe and Hensen (2011) summarize four benefits of uncertainty and sensitivity analysis in building performance simulation: model simplification, robustness analysis, quality assurance, and decision support. Augenbroe et al. (2013) investigate whether the fully coupled dynamic approach which model the HVAC system as an integral part of the building model could be replaced with an uncoupled sequential approach. The uncoupled approach introduces two types of error: (1) the effect of dynamic interaction is neglected, and (2) the HVAC simulation is simplified. The authors conclude that the uncoupled sequential simulation of building and HVAC system is acceptable when one is interested in (monthly) energy consumption. The authors point

out that the error from ignoring the dynamic interactions in different systems and building combination is still largely unknown. Lee, Sun, et.al (2013) introduce the Georgia Tech Uncertainty and Risk Analysis Workbench (GURA-W) that performs an uncertainty analysis on EnergyPlus models to explicitly capture the result of uncertainties in the physical properties of the building. The toolkit can sample the variables of interest based on stored distribution derived through extensive UQ exercises and performs Monte Carlo simulations with EnergyPlus 7.0. The output results in the form of distributions of selected outcomes are the predictions used in risk assessments and decision-making in general. The workbench has an embedded UQ Repository that includes the results of a set of UQ exercises-based uncertainty distributions for numerous parameters and model formulations as discussed below.

Based on their source, uncertainties are categorized into four types: weather, building envelope, HVAC system and occupant behavior. Insufficient knowledge of the local microclimate is one major source of uncertain in building energy prediction. Sun, Su, Wu, and Augenbroe (2015) develop a general framework to quantify model form uncertainty based on physical measurements and exemplify the approach on the solar diffuse irradiation on tilted surfaces. Sun et.al (2014) develop regression-based methods to develop statistical models that quantify the uncertainties of four microclimate variables: local wind speed, local temperature, wind pressure and solar irradiation which are used by building energy model to define external boundary conditions. Wang et al. (2012) investigate uncertainties in annual site energy consumption due to weather variation and operation parameters for a medium-size reference office.

The parameters associated with building envelope can be grouped into three types: thermal properties, surface properties, and other parameters including the parameters that describe infiltration rate, thermal bridging, convective heat transfer coefficient, and thickness of building materials. Macdonald (2002) derives detailed uncertainty estimates of thermal properties based on literature, including conductivity, density, and specific heat capacity. Sun (2014) conducts a study to quantify the uncertainty of ground albedo and convective heat transfer coefficients. Li et al. (2014) analyze the uncertainty of infiltration rate in the dormitory with natural ventilation. Moon (2005) conducts three simulation studies and quantified the effect of construction details on the temperature factor. Wang (2016) quantifies infiltration rate and thermal bridges issue related to workmanship issues.

Compared to other sources of uncertainty in building models, there are insufficient studies discussing the uncertainty associated with the HVAC system. It is usually assumed to operate in ideal conditions, although people learn from experience that this is seldom the case in the real situation. Many factors can impact the inability of the HVAC system to operate as idealized. It can result from inadequate design, such as duct routing, component sizing, deterioration, and deficient maintenance. Related studies typically focus on topics that are easier to capture in quantifiable effects in the form of uncertainty that can be propagated through the simulation model. Typical uncertainty studies consider the uncertainty in mechanical system efficiencies and quantify those by introducing probability distributions (Augenbroe, et al., 2013). Another type of uncertainty analysis investigates how to determine the size of HVAC components considering uncertainties (Gang, Wang, Shan, & Gao, 2015) (Sun, Gu, Wu, & Augenbroe, 2014) (Huang, Huang, & Wang, 2015) (Cheng, Wang, Yan, & Xiao, 2017) (Gang, et al., 2016). Other studies deal with the third

topic, system deterioration over time (de Wilde, Tian, & Augenbroe, 2011). Gang, Wang, et.al (2015) propose a cooling system sizing and configuration optimization method considering uncertainties in the cooling load calculation. The proposed method can determine the cooling system capacity with quantified confidence by presenting the probability distribution of the cooling load and the potential capital cost. Sun, Gu, Wu and Augenbroe (2014) propose a design method based on dynamic simulation considering quantified uncertainties to replace the safety factor in HVAC system sizing. Huang, Huang, and Wang (2015) propose a prototype of HVAC system design under peak load prediction uncertainty using a multi-criterion decision making technique which can assess the performance of a design at the design stage in terms of multiple performance indices and the customers' requirements and preferences. Huang and Huang (2017) investigate the uncertainty associated with the key parameters in predicting the maximum cooling loss in the HVAC systems. The authors use Bayesian inference and Markov Chain Monte Carlo method to calibrate uncertain distributions of the important parameters through combining prior information and in-situ data for decision making in retrofit analysis and HVAC system design. de Wilde et al. (2011) proposes a stochastic process model to model system deterioration with a gamma distribution. Smith, Luck and Mago (2010) present an analysis of a representative steady-state model of a combined cooling, heating, and power (CCHP) system under different operating strategies with input and model data uncertainties and demonstrate the importance of the use of uncertainty and sensitivity analysis in CCHP system performance predictions. Yan et.al (2017) investigate the uncertainties of outdoor air control of a specified system type. The authors identify the uncertain parameters, quantify their uncertainty patterns and map them to building performance simulation in

terms of energy consumption and ventilation requirement. The authors identify the inadequacy of the EnergyPlus model when neither outside air flow nor outside air ratio is kept constant when the outside air damper operates at a fixed minimum position in actual systems which is contrary to the model assumptions in EnergyPlus. Wang et al. (2012) investigate uncertainties in energy consumption due to different building operational practices. They argue that the different building operation strategies contribute a great portion in the overall uncertainties in annual site energy consumption.

Occupant behavior and its impact on building performance has become a popular research domain in recent years. Eguaras-Martínez, et.al (2014) emphasize the impact of occupancy behavior on building energy performance and claim that occupant behavior may lead to 30% differences in building energy performance based on their simulation result. They conclude that it is possible to save a great amount of energy by considering the occupancy patterns without architectural changes. The authors develop a deterministic occupant usage profile based on actual data on internal loads (people, schedules, type of lights, number and type of equipment) as input of a newly developed model. The study gives insight into the role of actual usage schedules of the building and how savings might be exaggerated if they are based on ideal control. Instead of comparing the outcome of their new model to a reference value that is predetermined over a large set of functionally equivalent buildings, the study compares the result of their model to a reference building that is generated from the same architectural design but with a default space usage template (for example provided as standard schedules in OpenStudio).

Davis III and Nutter (2010) investigate the occupancy profiles of six university building types. A simple method is developed to predict an occupancy diversity factor for

classroom-type university buildings by using a combination of the class scheduling data and an estimation of the number of office occupants. In general, building simulation tools allow the modeler to define occupant (behavior) that specifies occupant density and presence schedules in building zones. Occupant behavior models can be categorized into two types: implicit and explicit. The implicit models focus on modeling occupant interaction with building systems, such as lights and equipment. Ward, et.al (2016) explore the impact of different parameterizations of occupant-related internal loads in building energy simulation. Breesch and Janssens (2010) implement three scenarios (low, medium, and high) to represent the variations of internal heat gains. Wang (2016) develops an occupancy model to represent the variation of occupant presence and the associated lighting/appliance usage based on measured data. The author argues that stochastic nature of occupant presence and their control actions only moderately impacts monthly aggregated HVAC system consumption in most current buildings, provided that average occupancy is known at the weekly or monthly scale. Moreover, they show that the impact on monthly totals can be accurately predicted without needing dynamic simulation. Explicit models, on the other hand, derive the "state" of the occupant and its control actions by explicitly modeling the underlying logic that causes occupant behavior. Typical explicit models deploy Markov chain (Wang, Yan, & Jiang, 2011), agent-based approach (Luo, Lam, Chen, & Hong, 2017), and random walk (Ahn, Kim, Park, & Wilde, 2017). The Markov chain method generates stochastic predictions based on the conditional probabilities derived from measured data, whereas an agent-based approach generates the occupant behavior based on predefined rules. The rules are supposed to be calibrated on (video) observations, although these methods are new and unconfirmed. According to the

study conducted by Ahn et al. (2017), occupancy patterns can significantly vary depending on the building type. Accordingly, the energy prediction is significantly influenced by the characteristics of the client organization and its worker cohorts.

1.2 Motivation

The major function of an HVAC system in a building is to remove the thermal load and maintain the space at the desire condition. At the design stage, the prediction of the building thermal load is probabilistic in nature due to many sources of uncertainty in the actual realization, such as the weather condition, building envelope properties, infiltration and occupant behavior. Some parameter uncertainties can be small if managed properly during the realization of the building; others, mostly scenario parameters are inherently uncontrollable and stochastic in nature.

Besides the studies that discuss the manufacturing tolerance for HVAC system and their role in uncertain performance curves, many previous studies on uncertainty analysis of HVAC system performance focus on investigating the uncertainties of the building thermal load and HVAC sizing. For example, the HVAC equipment capacity is typically determined based on the peak heating and cooling load, which is affected by many factors, such as the assumption of a critical design day, the heat transfer through building envelope, internal heat gain, infiltration. There are two hidden assumptions in this. Firstly, it is assumed that the aggregated building thermal load from interior and exterior sources, is the load that needs servicing by the HVAC systems. Secondly, it is assumed that the thermal load can always be “perceived” by the HVAC system and the HVAC system is able to

satisfy the requirements by modifying its operational status according to the layout, system capacity and control strategies.

HVAC systems maintain predetermined thermal conditions to satisfy the requirements of occupant thermal comfort. In principle, loads in a space do not need to be fully addressed by the HVAC system when a space is not occupied. Yang and Becerik-Gerber (2014) quantify the heating/cooling loads associated with occupancy diversity and provide a generalizable framework to evaluate energy efficiency affected by eliminating the occupancy diversity based on zone-level HVAC start/stop schedules. Zhang et al. (2017) develop a probability distribution function to describe the spatial distribution characteristics based on field investigation and size the equipment by introducing a guaranteed rate, which corresponds to a confidence level assessment based on the probability distribution function.

These studies attempt to regulate the thermal load in a space considering the occupancy diversity and discuss the impact of the regulated thermal load on the performance of the HVAC system. However, the space load is not the directly measurable quantity. The HVAC system typically uses space condition, such as temperature, relative humidity and CO_2 concentration, as the directly measured quantities. The system monitors the space condition by sensors whereas a controller translates the measurement and known setpoints into a delivery requirement which then determines the operational status of the system through causal rules. In general, if the space condition cannot be sensed by the HVAC system, the delivery requirement in that space cannot be satisfied. This situation occurs frequently in buildings whose zonal distribution does not match the HVAC distribution topology.

Figure 0.4 diagrams the interaction between HVAC system, building space, and occupancy in the building system. The building provides a desired indoor environment to occupants to fulfill their working/living requirements. The thermal load is composed of two parts: the first part is the heat gain from the occupancy that includes the sensible and latent heat from not only the metabolism of occupants, but also the released heat of lighting and appliances; the second part of thermal load is from the outdoor environment introduced by the fresh air and heat transfer through the building envelope. To maintain the desired indoor environment, the HVAC system is required to deliver heating/cooling energy into the space to remove the thermal load. However, the thermal load is not a state variable; it rather is an "implicit" quantity with diminished observability and unlikely to be used by the HVAC control system. In reality, the space air temperature, instead of the thermal load, is used in the HVAC control system. The thermostat installed in the building space monitors the space condition and the HVAC system adjusts the delivered heating/cooling energy in order to maintain a predetermined ideal space condition that is deemed to satisfy the requirements of occupants based on the measured current state. As mentioned above, the role of the HVAC system in a building is to maintain the predetermined space thermal conditions that satisfy the thermal comfort requirements of occupants in those spaces. The interactions between the HVAC system and occupants are "intermediated" by the building space. Therefore, it is very important to investigate the relationship between the building space and the HVAC system as well as the interactions between occupant usage and the building space to determine how well the HVAC system performs its task and how much energy it consumes in doing so.

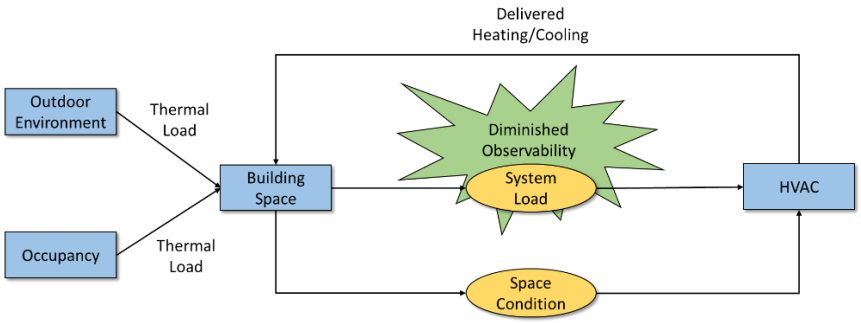

Figure 0.4 Interactions between HVAC, building space and occupant

Commonly used building energy models, such as EnergyPlus, use the concept of thermal zone instead of space (room) to link building and HVAC system. Sub-zones or spaces within a thermal zone share the uniform space air condition (temperature, relative humidity etc.) of the zone whose condition is maintained by a dedicated HVAC unit.

Taking the VAV system as an example, a VAV terminal unit usually serves more than one space in a practical situation and space conditions in different spaces are de facto assumed identical. The VAV terminal unit can only identify the condition of the space where the thermostat is located. Based on the feedback from the thermostat, the VAV box maintains the temperature in the monitored space at the setpoint while the heating/cooling is delivered to the serviced spaces in the (larger) zone. Therefore, the air condition in the spaces without thermostat cannot be monitored by the HVAC system and consequently the indoor air temperature in these spaces are not maintained at the setpoint since the energy delivered from the HVAC system may not balance the thermal load in the individual space. In reality, it is very common that the space air temperature in the monitored space is well maintained while the occupants in other rooms complain that their air temperature drifts away from the setpoint. The photos in Figure 0.5 are taken in the same office area in a

modern office building, it anecdotally illustrates that it might be too arbitrary to assume an identical space air temperature for all the spaces in a thermal zone.

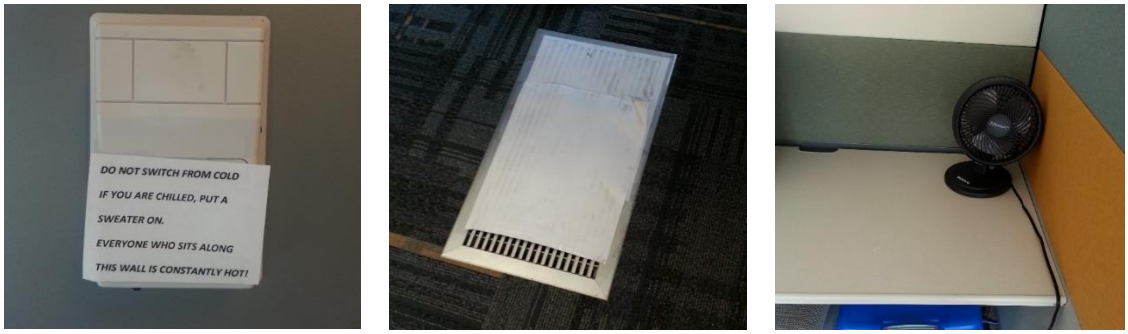

a. Unevenly distributed space air temperature

b. space air temperature always below the setpoint (74F)

c. space air temperature always above the setpoint (74F)

Figure 0.5 Measured space air temperature in the same office area

Take a typical VAV terminal box system layout shown in Figure 0.6 as an example, the terminal box serves three rooms and the thermostat is installed in room 1 (RM 1). The supply air flow of the VAV box is only determined by room 1 to maintain the indoor air temperature of room 1 at the setpoint, whereas room 2 (RM 2) and room 3 (RM 3) are air-conditioned but the supply air flow is not controlled based on their actual conditions.

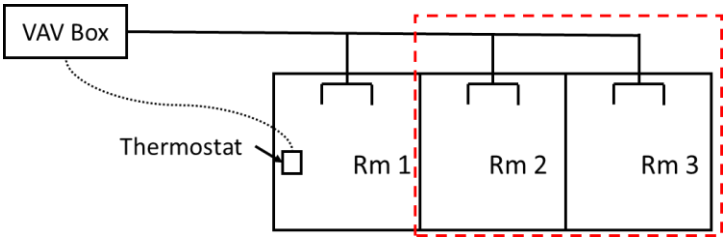

Figure 0.6 Typical layout of a VAV terminal box

To model the VAV terminal box system shown above in an EnergyPlus model, some simplifications are inevitably introduced due to the limitation of the software.

Although the modeling of the thermal zone of a VAV box system is highly dependent on the knowledge and preference of the modeler, two common zoning methods are typically used in the modeling process. The first zoning method is to combine the three rooms as one thermal zone based on the fact that the three rooms are served by only one VAV terminal box, shown as Figure 0.7. By using this zoning method, the three rooms are assumed as a well-mixed space sharing one uniform space air temperature T_i. The total supply air flow from the VAV box is calculated to satisfy the aggregated thermal load requirement of the entire thermal zone. On the other hand, the second zoning method is to define each room as an independent thermal zone, shown as Figure 0.8. Based on the second zoning method, the space air temperature in each room is independently maintained (T_i1, T_i2, and T_i3) by its dedicated virtual VAV terminal box. The supply air flow rate of each virtual VAV terminal box is adjusted independently to satisfy the thermal load of each space.

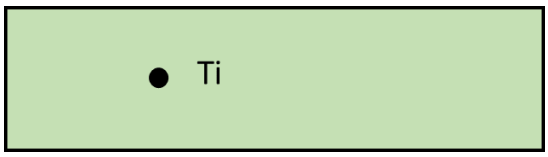

Figure 0.7 Zoning based on HVAC system layout

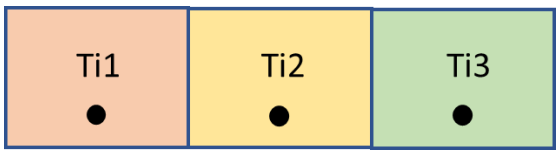

Figure 0.8 Zoning based on building partition layout

If the three rooms are grouped into one thermal zone, the system information of the VAV terminal box is embodied in the model, such as the service area and the size of HVAC components. However, this zoning method ignores the differences among the three rooms. First of all, the total heating/cooling energy is determined as an aggregated thermal load, which cannot distinguish the loads released in separate rooms. Secondly, the space

temperature (T_i) represents a virtual temperature that does not exist in reality and is most likely not the thermostat-monitored temperature of room 1 in the real situation. The second zoning method, contrarily, is based on layout of space partitions. It redefines the HVAC system layout and retains the information of the spaces, including the size, the space function, and the occupancy profile per room. To serve the three thermal spaces, three "virtual" VAV terminal box are added into the model and each space is regarded as a separate zone. Since the capacity of each virtual VAV terminal box is estimated based on the thermal load of the corresponding space, the total capacity of the three VAV system may not be equivalent to the capacity of the actual equipment. The second zoning method can independently maintain the space temperature for each thermal zone, whereas only the space temperature of room 1 can be measured and maintained in reality. Compared with the actual system shown in Figure 0.6, both zoning methods introduce distortions into the model. The distortions are inevitable because in EnergyPlus, building space and the HVAC system are coupled by the concept of thermal zone which is the atomic object to define physical characteristics, operational activities, and corresponding conditions. This forces us to reconsider whether it is indeed a reasonable constraint that building space and the HVAC system are coupled by the concept of thermal zone. As EnergyPlus mandates this as the only coupling, it must be identified as one source of discrepancy between model and reality. As introduced before, this is thus another instance of model form uncertainty in the low fidelity model and should be treated as such. The major challenge of this thesis is therefore to characterize and quantify the magnitude of this model form uncertainty (MFU). Once this is accomplished, it can be added to EnergyPlus as a stochastic term, similar to the inclusion of the other types of model form uncertainty as described in (Sun Y. , 2014),

where it is explained that at current there are 11 modules added to EnergyPlus to represent various sources of model form uncertainty. It should be noted that model form uncertainty cannot be defined as either parameter or scenario uncertainty that can be propagated through a Monte Carlo engine. It can in principle only be achieved by adding intrusive EnergyPlus code changes to the original software. It is therefore expected that likewise the model form uncertainty addressed in this thesis will also require an intrusive intervention by adding new code to the existing EnergyPlus software and recompiling the so adapted version. This however is not the primary objective of this thesis, as the emphasis is on quantifying the effect of the model discrepancy on different outcomes of interest. Based on these findings it will be left open to future work how the effect will be added to future use of EnergyPlus in everyday simulations. To show a road towards this, one example of the possible inclusion of MFU in the low fidelity model is shown in Chapter 6.

In particular, this study investigates the model discrepancy caused by simplified representations in EnergyPlus between the building space and the topology of the HVAC layout and controllability which, we argue, leads to significant misalignment with reality. An air-handling unit connected with VAV terminal boxes is chosen as the HVAC system for our study. This choice is motivated by the wide application of VAV systems. According to the literature, central VAV systems constitute 58.8% of centrally controlled HVAC systems in office buildings (Yang & Becerik-Gerber, 2014).

1.3 Thesis structure

The first chapter introduces the research background, followed by the literature reviews on the building energy performance gap and uncertainty quantification work. The

motivations for this thesis are presented and both the insufficient understanding and not well-quantified sources of uncertainty are discussed. Chapter 2 presents the ideal temperature control in EnergyPlus, followed by the introduction of two new characteristic parameters: alignment factor and occupant load diversity factor. An approach to derive sub-zone level occupant usage profiles from the zone level information is also presented in Chapter 2. In Chapter 3, we discuss the methods of characterization of model discrepancy and ensuing uncertainty quantification due to the misalignment of model and reality. A three-model approach is presented in this section. Chapter 4 contains the preliminary study with a specified spatial configuration in three usage diversity levels. Chapter 5 is the uncertainty analysis of the impact of the idealized temperature control of the EnergyPlus representation of VAV system considering the stochastic usage pattern of occupants in two space functions with five alignment configurations in three boundary situations focusing on the risk of underestimating energy consumption and over estimating occupant comfort (unmet hours in particular). Chapter 6 explores the characterizations of the results from the case studies and discusses the methodologies and steps for "post corrections" or MFU inclusion in the low fidelity model by using fan power as an example. Chapter 7 discusses the findings, conclusions of the study, and outlines ideas for future work.

IDEAL TEMPERATURE CONTROL AND ZONAL LOAD CALCULATION

1.4 The relationship between building spatial configuration and HVAC topology

In reality, HVAC control systems are typically closed loops. In the control loop of a VAV terminal box system shown as Figure 0.1, the space air temperature is the controlled state to be maintained at the setpoint. The temperature sensor measures the actual space air temperature and sends back a signal along the feedback path to the controller. The value of measured space temperature and the setpoint in the controller is compared. The difference between the setpoint and the measured value is known as the error signal. The error signal is transformed to a low voltage command signal delivered to the actuator. The actuator on the supply air damper (or on the reheat valve) reacts to the impulse received from the controller and modifies the supply air flow (or modify the flow of the hot water). It changes the space temperature and make it approach to the setpoint.

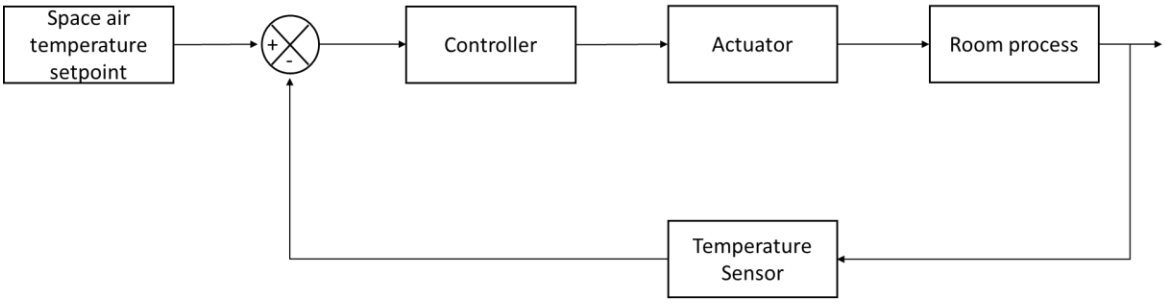

Figure 0.1 Schematic diagram for space air temperature control loop

However, only one controlled state (space air temperature) can be handled in the abovementioned VAV terminal box closed control loop. If there is more than one space served by the VAV terminal box, there are typically two methods to determine the control

state. The first method is to select one of the spaces as the primary space (or the most critical space) to install the thermostat to measure the indoor air temperature and use it as the control state whereas all other space air temperature will not be monitored. The second method is to compute an effective space temperature as the control state. The effective space temperature is calculated considering the indoor air temperature in more than one space. In either way, the single control state cannot fully represent the space conditions in all individual spaces in the thermal zone. It has two inevitable consequences: first, it is difficult to maintain the indoor air temperature in all spaces at the setpoint; second, the heating/cooling energy delivered from the VAV terminal box deviates consequently from the idealized load which is estimated based on the assumption that all spaces are maintained at the setpoint temperature.

Considering the cost and the robustness of the control sequences, the control state of the VAV control system is usually selected based on the first method, which means only one space is monitored and maintained at the desired indoor air temperature. Therefore, we can group the spaces in the service area of a VAV terminal box into two categories: the directly controlled area (DCA) and the indirectly controlled area (ICA). The DCA is the space where the thermostat is installed. The space air temperature of the DCA is measured and the control variables (flowrate and supply air temperature) of the VAV terminal box are determined based on the measured space air temperature and its corresponding setpoint. The space condition in the DCA is typically maintained well at the setpoint. The ICA is the space that is served by a VAV terminal box but has no thermostat of its own. The space air temperature of the ICA is not measured, and the control system “blindly” adjusts their

operating conditions without considering the space air temperature in the ICA. Thus, the space air temperature in the ICA may not be maintained at the setpoint.

In practice, it is very common that multiple spaces are served by one VAV terminal box. The control system is typically designed with insufficient capability to maintain conditions in all spaces, but only DCA is actively maintained at its setpoint whereas ICA is only "blindly" controlled as its real state cannot be "perceived" by the system.

1.5 Implementation in EnergyPlus

In the current EnergyPlus, thermal zone is the basic element to link the building space and the HVAC system. Only the zonal air temperature and to some extent its distribution within the space, is addressed, which allows surface heat transfer and air system heat balance calculations to be made considering the nature of thermal stratification of air and the different types of intentional air distribution designs, such as the underfloor or sidewall displacement ventilation that purport to extract room air at higher-than-mean temperatures. However, EnergyPlus does not have general methods to model room air that are universally applicable to every conceivable type of airflow distribution layout that might occur in a zone. Considering the computational cost of flow field simulation, the alternative, complete mixing room air model is widely accepted. Assuming uniform air temperature is the de-facto way of zonal modeling implying one "mean" air temperature and corresponding relative humidity.

To maintain the mean air temperature, the air systems in EnergyPlus provide hot or cold air to the zones to meet heating or cooling loads which is estimated based on the assumption that the zone mean air temperature is maintained at the setpoint. Taking the

VAV system in EnergyPlus as an example, each thermal zone is assigned to a VAV terminal box and the thermal zone typically cannot be further sub-divided. The space temperature in the overall thermal zone is represented by the unified zone air temperature, which is measured and maintained by the VAV terminal box system. If the air capacitance is neglected, the steady-state system output can be expressed as follow:

$$-\dot{Q}_{VAV,EP} = \dot{Q}_{int,z} + \sum_{i}^{n} h_i A_i (T_{si} - T_z) + \dot{m}_{inf} C_p (T_{OA} - T_z) \quad 2.1$$

$$\dot{m}_{VAV,EP} = \frac{\dot{Q}_{VAV,EP}}{C_p (T_{sup} - T_z)} \quad 2.2$$

$$T_z = T_{set}$$

Where:

$\dot{Q}_{VAV,EP}$: the delivered cooling/heating rate from the VAV terminal box into the space in EnergyPlus model (W);

$\dot{Q}_{int,z}$: the sum of the internal loads (W);

$\sum_i^n h_i A_i (T_{si} - T_z)$: the heat transfer from the zone surfaces (W);

$\dot{m}_{inf} C_p (T_{OA} - T_z)$: the heat transfer due to the infiltration of outside air (W);

$\dot{m}_{VAV,EP}$: the supply air mass flowrate of the VAV terminal box (kg/s);

C_p: the heat capacity of zone air (J/(kg·K));

T_{sup}: the supply air temperature (K);

T_z: the zone mean air temperature (K).

The equations above assume that the zone supply air mass flowrate exactly equals to the sum of the air flow rates leaving the zone through the system return air plenum and being exhausted directly from the zone. Both air streams exit the zone at the zone mean air temperature. On the basis of the inner workflow of EnergyPlus, the zone mean air temperature is estimated at the setpoint, and the zone load is predicted according to Equation 2.1, then the supply air flowrate of the VAV terminal box will be calculated based on Equation 2.2. The computational logic is shown in Figure 0.2.

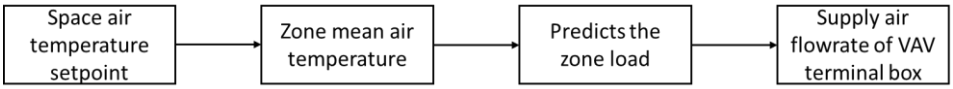

Figure 0.2 Computational logic of EnergyPlus

It is a reasonable approximation to use a single value to represent the space air temperature in the overall zone area if the thermal zone is a small open space. However, according to the internal computing process, traditional EnergyPlus cannot reflect the complexity between building spatial configuration and HVAC topology when the service area of a terminal unit is composed of more than one space because it cannot distinguish the indirectly controlled area from the directly controlled area. When we simplify the two spaces (the DCA and the ICA) as one thermal zone, the space air temperature in both DCA and ICA are assumed as the zone mean air temperature. The system load in EnergyPlus is calculated based on the zone mean air temperature and the aggregated load profile of the overall service area. Consequently, the heat gain released in the ICA plays a role in the aggregated load profile and eventually impacts the system load. However, the VAV system cannot sense the space condition in the ICA in the practical situation, and the system load

is only determined by the feedback of the measured space air temperature which only reflects the characteristics in the DCA.

As mentioned in the Chapter 1, there are two typical methods for zoning a service area with more than one enclosed space. The first method is to ignore the imperceptibility of ICA and combine the ICA with DCA as one space with an aggregated perceivable thermal load. This aggregated method neglects spatial configurations within the thermal zone. The second method is to add a virtual terminal unit in each ICA space thus assuming DCA and ICA as the individually controlled zones. The virtual terminal unit adds nonexistent controllability to the air system. Both models bring in simplifications that make up for the non-regarded interactions between the building spatial configuration and the HVAC topology, and introduce a discrepancy between the simulation outcomes and the measurement in reality. It is obvious that the level of complexity or mismatch between spatial configuration and HVAC layout topology has a major influence on the magnitude of the resulting discrepancy. Revealing the characteristics of the mismatch and the resulting discrepancy is the primary goal of this thesis.

1.6 Indicators of the complexity between spatial and HVAC configuration

1.6.1 Alignment factor

To study the impact of the complexity between spatial and HVAC configurations, we need to distinguish the DCA and the ICA in a service area instead of considering the whole area as a unified thermal zone. The steady-state system output of a VAV terminal box can be expressed as:

$$\dot{Q}_{VAV} = \dot{m}_{DCA} C_p \left(T_{Sup} - T_{DCA}\right) + \dot{m}_{ICA} C_p \left(T_{Sup} - T_{ICA}\right) \quad 2.3$$

In practice, the flowrate sensor is commonly installed to measure the total supply air flowrate of a VAV terminal box, and the flowrate is typically the area averagely distributed into the DCA and the ICA. Therefore, we use the total supply air flowrate of the VAV terminal box instead of the supply air flowrate of the DCA as the variable in the equations.

If we define:

$$\eta = \frac{A_{DCA}}{A_{DCA} + A_{ICA}} \quad 2.4$$

As the alignment factor to describe the "spatial-HVAC mismatch", which reflects the ratio of the controllable area to the total service area of a VAV terminal box, then we can derive Equation 2.3 as:

$$\dot{Q}_{VAV} = \eta \dot{m}_{VAV} C_p \left(T_{Sup} - T_{DCA}\right) + (1 - \eta) \dot{m}_{VAV} C_p \left(T_{Sup} - T_{ICA}\right) \quad 2.5$$

Where, $\dot{m}_{VAV}$ is the total supply air flowrate of the VAV terminal box.

The alignment factor (η) identifies the mismatch between the layout of building partitions and the topology of the VAV terminal box. The range of the alignment factor is from 0 to 1. If η equals to 1, it indicates that the entire space of the service area of the VAV terminal box is the DCA where the space temperature is measured by the thermostat. The supply air flowrate of the VAV terminal box is modulated to maintain the space

temperature at the setpoint based on the sensor data. In that case, the VAV terminal box has full controllability to maintain the space air temperature for the entire service area. If η equals to 0, it indicates that there is no thermostat installed in the space and the VAV terminal box can only blindly deliver heating/cooling into the space without sensing the space condition as feedback. In that case, the overall service area of the terminal box is out of control. It is an extreme condition and typically will not happen in the real situation. If η equals to a value between 0 and 1, it indicates that the service area of the VAV terminal box can be divided into the DCA and the ICA. The space temperature of the DCA is maintained by the terminal box. The total supply air flowrate of the terminal box is determined by the space temperature of the DCA. The distribution ratio of the supply air flowrate between the DCA and the ICA is determined by the value of η. Taking η equals to 1/5 as an example, it means that the amount of supply air to the DCA takes 1/5 of the total supply air flowrate of the VAV terminal box. The rest of the supply air is delivered into the ICA.

1.6.2 Occupant load diversity in the DCA and the ICA

According to Equation 2.5, the delivered cooling energy of the VAV terminal box includes two parts: the energy delivered to the DCA and the energy delivered to the ICA. The space air temperature in the DCA is the controllable state, which is well maintained by the modulated supply air flowrate from the VAV terminal box. Meanwhile, the space air temperature of ICA is affected by the heat gain in the ICA whereas the supply air flowrate delivered from the air system which is affected by the heat gain in DCA. The space air temperature in EnergyPlus model can always be maintained at the setpoint unless the capacity of the air supply system is not enough to handle the heat gain in the space. In

every time step, the thermal load released in the space will be handled by the HVAC system. However, the space air temperature of the ICA is not inherently maintained at the setpoint as reflected in the alignment factor introduced above. The question arises is in what condition the space air temperature of ICA can be maintained at the setpoint to make the EnergyPlus result valid. Take the cooling mode as an example, assuming:

At time step t_i,

$$T_{DCA} = T_{ICA} = T_{set}$$

Then:

For the DCA:

$$\eta \dot{m}_{VAV,ti} C_p \left(T_{Sup} - T_{set}\right) = -Load_{DCA,ti}$$

For the ICA:

$$(1-\eta) \dot{m}_{VAV,ti} C_p \left(T_{Sup} - T_{set}\right) = -Load_{ICA,ti}$$

Therefore, only if the thermal load of ICA at every time step satisfies the relationship shown as Equation 2.6, the result of sub-zone EnergyPlus model is valid.

$$\frac{Load_{DCA,ti}}{Load_{ICA,ti}} = \frac{\eta}{1-\eta} = \frac{A_{DCA}}{A_{ICA}} \qquad 2.6$$

$$\frac{Load_{DCA,ti}}{A_{DCA}} = \frac{Load_{ICA,ti}}{A_{ICA}} \quad 2.7$$

$$\frac{Load_{DCA,ti}}{Load_{DCA,ti} + Load_{ICA,ti}} = \frac{Load_{DCA,ti}}{Load_{total,ti}} = \eta \quad 2.8$$

Equation 2.6 illustrates that the space air temperature in the ICA can be maintained at the setpoint with the "blindly" supplied cooling air only if the ratio of the thermal load between the DCA and the ICA equals to the ratio of the space area. When Equation 2.6 is satisfied, the space conditions in DCA and ICA in the VAV terminal system can be balanced. We define the service area is operated with no spatial thermal load diversity in this situation. Under the no diversity situation, the thermal load is evenly distributed in the overall service area, shown as Equation 2.7.

if we define:

$$Diff_T = T_{obs} - T_{EP}$$

$$Diff_{\dot{Q}} = |\dot{Q}_{obs}| - |\dot{Q}_{EP}|$$

Where:

T_{obs}: the observed space air temperature which measured in the real situation (K);

T_{EP}: the predicted space air temperature by EnergyPlus (K);

$\dot{Q}_{obs}$: the delivered cooling/heating rate from the VAV terminal box measured in the real situation (W);

$\dot{Q}_{EP}$: the delivered cooling/heating rate from the VAV terminal box predicted by EnergyPlus (W).

There might still be a difference between the outcome of the sub-zone EnergyPlus model and the observations which can be influenced by case parameters. However, with no spatial thermal load diversity, the EnergyPlus model is expected to be a close approximation of reality.

However, the thermal load in DCA and ICA can vary dynamically as the result of many factors. Additionally, the correlations between the different space loads may be weak or non-existent. Therefore, the condition of no thermal load diversity mentioned above is an idealization that is unlikely to be achieved in any practical situation. If the condition cannot be satisfied, the delivered cooling/heating energy from the VAV box cannot meet the requirement of ICA and consequently, the space air temperature cannot be maintained at the setpoint. However, the EnergyPlus model cannot capture this and the outcomes of the model will deviate from the actual situation. According to Equation 2.8, the ratio of load of DCA to the total load of the overall service area must equal to the alignment factor during the time step t_i to make sure that the space conditions in both DCA and ICA are under control. In other words, if the ratio of load of DCA to the total load of the overall service area is larger than the alignment factor, the air system delivers extra cooling into the ICA and space air temperature of the ICA will be lower than the setpoint; if the ratio of load of DCA to the total load of the overall service area is smaller than the alignment factor, the cooling energy delivered by the air system is not enough to remove the thermal load of ICA and the space air temperature will be higher than the setpoint. Therefore, we make an assumption that for a determined alignment factor η, the discrepancies between

the simulation and observation result of the ICA condition are related to the ratio of the thermal load in these spaces, which can be expressed as:

$$Diff_{T,ti} = F_{\eta,ti}(\frac{Load_{DCA,ti}}{Load_{ICA,ti}})$$

$$Diff_{\dot{Q},ti} = G_{\eta,ti}(\frac{Load_{DCA,,ti}}{Load_{ICA,,ti}})$$

Where, $F_{\eta,ti}()$ and $G_{\eta,ti}()$ are the conversion functions to estimate the Diff T and Diff $\dot{Q}$ respectively based on determined η and internal loads in time step t_i.

However, the space (sub-zone level) thermal load is an implicit parameter that is affected by many factors. According to ASHRAE Handbook-Fundamentals (2013), the cooling load is affected by factors in four categories: external (envelop), internal (Occupant, lighting, and appliances), infiltration, and system (outside air, duct leakage, fan, and pump). Among these factors, internal load, which highly depends on the occupancy, is the key factor to determine the space thermal load, which is not only caused by the sensible and latent load released from the occupants but also the heat gain generated from the lighting and the equipment/appliances usage that are (in typical cases) to a large extent correlated with occupant presence. Therefore, we choose to use the occupant related load instead of the total thermal load to describe the level of spatial load diversity. To quantify the difference of the occupant load in the DCA and the ICA, we define the spatial occupant load diversity factor (θ) between the DCA and the ICA.

At time step t_i

$$\theta_{ti} = \frac{\dot{Q}_{int,DCA,t_i}/A_{DCA} - \dot{Q}_{int,ICA,t_i}/A_{ICA}}{\dot{Q}_{int,DCA,t_i}/A_{DCA}}$$

Where $\dot{Q}_{int,ICA,t_i}/A_{ICA}$ indicates the heat gain per unit area at time step t_i released by the occupants, lighting, and the equipment/appliances in ICA; $\dot{Q}_{int,DCA,t_i}/A_{DCA}$ indicates the heat gain per unit area at time step t_i released by the occupants, lighting and the equipment/appliances in DCA; θ describes the diversity of occupant related loads in DCA and ICA. The occupant related load is highly dependent on the presence of the occupants and therefore highly transient in nature, hence θ is a time dependent state variable.

1.7 The estimation of diversity factor in the sub-zone level

To estimate the value (distribution) of the diversity factor introduced in the previous section, it asks for more details of building usage information from zone level to the sub-zone level to generate the time series occupancy profile for both DCA and ICA. However, getting sub-zone level information is challenging and laborious which in many cases exceeds the available resources and stretches the modelers' case knowledge.

Internal heat gains vary with time and space because of occupancy variability. The space internal load information includes the load density and schedule of occupants, lights, and appliances. Wang (2016) conducts a survey and generates a stochastic occupancy profile based on the data-driven approach at the whole building level. Davis III et.al (2010) study six types of university buildings to generate stochastic occupancy schedules for each building type. Zhang et.al (2017) conduct a field investigation of forty-six tenants in seven office buildings to obtain the distribution of internal heat gains to determine the peak

cooling load. Chen et.al (2018) develop an occupancy simulator based on the agent-based method. Some of these studies deal with the stochastic nature of internal heat gains. The studies conducted by Wang and David III discuss the stochastic nature of occupancy schedules at the building level. Meanwhile, Zhang's work discusses the spatial diversity of internal heat gain density without considering the operation schedule since the study is focusing on estimating the size of chiller and AHU. To the best of authors' knowledge, there is a lack of research on predicting the diversity of internal heat gain at the sub-zone level. Therefore, we have no solid data to determine the range of the occupant load diversity factor. One way to overcome this is to derive sub-zone level information based on known zone level occupancy profiles. Wang (2016) establish a data-driven method to generate a stochastic occupancy profile based on a short period of measured data. The generated stochastic occupancy profile includes two sections: the mean occupancy profile and the day-to-day variability of occupancy variables. The basic assumption of the method is that the 24-hour profiles follow a multi-variant Gaussian distribution $N(\mu, \Sigma)$ with the value at each hour being a random variable. The distribution can be fully specified by the mean vector μ and covariance matrix Σ, where the covariance matrix Σ can be derived with the following equation:

$$\Sigma = \mathrm{D} \times \mathrm{C} \times \mathrm{D}$$

where matrix D is a diagonal matrix composed of the estimated standard deviation of the profile value at each hour. Matrix C is the correlation matrix between each hourly random variable which is derived from the data of ASHRAE Research Project 1093-RP (Abushakra, Sreshthaputra, Haberl, & Claridge, 2001). The day-to-day variability is generated from an

ARMA model, the coefficients of the autoregressive model is specified by the discrepancies between mean occupancy profile and the raw profile data.

With the abovementioned method, we can generate a time series occupancy profile for an area with a short period of occupancy profile. In this study, we use Occupant Simulator (Chen, Hong, Luo, & Xuan, 2018) which is an agent-based simulator released by LBNL to generate the dynamic occupant presence profile in the zone level as the measurement data to reflect the knowledge level of modelers in reality. The mean profile of the lighting and appliance usage and the correlation between the occupant presence and their operation of lighting and appliances is based on the measurement of a medium size building on the Georgia Tech campus conducted by Wang (2016). It can be assumed as a representative of a large volume of medium size office building, and we will use it to generate the lighting and appliance usage profiles based on the generated occupant presence profiles.

The sub-zone level occupancy profile will be derived from the zone level occupancy profile. For one space with a floor area of n square meters, $x_1, x_2, x_3, \dots, x_n$ represent the internal heat gain densities of each 1 m^2 floor area. X_n represents the internal heat gain density of the overall space. Then,

$$X_n = (x_1 + x_2 + x_3 + \cdots + x_n)/n$$

If $x_1, x_2, x_3, \dots, x_n$ follow the normal distribution function $N(\mu, \sigma^2)$, then X_n follows $N\left(\mu, \frac{\sigma^2}{n}\right)$. Zhang, et al. (2017) conduct an on-site investigation for forty-six tenants from seven office buildings to obtain the distribution of internal heat gains. The result

shows that the spatial distribution of the internal heat gain densities can be described by using normal distribution functions. Therefore, in this study, we assume the spatial distribution of the internal heat gain densities follow the normal distribution function.

Recall that we assume the 24-hour profiles of a zone ($X^1, X^2, X^3, \dots, X^{24}$) follow a multi-variant Gaussian distribution $N(\mu, \Sigma)$ with the value at each hour being a random variable. Then, if we divide the zone of interest into n sub-zones and assume each sub-zone keeps the same building function as the one in the entire zone. $x_m^1, x_m^2, x_m^3, \dots, x_m^{24}$ represent the 24-hour profile of the sub-zone m which follows a multi-variant Gaussian distribution $N(\mu, n\Sigma)$. Then

$$Corr(X^i, X^j) = \frac{E[(X^i - \mu_i)(X^j - \mu_j)]}{\sigma_i \sigma_j} \quad i, j = 1,2, \dots ,24$$

$$Corr(x_m^i, x_m^j) = \frac{E[(x_m^i - \mu_i)(x_m^j - \mu_j)]}{n\sigma_i \sigma_j} \quad i, j = 1,2, \dots ,24$$

$$Corr(x_m^i, x_m^j) = \frac{1}{n} Corr(X^i, X^j) \quad i, j = 1,2, \dots ,24$$

Recall that we use the correlation matrix between each hourly random variable which is derived from the data of ASHRAE Research Project 1093-RP. Then,

$$Corr(x_m^i, x_m^j) = \frac{1}{n}\, C_{ij} \quad i, j = 1,2, \dots ,24$$

From this, we derive the parameters of the sub-zone occupancy profile based on the information of zone level.

Taking alignment factor as 1/5 as an example to estimate the occupancy profile in the DCA and the ICA based on the zone level information that we obtained from the outcomes of Occupant Simulator, Figure 0.3 and Figure 0.4 shows the sampled occupant presence and lighting/appliance usage profiles during weekdays of one week. We can see that the profile in the larger area (in this scenario is ICA) has more significant influence on the zone level while the smaller area shows more variability compared to the larger area. The sampled profile shows the characteristics as our expectations.

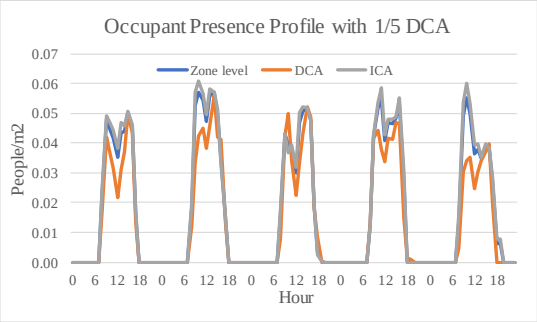

Figure 0.3 Sampled presence profile

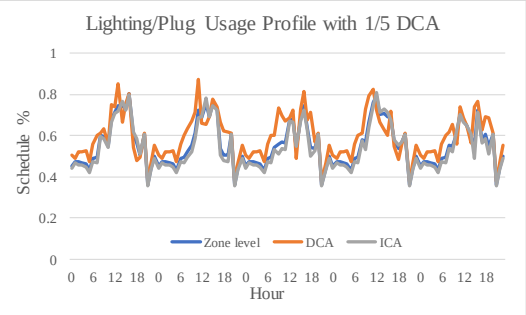

Figure 0.4 Sampled L/P usage profile

Based on the sampled occupant usage profiles, we can calculate the hourly occupant load diversity factor. Figure 0.5 diagrams the sampled diversity factor with the alignment factor as 1/5. Figure 0.5a shows the diversity factor during the weekdays in one week with a quite large hour-to-hour fluctuation. While Figure 0.5b shows the distribution of the diversity factor during the occupied hours (7am to 10pm) in the whole year. We can see that although the time series is a random sample, the distribution of diversity factor occurrences is fixed in a long enough sample period.

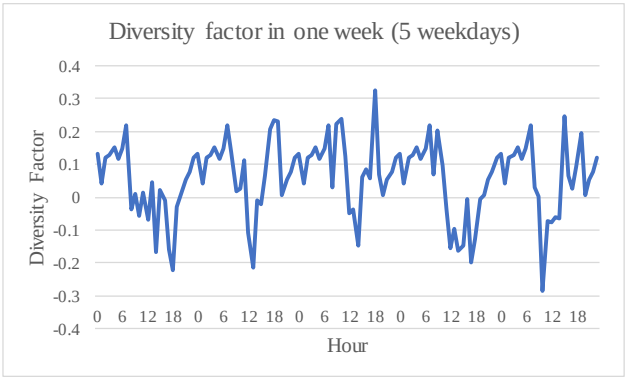

a

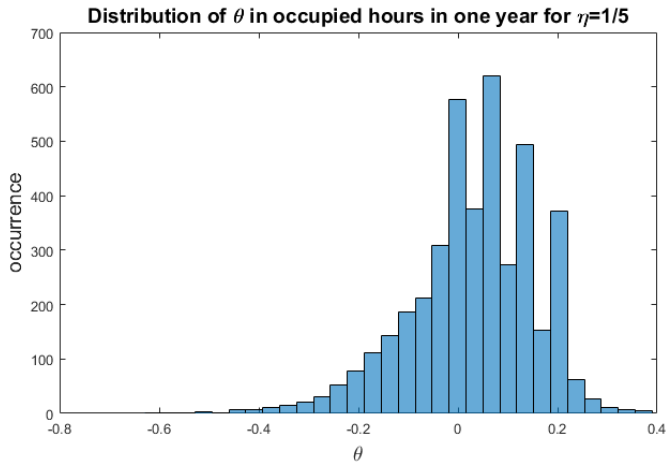

b

Figure 0.5 Sampled diversity factor with the alignment factor = 1/5

METHODOLOGY AND APPROACH

This chapter introduces the methodology typically used in the practice of uncertainty analysis, in particular a well-established methodology to quantify the model form uncertainty. The major simulation tools and the model configuration are introduced. In addition, the research approach and designed scenarios are presented in this chapter.

1.8 Model form uncertainty quantification

As state by George E.P. Box "All models are wrong, but some are useful", A computational models is an idealized representation of the real physical world with different levels of abstraction, in other words, a simulation model inevitably delivers only an approximate understanding of reality. If we denote a computational model as a function $G()$ that links input set u to the outputs $y = G(u)$, a discrepancy between the outputs y and the actual observations always exist even though the values of the model input set u are assigned to the true values, we identify this type of uncertainty (in G) as model form uncertainty (MFU). In order to quantify MFU we either need observation data from the physical reality or output from a higher fidelity model. As the intention is to estimate the uncertainty in the prediction of a not yet realized design, the first method is obviously not feasible unless on scale models. This study will therefore only use the second method to investigate the interactions between building and HVAC system in the operation stage comparing the low and high fidelity models. In EnergyPlus, the building is composed of thermal zones and the basic assumption is that the HVAC system layout is aligned with the thermal zones and the space condition in a thermal zone is uniform and well maintained by

the HVAC system. This basic assumption is an idealized understanding of reality and we will quantify the model form uncertainty caused by such model idealization.

The impact of MFU for a complex system, such as a building system, is hard to quantify at the entire system scale. Especially, it is difficult to collect high-quality observation data with limited input parameter uncertainties at the system scale. An effective way of conducting uncertainty quantification for complex systems is to develop a hierarchical structure that breaks down a complex system into subsystems and then into units (Sun Y. , 2014). At the unit level, we can collect high quality observation data with less noise and influence from input parameter uncertainties. Hence, this hierarchical structure should be utilized in model form uncertainty quantification, starting from the quantification at bottom level component and eventually moving up to the full system level. Let $G(u)$ denote the output of a computational model when input variables take values $u = (u_1, u_2, \dots, u_n)$. In this section, G is treated as a deterministic model and $G(u)$ has a fixed value by given a certain input set u. And the observation data y_{obs} is obtained from physical experiment or high-fidelity model. The model discrepancy refers to the difference between the observation data and the model output $G(u)$.

$$Diff(u, v) = y_{obs} - G(u)$$

We introduce additional parameters v along with the original input parameters u to represent the model discrepancy for a better representation of the model inadequacy if one expects that certain parameters (v) have a strong correlation with the resulting uncertainty. Once the discrepancy can be characterized by choosing the new defined parameter v, the output of a model can be modified by $Diff(u, v)$, so that the sum of $G(u)$ and $Diff(u, v)$

will be a better approximation of the observed value as it captures the correlation with certain parameters in the model.

If it is difficult to conduct the physical experiment, especially for the complex system, the observation data can be replaced by the outcomes $F(u)$ from a high-fidelity model, as shown as Figure 0.1. This method presumes the model inadequacy of the high-fidelity model merely has the secondary order effect compared to that of the low-fidelity model under study. Given the features of building simulation, we found it was useful to explore the high-fidelity model as an option to quantify the model form UQ of the low-fidelity model. An application of this approach is shown in Sun, Heo, et al. (2014), a high-order meteorological model was used as the high-fidelity model to quantify the uncertainty in a reduced order model of building microclimate.

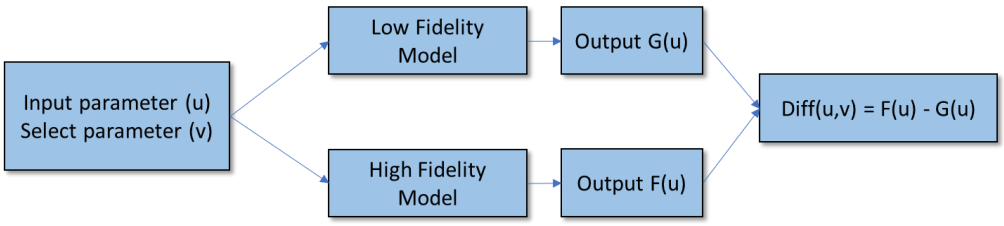

Figure 0.1 Model form uncertainty quantification by using a higher fidelity model

1.9 Methodology to study discrepancy between low and high fidelity models

A co-simulation model is introduced to mimic the reality of HVAC control as close as possible or at least better than a routine building simulation model. The co-simulation model is composed of (1) a routine building physical model and (2) a detailed HVAC model with fully modeled control logic. The building physical model is developed in EnergyPlus which includes the information of building envelope, occupancy, weather data,

zones and zone partitions. The HVAC model is specified in Modelica and implemented in Dymola. The service area of a VAV terminal box is divided into DCA and ICA. The VAV system is implemented as a detailed fully physics-based model in Dymola. The components (fan, damper, coil, etc.) in the HVAC system as well as the controllers, sensors, actuators in the control system are developed in the detailed HVAC model, which provides the flexibility to define the DCA and ICA based on sensor and actuator locations. The computing process of the co-simulation is different than the traditional EnergyPlus. In the co-simulation, the supply air flowrate of the VAV terminal box is modulated to maintain the space air temperature of the DCA at the setpoint. Then the supply air flowrate to the DCA and the ICA is determined by the embedded model of the ducting system (modeling flow and pressure). The distribution of the supply air flowrate into the service area of a terminal box depends on the ducting layout. In general, the supply air flow rate will be tuned as "area average distributed" during the commissioning process. The ratio of the supply air flowrate between the DCA and the ICA is kept constant determined by the fixed ratio of space area since the ducting characteristics typically keeps constant after commissioning process. For example, if the area of the DCA is one-fourth of the area of the ICA, the supply air flowrate to the DCA is always one-fourth of the supply air flowrate to the ICA. In other words, the system cannot adjust the ratio of delivered cooling energy based on the demand. The space air temperature is computed according to the thermal processes embedded in the building thermal model. The working process of the co-simulation is shown in Figure 0.2.

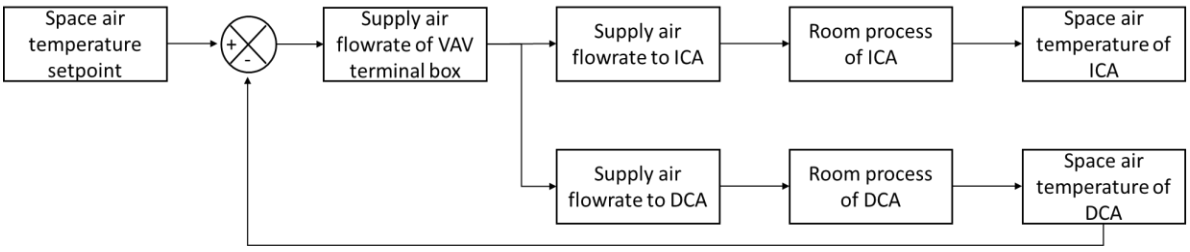

Figure 0.2 Working process of the co-simulation model

If the air capacitance is neglected, the steady-state system output can be expressed as:

$$Load_{DCA,T_{DCA}} = \dot{Q}_{int,DCA} + \sum_i^n h_i A_i (T_{si} - T_{DCA}) + \dot{m}_{inf} C_p (T_{OA} - T_{DCA})$$

$$\dot{m}_{DCA,co\_sim} = \frac{-Load_{DCA,T_{DCA}}}{C_p (T_{Sup} - T_{DCA})} \quad 3.1$$

For the ICA, the space air condition may not be guaranteed at the setpoint. Then:

$$Load_{ICA,T_{ICA}} = \dot{Q}_{int,ICA} + \sum_i^n h_i A_i (T_{si} - T_{ICA}) + \dot{m}_{inf} C_p (T_{OA} - T_{ICA})$$

$$\dot{m}_{ICA,co\_sim} = \frac{A_{ICA}}{A_{DCA}} \dot{m}_{DCA,co\_sim} = \frac{A_{ICA}}{A_{DCA}} \cdot \frac{-Load_{DCA,T_{DCA}}}{C_p (T_{Sup} - T_{DCA})} \quad 3.2$$

$$C \frac{dT_{ICA}}{dt} = Load_{ICA,T_{ICA}} + \dot{m}_{ICA,co\_sim} C_p (T_{Sup} - T_{ICA})$$

Where:

$\dot{m}_{DCA.co\_sim}$: the supply air flow delivered into the DCA;

$\dot{m}_{ICA,co\_sim}$: the supply air flow delivered into the ICA;

A_{ICA} and A_{DCA}: the space area of the ICA and the DCA, respectively.

Based on Equation 3.1 and Equation 3.2, we can find that the space air temperature in the two sub-zone areas may differ, the linkage between the two spaces in the air system is the ratio of supply air flowrate. The delivered cooling/heating rate in the steady-state system output can be expressed as follow:

$$\dot{Q}_{VAV,co\_sim} = \dot{m}_{DCA,co\_sim} C_p \left(T_{Sup} - T_{DCA}\right) + \dot{m}_{ICA,co\_sim} C_p \left(T_{Sup} - T_{ICA}\right)$$

$$= \dot{m}_{DCA,co\_sim} C_p \left(T_{Sup} - T_{DCA}\right) + \frac{A_{ICA}}{A_{DCA}} \cdot \dot{m}_{DCA,co\_sim} C_p \left(T_{Sup} - T_{ICA}\right) \quad 3.3$$

Where:

$\dot{Q}_{VAV,co\_sim}$: the delivered cooling/heating rate from the VAV terminal box into the space;

$\dot{m}_{VAV,co\_sim}$: the supply air flowrate of the VAV terminal box.

1.9.1 Model comparison and simulation outcomes

Equation 3.1 to Equation 3.3 express the space conditions and delivered cooling energy of the co-simulation model, it illustrates that the co-simulation has the capability to reflect the characteristics of the complexity between the building spatial configuration and the HVAC topology. The major assumption of this study is that the co-simulation model is such a good approximation of reality that it can be used as the reference to quantify the discrepancy of the stand-alone EnergyPlus simulation (Wang Q. , 2016). To limit the scope, this study is conducted only for systems with VAV terminal reheat boxes. Based on the two zoning methods (explained in Chapter 1.2), two EnergyPlus models are developed. The first EnergyPlus model aggregates the DCA and the ICA as one space (we call it as the aggregated-zone EnergyPlus model) and the second EnergyPlus model separates the

DCA and the ICA into two different zones (we call it as the sub-zone EnergyPlus model). The DCA and the ICA is represented by a virtual unified space air temperature in the aggregated-zone EnergyPlus model. The operating status of the VAV terminal box is determined by the aggregated thermal load of the DCA and ICA. The model has no capability to distinguish if the heat gain released from the DCA or from the ICA. In the second model on the other hand, the DCA and the ICA are controlled individually in the sub-zone EnergyPlus model. The two spaces are maintained by two independent HVAC system and the supply air flowrates are modulated independently. Equation 3.4 to Equation 3.7 shows the calculation process of space condition as well as the delivered cooling energy of the two EnergyPlus models.

For the aggregated-zone EnergyPlus model, the output in the steady-state system can be expressed as:

$$T_{DCA} = T_{ICA} = T_z$$

$$-\dot{Q}_{VAV,EP\_agg} = Load_{DCA,T_z} + Load_{ICA,T_z} \quad 3.4$$

$$\dot{m}_{VAV,EP\_agg} = \frac{\dot{Q}_{VAV,EP\_Agg}}{C_p\left(T_{Sup} - T_z\right)} \quad 3.5$$

For the sub-zone EnergyPlus model, the output in the steady-state system can be expressed as:

$$-\dot{Q}_{VAV,EP\_sub} = Load_{DCA,T_{DCA}} + Load_{ICA,T_{ICA}} \quad 3.6$$

$$\dot{m}_{VAV,EP\_sub} = \dot{m}_{DCA,EP\_sub} + \dot{m}_{ICA,EP\_sub} \quad 3.7$$

$$\dot{m}_{DCA,EP\_sub} = \frac{-Load_{DCA,T_{DCA}}}{C_p(T_{Sup} - T_{DCA})}$$

$$\dot{m}_{ICA,EP\_sub} = \frac{-Load_{ICA,T_{ICA}}}{C_p(T_{Sup} - T_{ICA})}$$

According to Equation 3.1, 3.2, 3.5 and 3.7, we can see that the outcomes of the three models may result in different predictions of the overall supply air flowrate and the space air temperature in the ICA even if we assume the space air temperature in the DCA is always maintained at the setpoint. Consequently, the delivered cooling energy outcomes from the three models will be different. The results may impact the occupant thermal comfort, cooling demand and the total cooling energy consumption. To quantify the differences between the model outcomes caused by the simplification introduced by the routine EnergyPlus models, we focus on space air temperature, and cooling energy in different time interval (hourly, daily, and monthly). We will also calculate the unmet hours based on the outcomes of the space air temperature and evaluate the impacts on the thermal comfort. The discrepancies in the supply air flowrate also affect the fan power estimation which can be a significant part of total energy consumption. In EnergyPlus, the VAV system does not perform pressure-based simulation with all terminal boxes operating independently. The fan power consumption for a variable speed fan is simply calculated based on a part load factor (DoE, 2017).

$$f_{flow} = \dot{m}/\dot{m}_{design}$$

$$f_{pl} = c_1 + c_2 \cdot f_{flow} + c_3 \cdot f_{flow}^2 + c_4 \cdot f_{flow}^3 + c_5 \cdot f_{flow}^4 \quad 3.8$$

$$\dot{Q}_{tot} = f_{pl} \cdot \dot{m}_{design} \cdot \Delta P / (\varepsilon_{tot} \cdot \rho_{air}) \quad 3.9$$

Where：

$\dot{Q}_{tot}$: the fan power (W);

$\dot{m}$: the air mass flow (kg/s);

$\dot{m}_{design}$: the design (maximum) air flow (kg/s);

ΔP: the fan design pressure increase (Pa);

ε_{tot}: the fan total efficiency;

f_{flow}: the flow fraction or part-load ratio;

f_{pl}: the part load factor.

The Modelica model better approximates the reality by involving pressure-based simulation. The supply air flowrate for a given VAV terminal box is calculated not only based on its own damper position, but also the damper characteristics, fan speed, fan performance curve, and the overall duct network including other movable components. This study does not aim to investigate the essential differences between the air system loop in EnergyPlus and Modelica model but attempts to investigate the discrepancies in the predicted flowrate and fan power from the three models.

The differences found from this exercise for a variety of configurations will be used to characterize and quantify the model discrepancy resulting from simplified HVAC control modeling in a generic way.

1.10 Simulation tools

EnergyPlus is the flagship building simulation tool supported by the United States Department of Energy (DOE). As an open source program, EnergyPlus provides many simulation capabilities including sub-hourly time-steps, thermal comfort, co-simulation with external interfaces, and user customizable energy management system (EMSs). Certain simulation capabilities of EnergyPlus, i.e. sub-hourly time-steps, co-simulation with external interfaces, and external schedules are heavily relied on in this study. The EnergyPlus model (identified as the low-fidelity model in this study) consists of the building physical model with embedded abstract HVAC system model. For the high-fidelity variant, a co-simulation model is adopted including an EnergyPlus building physical model and a detailed Modelica HVAC system model. Modelica is an equation-based object-oriented modeling language that specializes in describing and analyzing complex system represented by differential algebraic and discrete equations (Elmqvist, Mattsson, & Otter, 1998) (Modelica, 2019). The building library in Modelica, developed by LBNL, is a free open-source library with dynamic simulation models for building and district energy and control systems (LBNL, 2019). The primary use of the library is for flexible and fast modeling of new and existing buildings. In the Modelica model of the VAV system, the system components such as VAV box, fan, and air duct, are modeled and operated with actual control sequences (Wetter, 2009). The component modulates its operation state based on physical variable measured by a specified sensor instead of the idealized thermal load that is used in many building simulation tools including "stand-alone" EnergyPlus. By integrating the room level EnergyPlus model and the Modelica VAV system model, the co-simulation model is able to represent the actual physical connectivity between the VAV system components and building spaces, thereby

decoupling the VAV terminal box service area and the space partitions and is therefore able to reflect zoning complexity and occupant usage diversity.

1.11 Co-Simulation of the EnergyPlus building and Modelica HVAC system

The high-fidelity co-simulation model includes three parts: the EnergyPlus building module, the Modelica HVAC system module, and the BCVTB co-simulation platform which links the building model and the HVAC system model.

1.11.1 Configuration of the EnergyPlus building model

The EnergyPlus building module dynamically simulates the thermal response of the spaces considering weather condition, building envelope, internal load as well as the supplied cooling/heating energy. In the co-simulation loop, the building module receives the cooling/heating energy from the Modelica HVAC module and provides the space conditions (temperature and relative humidity) of each room back to the HVAC module. In the EnergyPlus building module, we use the "Other Equipment" objects in the "Internal Gain" section associated with schedule values as the interface to represent the sensible and latent heat gain resulting from the supply and return airflow in and out the space boundary. The schedule value associated with each sensible and latent heat gain is dynamically adjusted by the Modelica HVAC module in each timestep. The space temperature and relative humidity in each room are the output variables of the building module. A simplified configuration of EnergyPlus with schedules is shown in Figure 0.3.

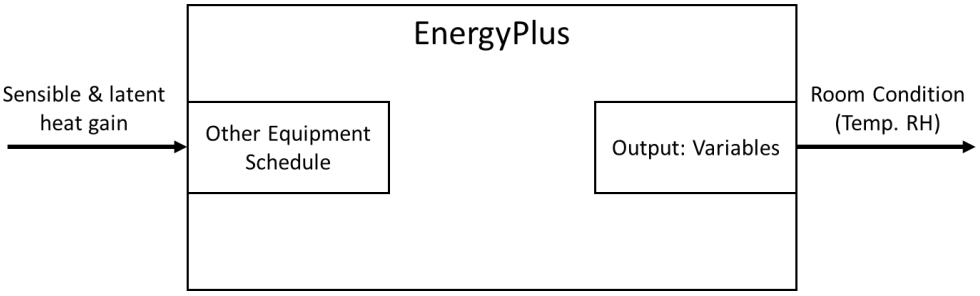

Figure 0.3 Configuration of EnergyPlus

1.11.2 Configuration of the Modelica HVAC system

Since the building physical model in EnergyPlus is developed without HVAC system, the sensible and latent energy from the HVAC system are implemented as the internal heat gains for each room in the building model. A predefined component named as "Buildings.Utilities.IO.BCVTB.MoistAirInterface" in the Modelica building library is implemented in the HVAC module to calculate the amount of the sensible and latent heat flow into each space boundary considering the enthalpy and mass flow rate of supply and return air stream. The component takes the air temperature, relative humidity and, optionally, a bulk mass flow rate into or out of the system boundary as input signals. The outputs of this component are the sensible and latent heat exchanged across the system boundary. The state of the fluid that flows out of this component will be at the system (room) temperature and relative humidity. The computed sensible and latent heat flows of each space will be sent as the input signal to a component named as "Buildings.Utilities.IO.BCVTB.BCVTB" which is the block for data exchanging between the simulation programs coupled in the BCVTB environment. The outputs of the data exchanging component are the air temperature and relative humidity of each room simulated by the EnergyPlus building module. The data is exchanged between the

Modelica module and the BCVTB platform at each sampling interval. At the start of the simulation, the data exchanging block establishes a socket connection using the Berkeley Software Distribution socket (BSD socket).

Since the Modelica HVAC module does not have the feature to auto-size the equipment, the modeler has to supply component capacities. To realize this, the design supply air flows for each zone from the auto-sizing result in the low-fidelity EnergyPlus model are implemented as the input for the system components in the Modelica module. Therefore, the system in the low-fidelity EnergyPlus model and the high-fidelity co-simulated model share the same system component capacities. The EnergyPlus building model developed in this study does not perform the airflow network simulation, therefore, the co-simulation simply assumes that the supply air stream and the return air stream have identical values, which means that infiltration and inter-zone air flows are not considered. This is in line with the primary objective of this thesis which is to "isolate" the effect of spatial-HVAC misalignment and occupancy diversity.

1.11.3 Configuration of the BCVTB co-simulation model

The Building Controls Virtual Test Bed (BCVTB) is a software environment that allows users to couple different simulation programs for co-simulation, and to couple simulation programs with actual hardware. The BCVTB is based on the Ptolemy II software environment. The configuration of the co-simulation model is shown in Figure 0.4.

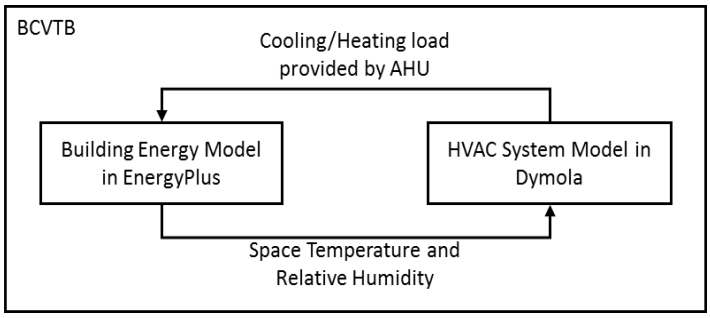

Figure 0.4 The configuration of the co-simulated model

Data is exchanged between the different clients using a fixed synchronization time step in BCVTB. There is no iteration between the clients. The algorithm for exchanging data between clients is as follows: Suppose we have a system with two clients, where each client solves an initial value ordinary differential equation that is coupled to the ordinary differential equation of the other client (Wetter & Nouidui, 2016). Let $N \in \mathbb{N}$ denote the total number of time steps and let $k \in \{0, \dots, N\}$ denote the time steps. For some $n_1, n_2 \in \mathbb{N}$, let f_1 and f_2 denote the functions that compute the next value of the state variables x in simulator 1 and 2. Note that these functions are defined by the sequence of code instructions executed in the respective simulator. The simulator 1 computes, for $k \in \{0, \dots, N-1\}$, the sequence

$$x_1(k+1) = f_1(x_1(k), x_2(k)),$$

and, similarly, the simulator 2 computes the sequence

$$x_2(k+1) = f_2(x_2(k), x_1(k)),$$

With initial condition $x_1(0) = x_{1,0}$ and $x_2(0) = x_{2,0}$. At $k = 0$, both simulators exchange their initial value $x_{1,0}$ and $x_{2,0}$. To advance from time k to k+1, each simulator

uses its own time integration algorithm. At the end of the time step, the simulator 1 sends the new state $x_1(k+1)$ to the BCVTB and it receives the state $x_2(k+1)$ from the BCVTB. The same procedure is done by the simulator 2. The BCVTB synchronizes the data in such a way that it does not matter which of the two simulators is called first.

The data exchange between the two simulators is analogous to an explicit Euler integration. Therefore, in the simulation where the differential equation is integrated over time using co-simulation the algorithm becomes:

Step 0:

Initialize counter k = 0 and number of steps $n \in \mathbb{N}$

Set initial states $x_1(k) = x_{1,0}$ and $x_2(k) = x_{2,0}$.

Set time step $\Delta t = 1/N$.

Step 1:

Compute new states

$x_1(k+1) = x_1(k) + f_1(x_1(k), x_2(k))\Delta t$, and

$x_2(k+1) = x_2(k) + f_2(x_2(k), x_1(k))\Delta t$.

Replace k by k+1.

Step 2:

If k=N stop, else go to Step 1.

This algorithm is implemented in the BCVTB. It does not require an iteration between the two simulators.

1.12 Set-up of the study

1.12.1 Scenario design

This study aims to quantify the model form uncertainty of the idealization of temperature controllability of the VAV system in multiple spaces introduced by EnergyPlus which is caused by the simplification of the linkage between building spatial configuration and HVAC system topology. The predicted space air temperature and its corresponding energy consumption are the targeted outcomes of the simulations for the purpose of assessing thermal comfort and system efficiency. Therefore, we choose the space air temperature, daily unmet hours as the outcomes to investigate the impact of the simplification on the thermal comfort. Hourly, daily and monthly aggregated cooling energy as well as fan power consumptions are the target outcomes to evaluate the impact of the model simplification on energy consumptions. As explained above, we postulate that the spatial configuration, HVAC layout, occupancy variability are the three major influences that play a role in the quantification. The first task of the study is to investigate if indeed the model simplification leads to discrepancies on the target outcomes. If so, the second task of the study is to characterize the discrepancies in terms of correlation with the leading parameters, i.e. alignment factor and occupant load diversity factor. The alignment factor (η) is developed to reflect the relationship between spatial configuration and HVAC layout. Occupant load spatial diversity factor (θ) is introduced to describe the occupancy variability in the sub-zone level spatial configuration. It is expected that these roles can be effectively captured in the additional parameter set (η, θ) that we introduced above. We assume that these two factors have a dominant correlation with the discrepancies, de facto leading to a dimensionality of two for the vector (η, θ).

The occupant load diversity factor is the indicator to describe the occupancy spatial variability which only considers the heat gains released by occupant as well as the lights

and equipment in the space. However, the thermal load of a service area not only depends on the internal load released by the occupant, lights, and the equipment, but also includes the heat gains through the space boundaries, such as the heat convection from internal building surfaces, solar radiation, and air infiltration. Therefore, we develop three typical spatial configurations of VAV terminal service areas to reflect different situations with different convective loads and solar heat gains. The first configuration is an perimeter zone with only one external façade (Figure 0.5.a); the second configuration is an perimeter zone with two external façades (Figure 0.5.b); and the third spatial configuration is an core zone with no external façade (Figure 0.5.c).The area labeled with blue in the Figure 0.5 is the target area where we conduct our studies.

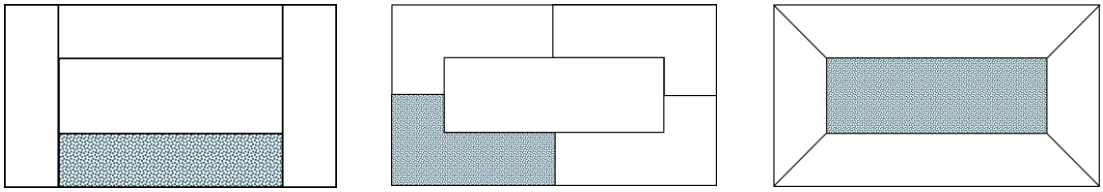

a b c

Figure 0.5 Three typical situations for building zones used in this study

For each zone, a variety of spatial DCA-ICA configurations are considered. A spatial configuration is characterized by an alignment factor to define the relative area of DCA versus ICA which reflects the mismatch between the spatial configuration and HVAC topology. Two low-fidelity EnergyPlus models and one high-fidelity co-simulation models are developed for each configuration. The outcomes of the models are compared to quantify discrepancies in selected outcome quantities.

The base case for the study is the three-story new construction medium office building from the DOE reference building pool (Deru, et al., 2011) .We use the second floor, which consists of a core zone and four perimeter zones, as the target area to conduct this study. The entire space on the second floor is served by a VAV system with five terminal boxes. The spatial configuration of the VAV is selected from the three typical configurations shown in Figure 0.5. Different layouts of the VAV terminal box system are selected to reflect different values of the alignment factor. We choose layouts that correspond to alignment factors 1/5, 2/5, 3/5, 4/5, and 1. The partition between the DCA and ICA is assumed as the perpendicular wall to the external façade. Take the spatial configuration in Figure 0.5.a as an example, the configuration of the DCA and ICA is shown in Figure 0.6.

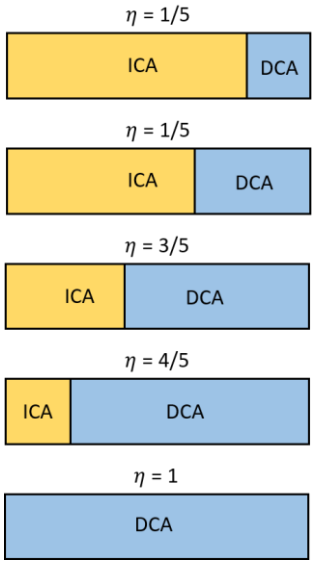

Figure 0.6 Schematic diagram of the configuration of DCA and ICA

As well as considering the impact of heat gain from the outdoor environment, we also investigate the influence on the simulation outcomes if multiple building functions are

applied in the same service area. In our study, we put meeting room as the second building function into our investigation. As the configuration shown in Figure 0.6, we will assign the ICA as the meeting rooms instead of the office area. The occupant presence profile for the meeting rooms is generated by Occupant Simulator and the lighting/plug use profile will be generated based on the occupant profile. We consider four cases with the alignment factor as 1/5, 2/5, 3/5, and 4/5 to represent the different layouts between the office area and the meeting area.

1.12.2 Workflow of study

For each case (identified by a distinct spatial configuration, value of the alignment factor, and building functions), the overall process of the study is done in three phases: case preparation, modeling and simulation, and uncertainty quantification.

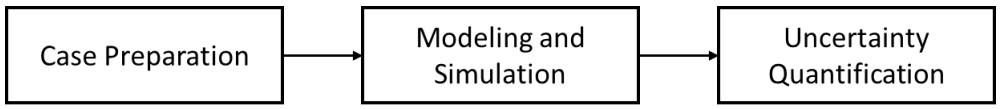

1.12.2.1 Case preparation

The case preparation phase involves the following: (1) select a spatial configuration (DCA and the ICA); (2) determine the equipment size of the VAV system; (3) develop stochastic occupant profiles for the DCA and ICA and calculate the corresponding occupant load diversity factor. The procedure of the data processing phase is shown in Figure 0.7. The blue blocks represent the input information. The yellow blocks identify the resulting case identifiers.

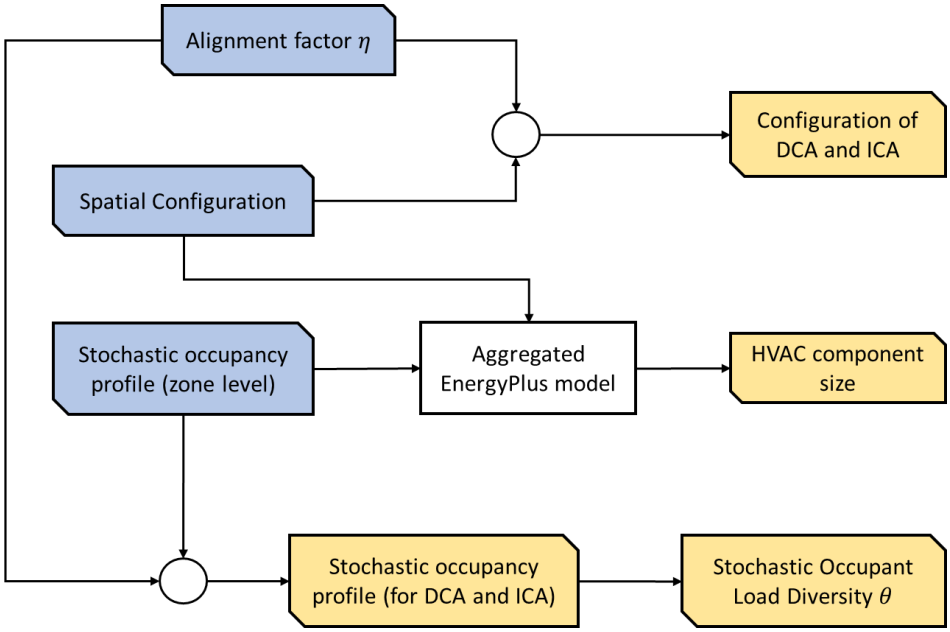

Figure 0.7 The procedure of the case preparation

The target service area of the VAV terminal box is selected from the three predetermined spatial configurations. The overall service area is divided into DCA and ICA to reflect a chosen alignment factor. If the alignment factor equals to 1/5, which means the area of the DCA is 1/5 of the overall service area.

As stated before, we utilize the auto-sizing outcomes from the aggregated-zone EnergyPlus model to assign the equipment size in the Modelica model. The aggregated-zone EnergyPlus model includes the construction information with the floor area divided into five zones without considering the difference between the DCA and the ICA. The equipment size defines the capacity of the HVAC component, such as the maximum flowrate of the VAV terminal box, which is not affected by the segmentation of the zone. Nevertheless, the distribution of the supply air flow from a HVAC component is indeed

affected by the segmentation of the DCA and the ICA. We assume the airflow is evenly distributed over the area of the space linking the space area and air flowrate.

For a predetermined alignment factor η, the stochastic occupancy profile (including occupants, lighting, and appliances) for the entire service area is generated by using Occupant Simulator with the measurement data of a Georgia Tech campus building (Wang Q. , 2016). The sub-zone level occupancy profiles are generated according to the zone level information by using the stochastic method introduced in Chapter 2.4. The hourly occupant load diversity factor is calculated based on the sub-zone level occupancy profile.

1.12.2.2 Modeling and simulation

In the modeling and simulation step, the simulation models are developed with the procedures shown in Figure 0.8. The first model is the aggregated-zone EnergyPlus model which we already developed for the component size estimation. The second model is the sub-zone EnergyPlus model. The difference between the first and the second models is the configuration of service area and its corresponding occupancy profiles. The sub-zone EnergyPlus model divides the service area into two zones based on the spatial configuration of the DCA and the ICA. The occupancy profile of the DCA and the ICA will be input separately based on the stochastic occupancy profiles generated in the case preparation phase. The last model is the co-simulation model which integrates an EnergyPlus building model and a Modelica HVAC model on the BCVTB platform.

In the co-simulation model, the HVAC system is removed from the EnergyPlus model and the cooling/heating energy delivered from the HVAC system is assigned as an external input that is imported from the Modelica module at every time step. The space air

temperature and relative humidity are exported from the building module to the Modelica HVAC model at every time step as well.

The VAV system is fully specified and developed in the Modelica model, which comprises of one AHU with five VAV terminal boxes. Both DCA and ICA are served by the same VAV terminal box and only the space air temperature in DCA is the control variable of the VAV terminal box. The VAV terminal box modulates its operating status to maintain the monitored space air temperature. The size of each VAV is determined based on the auto-sizing result from the aggregated EnergyPlus model (the first model).

The output from the three models includes: the hourly space air temperature of the DCA and the ICA, the cooling energy of the VAV box and the fan power consumption in hourly, daily, and monthly interval. Since the aggregated-zone EnergyPlus model generates a mean air temperature to represent the space condition in the DCA and the ICA with no distinction, the unmet hours of the aggregated-zone EnergyPlus model is based on the virtual mean air temperature for the zone level instead of generating the unmet hour for the sub-zone level respectively.

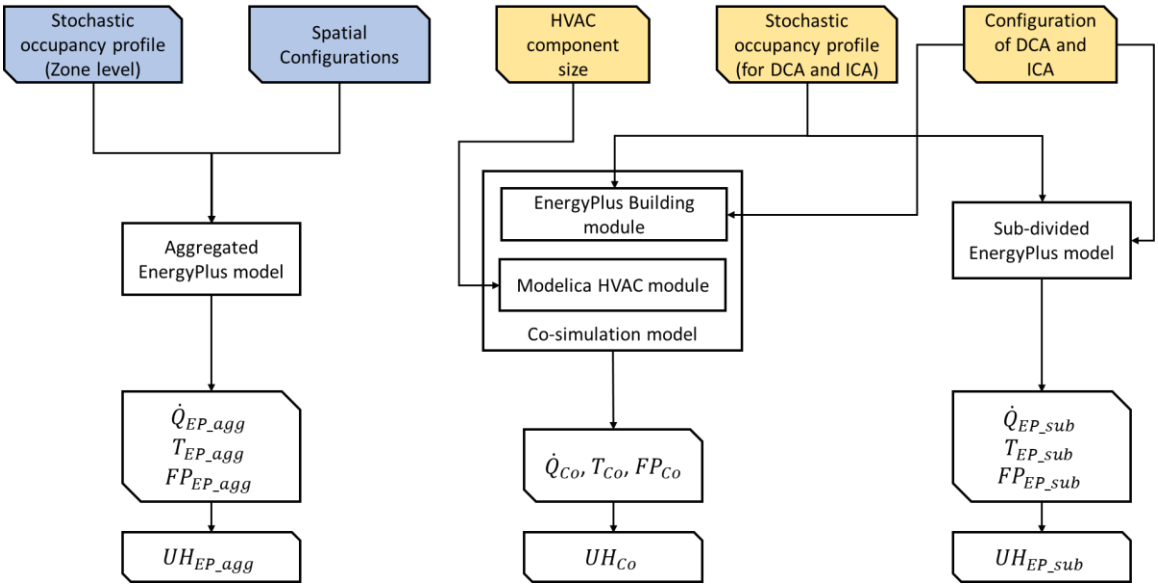

Figure 0.8 The procedure of the modeling and simulation phase

1.12.2.3 Uncertainty quantification

The third phase of the study is the uncertainty quantification. It uses the outcomes of the co-simulation model as reference, revealing the discrepancies of selected outcomes with the two EnergyPlus models. The next step is to characterize the discrepancies in the form of differences for each mentioned outcome, i.e. quantity of interest (QoI) in terms of alignment factor η and occupant load diversity factor θ. The procedure of the uncertainty quantification is shown in Figure 0.9.

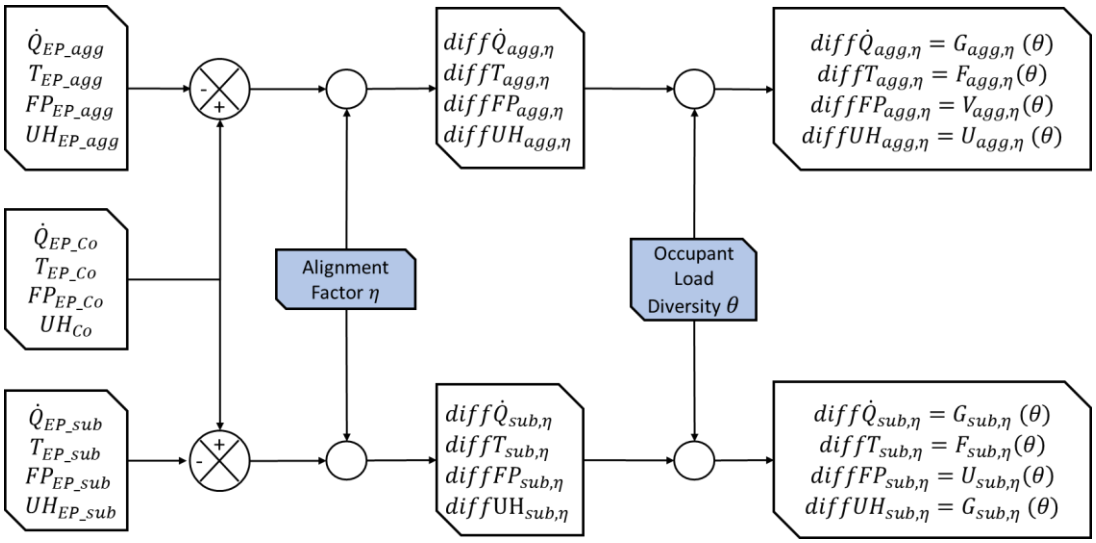

Figure 0.9 The procedure of the uncertainty quantification

PRELIMINARY STUDY

The premise of this thesis is that EnergyPlus has insufficient capability to reflect the complexity between the building physical partition layout and the HVAC system topology at the sub-zone level. Therefore, as explained before the goal is to quantify the uncertainty in simulation outcomes that is introduced by the inadequacy of EnergyPlus. As stated, we use a high-fidelity model, which is able to capture physical behaviors neglected in the EnergyPlus model and apply that to a (large) set of cases with different spatial-HVAC layouts and occupancy load diversity. In this chapter a preliminary study is performed to verify the suitability of the proposed approach and test the feasibility to perform this on a set of cases. The is not trivial as the development of the high-fidelity model is time consuming which may limit the set of cases that can be studied in this thesis. Limiting the set of cases will obviously make the outcome of the UQ exercise less generic and thus limit its applicability.

We assume that discrepancies between the low and high fidelity models has strong correlation with the misalignment between the topology of HVAC space temperature controllability and the physical building partition layouts. The occupancy variation between the directly controlled area and the indirectly controlled area is a second major influence as this will exacerbate the discrepancies that result from misalignment.

Therefore, there are two tasks for the preliminary study. The first task is to demonstrate the low and high fidelity models are comparable. Two models with different fidelity levels are expected to provide similar outcomes if there is no misalignment between the HVAC topology and the building partition layout. If the models are proven to be

comparable, the second task in the preliminary study is to investigate that if the co-simulation system can reveal the discrepancies in the predicted space condition, supply air flow and delivered heating/cooling energy caused by the misalignment. Additionally, we will also attempt to evaluate if how discrepancies are magnified by an increase of the occupant load diversity. A baseline case (section 4.1) is conducted to investigate task one, whereas a second case (section 4.2) is developed to investigate task two.

1.13 Baseline case

The major difference between the low-fidelity EnergyPlus model and the high-fidelity co-simulation model is the way the HVAC system, and in particular its control is represented. In the EnergyPlus model, the HVAC system is an abstract system which is controlled based on the thermal load. In the co-simulation case, the components of the HVAC system are fully developed in Modelica and the system is modulated according to the space air temperature centered control logic. The purpose of the baseline case is to investigate whether the low and high fidelity models provide close enough outcomes in buildings without misalignment. If the models can maintain space air temperature within a narrow margin, and with similar supply air flowrate, we conclude that both representations of the HVAC system and its corresponding control logics form a strong basis to conduct the further analysis.

The baseline building is a three-story office building in Atlanta based on the new construction medium office building from the DOE reference building pool (Deru & etc. (2011)). We take the second floor as the case study which consists of four perimeter zones and a core zone, as shows in Figure 0.1. The gross floor area of the second floor is 900 m^2

with dimensions of $\mathrm{L} \times \mathrm{W} \times \mathrm{H} = 30\mathrm{m} \times 30\mathrm{m} \times 3\mathrm{m}$. the window to wall ratio on each exterior wall is 0.4. With a width of 5 meters, the size of each perimeter zone is $25\mathrm{m} \times 5\mathrm{m} = 125m^2$ and the size of the core zone is $20\mathrm{m} \times 20\mathrm{m} = 400m^2$. The south perimeter zone is the area of interest which is assumed as an open space with a uniform space air condition which can be measured by the thermostat. All the area in the south perimeter zone is the directly controlled area. In that case, the alignment factor (η) of the area equals to one and the occupancy usage is represented by an aggregated occupant load profile with uniform spatial distribution of load release. We use the occupancy usage profile as specified by ASHRAE and as used in the DOE medium office reference building.

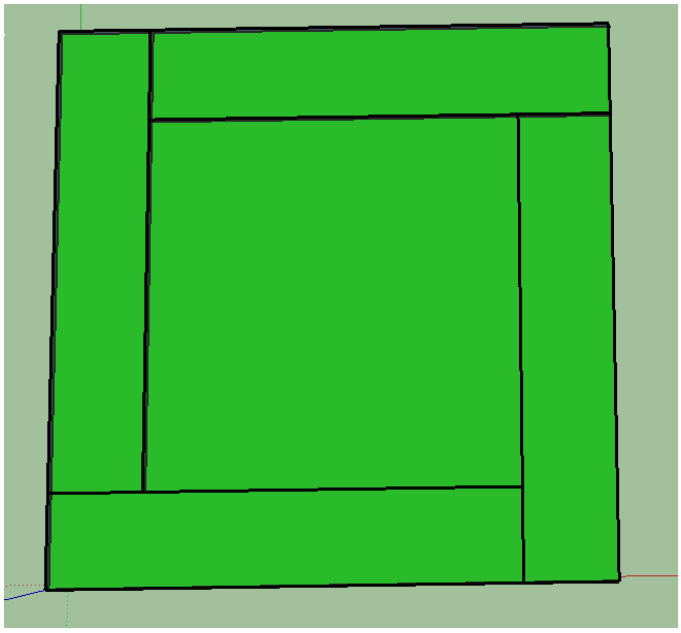

Figure 0.1 The floor plan on the 2nd floor in the building used for the baseline case study

In the low-fidelity model, the second floor is served by an AHU system with five VAV terminal boxes, each one serving a single zone. The operating period of the HVAC system is from 7 am to 10 pm with a cooling setpoint at 24 ℃.

For the high-fidelity model, the HVAC system is developed in Modelica. The components in the VAV system are developed based on the VAV with reheat system components in the Modelica Buildings library version 5.1.0. The VAV system consists of an economizer, a heating coil, a cooling coil, and a supply fan in the air handler unit. There is also a reheat coil and an air damper in each of the five zone inlet branches. The minimum flowrate of each VAV box is 25% of the design flowrate. A schematic drawing of the system is shown in Figure 0.2

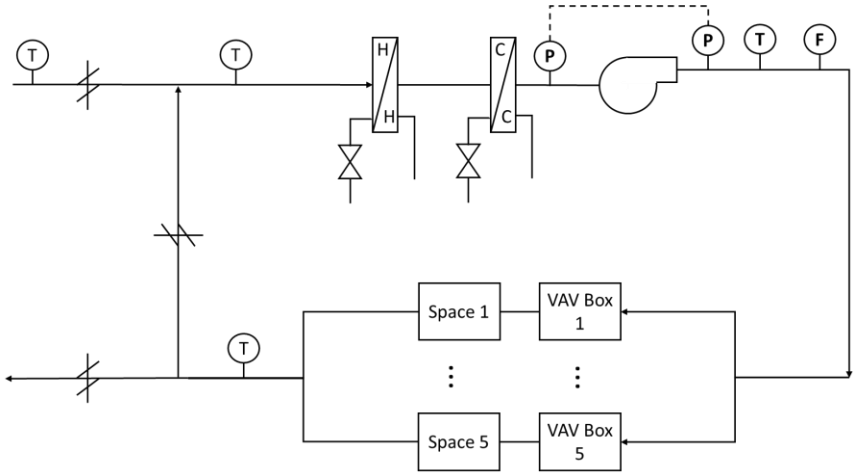

Figure 0.2 Schematic drawing of the AHU system

The control is an implementation of the control sequence VAV 2A2-21232 of the Sequences of Operation for Common HVAC Systems (ASHRAE, 2006). In this control sequence, the supply fan speed is regulated based on the duct static pressure. The duct static pressure is adjusted so that at least one VAV damper is 90% open. The economizer dampers are modulated to track the setpoint for the mixed air dry-bulb temperature. Priority is given to maintain a minimum outside air volume flow rate. In each zone, the VAV damper is adjusted to meet the room temperature setpoint for cooling, or fully opened during heating. The room temperature setpoint for heating is tracked by varying the water flow rate through

the reheat coil. There is also a finite state machine that transitions the mode of operation of the HVAC system between the modes occupied, unoccupied off, unoccupied night set back, unoccupied warm-up and unoccupied pre-cool. In the VAV model, all air flows are computed based on the duct static pressure distribution and the performance curves of the fans. Local loop control is implemented using proportional and proportional-integral controllers, while the supervisory control is implemented using a finite state machine.

Figure 0.3 and Figure 0.4 show the overall Modelica VAV system model and a partial enlargement for the zone inlet branches.

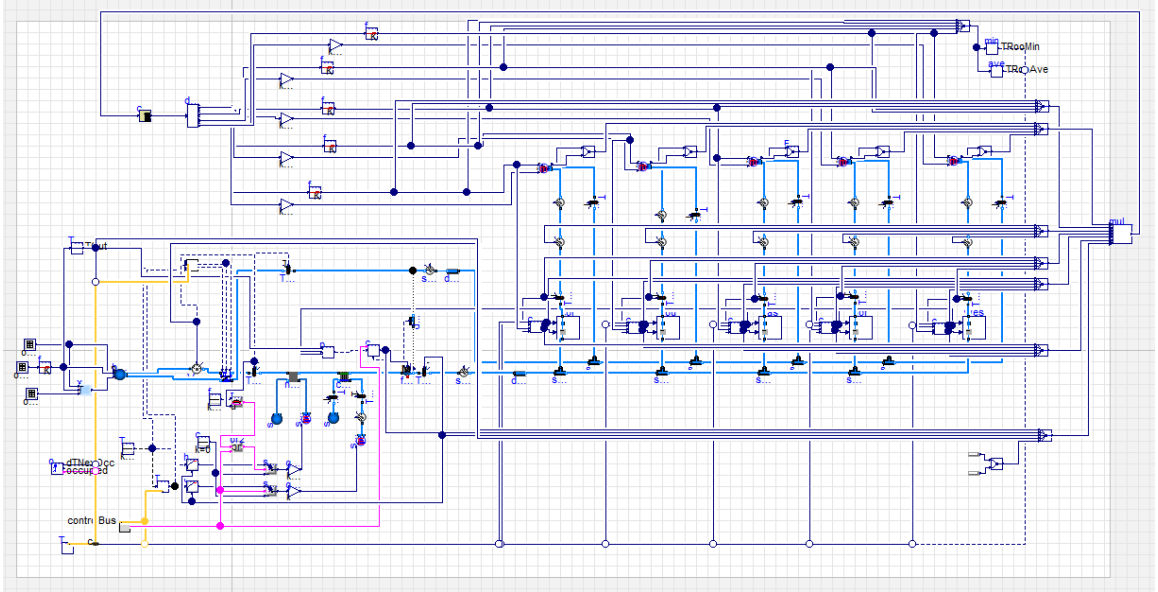

Figure 0.3 The diagram of the overall Modelica VAV system model

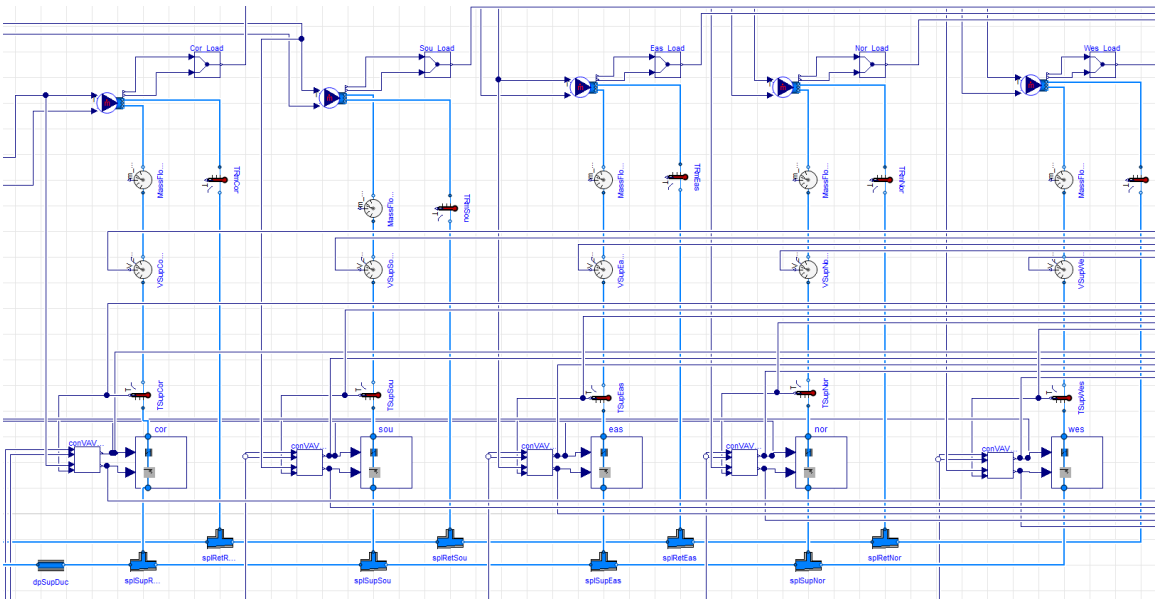

Figure 0.4 Zone inlet branches

The size of the VAV terminal boxes in the Modelica model is based on the auto sizing results of the low fidelity EnergyPlus model since Modelica has no function to estimate the size of component. Table 0.1 shows the design flowrate of each VAV terminal box.

Table 0.1 The auto sizing result of each VAV terminal box

	Core	South	East	North	West
Design Size Maximum Air Flow Rate [m3/s]	1.04	0.42	0.577	0.389	0.614

We take the design supply airflows for each zone from the EnergyPlus sizing results as the input parameters in the Modelica VAV system model. By using the 2017 TMY weather file of Atlanta, we conduct the simulation for the EnergyPlus model and the co-simulation model for part of the cooling season, from 6/24 to 7/31.

The comparison of the simulation results is shown in Figure 0.5, the space air temperature of the south perimeter zone generated by the EnergyPlus and co-simulation

model follow the same trend. The differences between the two results is that the space air temperature estimated by the co-simulation model fluctuates around the cooling setpoint which is mainly because the Modelica model introduces the characteristics of the actual system components with imperfect control. The Normalized Mean Bias ($NMB = \frac{\sum_1^n (M-O)}{\sum_1^n O}$) of the EnergyPlus model is only -0.12% if we regard the co-simulation results as the high-fidelity baseline with zero error.

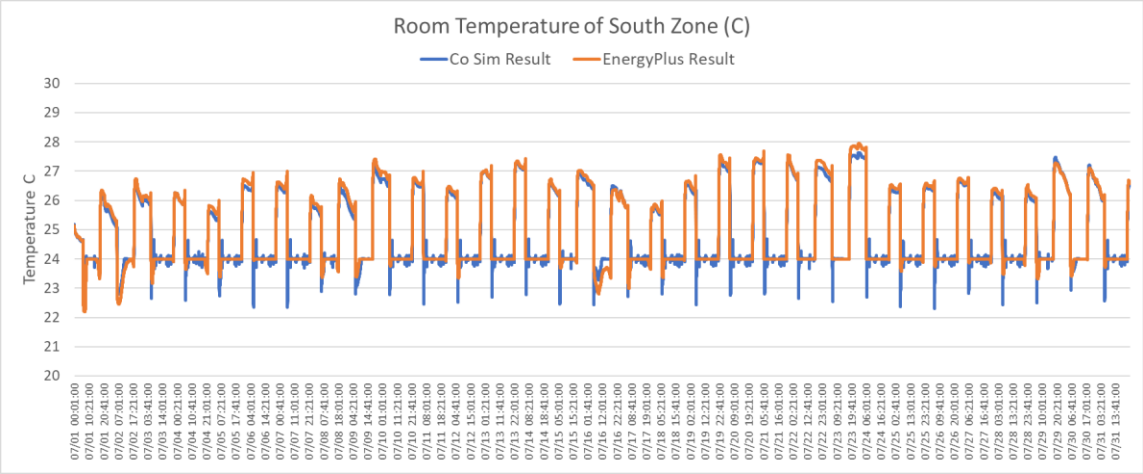

Figure 0.5 Comparison of space air temperature of south perimeter zone in July for baseline case ($\boldsymbol{\eta = 1}$)

Figure 0.6 shows the comparison of supply air flowrate for the south perimeter zone. We can see both the EnergyPlus model and the co-simulation model capture similar variability of the supply air flowrate. The differences are small; the normalized mean bias of EnergyPlus is 5.39%.

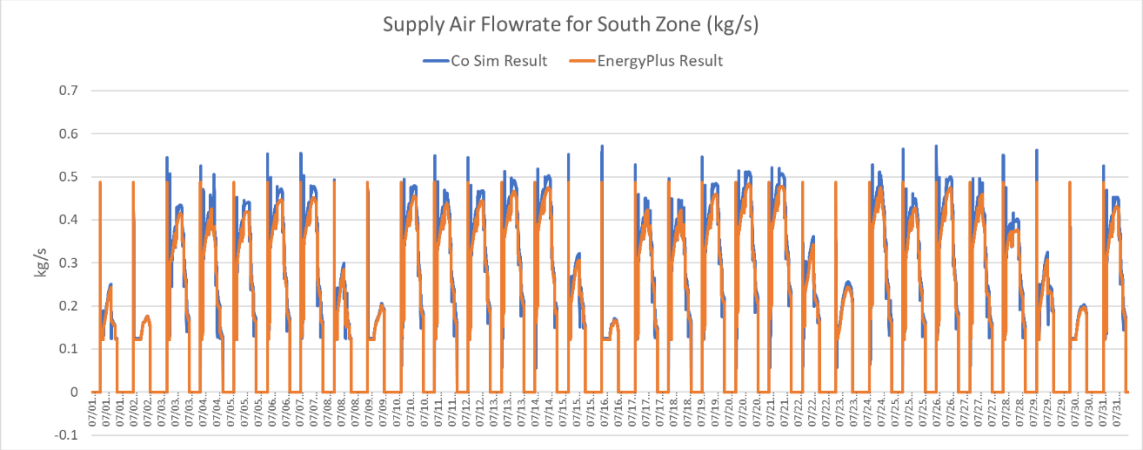

Figure 0.6 Comparison of supply air flowrate for the south perimeter zone in July for baseline case ($\boldsymbol{\eta = 1}$)

The results of the baseline case show that, even in the case of full alignment, there is a difference between the outcomes of the low and high fidelity models. It is to be expected that this discrepancy is influenced by the specific case selection. But the result is good enough to prove that the low-fidelity EnergyPlus model with idealized HVAC control logics is a close approximation of the high-fidelity outcomes when no misalignment is present in the building.

1.14 Case with 1/5 misalignment

1.14.1 Model description

To evaluate whether the methodology and approach are valid to investigate the impact of misalignment and usage variability, we conduct a preliminary study with an alignment factor $\eta = 1/5$. We use the same building floor plan as in the baseline case and the south perimeter zone on the second floor is again the area of interest. We divide the south perimeter zone into two parts, one part is the directly controlled area (DCA) and the other part is the indirectly controlled area (ICA). Based on the definition of the alignment

factor, the area of DCA is 1/5 of the overall area of the south perimeter zone, and the area of the ICA is 4/5 of the total area of the south perimeter zone. The floor plan is shown in Figure 0.7.

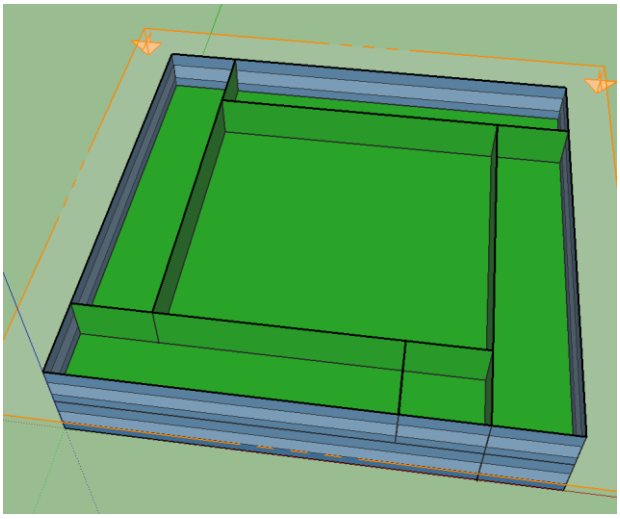

Figure 0.7 The floor plan of the preliminary study, alignment $\boldsymbol{\eta = 1/5}$

Since the south perimeter zone is divided into the DCA and the ICA, the second floor is now composed of six thermal zones in the building model. To serve the overall south perimeter zone with two thermal zones, we develop two virtual VAV terminal boxes to serve the DCA and ICA independently, instead of use a single VAV terminal box, in the sub-divided zone EnergyPlus model. For the high-fidelity model, the main modification in the Modelica HVAC module occurs in the south zone inlet branch (Figure 0.8). The supply air is bifurcated into two sub-branches by the splitter after passing through the VAV terminal box. One sub-branch delivers the supply air into the DCA and the other sub-branch sends the supply air into the ICA. The design flowrates of the air streams are established based on the alignment factor $\eta = 1/5$ since we assume the air flow is supplied in an "area average distributed" way into the space. The space air temperature of DCA is measured by a thermostat and sent back to the controller of VAV terminal box. The VAV terminal box

modifies its operating condition based on the measured condition to maintain the space temperature at the setpoint in the DCA. The ICA is conditioned by the VAV terminal box without space air temperature feedback.

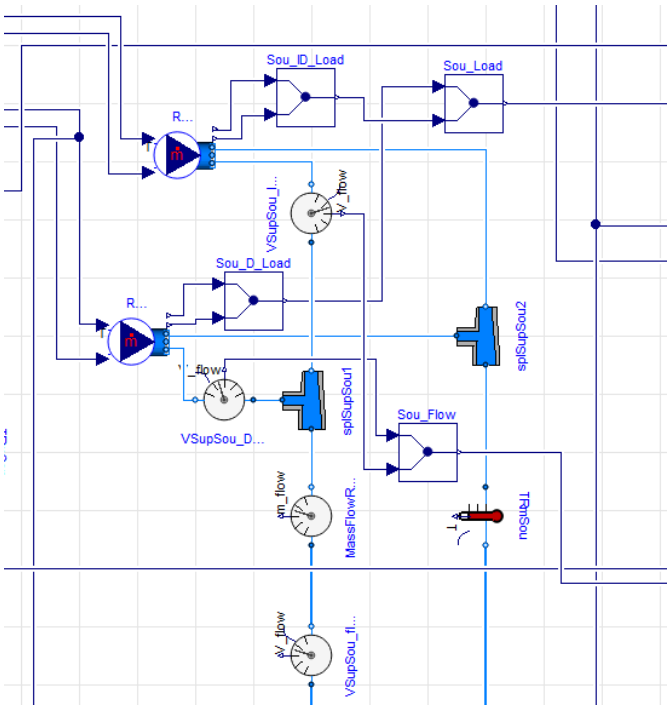

Figure 0.8 The south zone inlet branch

The occupancy load profile in EnergyPlus includes the information of load density and schedule for occupant, lights and plug load, per thermal zone. In the baseline case, we provide the zone level occupant load profile by using the ASHRAE occupancy load profile as mentioned above. With the zone level occupancy load, we neglect the diversity of load release in the sub-zone level. In this preliminary study, we generate four occupant load diversity levels: no diversity, low diversity, medium diversity, and high diversity. They are used to evaluate the impact of occupant load diversity in the sub-zone level. The definition of the four diversity levels are shown in Table 0.2. For each occupant load diversity

scenario, we run the simulation from 6/24 to 7/31. It has 26 weekdays during that simulation period, which include 390 occupied hour data points for each diversity scenario.

Table 0.2 The definition of occupant load diversity level

Occupant load diversity level	Definition
No diversity	$\theta = 0$
Low diversity	$\lvert\theta\rvert \leq 0.3$
Medium diversity	$0.3 < \lvert\theta\rvert \leq 0.6$
High diversity	$\lvert\theta\rvert > 0.6$

The purpose of the preliminary study is to investigate whether and how the occupant load diversity affects the outcomes of models. Therefore, we introduce four diversity levels to conduct a parametric study. For each diversity level, we randomly select one value (from the available range) as the daily diversity factor and assume it remains constant for every hour in that day. Then, the occupancy usage schedule for the DCA and the ICA can be generated by using the selected diversity factor based on the zone level information. Taking the occupant schedule as an illustration, Figure 0.9 to Figure 0.11 show the occupant schedules in an arbitrary week for DCA (blue line) and ICA (red line) with low diversity, medium diversity and high diversity. Comparing to the diversity factor profile we generate in Chapter 2.4, the daily based sampling method we used in the preliminary study may overestimate the impact of the diversity in the daily interval, which may lead to a strong correlation between the quantity of interest and the daily diversity factor.

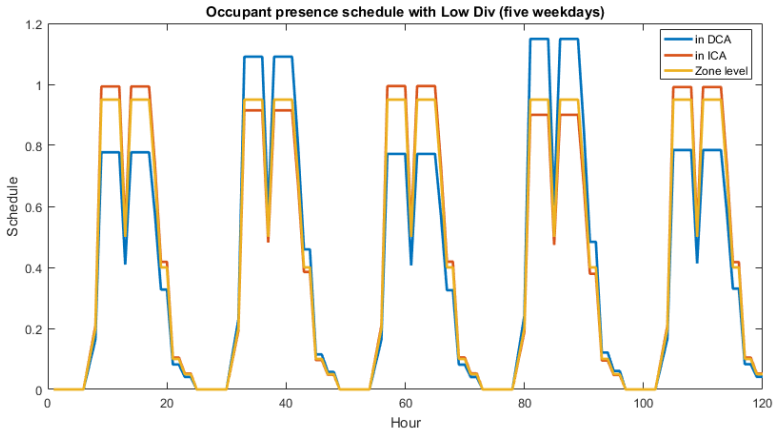

Figure 0.9 The weekday occupant schedules at different scale with low diversity level

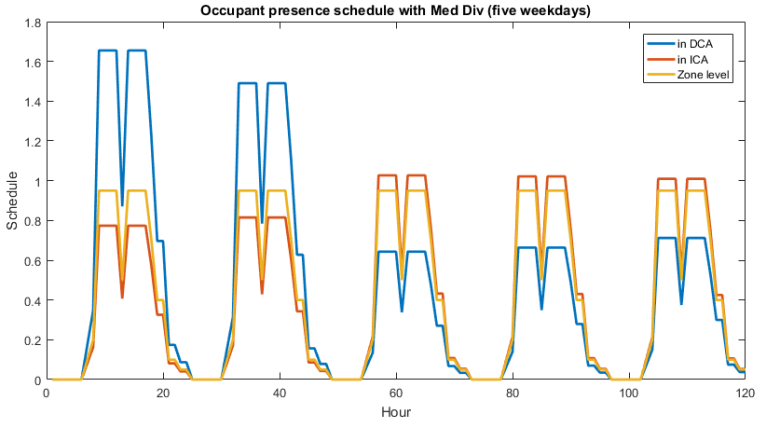

Figure 0.10 The weekday occupant schedules at different scale with medium diversity level

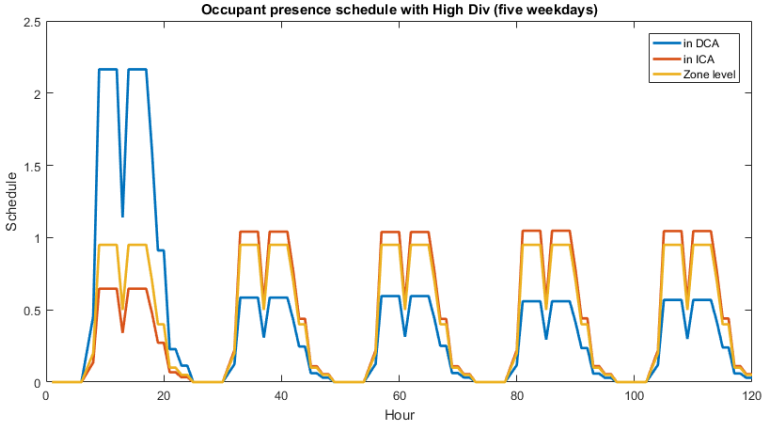

Figure 0.11 The weekday occupant schedules at different scale with high diversity level

If we integrate the schedule information of the DCA and the ICA, the zone level information is calculated which is indicated by the yellow line. Based on the result, we can see that the schedule value in the sub-zone level can be larger than one, which represents the number of occupants in that area is more than the design value. This reflects what happens in real life. It is common that small group meetings or short meetings are held in the manager's office instead of the meeting room. The number of occupants in the manager's office will be larger than the design value during that period.

Now we have three models to compare: (1) a five-zone EnergyPlus model aggregating the two spaces (DCA and ICA) as one thermal zone; (2) a six-zone EnergyPlus model (setting the DCA and the ICA as separate thermal zones); and (3) the six-zone co-simulation model. We refer to them as Model-1, Model-2 and Model-3. Model-1 neglects the sub-divided room in the zone and consequently ignores the diversity of the occupant loads in the sub-zone level. Model-2 distinguishes the ICA from the DCA as the independent zone and puts the occupant load diversity in the sub-zone level into the consideration. However, it creates two instead of one VAV terminal box to serve the overall south perimeter area, which provides a deceptive functionality to maintain the two rooms independently which violates reality. Model-3 not only considers the occupant load diversity in the different spaces but also reflects the actual VAV system with one terminal box serving the two areas. Recall that since Model-3 is able to capture physical behaviors neglected in Model-1 and Model-2, we regard it as the high-fidelity reference model.

1.14.2 Impact of misalignment between building partition and HVAC topology

To analyze the impact of misalignment between spatial partitions and HVAC supply topology, we compare the simulation outcomes between Model-1 and Model-3 as well as the outcomes between Model-2 and Model-3 without the occupant load diversity. Figure 0.12 shows the comparison result on space air temperature in DCA and ICA during weekdays. The boxplot results are generated by taking hourly values for all simulated weekdays in the period from 6/24 to 7/31.

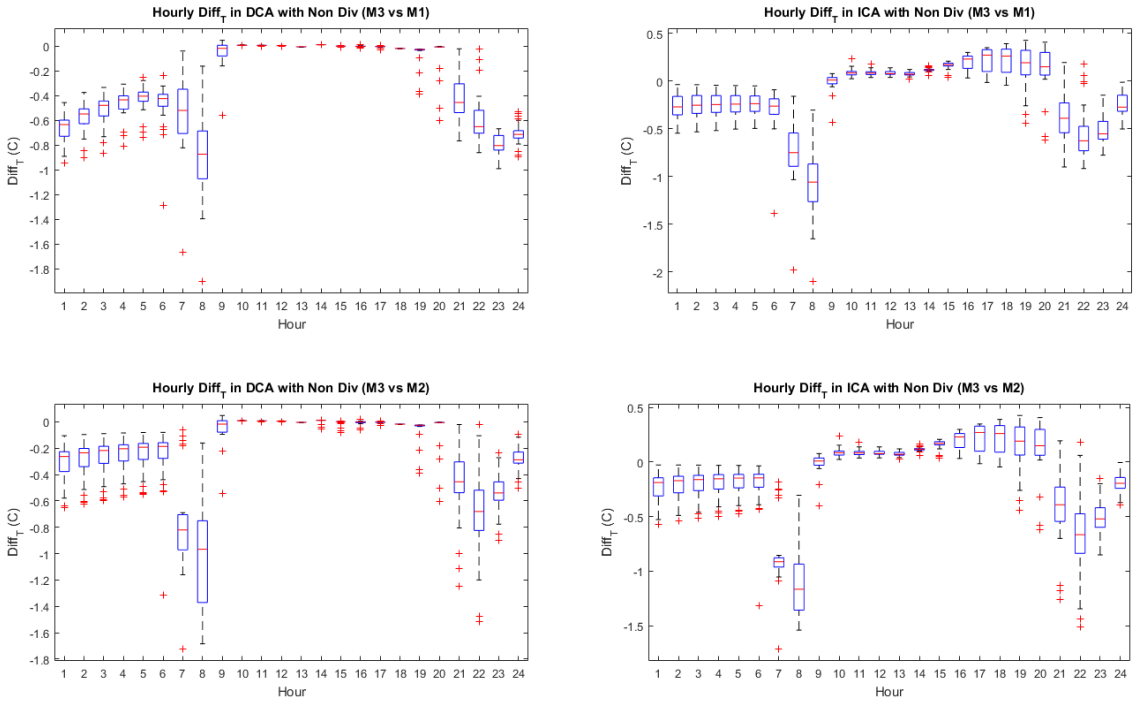

Figure 0.12 Hourly **Diff$_T$** during weekday with no occupant load diversity

Model-1 only estimates a zone mean temperature for the overall space. In the comparison, both the space air temperature of DCA and ICA estimated by Model-1 are represented by this zone mean temperature. Based on Figure 0.12.a and Figure 0.12.c, we conclude that the space air temperature of DCA can be well maintained and the Diff$_T$ between Model-1/2 and Model-3 are small during the occupied hours except the first two hours. The latter is due to the implemented actual, and hence imperfect control in Model-

3. Differences occur mainly in the space air temperature of ICA according to Figure 0.12.b and Figure 0.12.d, the predicted space air temperature of ICA by Model-1/2 deviate from the result of Model-3, especially during the afternoon. In the chosen case, the DCA is only affected by the south façade while both south and west façade affect the ICA. In the afternoon, the heat gain from the west façade becomes more significant than that in the morning which makes the difference between the thermal load in ICA and DCA more noticeable. Since the VAV terminal box in model-3 is "blindly" delivering cooling to the ICA, the space air temperature of ICA cannot be well maintained at the setpoint.

The results indicate that: (1) misalignment between the building space partition and HVAC topology affects the simulation outcomes; (2) the spatial configuration of perimeter zones may affect the simulation outcomes due to effects stemming from facade orientation.

1.14.3 Impact of occupant load diversity

Based on the four occupancy load profiles (reflecting the different diversity levels), we compare the results of Model-2 and Model-3. Model-1 keeps using the same zone level occupancy load profile but obviously without considering the spatial occupant load diversity.

1.14.3.1 Space air temperature

Figure 0.13 to Figure 0.16 show the comparison of the simulated space air temperature with different occupant load diversity scenarios during the weekdays from 7/3 to 7/7 (Monday to Friday, considering 7/4 as a normal working day).

When occupant load in the DCA and ICA have no diversity, both model-1 and model-2 maintain the space air temperature well at the setpoint. Model-3 outcomes show that the space air temperature in both DCA and ICA are basically maintained at the setpoint although the air temperature in ICA has some minor fluctuation in the afternoon which is affected by the heat gain from the west façade.

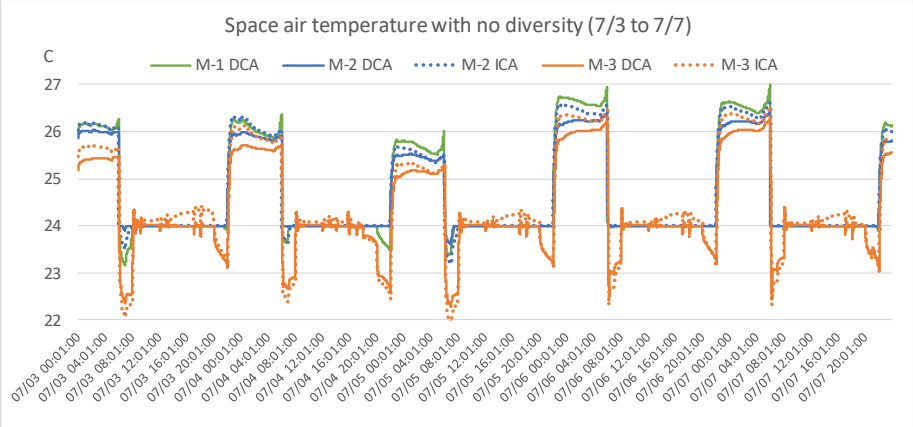

Figure 0.13 The comparison of space air temperature with no occupant load diversity

When we introduce low occupant load diversity into the models, the outcomes of Model-1/2 keep showing well-maintained space air temperature around the setpoint. However, the outcomes of Model-3 show the space air temperature of ICA cannot be kept at the setpoint while the space air temperature of DCA is well-maintained at the setpoint. When the occupant load per area in DCA is smaller than that in ICA, the space air temperature of ICA is higher than the setpoint. Otherwise the space air temperature of ICA is lower than the setpoint. This is in line with our expectation.

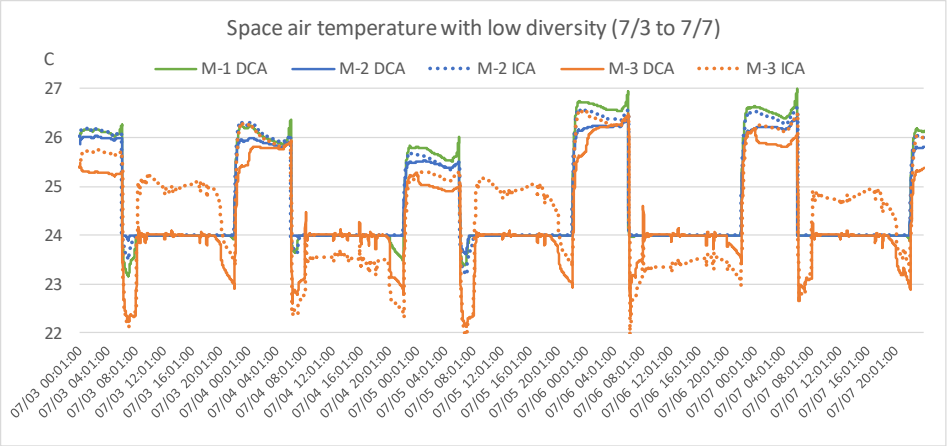

Figure 0.14 The comparison of space air temperature with low occupant load diversity

If we increase the occupant load diversity to the medium level, the simulation results from Model-1 show no significant changes. The space air temperature predicted by Model-2 are well maintained in most of the occupied period while overcooling more often occurs because of the minimum supply air flow setpoint. The results of Model-3 show that the air temperature of DCA is basically well maintained at the setpoint while the temperature of ICA has a larger deviation than that in the low load diversity scenario.

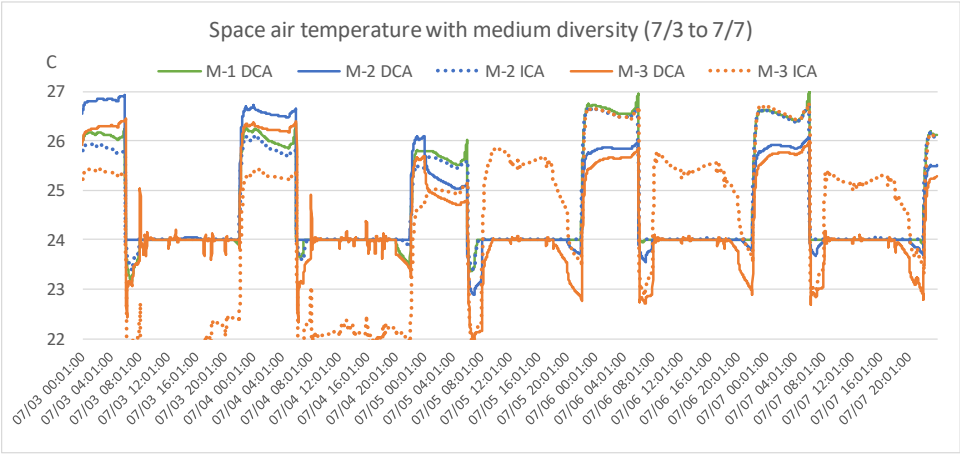

Figure 0.15 The comparison of space air temperature with medium occupant usage diversity

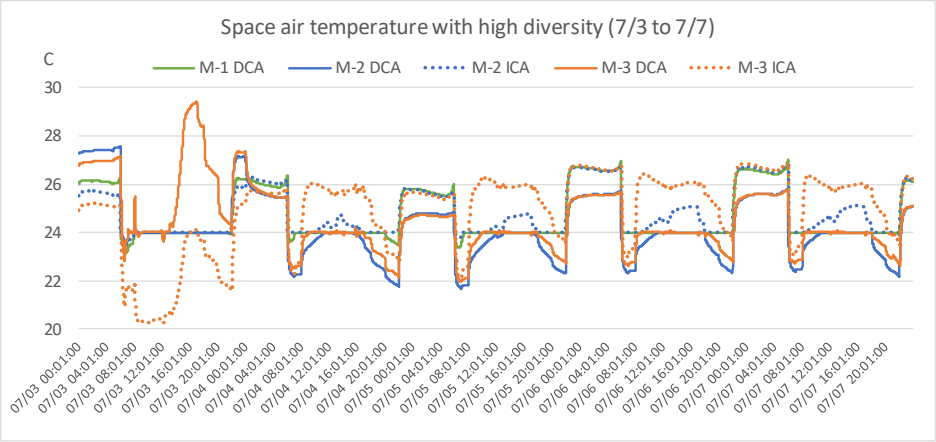

Figure 0.16 The comparison of space air temperature with high occupant usage diversity

With high occupant load diversity, the thermal load characteristics in the two areas (the DCA and the ICA) become more diverse without impacting the zone level occupant load profile. Model-1 hence shows no impact with remaining well-maintained space air temperature shown in Figure 0.16. Nevertheless, the space air temperature outcome from Model-2 is not maintained at the setpoint in some situations. This is because the supply air hits its minimum or maximum flowrate boundary when the space encounters extreme load conditions, the delivered cooling is unmatched to the thermal load during that periods. The outcomes of Model-3 show that overcooling is aggravated in the DCA from 7/4 to 7/7. Figure 0.17 displays that the VAV damper stays at the minimum opening position in the morning and afternoon without any more margin to close, and the space is overcooled during that period. Meanwhile, the ICA is in fact undercooled from 7/4 to 7/7 and the magnitude of the temperature downdrift in high diversity scenario becomes larger compared to the drift in the medium diversity scenario.

The simulation results from Model-3 show a special phenomenon on 7/3. Both DCA and ICA are undercooled, and the space temperature has dramatic fluctuations in a

short period. Figure 0.18 shows the space air temperature, supply air damper position, and the supply air flowrate on 7/3 of the outcomes from Model-3. We see that the supply air flowrate drops, nevertheless the supply air damper keeps fully open when the space air temperature increase. That is because the speed of the supply fan decreases after the damper position exceeds 90% opening ratio. According to the control sequence, the supply fan speed is regulated based on the duct static pressure. The duct static pressure is adjusted to maintain at least one VAV damper is 90% open. Figure 0.19 shows the trend of VAV damper position and the speed of supply fan. In this case, the VAV system and the corresponding control sequences experience a failure and the space condition ends up out of control.

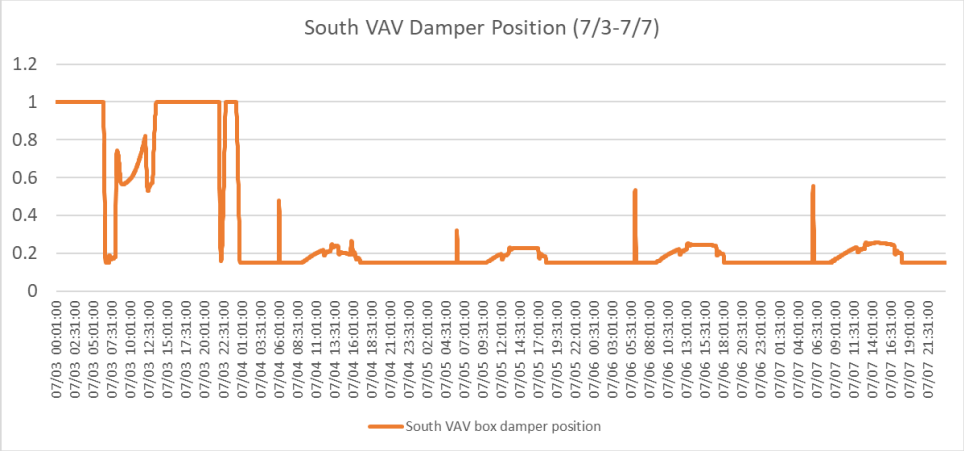

Figure 0.17 The damper position of the south VAV terminal box

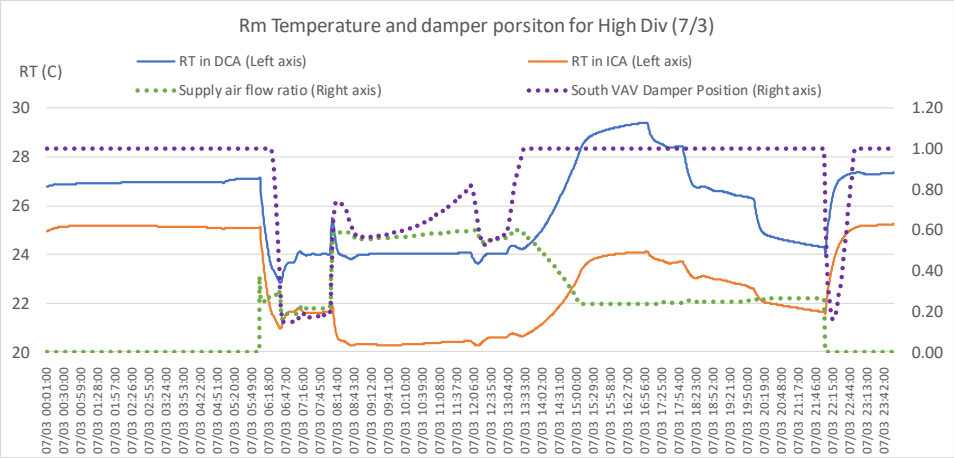

Figure 0.18 Space conditions and system operation status of the south VAV terminal box

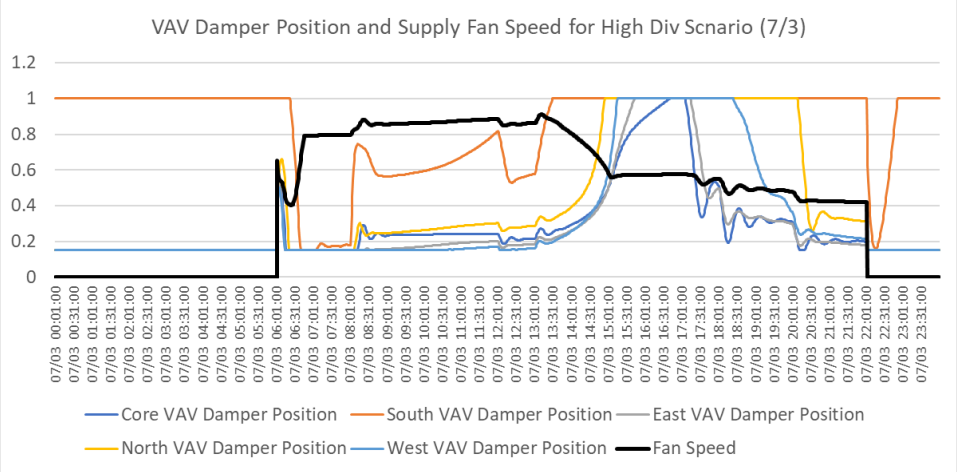

Figure 0.19 The trend of VAV damper position and supply fan speed

Model-3 outcomes show that increasing the load diversity leads to a larger deviation in space air temperatures between DCA and ICA. Figure 0.20 shows the discrepancies in space air temperature between the DCA and the ICA predicted by Model-3 under different occupant load diversity scenarios with an alignment factor of 1/5. As explained, Model-1 and Model-2 are not able to capture this phenomenon.

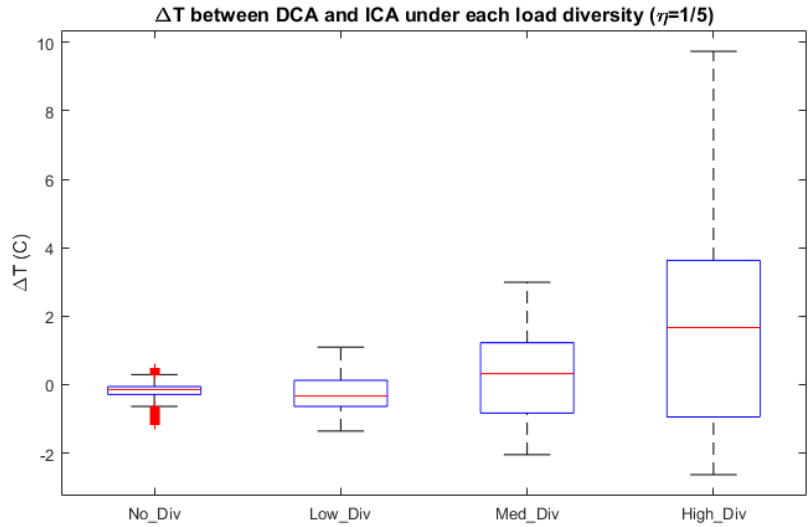

Figure 0.20 **ΔT** between DCA and ICA under different occupant load diversity scenarios predicted by Model-3

Figure 0.21 shows the comparison between the outcomes of space air temperature from Model-1 and Model-2. Based on the result, both Model-1 and Model-2 approximate space air temperatures fairly well in the no diversity, low diversity, and medium diversity scenarios. The discrepancies between the outcomes from Model-1 and Model-2 become significant under the high diversity scenario. It is because the limitation of the setpoint of the supply air flowrate.

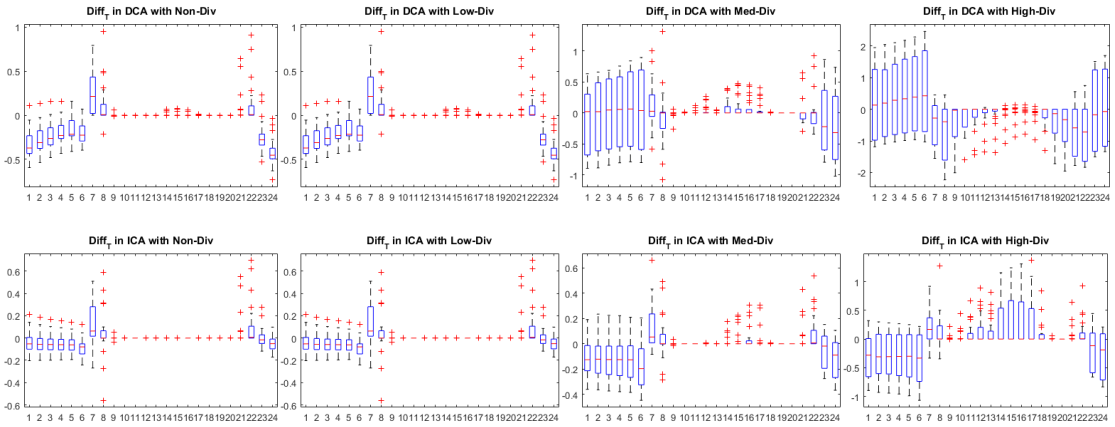

Figure 0.21 Comparison of the outcomes of weekday space air temperature between Model-1 and Model-2

Figure 0.22 shows that both Model-2 and Model-3 reasonably approximate space air temperature in DCA while the results of space air temperature in ICA has significant deviations under the low and medium diversity scenarios. The deviation expands from +/- 1℃ to +/- 2℃ as load diversity increases. The space air temperature result shows extreme deviation in the high diversity scenario since the space air temperature cannot be maintained in Model-3 because of the failure of the control strategies.

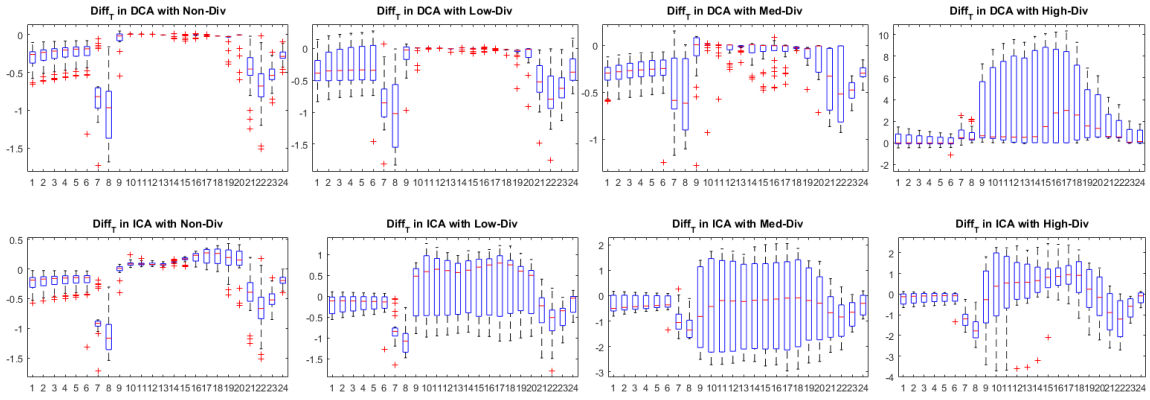

Figure 0.22 Comparison of the outcomes of weekday space air temperature between Model-2 and Model-3

If we eliminate the impact of the control failure, we should plot the relationship between the $Diff_T$ (Model-3 minus Model-1/2) only for low and medium diversity. Figure 0.23 shows that the $Diff_T$ of DCA does not correlate with the diversity factor while the $Diff_T$ of ICA shows a strong correlation with the diversity factor. When the diversity factor is negative (the occupant load per unit area in DCA is smaller than that in ICA), Model-1/2 underestimates the space air temperature of ICA; when the diversity factor is positive (the occupant load per unit area in DCA is larger than that in ICA), the EnergyPlus models overestimates the space air temperature of ICA.

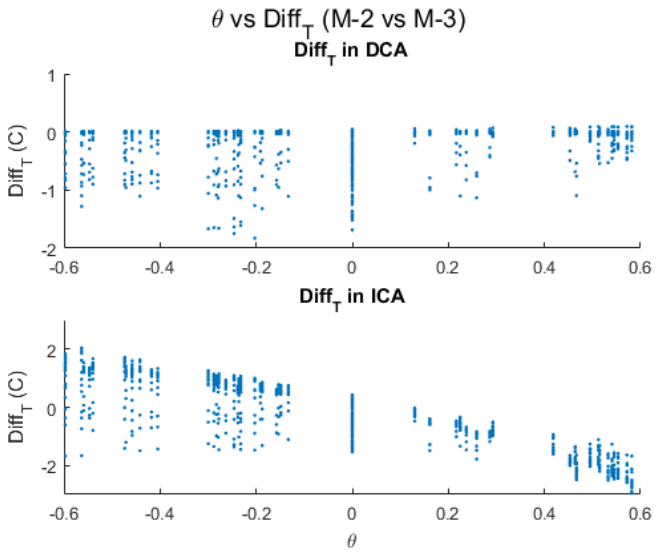

Figure 0.23 Relationship between $\mathbf{Diff_T}$ and diversity factor

1.14.3.2 Thermal comfort

In this section, we use unmet hours to evaluate thermal comfort. According to the space air temperature result, we calculate unmet hours for the south perimeter zone following the rules below: an hour will be counted as an unmet hour if the space air temperature of one or more spaces is outside of the setpoint plus or minus 1°C. Figure 0.24

shows the result of unmet hours in the 390 data points. We can see the EnergyPlus models underestimate the number of unmet hours for all diversity levels. Based on the co-simulation model result, the HVAC system cannot maintain the entire south perimeter zone within the unmet hour tolerance when the internal load reaches to the medium and high diversity levels.

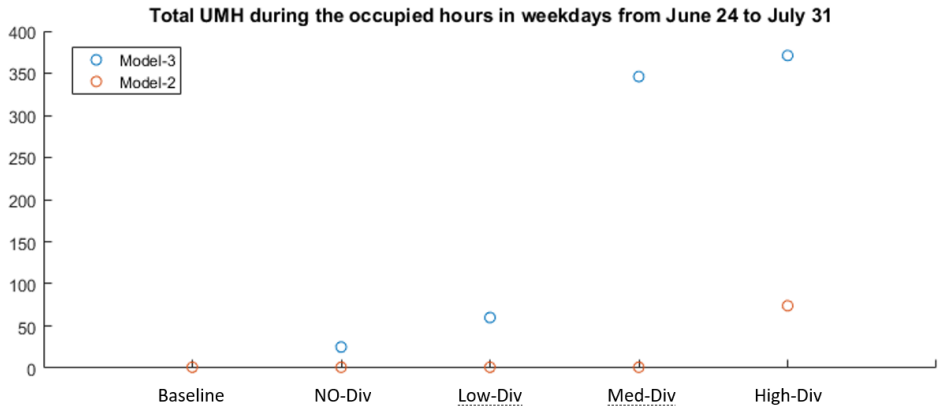

Figure 0.24 The unmet hour results of Model-2 and Model-3

1.14.3.3 Supply air flowrate

We also compare the total supply airflow rate for the overall south perimeter zone by using the percentage of difference between the hourly airflow rate ($\text{Diff}_{\text{Flow}}$) predicted by Model-2 and Model-3. The percentage of the Diff flow is calculated by:

$$Diff_{Flow} = (SAF_{Co-sim} - SAF_{EP})/SAF_{EP}$$

We plot the relationship between the $\text{Diff}_{\text{Flow}}$ and the diversity factor in Figure 0.25 (excluded the data point obtained for the high diversity scenario to eliminate the bias of control failures in the targeted correlations). We can see that the $\text{Diff}_{\text{Flow}}$ is strongly correlated with the diversity factor. Model-2 underestimates the supply air flowrate when

the diversity factor is positive and overestimates the flowrate when the diversity factor is negative. It is because the EnergyPlus model estimates the supply airflow rate based on the thermal load released in both DCA and ICA while the co-simulation model determines the supply airflow rate only based on the space condition of DCA.

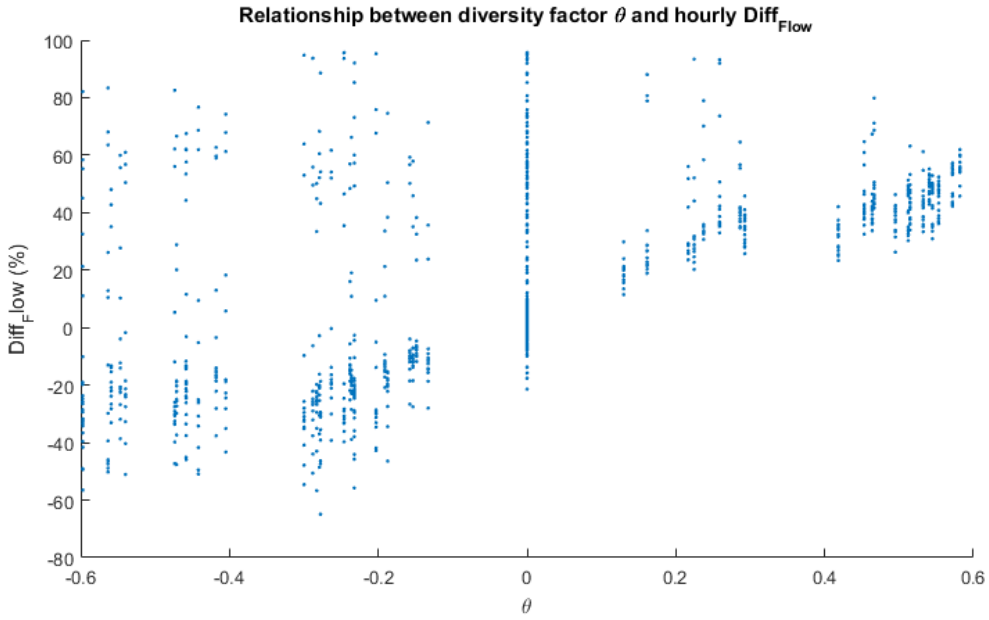

Figure 0.25 Relationship between the $\mathbf{Diff_{Flow}}$ and the diversity

1.14.3.4 Delivered cooling energy

The delivered cooling energy is compared in three different time intervals: hourly, daily and monthly. We compare the outcomes of the hourly delivered cooling between Model-1 and Model-3 as well as between Model-2 and Model-3. The dataset includes 1,170 hourly data points during the occupied period of weekdays under no diversity, low diversity, and medium diversity scenarios (after excluding the high diversity case). We use the percentage of $\mathrm{Diff_{Cooling}}$ to show the relationship between the delivered cooling and the diversity factor, the percentage of $\mathrm{Diff_{Cooling}}$ is calculated by:

$$Diff_{Cooling} = (Cooling_{Co-sim} - Cooling_{EP})/Cooling_{EP}$$

Figure 0.26 shows that the hourly $\text{Diff}_{\text{Cooling}}$ increases for a larger diversity factor.

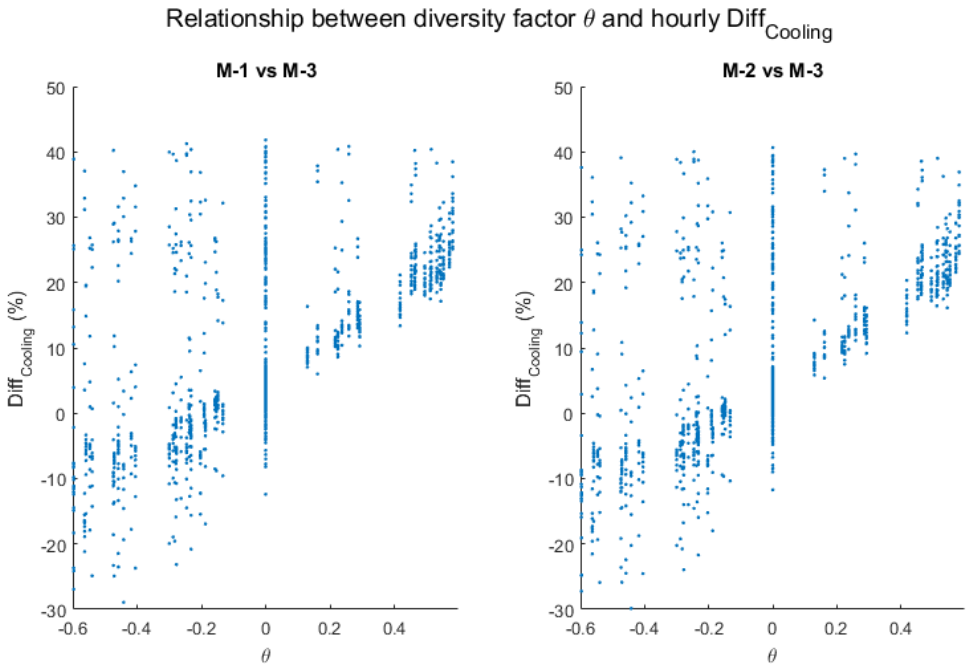

Figure 0.26 Relationship between the hourly $\mathbf{Diff_{Cooling}}$ and the diversity (left: Model-1 vs Model-3; right: Model-2 vs Model-3)

The total simulation period includes 26 weekdays, so we compare the daily delivered cooling for the 26 days. The dataset has 78 data points including the daily delivered cooling result under no diversity, low diversity and medium diversity scenarios. Figure 0.27 shows the percentage of difference on daily delivered cooling energy. Based on the result, we can see that the $\text{Diff}_{\text{Cooling}}$ varies from –5% to 35% along with the increase of the diversity factor. The $\text{Diff}_{\text{Cooling}}$ is about 6% when the building under the no diversity scenario which can be influenced by specific parameters of the case under study.

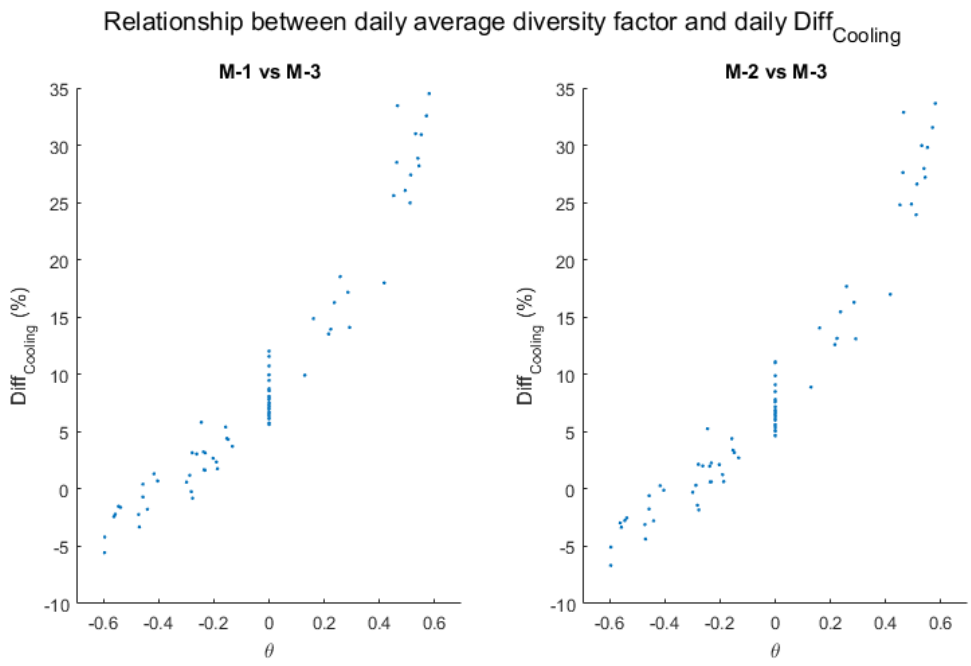

Figure 0.27 Relationship between the daily **Diff$_{Cooling}$** and the daily average diversity (left: Model-1 vs Model-3; right: Model-2 vs Model-3)

The monthly delivered cooling results in July estimated by the three models are compared. Figure 0.28 shows the comparison between the three models. Based on the result, the monthly Diff$_{Cooling}$ result has about 8% deviation between Model-1 and Model-3 under no diversity scenario which can be influenced by the specific case or the imperfect control of HVAC system. When we introduce the occupant load diversity into the model, there appears to a very strong correlation between the percentage of Diff$_{Cooling}$ and the diversity level, which is because we randomly sample the diversity factor in the daily level. Models 1 and 2 underestimate the delivered cooling when the diversity factor is positive and otherwise the delivered cooling will be overestimated. However, by the same token, the accumulated monthly result shows much less correlation with the diversity factor as the effect of uncorrelated daily values even out over the month.

Model-1 predicts the same result for all diversity scenarios since it cannot reflect the spatial occupant load diversity. Figure 0.28 shows that the difference between Model-3 and Model-1 become smaller when we introduce high occupant load diversity into the model. It indicates that the building may consumes less cooling energy when there is significant spatial occupant load diversity in the space where the space temperature drifts from (above) the setpoint. This is an example where the real building consumes less energy than predicted. But this comes obviously at the expense of non-maintained setpoint temperatures and hence increased discomfort.

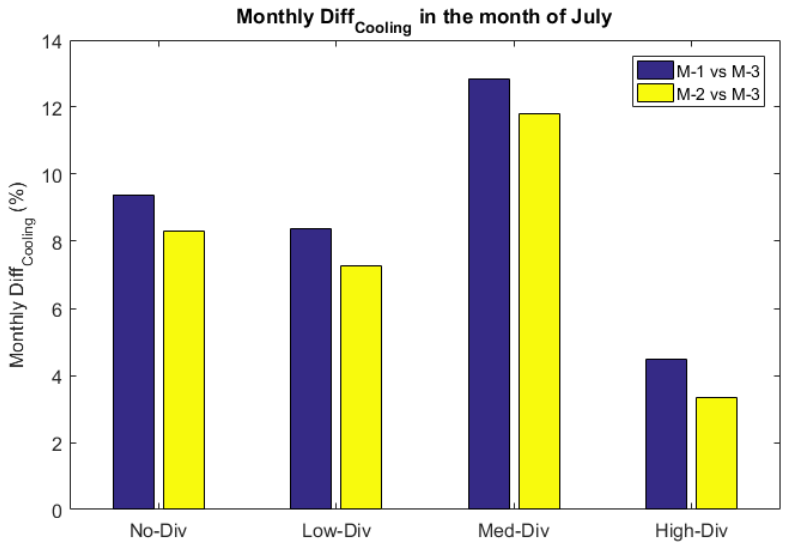

Figure 0.28 Comparison of monthly delivered cooling: (blue) the comparison between Model-1 and Model-3; (yellow) the comparison between Model-2 and Model-3)

1.15 Discussion

The preliminary study includes two case studies: the baseline case and the load diversity case with deterministic load patterns. Based on the result of the two cases, we learn that:

(1): The EnergyPlus model with an idealized HVAC control is able to provide a close approximation result to the co-simulation with detailed HVAC system and control strategies when there is no misalignment between the building partition and HVAC topology

(2): The level of misalignment affects the simulation outcomes; this means specifically that the spatial configuration of spaces within a zone affects the simulation outcomes.

(3): Occupant load diversity exacerbates the impact of the misalignment at low and medium diversity, while high diversity leads to serious problems that go undetected in model 1 and 2. This is linked to the observation that control strategies of the HVAC system may experience failure when extreme spatial occupant load diversity occurs in the space.

GAP ANALYSIS

We choose a three-story new construction medium office building model to conduct the uncertainty analysis. The parameters of building material and constructions are based on the ASHARE Standard 90.1-2010 prototype medium office building. The dimension of the second floor is $45\text{m (L)} \times 30\text{m(W)} \times 3\text{m(H)}$ with an overall floor area at 1,350 m^2. As the same settings as used in the preliminary study, the indoor floor area is assumed to be served by an AHU with five VAV terminal boxes with reheat. To evaluate the impact of convective loads and solar heat gains from ambient environment, we implement different zoning configurations with single external façade, two external facades, and no external façade as detailed in the following sections.

1.16 Single external façade case

1.16.1 Model configurations

The zone of interest in the single external façade case has only one orientation with external façade and all other zone boundaries are adjacent to other indoor areas. We partition the service area of the VAV terminal boxes as shown in Figure 0.1a. The south perimeter zone is the area of interest with a dimension of $35\text{m (L)} \times 5\text{m(W)}$, the total area of the zone is 175m^2. We assume the entire south perimeter zone are office area and the occupants share the similar space using pattern, therefore, the spatial distribution of the internal heat gain densities can be described by using normal distribution functions. We design five sub-zone configurations with different alignment factor (η) values to reflect the levels of mismatch as shown from Figure 0.1b to Figure 0.1f. The marked area is the

directly controlled area (DCA). The basic control strategies and setpoints of the HVAC system in the low-fidelity model and Modelica model are kept the same as in the preliminary study.

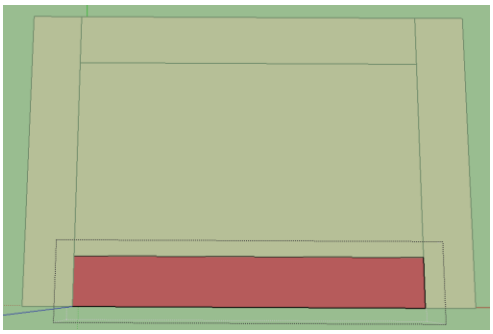

a. Zone configuration with single external façade

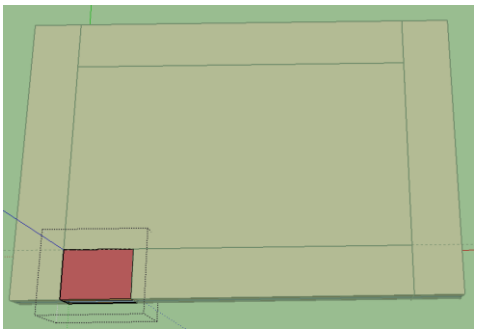

b. $\eta = 1/5$

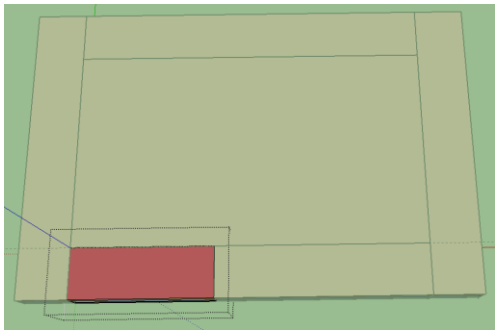

c. $\eta = 2/5$

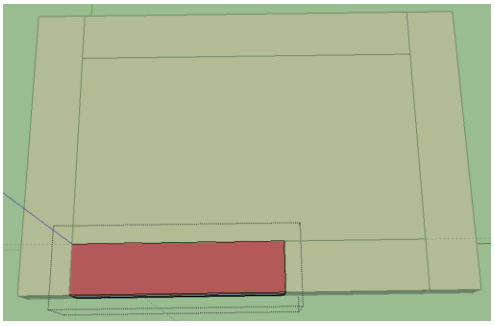

d. $\eta = 3/5$

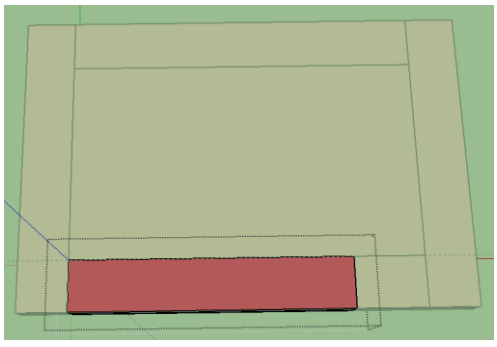

e. $\eta = 4/5$

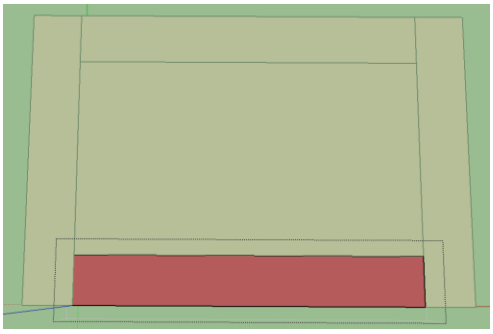

f. $\eta = 1$

Figure 0.1 Zoning configurations of single external façade case

1.16.2 Occupancy profile and diversity factor

As mentioned in Chapter 2, we want to include the stochastic nature of occupant presence and their influence on lighting and plug loads in our consideration. We assume the modeler has good knowledge about the zone level occupancy profile, and that the unknown sub-zone level occupancy profiles can be derived from available information. The selected office building has a north perimeter zone with meeting rooms while the remaining space is office area. The design value of occupants in the meeting rooms is zero since the meeting rooms are occupied only if there are meetings. Based on the reference value (18.58m^2/person) of the occupant density specified by ASHRAE, the design value of the number of occupants in each zone is defined as shown in Table 0.1

Table 0.1 Design values of the number of occupants in each zone

	Core	South	East	North	West	Total
Number of total occupant (p)	38	9	8	0	8	64

According to the settings above, we use Occupant Simulator to generate zone level occupant presence schedules and treat them as the client supplied or measurement data. Figure 0.2 shows the generated occupant presence profile for the south perimeter zone from June 1st to July 31st.

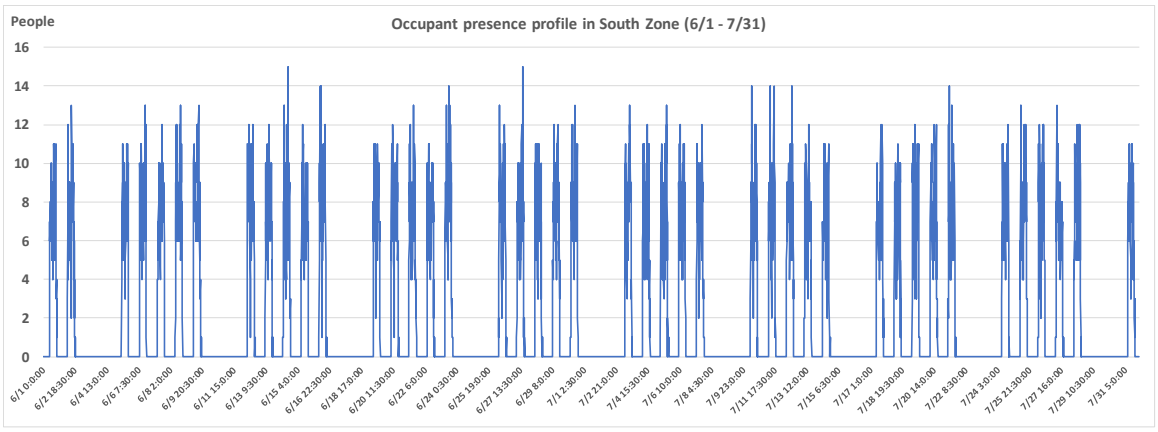

Figure 0.2 The generated occupant presence profile from June 1st to July 31st for the south zone

The number of occupants in the south perimeter zone fluctuates from 1 to 15 people with a mean value of 7 during the working hours. It illustrates the fact that the occupants move between spaces during working hours; sometimes people gather together in an area with the number far beyond the design capacity of that area. The mean profile of the lighting and appliance usage and the correlation between the occupant presence and the lighting/appliances usage is derived from Wang's (2016) on-site measurement. Based on the zone level occupancy, lighting and appliance information, we sample the sub-zone level occupancy profiles for each alignment factor configuration by using the method introduced in Chapter 2.4. Since the occupancy profile during the weekends and after hours has very limited fluctuation, we select 4,160 working hours from the 8,760 hours in total to calculate the corresponding hourly diversity factors for each configuration case. Figure 0.3 depicts the distribution of diversity factor in each case. The range of the value of diversity factor is mainly from -0.5 to 0.5 with the mean value close to 0. It indicates that the occupant usage varies in DCA and ICA. Actually, the occupant usage in DCA and ICA are not identical most of the time.

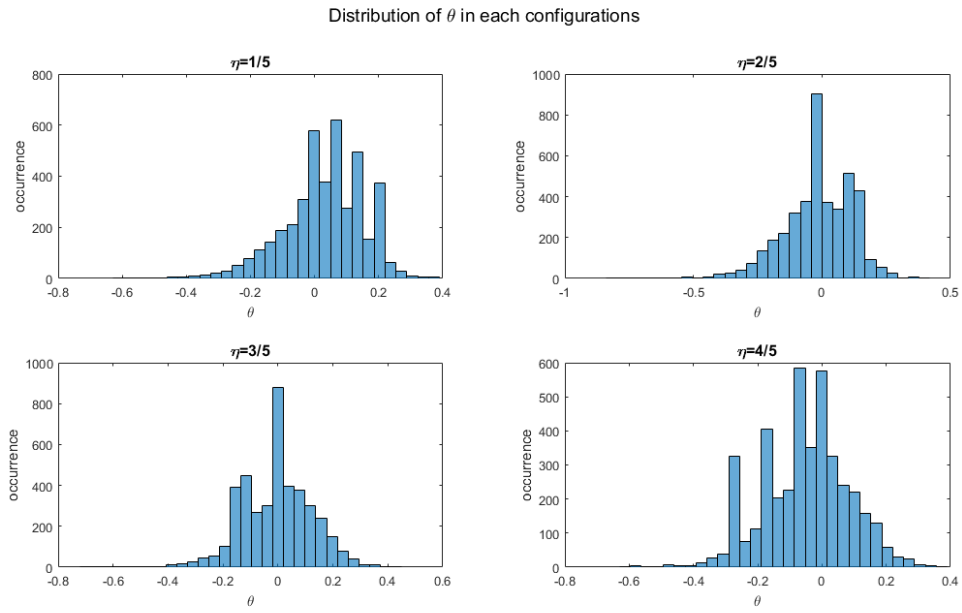

Figure 0.3 Distribution of hourly diversity factor in single façade case

Figure 0.4 is the boxplot to show the variations of diversity factor in different configuration cases. We can see that the medium is close to zero and the spacings between the first quartile and third quartile is not wide, but some outliers with large absolute value exist in the relatively long tails. According to the knowledge we obtained from the preliminary study, these outliers may introduce control or discomfort issues into the space.

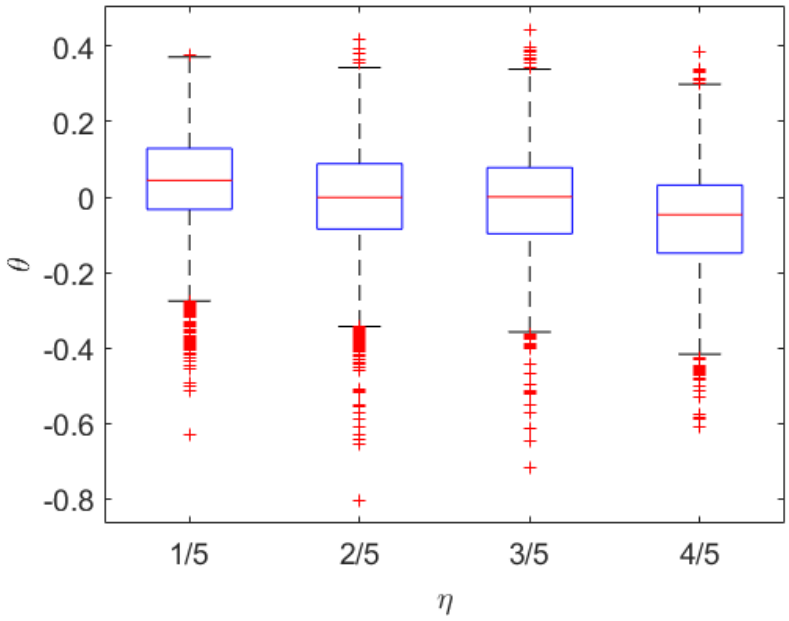

Figure 0.4 Value of diversity factor in single façade case

To analyze the impacts of the diverse usage on space condition and energy consumptions, we utilize the sub-zone level occupancy profiles to assign the internal loads in the three models: the aggregated EnergyPlus model (Model-1), the sub-divided EnergyPlus model (Model-2), and the co-simulation model (Model-3). Since Model-1 does not distinguish the ICA from the DCA, we combine the two occupancy profiles together to assign the internal loads. The simulation period is from 6/24 to 7/31 and the predictions for July are used to conduct the following analysis.

1.16.3 Model-1 vs Model-2

Before investigating the discrepancies between the co-simulation model and the EnergyPlus models, we compare the outcomes from the two EnergyPlus models. As Model-2 requires higher resolution of the input information, i.e. at sub-zone level, we want to inspect if the extra information could bring improvements to the simulation outcomes.

Recall that we use the auto-sizing result of Model-1 as the size parameter when developing the co-simulation model and analyze the outcomes between Model-2 and Model-3. Thus, it is necessary to determine if the auto-sizing of Model-1 and Model-2 leads to comparable values. Figure 0.5a shows the design airflow sizes of VAV box for the south perimeter zone estimated by Model-1 and Model-2. The maximum difference is no larger than 2%. Figure 0.5b depicts the correlation between the alignment factor and the ratio of design size of DCA to the design size of the overall south perimeter zone. The results illustrate that the two models provide auto-sizing results that are close. As Figure 0.5 shows, the design size of the virtual VAV boxes at the sub-zone level can in fact be derived based on the value of the alignment factor, at least in the single external façade case.

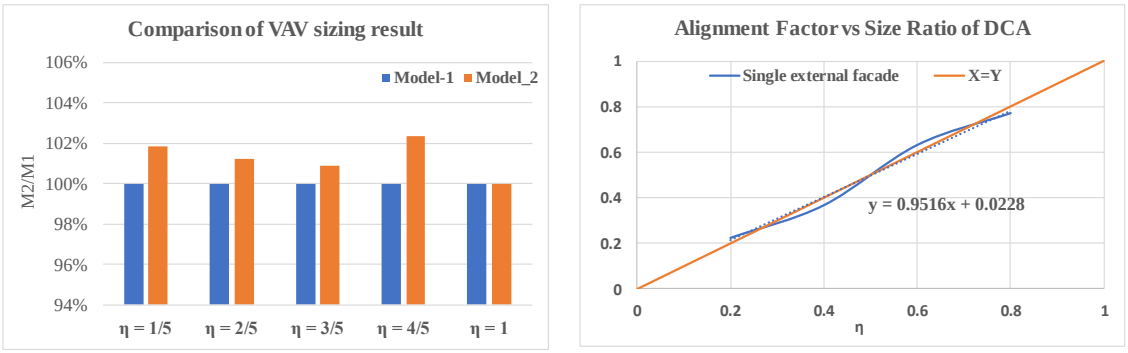

a b

Figure 0.5 Comparison of the auto sizing result between Model-1 and Model-2 for single façade case

Figure 0.6 shows the differences (Diff) of the hourly outcomes in the south perimeter zone between Model-1 and Model-2 for the five alignment factors, including room air temperature (RT) of ICA, supply air flowrate (AF), delivered cooling (Q), and fan power (FP). The comparison depicts that increasing the resolution of the EnergyPlus model

from zone level (Model-1) to sub-zone level (Model-2) has little impact on the simulation outcomes for the thermal zone in the single external façade case.

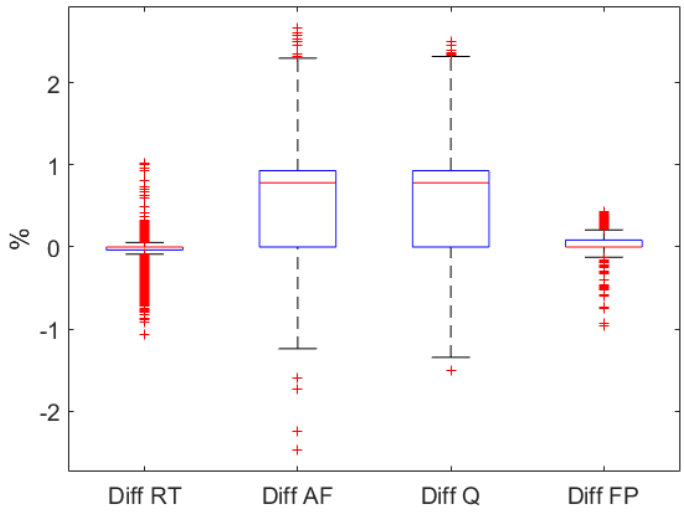

Figure 0.6 Outcome comparison between Model-1 and Model-2 for single façade case

1.16.4 Data pre-processing

The occupied hour of the space is from 8am to 9 pm, to maintain the space temperature at 24 ℃ during that period, the operating period of the HVAC system is from 7 am to 10 pm. The first (7-8 am) and the last (9-10 pm) operating hour is where the transition happens. The controlled variable in Model-3 is the supply air flowrate which is determined by the difference between the temperature setpoint and its measured value. In the first operating hour, the space temperature setpoint shifts from the unoccupied setpoint (26.7 ℃) to the occupied setpoint (24℃) which results in a large difference between the setpoint to the actual space temperature, the damper control then leads to an overshoot which oversupplies cooling which results in extra delivered cooling energy. In the last operating hour, the space requires less supply air along with the decrease of the occupant

usage intensity. However, the supply air flowrate cannot reduce further when the damper hit its minimum damper position setpoint even if the space air temperature already drops below the setpoint. On the other hand, Model-2 only experiences a short transition period since the delivered energy is estimated based on the thermal load. Therefore, it inevitably leads to the bias between the Model-2 and Model-3 in space air temperature, delivered cooling, and fan power consumption. Figure 0.7 to Figure 0.9 show the daily curve of difference in space air temperature, delivered cooling, and supply air flowrate in ICA during the weekdays in July, which diagram that Model-3 predicts much higher cooling consumption and supply air flowrate during the transition hours, and consequentially the space experiences overcooling during that period. While Figure 0.10 depicts that the value of diversity factor stays within a moderate level during the transition period. It means that the diversity factor is not the main driver of the difference between Model-2 and Model-3 outcomes for the quantities of interest. Recall that in this study we attempt to describe the difference of quantities of interest by diversity factor, Therefore, we remove the datapoints measured in the first and the last occupied hour from the occupied hour dataset to eliminate the impact of the transition period. The new dataset is used for the hourly interval regression analysis in the next three sections to evaluate the impact of the diversity factor on the outcomes of quantities of interest.

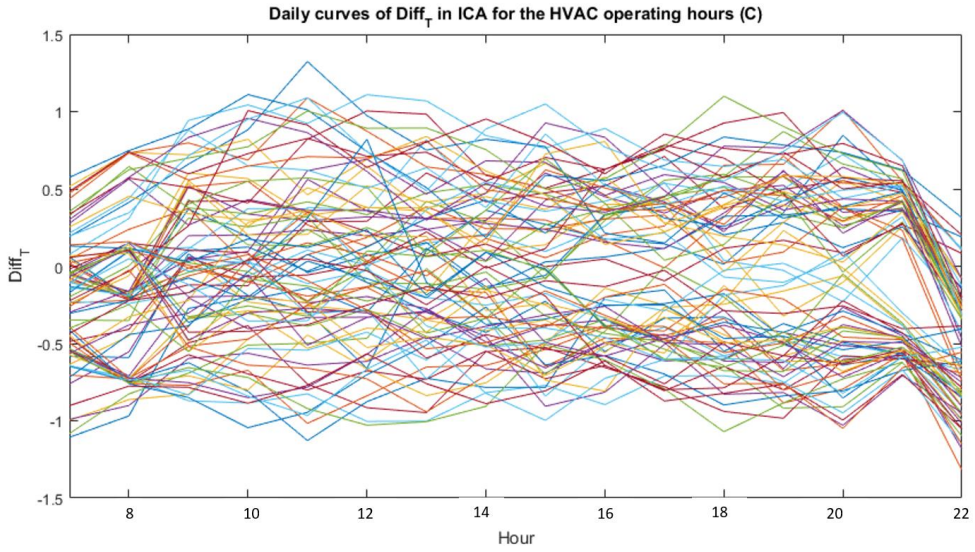

Figure 0.7 Daily curves of $\mathbf{Diff_T}$ in ICA from 7am to 10pm (°C)

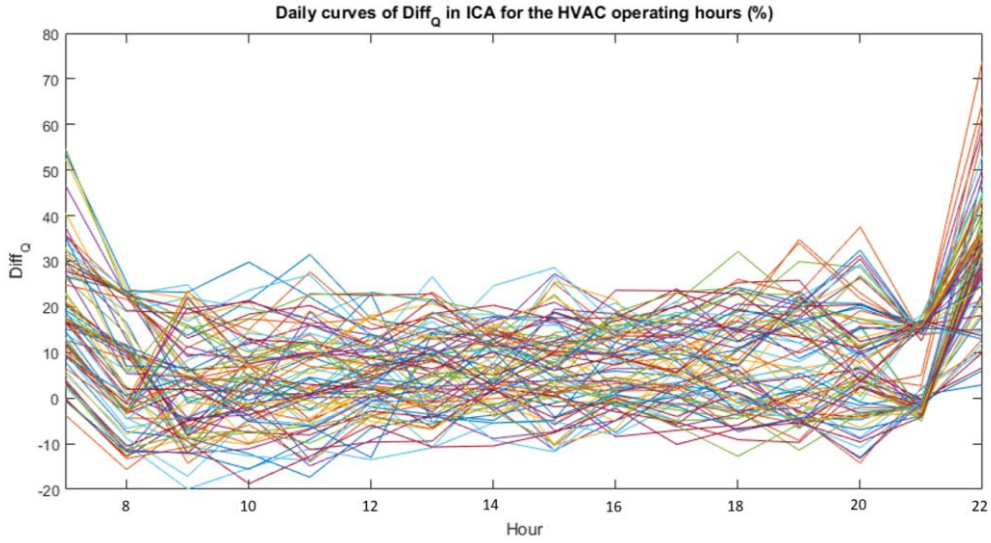

Figure 0.8 Daily curves of $\mathbf{Diff_{Cooling}}$ in ICA during from 7am to 10pm (Wh/m2)

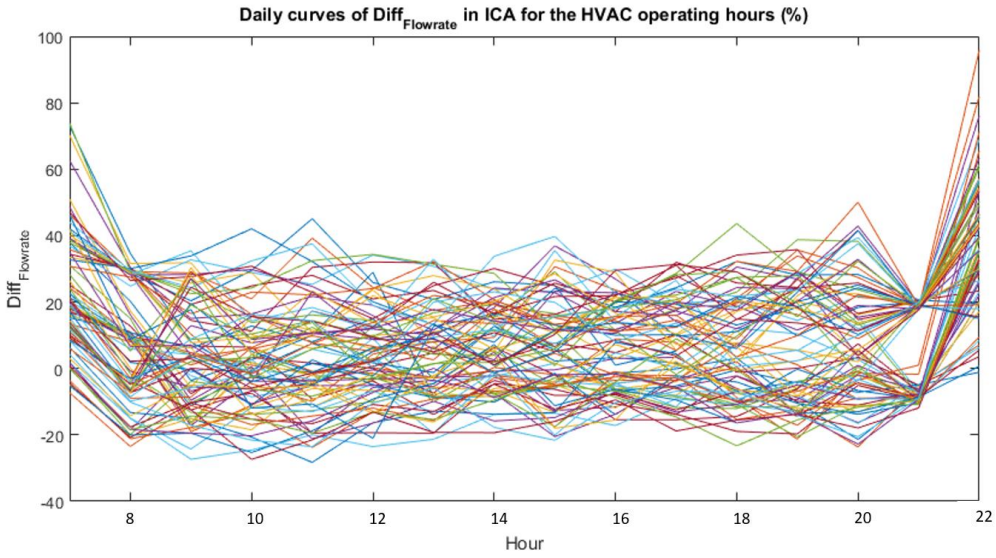

Figure 0.9 Daily curves of **Diff$_{Flowrate}$** in ICA from 7am to 10pm (%)

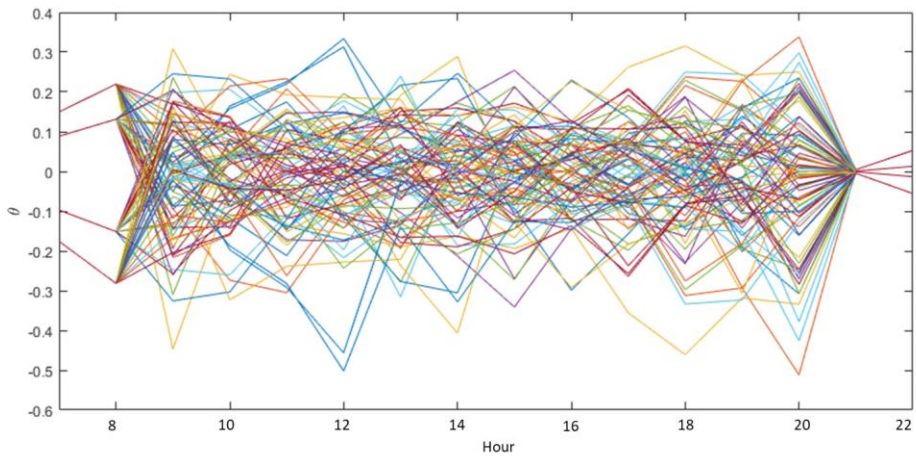

Figure 0.10 Daily curves of diversity factor from 7am to 10pm

1.16.5 Impact on space air temperature

Figure 0.11 shows the histogram of the differences between Model-2 and Model-3 in the predicted hourly space air temperature. The dataset includes 1,176 occupied hour data for the single façade cases with alignment factor 1/5, 2/5, 3/5, and 4/5. The left figure shows that the two models predict the temperature of DCA closely. The right figure shows

noticeable differences in the predicted space air temperature of ICA estimated by Model-2 and Model-3 within a range from -1.3°C to 1.3°C. The result indicates that in spite of the low fidelity of Model-2 the HVAC system maintains the space air temperature within an acceptable range for the stated alignment factors. This result applies to the office area located in a perimeter zone with single external façade.

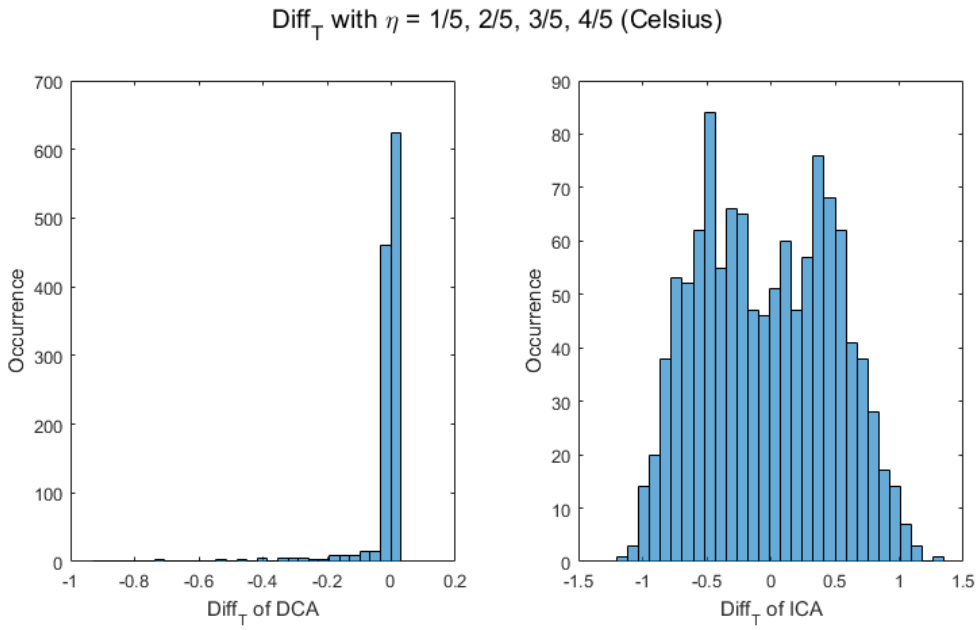

Figure 0.11 $\mathbf{Diff_T}$ between Model-2 and Model-3 when $\boldsymbol{\eta}$ = 1/5, 2/5, 3/5, 4/5 for single façade case

In the preliminary study in Chapter 4 we learned that diverse occupant usage of the ICA may be the root cause for larger discrepancies. Therefore, we need to build a statistical adjustment to the prediction difference from the EnergyPlus model using the high-fidelity co-simulation model result. For this reason, we perform a linear regression fitting to the temperature discrepancy term against the diversity factor with the unit of temperature as Celsius. In this study we assign the occupant usage by using the sampled time series sub-zone level profile. Based upon the input profiles, we can calculate the corresponding

diversity factor for each hour. To eliminate the impact of the transition period as introduced above, the dataset we use in the following hourly interval analysis includes the simulation outcomes from 8 am to 9 pm of the weekdays in July. Figure 0.12 shows the correlation between the diversity factor and the $\mathrm{Diff_T}$ in each alignment case (red line). The fitted coefficients are shown in Table 0.2. The band between the yellow and purple lines has a width of 4 standard deviations.

Table 0.2 Fitted linear equations for $\mathbf{Diff_T}$ of ICA (Celsius) against diversity factor ($\boldsymbol{\theta}$) for single façade case

η	Fitted equations
1/5	$\mathrm{Diff_T} = -1.65\theta + 0.25 + \varepsilon, \varepsilon \sim \mathrm{N}(0,0.15), R^2 = 0.68$
2/5	$\mathrm{Diff_T} = -1.61\theta - 0.61 + \varepsilon, \varepsilon \sim \mathrm{N}(0,0.13), R^2 = 0.70$
3/5	$\mathrm{Diff_T} = -1.37\theta + 0.54 + \varepsilon, \varepsilon \sim \mathrm{N}(0,0.20), R^2 = 0.40$
4/5	$\mathrm{Diff_T} = -1.49\theta - 0.36 + \varepsilon, \varepsilon \sim \mathrm{N}(0,0.16), R^2 = 0.64$

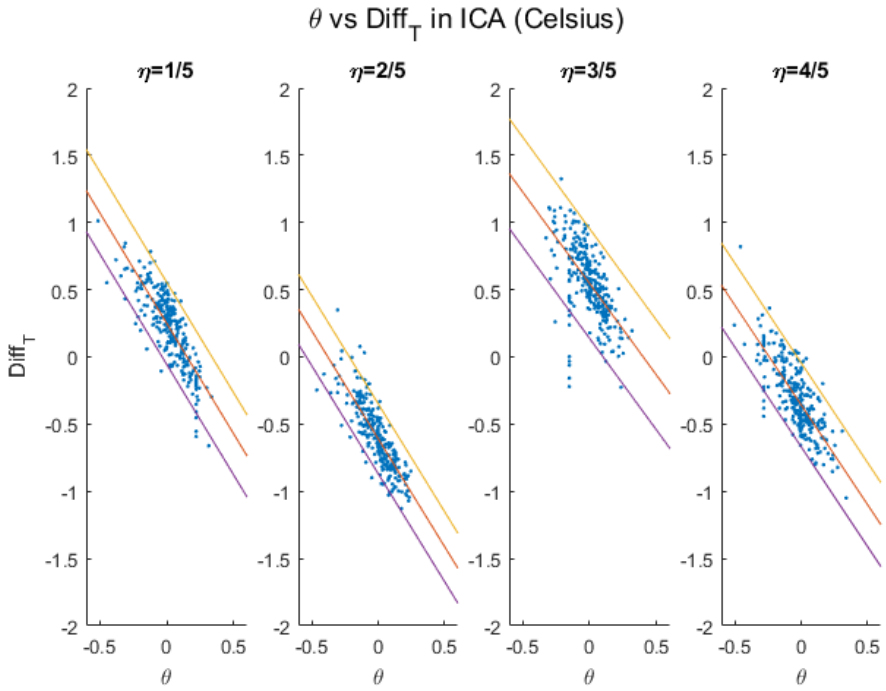

Figure 0.12 $\mathbf{Diff_T}$ (Celsius) of ICA as function of diversity for single façade case

According to the outcomes in space air temperature, we calculate the number of unmet hours during the occupied period (weekday from 8 am to 9 pm) in July to evaluate thermal comfort: an hour will be counted as an unmet hour if the space air temperature is outside of the setpoint plus or minus 1℃. The dataset includes 294 occupied hours in July for each alignment case and the number of unmet hours is shown in Figure 0.13. We can see that Model-2 and Model-3 have similar prediction of the unmet hours for the DCA while the Model-2 underestimates the unmet hours for the ICA. The latter indicates that in reality the space experiences discomfort issue that are not detected by routine EnergyPlus simulations. This is due to the HVAC system's limited controllability as exposed in Model-3 and not due to hardware faults in the control as sometimes believed by onsite auditors.

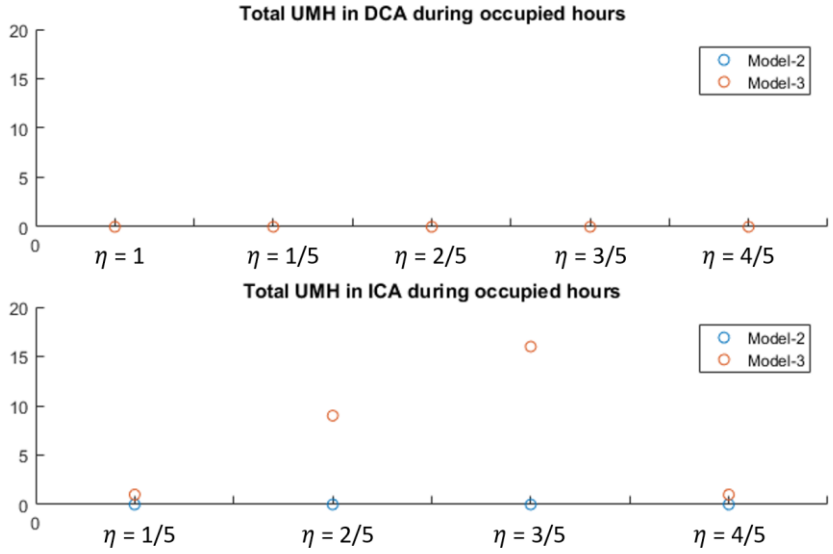

Figure 0.13 Outcomes of unmet hours from Model-2 and Model-3 for single façade case for month of July

1.16.6 Impact on delivered cooling energy

The south perimeter zone is served by one VAV terminal system which is the atomic unit to regulate the delivered cooling. Therefore, we firstly calculate the hourly

$\text{Diff}_{\text{Cooling}}$ between the outcomes of Model-2 and Model-3 for the entire south perimeter zone containing DCA and ICA. The differences are calculated based on the equations introduced in Chapter 4 for the fixed daily occupancy schedules.

The dataset, contains 1,470 datapoints, is divided into two groups: the first group includes 294 datapoint of the case with alignment factor 1, and the second group contains the rest 1,176 datapoints of the other four alignment cases with alignment factor 1/5, 2/5, 3/5 and 4/5. The left figure in Figure 0.14 depicts the distribution of data group one; and the right figure presents the distribution of the data group two. By performing a distribution fitting, we obtain: $Diff_{cooling,\eta=1} \sim LogLogistic(0.011,0.065,18.25)$ and $Diff_{cooling,\eta\neq1} \sim N(0.057,0.053)$. When $\eta = 1$, the difference has a positive mean value with a narrow distribution which indicates that the EnergyPlus model slightly underestimates the delivered cooling energy by implementing the virtual ideal HVAC system. When $\eta \neq 1$, the discrepancy has a much wider distribution and the value can be negative in some cases. Based on the statistic result, the differences in the hourly delivered cooling can reach to 20%. The negative value illustrates that in reality the HVAC system may deliver less cooling than is predicted by the routine EnergyPlus model (Model-2), implying that it does not always meet the required cooling supply.

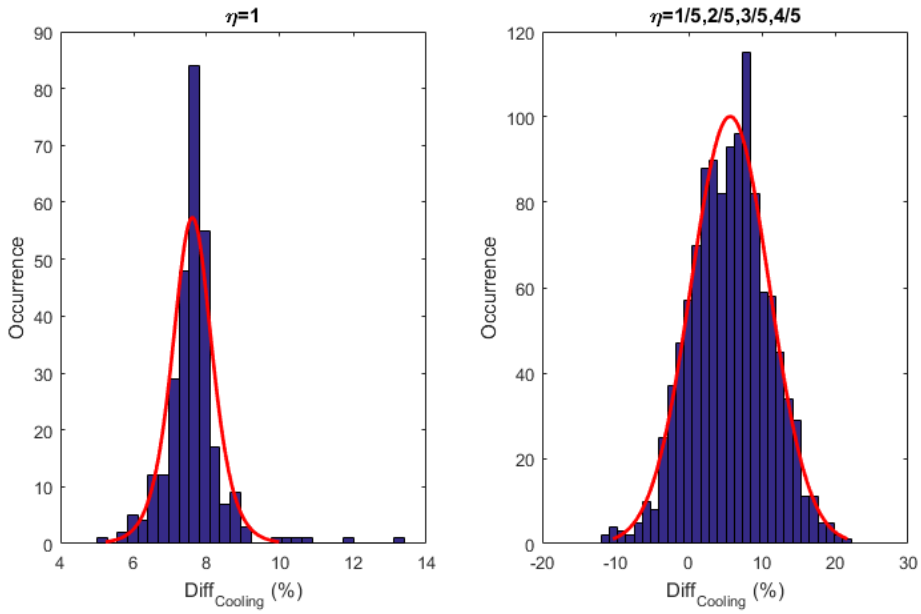

Figure 0.14 Distribution of $\mathbf{Diff_{Cooling}}$ between the predictions of Model-2 and Model-3 for single façade case

We plot the distribution of $\mathrm{Diff_{Cooling}}$ for each alignment case and perform distribution fitting for the $\mathrm{Diff_{Cooling}}$ (%) with the coefficients shown as Table 0.3.

Table 0.3 Fitted distributions of $\mathbf{Diff_{Cooling}}$ (%) for each alignment factor

$\eta = 1/5$	$\eta = 2/5$	$\eta = 3/5$	$\eta = 4/5$
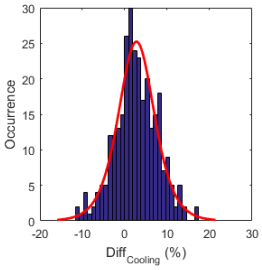	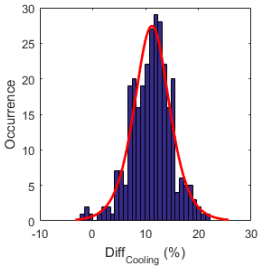	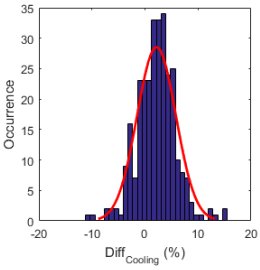	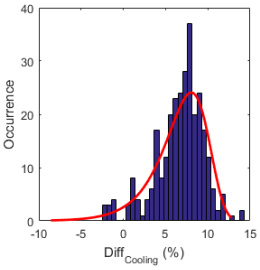
$N(0.027,0.05)$	$N(0.111,0.039)$	$N(0.022,0.037)$	$N(0.067,0.029)$

To investigate the impact of diversity factor on the delivered cooling energy, we plot the correlation between the zone level $\mathrm{Diff_{Cooling}}$ and the corresponding hourly diversity factor for each alignment case (red line), as shown in Figure 0.15. The band between the yellow and purple lines has a width of 4 standard deviations.

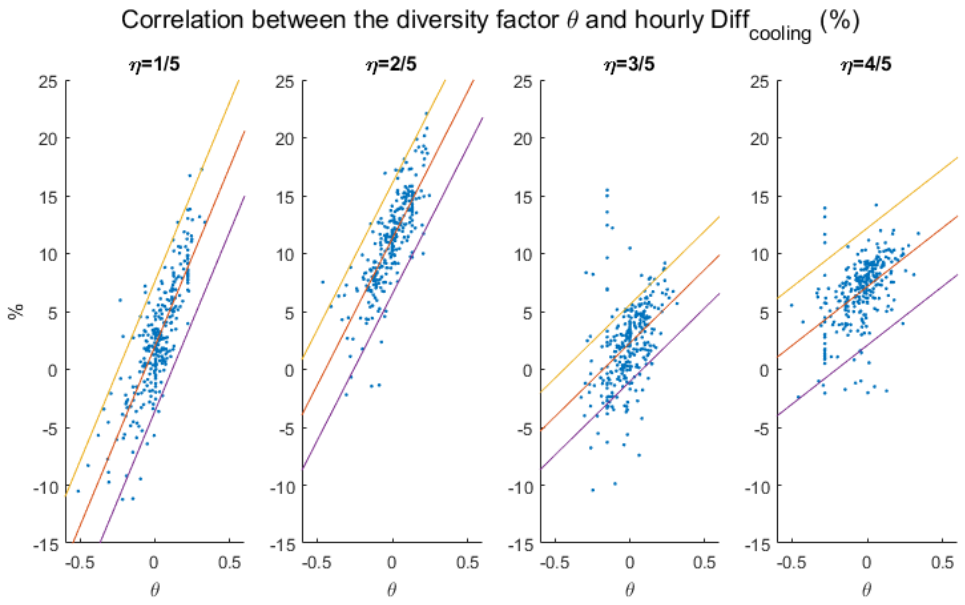

Figure 0.15 Correlation between diversity factor ($\boldsymbol{\theta}$) and hourly $\mathbf{Diff_{Cooling}}$ (%) in the zone level for single façade case

We notice that the correlation between the $Diff_{Cooling}$ and the diversity factor (θ) is getting weak along with the increase of the alignment factor (η). It is in line with our expectations since the impact of the undetectable occupant usage on the total cooling energy mitigates along with the increase of the directly controlled area. The result prompts that we should derive the linear correlation between the diversity factors and the $Diff_{Cooling}$ of ICA instead of the $Diff_{Cooling}$ of the entire thermal zone.

We can obtain the straightforward result shown in Figure 0.16 when we investigate the correlation between the $Diff_{Cooling}$ of ICA and the diversity factor by performing a linear regression (red line). Table 0.4 shows the fitted linear equations of $Diff_{Cooling}$ of ICA against the diversity factor in each alignment factor case. The band between the yellow and purple lines has a width of 4 standard deviations.

Table 0.4 Fitted linear equations of hourly $\mathbf{Diff_{Cooling}}$ (%) of ICA against diversity factor ($\boldsymbol{\theta}$) for single façade case

η	Fitted equations
1/5	$\mathrm{Diff}_{\mathrm{Cooling}} = 0.39\theta + 0.01 + \varepsilon, \varepsilon \sim N(0,0.03), R^2 = 0.74$
2/5	$\mathrm{Diff}_{\mathrm{Cooling}} = 0.35\theta + 0.13 + \varepsilon, \varepsilon \sim N(0,0.03), R^2 = 0.72$
3/5	$\mathrm{Diff}_{\mathrm{Cooling}} = 0.40\theta - 0.04 + \varepsilon, \varepsilon \sim N(0,0.04), R^2 = 0.55$
4/5	$\mathrm{Diff}_{\mathrm{Cooling}} = 0.39\theta + 0.11 + \varepsilon, \varepsilon \sim N(0,0.04), R^2 = 0.68$

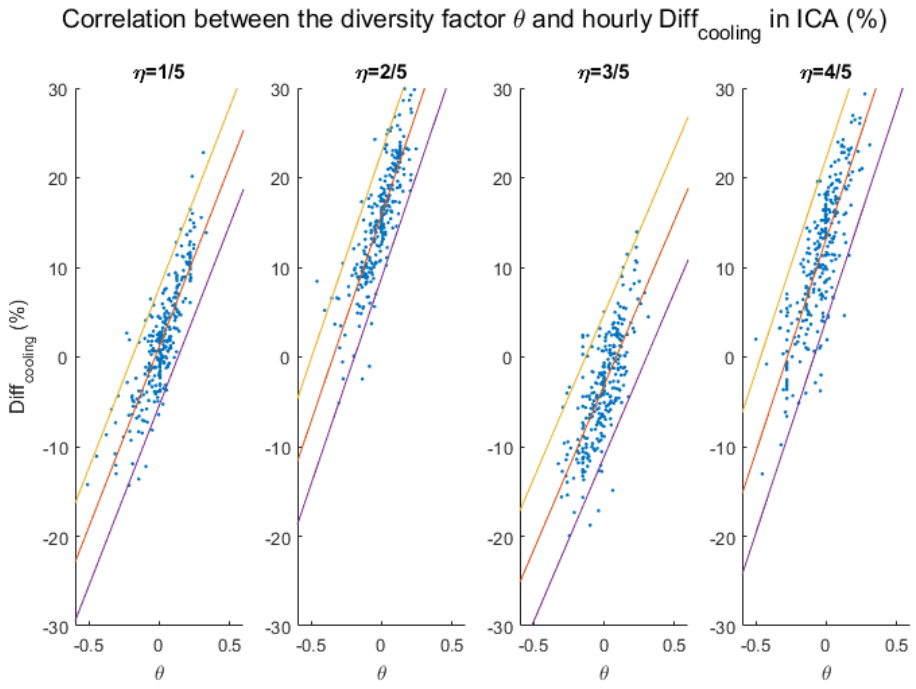

Figure 0.16 Correlation between diversity factor ($\boldsymbol{\theta}$) and hourly $\mathbf{Diff_{Cooling}}$ (%) of ICA for single façade case

The abovementioned cooling energy is for one-hour intervals. It is more relevant to conduct the analysis also for daily and monthly intervals. The dataset of daily $\mathrm{Diff}_{\mathrm{Cooling}}$ of the entire south zone contains 105 datapoints for the five alignment factor cases. Figure 0.17 shows the distribution of daily $\mathrm{Diff}_{\mathrm{Cooling}}$ for the overall south perimeter zone. The result depicts the daily cooling predicted by the EnergyPlus model is on average 20-30

Wh/m^2 smaller than the outcomes of co-simulation model, which is about 7-8% of the predicted value by the EnergyPlus model.

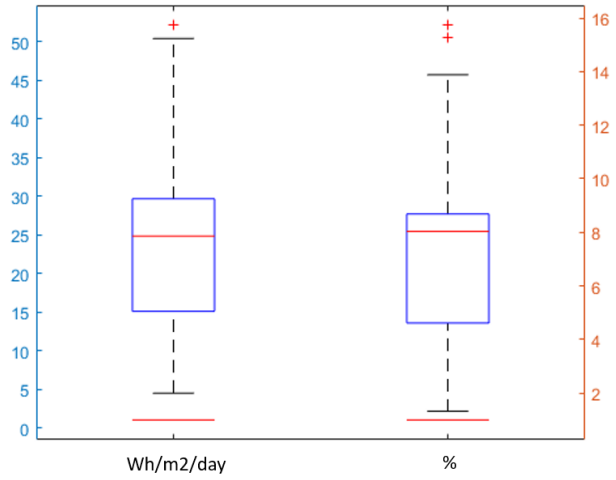

Figure 0.17 Distribution of daily **Diff$_{\mathbf{Cooling}}$** for single façade case

Figure 0.18 displays the comparison of monthly delivered cooling energy between the EnergyPlus model and the co-simulation model. The left figure depicts the predicted delivered cooling energy per square meter, the yellow bar is the outcomes of EnergyPlus model while the blue bar is the result of co-simulation model. The right figure shows the percentage of monthly Diff$_{\mathrm{Cooling}}$. The result presents that Diff$_{\mathrm{Cooling}}$ can reach to 8% when we include a detailed HVAC system with imperfect control in Model-3 with an alignment factor at 1; and the Diff$_{\mathrm{Cooling}}$ can be further increased 1% to 9% for the cases with an alignment factor at 1/5, 2/5, 3/5, and 4/5. It illustrates that the difference between the simulation result in delivered cooling energy is more noticeable when limited controllability of the HVAC system is present in the model.

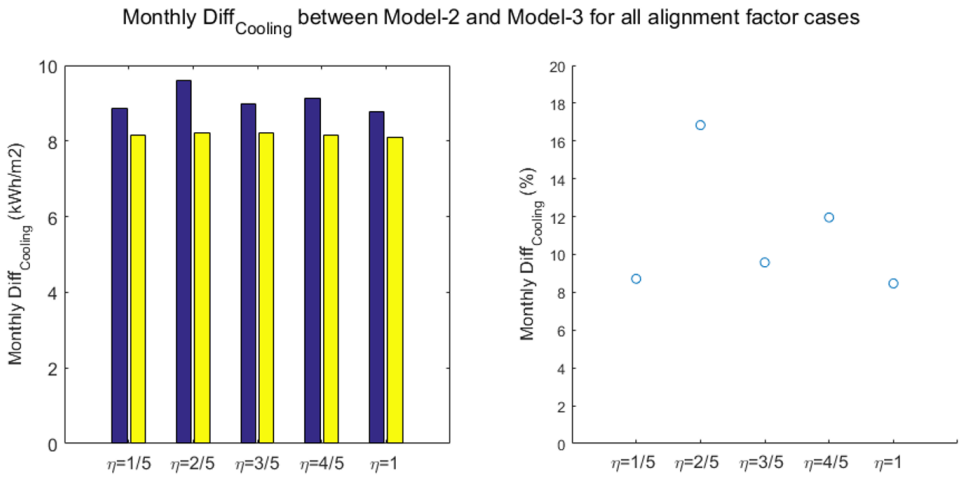

Figure 0.18 Comparison between Model-2 and Model-3 in monthly cooling energy for single façade case

1.16.7 Impact on air flowrate

The difference of flowrate is presented as a percentage calculated by the equation introduced in Chapter 4 for the fixed daily occupancy schedules. The dataset contains 294 datapoints for alignment factor 1, and 1,176 datapoints for alignment factor 1/5, 2/5, 3/5, and 4/5. Figure 0.19 shows the hourly $\text{Diff}_{\text{Flow}}$ between Model-2 and Model-3. The $\text{Diff}_{\text{Flow}}$ diagrammed in Figure 0.19 is for the total supply air flowrate of the VAV box. The left figure shows that the $\text{Diff}_{\text{Flow}}$ has a narrow range within 3% to 8% with a mean value of 5.5%. It illustrates that the EnergyPlus model slightly underestimates the supply air flowrate when no misalignment occurs for single external façade case. This is mainly caused by the unavoidably imperfect control by the real control system. The right figure in Figure 0.19 shows the distribution of $\text{Diff}_{\text{Flow}}$ for alignment factor 1/5, 2/5, 3/5, and 4/5. By performing a Gaussian distribution fitting, we obtain: $Diff_{flow,\eta\neq1} \sim N(0.040, 0.078)$. The distribution of the differences with misalignment is much wider than that for the no-

misaligned case, which confirms that misalignment impacts significantly on the flowrate prediction.

We plot the distribution of $\mathrm{Diff_{Flow}}$ for the four alignment cases and perform Gaussian distribution fittings, the results are shown as Table 0.5.

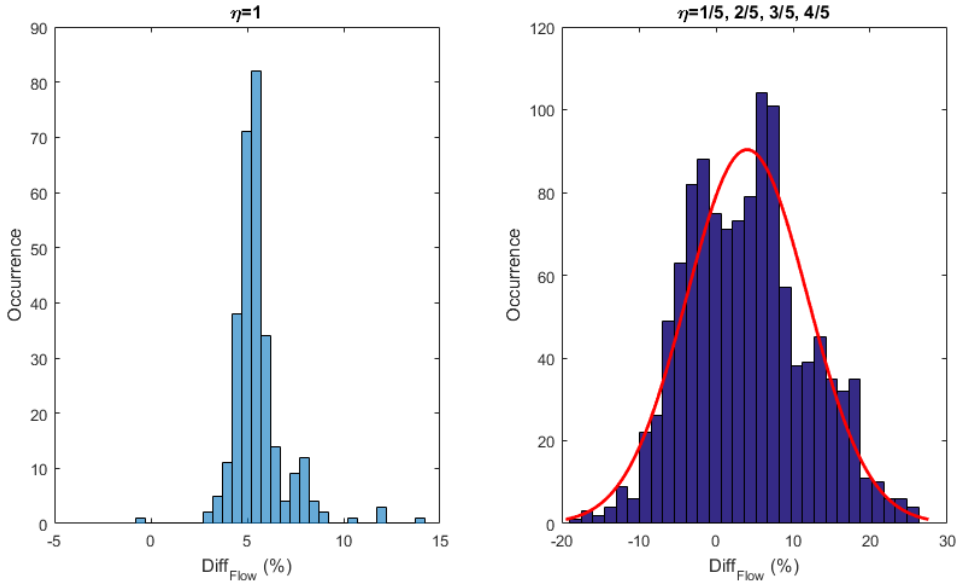

Figure 0.19 Distribution of $\mathbf{Diff_{Flow}}$ between the predictions of Model-2 and Model-3 for single façade case

Table 0.5 Fitted distributions of $\mathbf{Diff_{Flow}}$ for single façade case

$\eta = 1/5$	$\eta = 2/5$	$\eta = 3/5$	$\eta = 4/5$
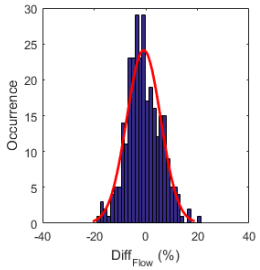	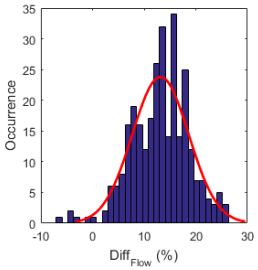	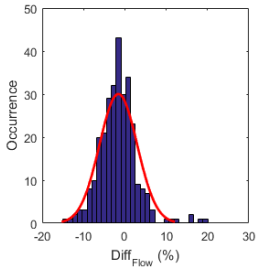	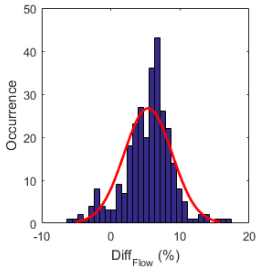
$N(-0.008, 0.066)$	$N(0.132, 0.055)$	$N(-0.016, 0.046)$	$N(0.054, 0.035)$

we also investigate the correlation between the $\mathrm{Diff_{Flow}}$ of south zone against the diversity factor (red line), as shown in Figure 0.20. The band between the yellow and purple

lines has a width of 4 standard deviations. The correlation between the zone level $\text{Diff}_{\text{Flow}}$ and the diversity factor gets weak with the increase of the alignment factor. We attempt to derive the linear correlation between the diversity factors and the $\text{Diff}_{\text{Flow}}$ of ICA instead of the $\text{Diff}_{\text{Flow}}$ of the entire thermal zone.

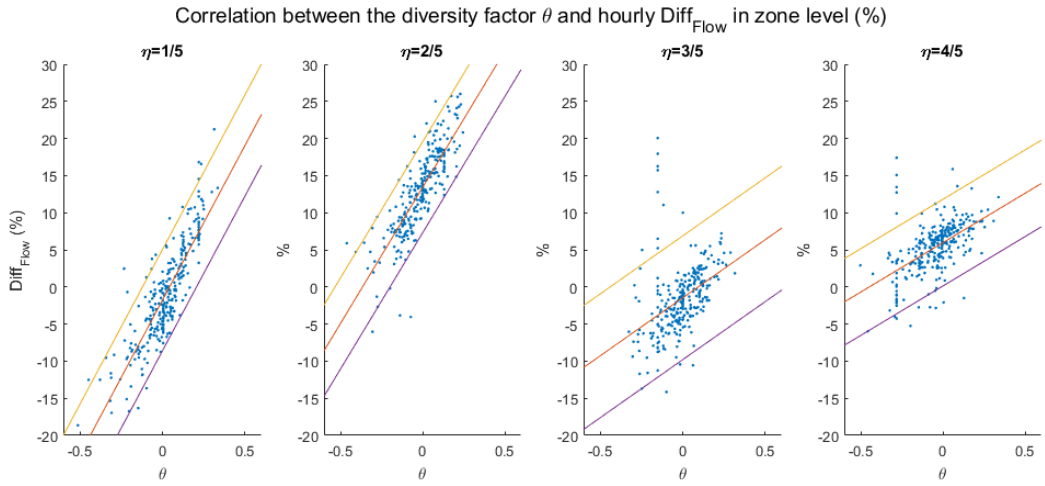

Figure 0.20 Correlation between the diversity factor ($\boldsymbol{\theta}$) and hourly $\mathbf{Diff_{Flow}}$ (%) in the overall south perimeter zone for single façade case

Figure 0.21 shows the correlation between the $\text{Diff}_{\text{Flow}}$ of ICA and the diversity factor by performing a linear regression. The band between the yellow and purple lines has a width of 4 standard deviations. The fitted linear equations are shown in Table 0.6.

Table 0.6 Fitted linear equations of the $\mathbf{Diff_{Flow}}$ (%) of ICA against diversity factor ($\boldsymbol{\theta}$) for single façade case

η	Fitted equations
1/5	$\text{Diff}_{\text{Flow}} = 0.54\theta - 0.03 + \varepsilon, \varepsilon \sim N(0,0.04), R^2 = 0.75$
2/5	$\text{Diff}_{\text{Flow}} = 0.67\theta + 0.21 + \varepsilon, \varepsilon \sim N(0,0.05), R^2 = 0.75$
3/5	$\text{Diff}_{\text{Flow}} = 0.46\theta - 0.10 + \varepsilon, \varepsilon \sim N(0,0.05), R^2 = 0.58$
4/5	$\text{Diff}_{\text{Flow}} = 0.65\theta + 0.15 + \varepsilon, \varepsilon \sim N(0,0.06), R^2 = 0.72$

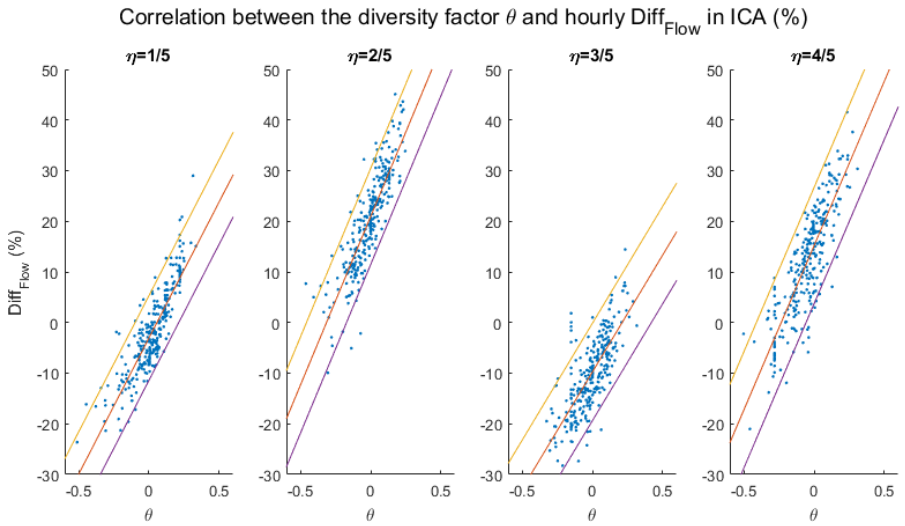

Figure 0.21 Correlation between the diversity factor ($\boldsymbol{\theta}$) and hourly $\mathbf{Diff_{Flow}}$ (%) of ICA for single façade case

1.17 Two external façades case

1.17.1 Model configurations

The zone of interest in the two external façades case has only two orientations with external façade and all other zone boundaries adjacent to other indoor areas. We partition the service area of the VAV terminal boxes as shown in Figure 0.22a. We select the southwest perimeter zone as the area of interest to conduct the study. The area of southwest perimeter zone is 162.5m^2 with a south external facade of 22.5m and a west external facade of 15m. We assume the entire southwest perimeter zone are office area and the occupants share the similar space using pattern, therefore, the spatial distribution of the internal heat gain densities can be described by normal distribution functions. The five sub-zone configurations with different alignment factor values are shown from Figure 0.22b to Figure 0.22f. The marked area is the directly controlled area. The basic control strategies

and setpoints of the HVAC system in the low-fidelity model and Modelica model are the same as the settings in the preliminary study in Chapter 4.

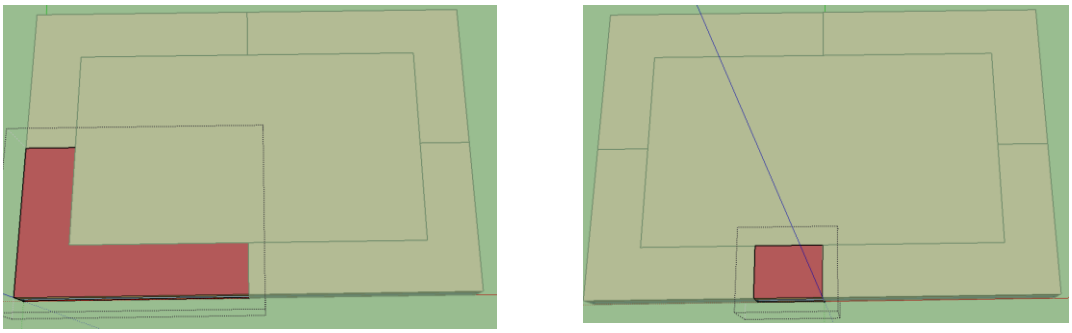

a. Zone configuration with double external façades

b. $\eta = 1/5$

c. $\eta = 2/5$

d. $\eta = 3/5$

e. $\eta = 4/5$

f. $\eta = 1$

Figure 0.22 Zoning configurations of the case with two external façades

1.17.2 Occupancy profile and diversity factor

As same as the single façade case, we use Occupant Simulator to generate the zone level occupant presence schedules for one entire year as the measurement data. The design value of the number of occupants in southwest zone is 9 based on the reference value (18.58m^2/person) of ASHRAE. Figure 0.23 shows the generated occupant presence profile for the southwest perimeter zone from June 1st to July 31st.

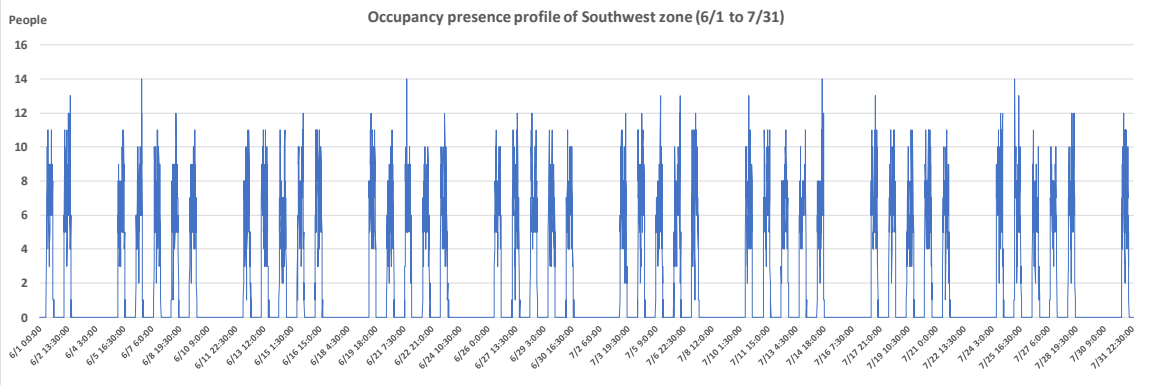

Figure 0.23 The generated occupant presence profile from June 1st to July 31st for the southwest zone

According to the simulation outcomes, the number of occupants in the southwest perimeter zone varies from 1 to 14 people with a mean value of 6 people during the working hours. The mean profile of the lighting and appliance usage and the correlation between the occupant presence and the lighting/appliances usage is derived from Wang's (2016) on-site measurement. Based on the zone level occupancy, lighting and appliance information, we sample the sub-zone level occupancy profiles for each alignment factor configuration by using the method introduced in Chapter 2.4. Then we calculate the corresponding hourly diversity factors in the working hours. Figure 0.24 depicts the distribution of hourly diversity factor in each alignment factor case with a range from -0.5 to 0.5 and a mean value close to 0.

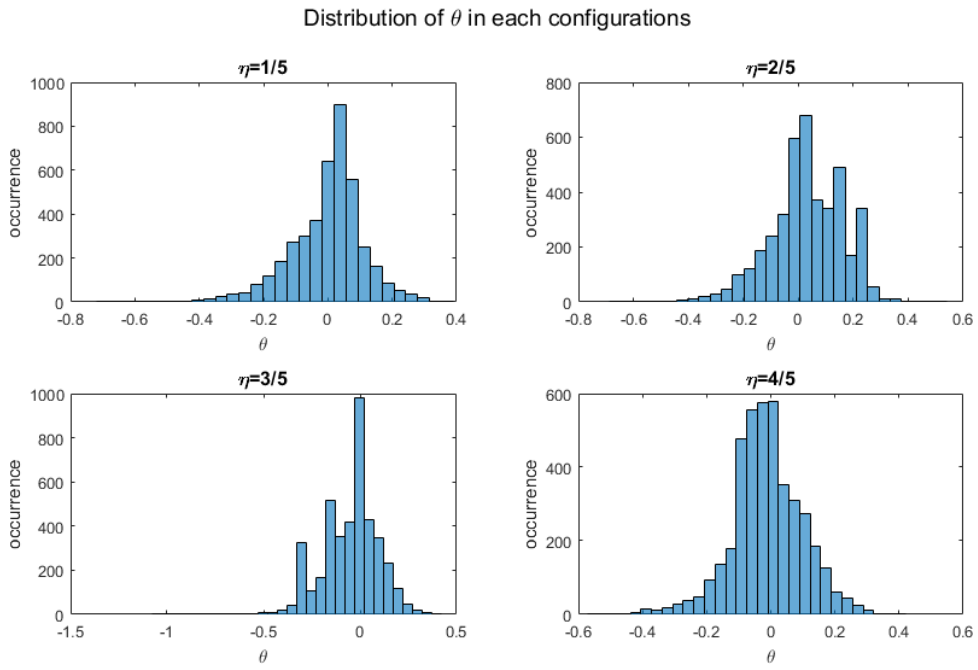

Figure 0.24 Distribution of diversity factor ($\boldsymbol{\theta}$) in two façades case

Figure 0.25 is the boxplot to show the variations of diversity factor for different alignment factor cases. We can see that the medium value is very close to zero, and the spacings between the first quartile and the third quartile is not wide, but with many outliers which may introduce control and discomfort issues into the space.

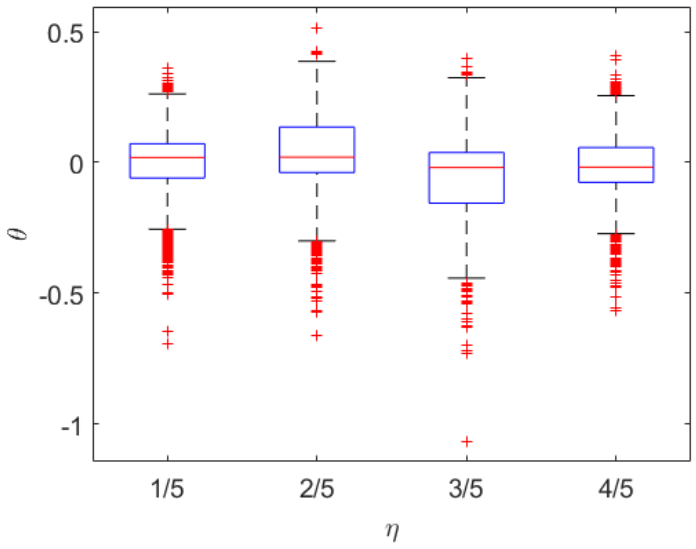

Figure 0.25 Distribution of diversity factor in two façades case

We utilize the sub-zone level occupancy profiles to assign the internal loads in the three models: the aggregated EnergyPlus model (Model-1), the sub-divided EnergyPlus model (Model-2), and the co-simulation model (Model-3). As Model-1 has no sub-zones, we combine the profiles as the zone level input. The simulation period is from 6/24 to 7/31 and the predictions for July are used to conduct the following analysis.

1.17.3 Model-1 vs Model-2

In this section, we compare the outcomes of auto-sizing and the quantities of interest predicted by Model-1 and Model-2. Figure 0.26a shows the design airflow sizes of the VAV box for the southwest perimeter zone given by Model-1 and Model-2. The maximum difference is about 4%, which is larger than the result of the single façade case. Figure 0.26b depicts the correlation between the alignment factor and the ratio of design size for DCA to the design size of the overall southwest perimeter zone. The results indicate that the two models provide similar auto-sizing results at the zone level, but the required

system size for each sub-zone cannot be simply scaled by the alignment factor when the sub-zone area is adjacent to different external thermal boundary conditions (i.e. façade orientations).

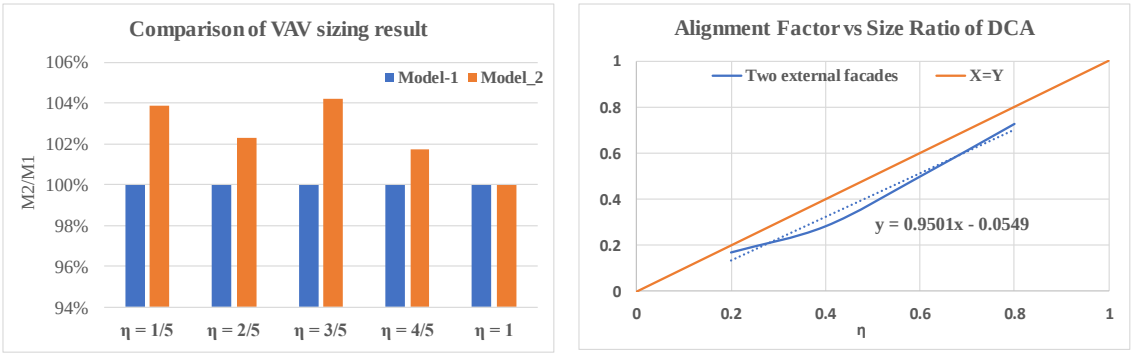

a b

Figure 0.26 Comparison of the auto sizing result between Model-1 and Model-2 for two façades case

Figure 0.27 shows the differences of the hourly outcomes in the southwest perimeter zone between Model-1 and Model-2 for the five alignment cases in room air temperature (RT), supply air flowrate (AF), delivered cooling (Q), and fan power (FP). The comparison reveals that the temperature results show consistence between the two models. The other predicted quantities of interest show that the medium value is very close to zero, and the spacings between the first quartile and the third quartile is narrow, but many outliers exist with indicating a wide distribution with long tails. However, the outliers have apparently little impact on the monthly result as the differences are no larger than 1.5% shown in Figure 0.28.

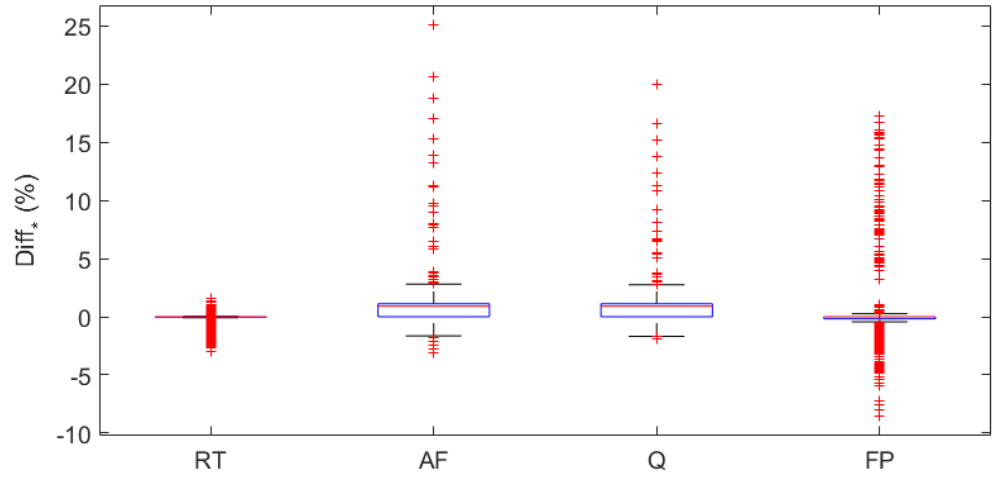

Figure 0.27 Outcome comparison between Model-1 and Model-2 for two façades case

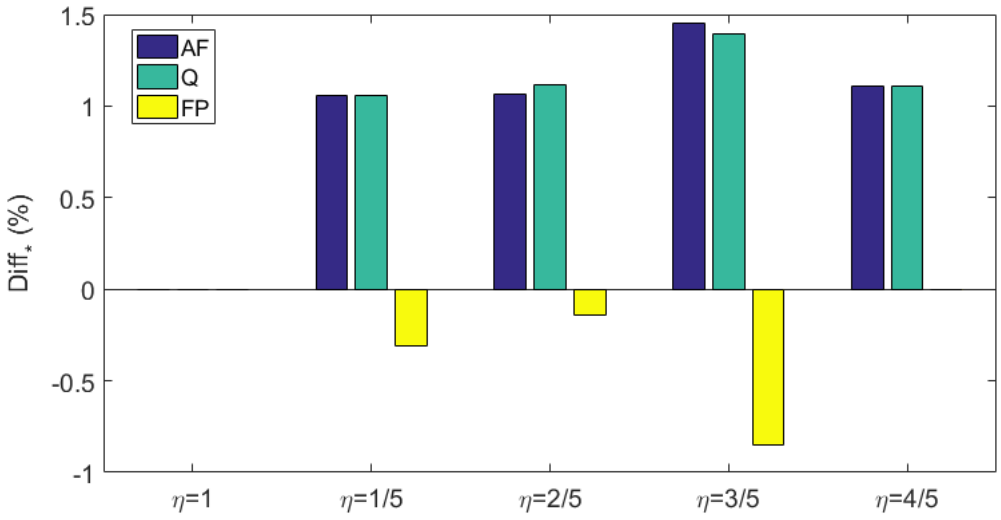

Figure 0.28 Differences of monthly predictions between Model-1 and Model-2 for two façades case

1.17.4 Data pre-processing

Similar to the single façade case there is the need to eliminate the impact of the transition period. For this reason, we take similar action, i.e. by removing the datapoints of the first and the last operating hour of HVAC system from the dataset and conduct the curve fitting analysis discussed below.

1.17.5 Impact on space air temperature

Figure 0.29 shows the histogram of the differences between Model-2 and Model-3 predicted hourly space air temperature. The dataset includes 1,176 occupied hour data for the cases with the alignment factor 1/5, 2/5, 3/5, and 4/5. The left figure shows that the two models predict similar space air temperature in DCA. On the other hand, the right figure shows noticeable bias in the space air temperature of ICA predicted by Model-2 and Model-3. By performing a Gaussian distribution fitting, we obtain $Diff_{T,ICA} \sim N(-1.33, 0.5)$; the result indicates that in reality the limited controllability of HVAC system may not meet the space temperature requirement for office areas located in a perimeter zone with multiple façade orientation exposures.

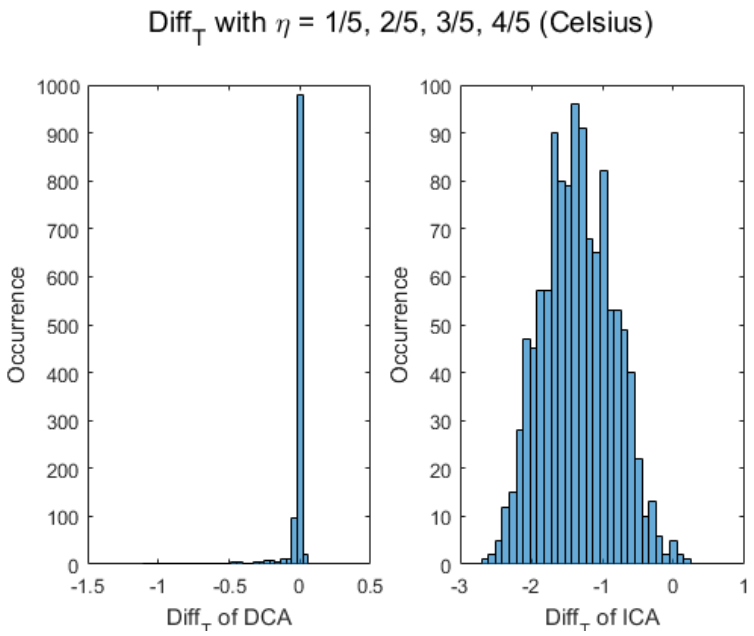

Figure 0.29 $\mathbf{Diff_T}$ between the prediction of Model-2 and Model-3 when $\boldsymbol{\eta}$ = 1/5, 2/5, 3/5, 4/5 for two façades case

From the fixed daily occupancy schedule case, we learned that the diverse occupant usage in the ICA may be the root cause of the differences. To correlate the $Diff_T$ with

situational parameters, we perform a linear regression fitting to the $\mathrm{Diff_T}$ term against the diversity factor with the unit of temperature as Celsius. As same as the single façade case, we use the sampled time series sub-zone level occupant usage profile we introduced in Section 5.2.2 to assign the occupant usage in the models. And the diversity factor for each hour is calculated accordingly. Figure 0.30 shows the correlation between the diversity factor and the $\mathrm{Diff_T}$ in each alignment case (red line). The fitted coefficients are shown in Table 0.7. The band between the yellow and purple lines has a width of 4 standard deviations. The linear fitting results depict that the correlations between diversity and $\mathrm{Diff_T}$ become weak when the sub-zone area is impacted by both façades.

Table 0.7 Fitted linear equations for $\mathbf{Diff_T}$ of ICA (Celsius) against diversity factor ($\boldsymbol{\theta}$) for two façades case

η	Fitted equations
1/5	$\mathrm{Diff_T} = -1.71\theta - 0.77 + \varepsilon, \varepsilon \sim \mathrm{N}(0,0.23), R^2 = 0.46$
2/5	$\mathrm{Diff_T} = -1.89\theta - 1.59 + \varepsilon, \varepsilon \sim \mathrm{N}(0,0.25), R^2 = 0.55$
3/5	$\mathrm{Diff_T} = -1.32\theta - 1.71 + \varepsilon, \varepsilon \sim \mathrm{N}(0,0.32), R^2 = 0.32$
4/5	$\mathrm{Diff_T} = -1.55\theta - 1.32 + \varepsilon, \varepsilon \sim \mathrm{N}(0,0.23), R^2 = 0.40$

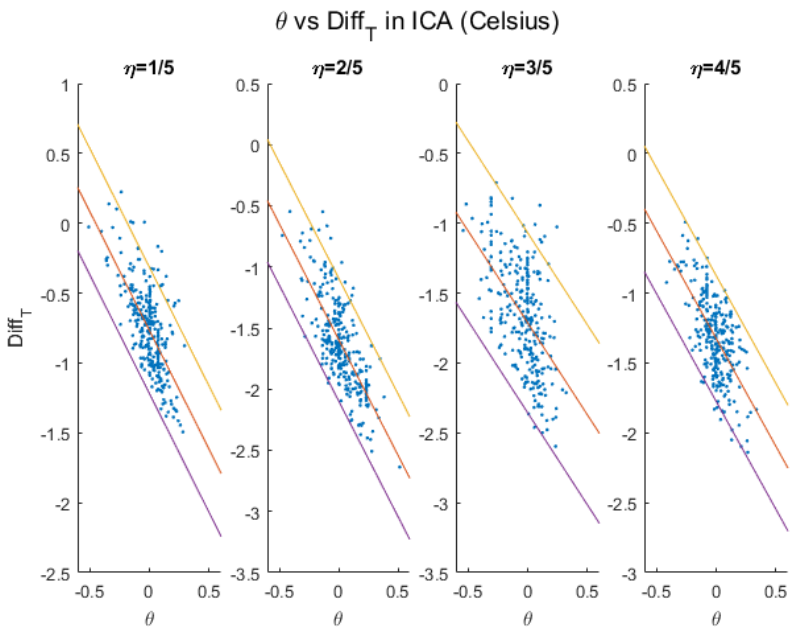

Figure 0.30 $\mathbf{Diff_T}$ (Celsius) of ICA as function of diversity for two façades case

With outcomes of space air temperature, we calculate the number of unmet hours during the occupied period (weekday from 8 am to 9 pm) in July to evaluate thermal comfort: an hour will be counted as an unmet hour if the space air temperature is outside of the setpoint plus or minus 1℃. The dataset includes 294 occupied hours in July for each alignment case and the number of unmet hours is shown in Figure 0.31. It proves that Model-2 and Model-3 has similar predictions of the unmet hours for the DCA, while EnergyPlus underestimates the unmet hours in the ICA. The result indicates that in reality the space can experience severe comfort issue because the HVAC system operates with limited controllability which is unrecognized by Model-2.

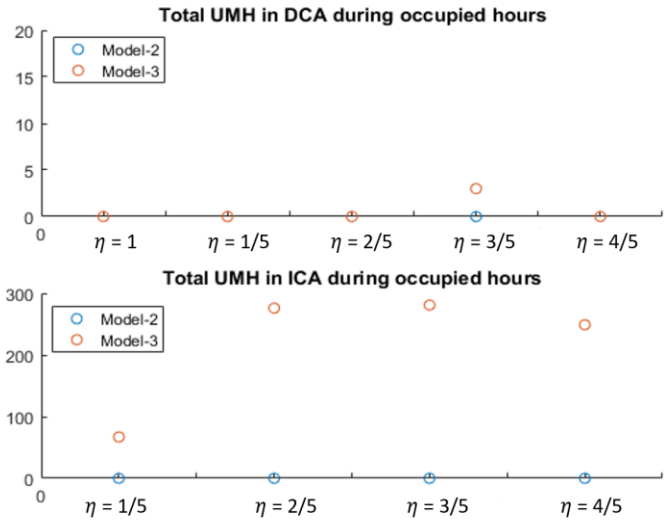

Figure 0.31 Predicted unmet hours by Model-2 and Model-3

1.17.6 Impact on delivered cooling energy

We firstly calculate the hourly $\text{Diff}_{\text{Cooling}}$ between the outcomes of Model-2 and Model-3 for the southwest perimeter zone as a whole. The $\text{Diff}_{\text{Cooling}}$ is calculated based on the equation shown in the preliminary study in Chapter 4.

The dataset, containing 1,470 datapoints, is divided into two groups: the first group includes 294 datapoint of the case with alignment factor 1, and the second group contains the remaining 1,176 datapoints of the other four cases with alignment factor 1/5, 2/5, 3/5 and 4/5. The left figure in Figure 0.32 depicts the distribution of data group one; and the right figure presents the distribution of the data group two. By performing a distribution fitting, we obtain: $Diff_{cooling,\eta=1} \sim Logistic(0.075, 0.003)$ and $Diff_{cooling,\eta\neq1} \sim LogLogistic(-0.08, 0.22, 6.46)$. When $\eta = 1$, the $\text{Diff}_{\text{Cooling}}$ have a positive mean value (5%) with a narrow distribution which illustrates that the EnergyPlus

model slightly underestimates the delivered cooling energy. When $\eta \neq 1$, the $\mathrm{Diff}_{\mathrm{Cooling}}$ have a much wider distribution, up to 40%.

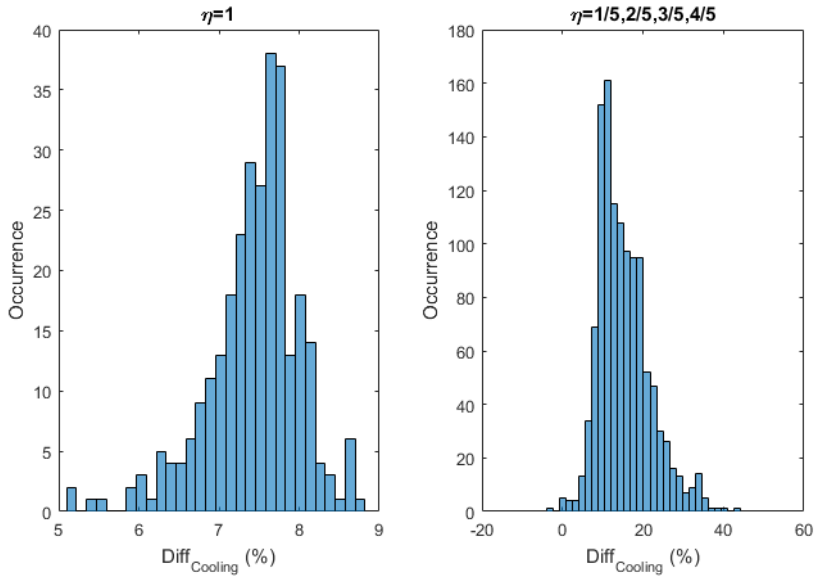

Figure 0.32 Distribution of $\mathbf{Diff_{Cooling}}$ between the prediction of Model-2 and Model-3 for two façades case

We plot the distribution of $\mathrm{Diff}_{\mathrm{Cooling}}$ for each alignment factor and perform distribution fitting for the $\mathrm{Diff}_{\mathrm{Cooling}}$ (%) with the coefficients shown as Table 0.8.

Table 0.8 Fitted distributions of $\mathbf{Diff_{Cooling}}$ for each alignment factor

$\eta = 1/5$	$\eta = 2/5$	$\eta = 3/5$	$\eta = 4/5$
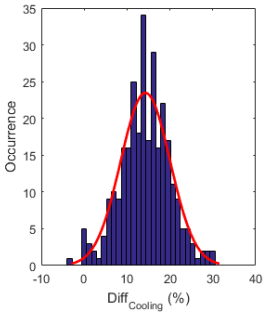	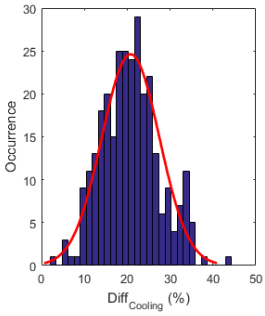	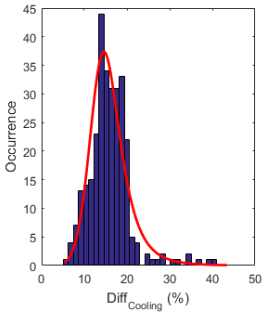	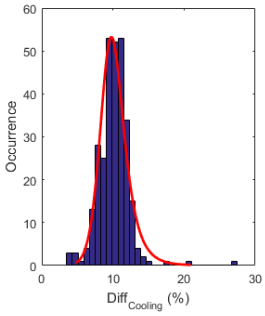
$N(0.143,0.057)$	$N(0.208,0.067)$	$LL(-0.045,0.20,8.3)$	$LL(-0.21,0.31,28.8)$

To investigate the impact of the diversity factor on the delivered cooling energy, we plot the correlation between the diversity factor and the $\mathrm{Diff}_{\mathrm{Cooling}}$ for each alignment factor. Based on the knowledge we learned from the single façade case, we derive the linear correlation between the diversity factors and the $\mathrm{Diff}_{\mathrm{Cooling}}$ of ICA (red line), as shown in Figure 0.33. The fitted linear equations are shown in Table 0.9. The band between the yellow and purple lines has a width of 4 standard deviations.

The result shows that the correlation between the diversity factor and the $\mathrm{Diff}_{\mathrm{Cooling}}$ of ICA become weaker when the sub-zone area is impacted by both facades.

Table 0.9 Fitted linear equations of hourly $\mathbf{Diff_{Cooling}}$ (%) of ICA against diversity factor ($\boldsymbol{\theta}$) for two façades case

η	Fitted equations
1/5	$\mathrm{Diff}_{\mathrm{Cooling}} = 0.46\theta + 0.17 + \varepsilon, \varepsilon \sim \mathrm{N}(0,0.05), R^2 = 0.57$
2/5	$\mathrm{Diff}_{\mathrm{Cooling}} = 0.70\theta + 0.30 + \varepsilon, \varepsilon \sim \mathrm{N}(0,0.07), R^2 = 0.67$
3/5	$\mathrm{Diff}_{\mathrm{Cooling}} = 0.30\theta + 0.34 + \varepsilon, \varepsilon \sim \mathrm{N}(0,0.09), R^2 = 0.23$
4/5	$\mathrm{Diff}_{\mathrm{Cooling}} = 0.44\theta + 0.28 + \varepsilon, \varepsilon \sim \mathrm{N}(0,0.06), R^2 = 0.40$

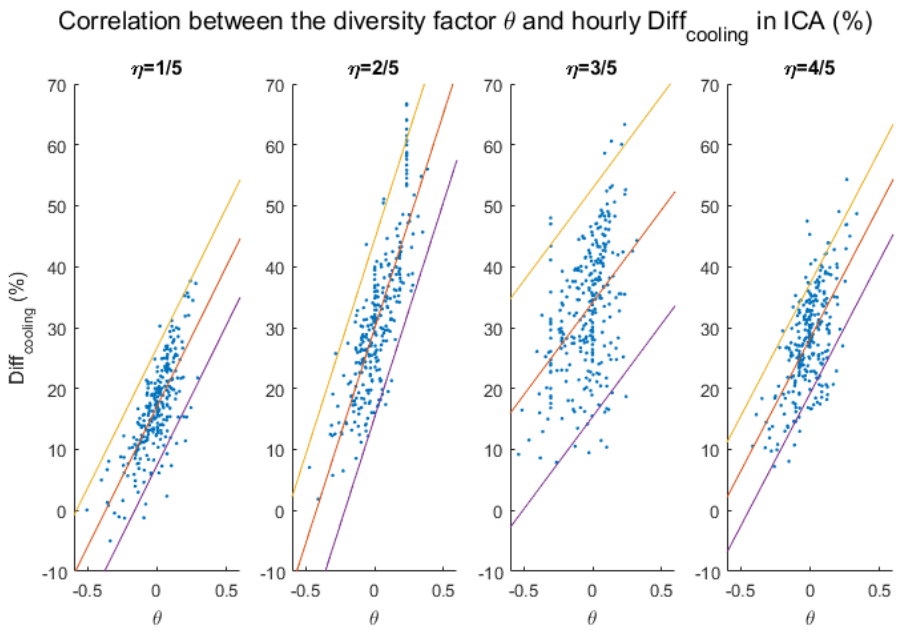

Figure 0.33 **$\mathbf{Diff_{Cooling}}$** (%) of ICA as function of diversity for two façades case

The abovementioned cooling energy is for hourly intervals. This needs to repeated daily and monthly intervals. The dataset of daily $\mathrm{Diff_{Cooling}}$ for the southwest zone contains 105 datapoints for the five alignment factor cases. Figure 0.34 depicts the distribution of daily $\mathrm{Diff_{Cooling}}$ for southwest perimeter zone as a whole. The result presents the daily cooling predicted by the EnergyPlus model is on average 60 Wh/m2 smaller than the outcomes of co-simulation model, which means that it underpredicts the real cooling energy on a daily basis by around 15%.

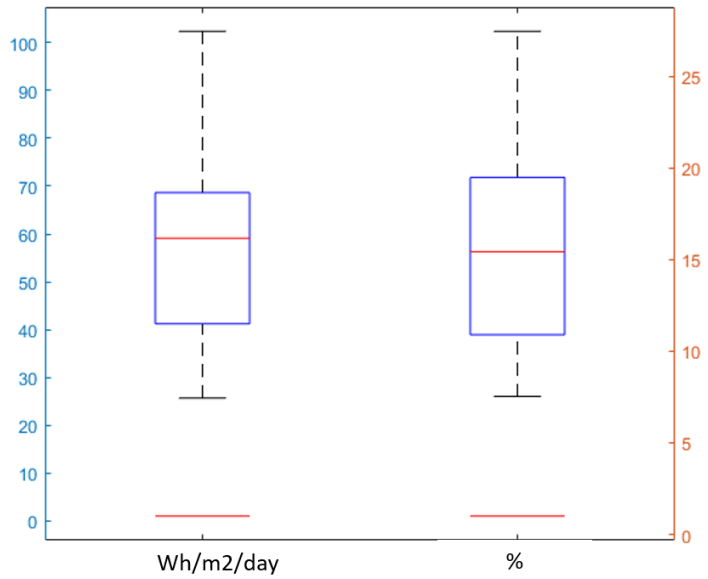

Figure 0.34 Distribution of daily **$\mathbf{Diff_{Cooling}}$** for two façades case

Figure 0.35 displays the comparison of predicted monthly delivered cooling energy between the EnergyPlus model and the co-simulation model. The left figure depicts the predicted delivered cooling energy per square meter, the yellow bar is the outcomes of EnergyPlus model while the blue bar is the result of co-simulation model. We can see the $\mathrm{Diff_{Cooling}}$ are more noticeable when the misalignment is present in the thermal zone. The right figure shows the percentage of monthly $\mathrm{Diff_{Cooling}}$. The result presents that $\mathrm{Diff_{Cooling}}$ can reach to 8% when we include a detailed HVAC system with imperfect control in Model-3 with an alignment factor at 1; and the $\mathrm{Diff_{Cooling}}$ further increases by 8% to 18% for the cases with an alignment factor at 1/5, 2/5, 3/5, and 4/5. It confirms that misalignment impacts significantly on the prediction of delivered cooling energy.

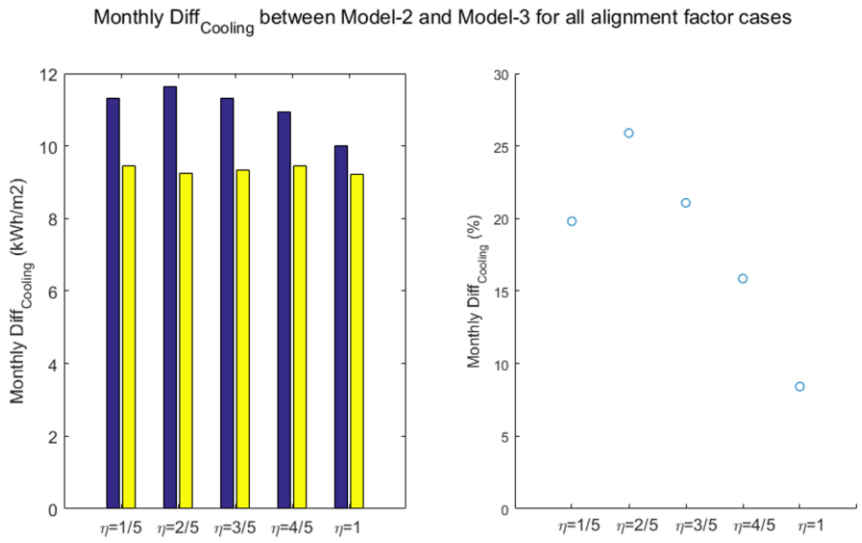

Figure 0.35 Comparison between Model-2 and Model-3 in monthly cooling energy for two façades case

1.17.7 Impact on air flowrate

The difference of flowrate is presented as a percentage calculated by the equation introduced in Chapter 4 for the fixed daily occupancy schedules. The dataset contains 294 datapoints for alignment factor 1, and 1,176 datapoints for alignment factor as 1/5, 2/5, 3/5, and 4/5. Figure 0.36 shows the hourly $\text{Diff}_{\text{Flow}}$ between Model-2 and Model-3. The $\text{Diff}_{\text{Flow}}$ in Figure 0.36 is for the total supply air flowrate of the VAV box. The left figure shows that $\text{Diff}_{\text{Flow}}$ has a narrow range mainly from 3% to 9% with a mean value at 5.3%, which follows a loglogistic distribution $LL(-0.07,0.12,21.8)$. It illustrates that the EnergyPlus model slightly underestimates the supply air flowrate when no misalignment occurs for two external façades case. This is mainly caused by the imperfect control in the real control system. The right figure in Figure 0.36 shows the distribution of $\text{Diff}_{\text{Flow}}$ for alignment factor 1/5, 2/5, 3/5, and 4/5. By performing a Lognormal distribution fitting, we obtain: $Diff_{flow,\eta\neq1} \sim Lognormal(0.42,0.16)$. The mean value of the $\text{Diff}_{\text{Flow}}$ is 22%

with much wider distribution than that for the no-misaligned case, which again confirms that misalignment impacts significantly on the flowrate prediction.

We plot the distribution of $\mathrm{Diff}_{\mathrm{Flow}}$ for the four alignment factor cases and perform distribution fittings, the results shown as Table 0.8.

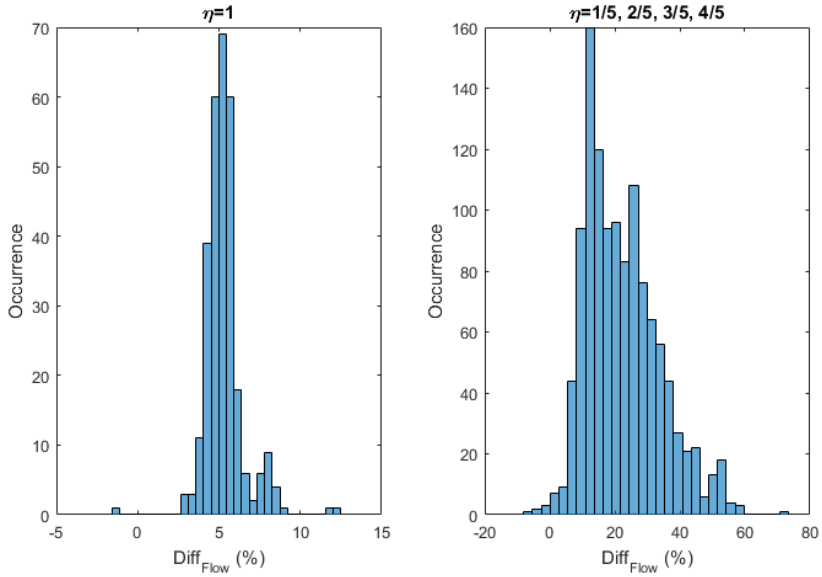

Figure 0.36 Distribution of $\mathbf{Diff_{Flow}}$ between the predictions of Model-2 and Model-3 for two façades case

Table 0.10 Fitted distributions of $\mathbf{Diff_{Flow}}$ for two façades case

$\eta = 1/5$	$\eta = 2/5$	$\eta = 3/5$	$\eta = 4/5$
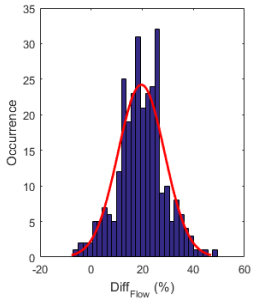	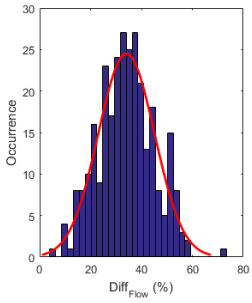	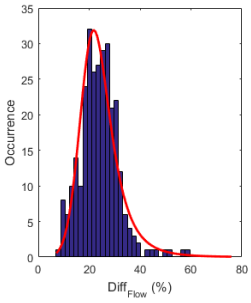	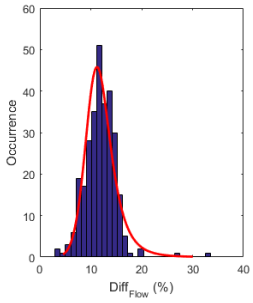
$N(0.196,0.091)$	$N(0.341,0.111)$	$LL(-0.252,0.487,12)$	$LL(-0.271,0.39,24.1)$

To investigate the impact of diversity factor on the supply air flowrate, we plot the correlation between the diversity factor and the $\text{Diff}_{\text{Flow}}$ for each alignment factor case. Based on the knowledge we learned from the single façade case, we derive the linear correlation between the $\text{Diff}_{\text{Flow}}$ of ICA against the diversity factor, as shown in Figure 0.37. The band between the yellow and purple lines has a width of 4 standard deviations. The fitted linear equations are shown in Table 0.11.

Table 0.11 Fitted linear equations of the $\mathbf{Diff_{Flow}}$ (%) of ICA against diversity factor ($\boldsymbol{\theta}$) for two façades case

η	Fitted equations
1/5	$\text{Diff}_{\text{Flow}} = 0.70\theta + 0.24 + \varepsilon, \varepsilon \sim \text{N}(0,0.08), R^2 = 0.53$
2/5	$\text{Diff}_{\text{Flow}} = 1.16\theta + 0.52 + \varepsilon, \varepsilon \sim \text{N}(0,0.12), R^2 = 0.67$
3/5	$\text{Diff}_{\text{Flow}} = 0.60\theta + 0.59 + \varepsilon, \varepsilon \sim \text{N}(0,0.16), R^2 = 0.28$
4/5	$\text{Diff}_{\text{Flow}} = 0.75\theta + 0.45 + \varepsilon, \varepsilon \sim \text{N}(0,0.10), R^2 = 0.43$

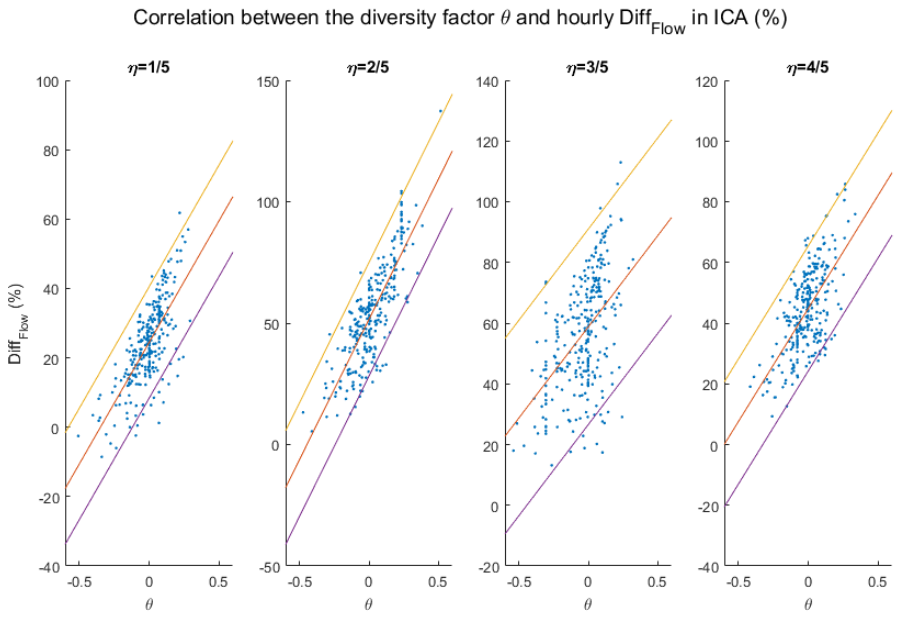

Figure 0.37 Correlation between the diversity factor ($\boldsymbol{\theta}$) and hourly $\mathbf{Diff_{Flow}}$ (%) of ICA for two façades case

1.18 Interior case

1.18.1 Model configurations

The zone of interest in the interior case is the central area of the second floor with all boundaries adjacent to indoor conditioned areas. We partition the service area of the VAV terminal boxes as shown in Figure 0.38. The area of core zone is 700m^2 with a length of 35m and a width of 20m. We assume the entire zone are office area and the occupants share the similar space using pattern. Therefore, the spatial distribution of the internal heat gain densities can be described by normal distribution functions. The five sub-zone configurations with different alignment factor values are shown from Figure 0.38b to Figure 0.38f. The marked area is the directly controlled area. The basic control strategies and setpoints of the HVAC system in the low-fidelity model and Modelica model are the same as the settings in the preliminary study in Chapter 4.

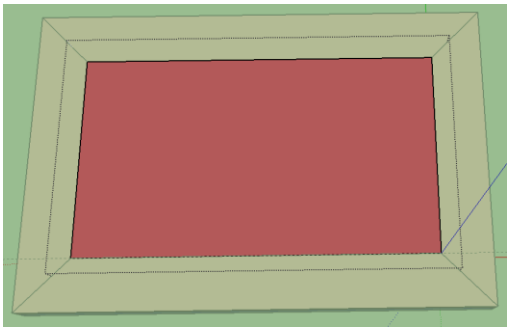

a. Zone with no external façade

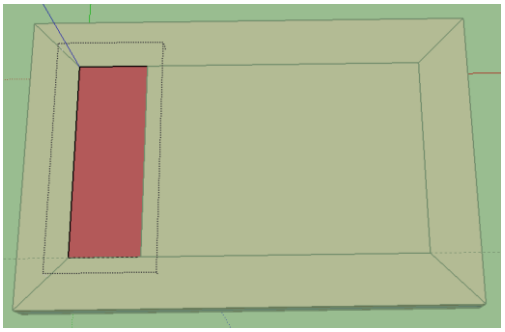

b. $\eta = 1/5$

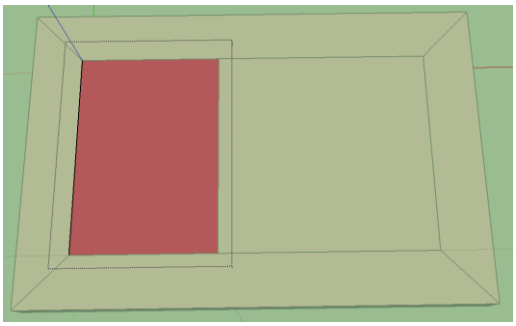

c. $\eta = 2/5$

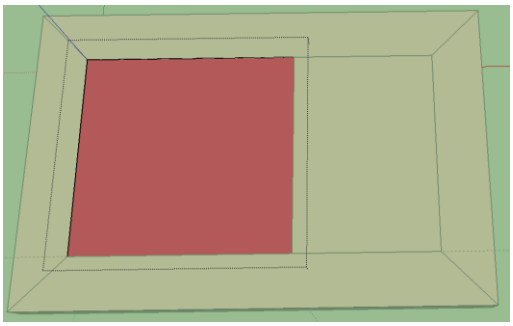

d. $\eta = 3/5$

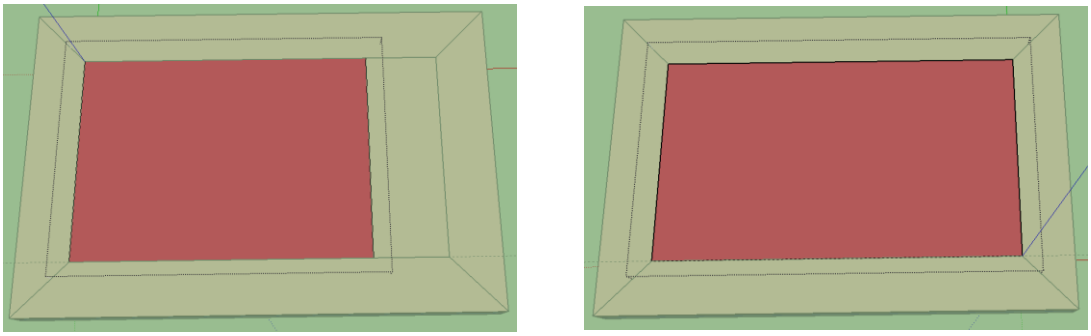

e. $\eta = 4/5$ f. $\eta = 1$

Figure 0.38 Zoning configurations of the interior case

1.18.2 Occupancy profile and diversity factor

As same as the case studies above, we use Occupant Simulator to generate the zone level occupant presence schedules as the measurement data. The design value of the number of occupants in core zone is 38 based on the reference value (18.58m^2/person) of ASHRAE. Figure 0.39 shows the generated occupant presence profile for core zone from June 1st to July 31st.

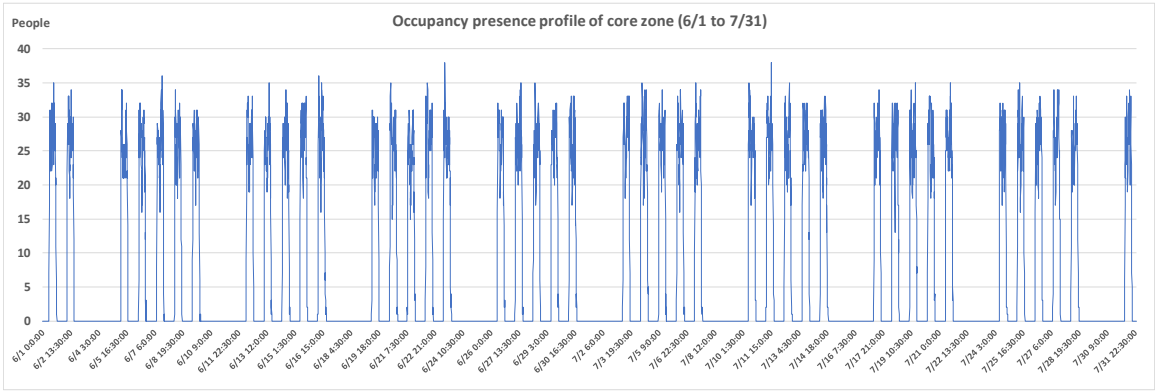

Figure 0.39 The generated occupant presence profile from June 1st to July 31st for the core zone

According to the simulation outcomes, the number of occupants in the core zone varies from 1 to 38 people with a mean value of 23 people during the working hours. The

mean profile of the lighting and appliance usage and the correlation between the occupant presence and the lighting/appliances usage is derived from Wang's (2016) on-site measurement. Based on the zone level occupancy, lighting and appliance information, we sample the hourly sub-zone level occupancy profiles for each alignment factor configuration by using the method introduced in Chapter 2.4. Then we calculate the corresponding hourly diversity factors in the working hours. Figure 0.40 depicts the distribution of diversity factor in each alignment factor. The range of diversity factor is mainly from -0.4 to 0.4 with the mean value close to 0.

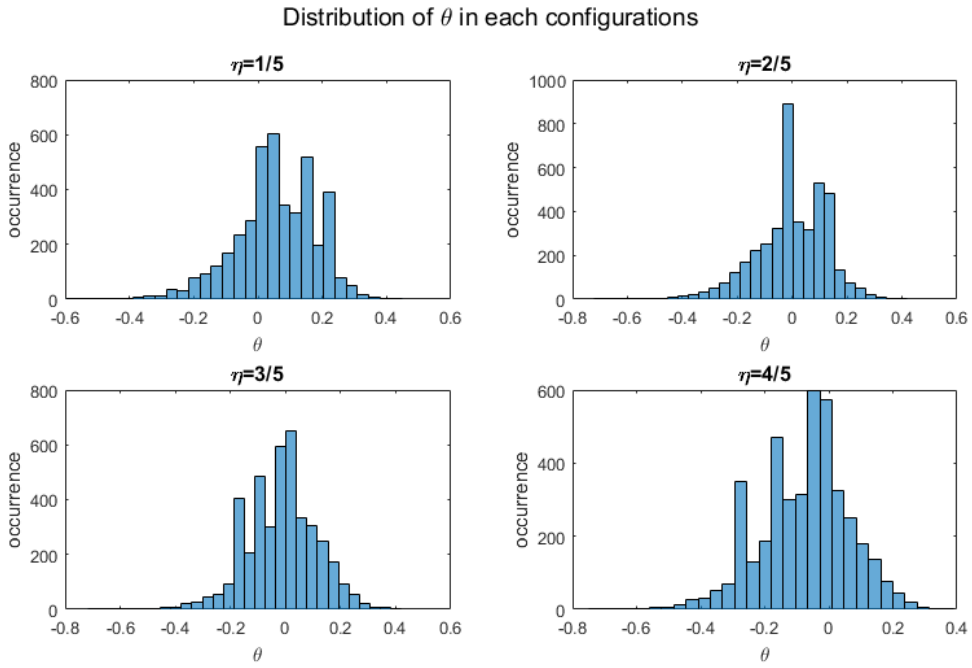

Figure 0.40 Distribution of diversity factor ($\boldsymbol{\theta}$) for interior case

Figure 0.41 is the boxplot to show the variations of diversity factor for different alignment factor cases. We can see that the medium value is very close to zero, and the spacings between the first quartile and the third quartile is not wide, but with many outliers which may introduce control and discomfort issues into the space.

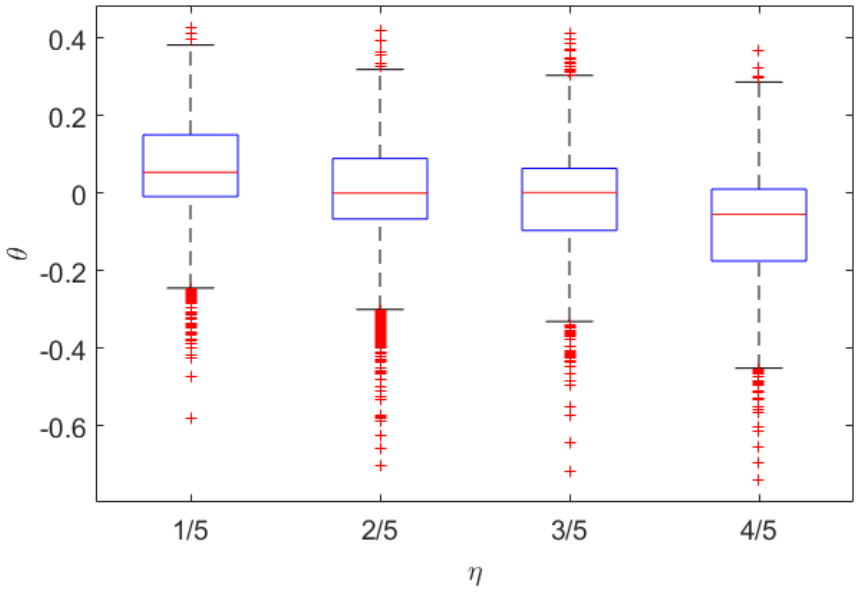

Figure 0.41 Distribution of diversity factor ($\boldsymbol{\theta}$) for interior case

We utilize the sub-zone level occupancy profiles to assign the internal loads in the three models: the aggregated EnergyPlus model (Model-1), the sub-divided EnergyPlus model (Model-2), and the co-simulation model (Model-3). As Model-1 has no sub-zones, we combine the profiles as the zone level input. The simulation period is from 6/24 to 7/31 and the predictions for July are used to conduct the following analysis.

1.18.3 Model-1 vs Model-2

In this section, we compare the outcomes of auto-sizing and the quantities of interest predicted by Model-1 and Model-2. Figure 0.42a shows the design airflow sizes of VAV box for the core zone given by Model-1 and Model-2. The maximum difference is about 5%. Figure 0.42b depicts the correlation between the alignment factor and the ratio of design size for DCA to the design size of the overall core zone. The results illustrate that two models provide similar auto-sizing results at the zone level and the design size of the

virtual VAV boxes at the sub-zone level can in fact be derived based on the value of the alignment factor in the interior case.

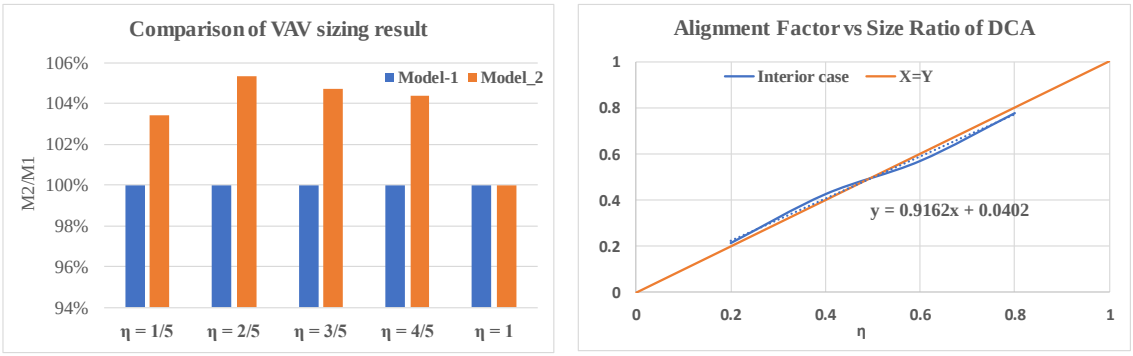

a b

Figure 0.42 Comparison of the auto sizing result between Model-1 and Model-2 for interior case

Figure 0.43 shows the differences of the hourly outcomes in the core zone between Model-1 and Model-2 for the five alignment cases in room air temperature (RT), supply air flowrate (AF), delivered cooling (Q), and fan power (FP). The comparison depicts that increasing the fidelity of EnergyPlus model from zone level to sub-zone level has little impact on the simulation outcomes for the interior thermal zone.

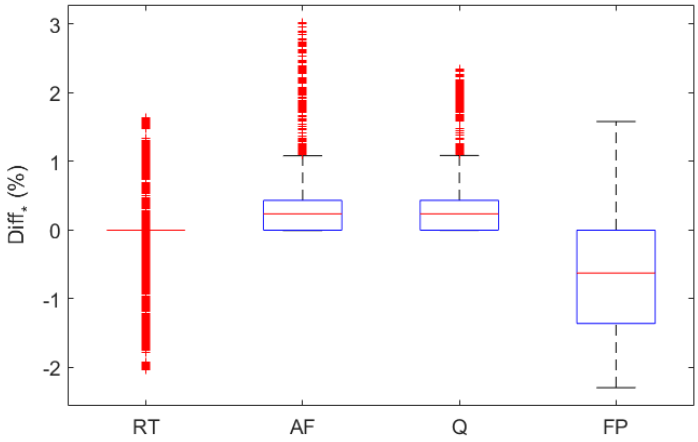

Figure 0.43 Outcome comparison between Model-1 and Model-2 for interior case

1.18.4 Data pre-process

Similar to the single façade case there is the need to eliminate the impact of the transition period. For this reason, we take similar action, i.e. by removing the datapoints of the first and the last operating hour of HVAC system from the dataset and conduct the curve fitting analysis discussed below.

1.18.5 Impact on space air temperature

Figure 0.44 shows the histogram of the differences between Model-2 and Model-3 predicted hourly space air temperature. The dataset includes 1,176 occupied hour data for the cases with the alignment factor 1/5, 2/5, 3/5, and 4/5. The left figure shows the two models predict similar space air temperature in DCA. On the other hand, the right figure shows noticeable bias in the space air temperature of ICA predicted by Model-2 and Model-3. By performing a Gaussian distribution fitting, we obtain $Diff_{T,ICA} \sim N(0,0.5)$; the result indicates that in spite of the low fidelity of Model-2 the HVAC system maintains

the space air temperature within an acceptable range for the stated alignment factors. This result applies to the office area located in an interior zone with no external façade.

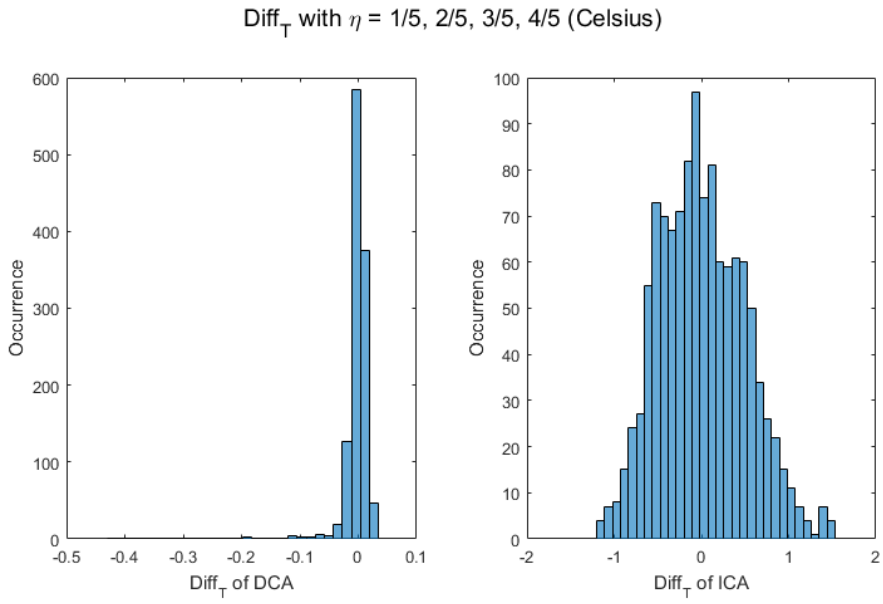

Figure 0.44 $\mathbf{Diff_T}$ between Model-2 and Model-3 when $\boldsymbol{\eta}$ = 1/5, 2/5, 3/5, 4/5 for interior case

From the fixed daily occupancy schedule case, we learned that the diverse occupant usage in the ICA may be the root cause for the discrepancies. To correlate the $\mathrm{Diff_T}$ with situational parameters, we perform a linear regression fitting to the $\mathrm{Diff_T}$ term against the diversity factor with the unit of temperature as Celsius. As same as the single façade case, we use the sampled time series sub-zone level occupant usage profile we introduced in Section 5.3.2 to assign the occupant usage in the models. And the diversity factor for each hour is calculated accordingly. Figure 0.45 shows the correlation between the diversity factor and the $\mathrm{Diff_T}$ in each alignment case (red line). The fitted coefficients are shown in Table 0.12. The band between the yellow and purple lines has a width of 4 standard deviations. The linear fitting results depict that the usage diversity and $\mathrm{Diff_T}$ show linear correlation for the interior case.

Table 0.12 Fitted linear equations for $\mathbf{Diff_T}$ of ICA (Celsius) against diversity factor ($\boldsymbol{\theta}$) for interior case

η	Fitted equations
1/5	$\mathrm{Diff_T} = -2.95\theta + 0.19 + \varepsilon, \varepsilon \sim \mathrm{N}(0,0.28), R^2 = 0.66$
2/5	$\mathrm{Diff_T} = -3.19\theta + 0.25 + \varepsilon, \varepsilon \sim \mathrm{N}(0,0.25), R^2 = 0.74$
3/5	$\mathrm{Diff_T} = -2.79\theta - 0.22 + \varepsilon, \varepsilon \sim \mathrm{N}(0,0.25), R^2 = 0.77$
4/5	$\mathrm{Diff_T} = -2.35\theta - 0.27 + \varepsilon, \varepsilon \sim \mathrm{N}(0,0.24), R^2 = 0.67$

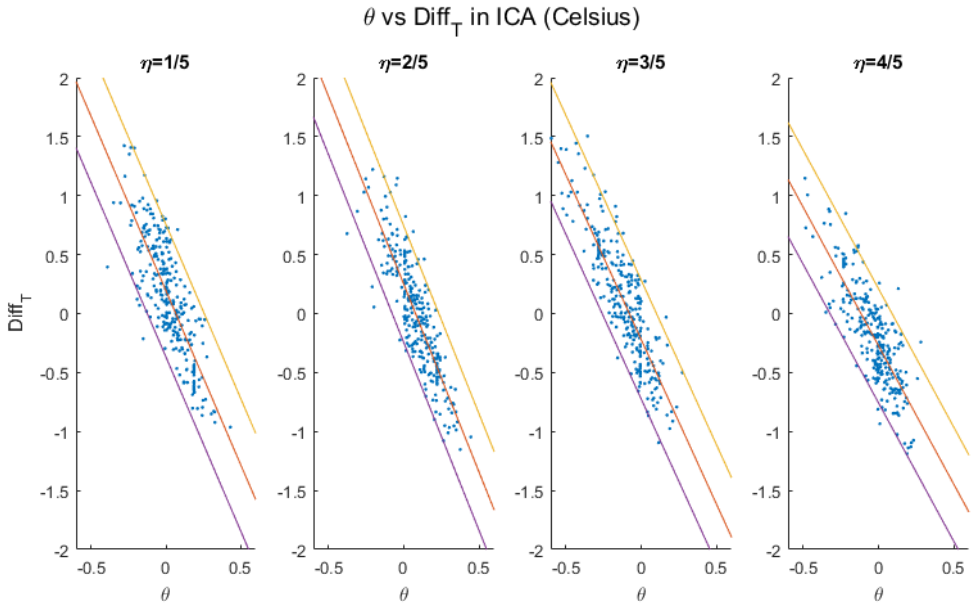

Figure 0.45 $\mathbf{Diff_T}$ (Celsius) of ICA as function of diversity for interior case

According to the outcomes of space air temperature, we calculate the number of unmet hours during the occupied period (weekday from 8 am to 9 pm) in July to evaluate thermal comfort: an hour will be counted as an unmet hour if the space air temperature is outside of the setpoint plus or minus 1℃. The dataset includes 294 occupied hours in July for each alignment case and the number of unmet hours is shown in Figure 0.46. It proves that Model-2 and Model-3 has similar predictions of the unmet hours for the DCA, while EnergyPlus underestimates the unmet hours in the ICA. The result indicates that in reality the space can experience discomfort issue because the HVAC system operates with limited controllability which is unrecognized by Model-2.

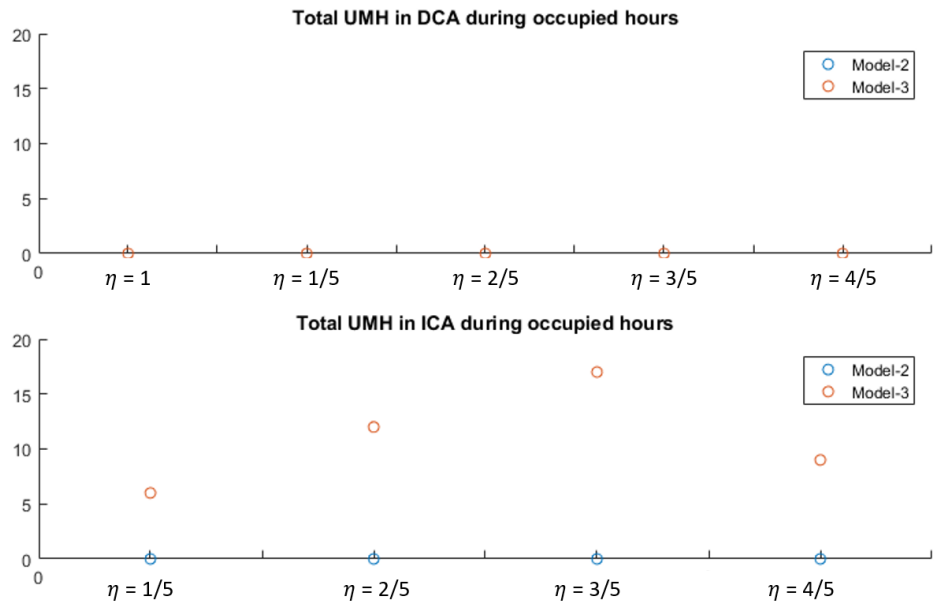

Figure 0.46 Outcomes of unmet hours from Model-2 and Model-3

1.18.6 Impact on delivered cooling energy

We firstly calculate the hourly $\text{Diff}_{\text{Cooling}}$ between the outcomes of Model-2 and Model-3 for the core zone as a whole. The $\text{Diff}_{\text{Cooling}}$ is calculated based on the equation shown in the preliminary study in Chapter 4.

The dataset, containing 1,470 datapoints, is divided into two groups: the first group includes 294 datapoint of the case with alignment factor 1, and the second group contains the remaining 1,176 datapoints of the other four cases with alignment factor 1/5, 2/5, 3/5, and 4/5. The left figure in Figure 0.47 depicts the distribution of data group one; and the right figure presents the distribution of data group two. By performing a distribution fitting, we obtain: $Diff_{cooling,\eta=1} \sim Logistic(0.075, 0.003)$ and $Diff_{cooling,\eta\neq1} \sim N(0.055, 0.059)$. When $\eta = 1$, the $\text{Diff}_{\text{Cooling}}$ have a positive mean value (7.4%) with a narrow distribution which illustrates that the EnergyPlus model slightly

underestimates the delivered cooling energy. When $\eta \neq 1$, the $\mathrm{Diff}_{\mathrm{Cooling}}$ has a much wider distribution and the value can be negative in some cases. Based on the statistic result, the hourly $\mathrm{Diff}_{\mathrm{Cooling}}$ can reach to ±20%. The negative value illustrates that in reality the HVAC system may deliver less cooling than is predicted by the routine EnergyPlus model (Model-2), implying that it does not always meet then required cooling supply.

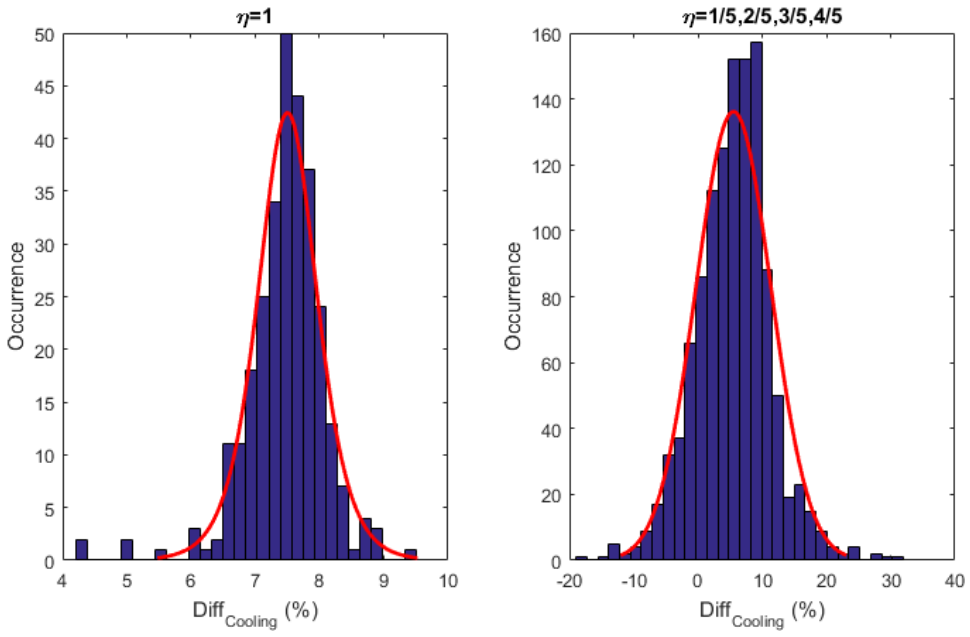

Figure 0.47 Distribution of $\mathbf{Diff_{Cooling}}$ between the predictions of Model-2 and Model-3 for interior case

We plot the distribution of $\mathrm{Diff}_{\mathrm{Cooling}}$ for each alignment factor and perform distribution fitting for the $\mathrm{Diff}_{\mathrm{Cooling}}$ (%) with the coefficients shown as Table 0.13.

Table 0.13 Fitted distributions of $\mathbf{Diff_{Cooling}}$ for interior case

$\eta = 1/5$	$\eta = 2/5$	$\eta = 3/5$	$\eta = 4/5$
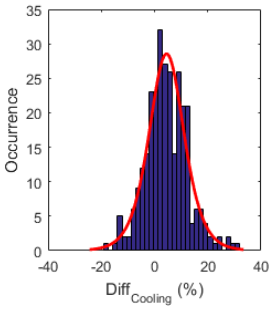	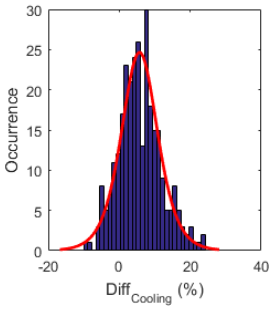	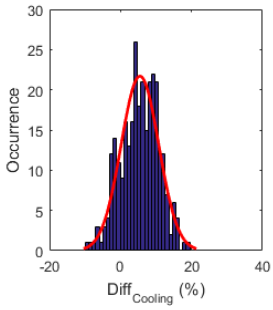	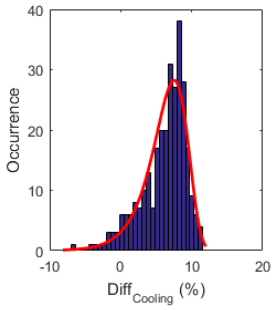
$L(0.045,0.044)$	$L(0.057,0.034)$	$N(0.055,0.053)$	$EV(0.075,0.024)$

To investigate the impact of diversity factor to the delivered cooling energy, we plot the correlation between the diversity factor and the $\text{Diff}_{\text{Cooling}}$ for each alignment factor. Based on the knowledge we learned from the studies above, we derive the linear correlation between the diversity factors and the $\text{Diff}_{\text{Cooling}}$ of ICA (red line), as shown in Figure 0.48. The fitted linear equations are shown in Table 0.14. The band between the yellow and purple lines has a width of 4 standard deviations.

Table 0.14 Fitted linear equations of hourly $\mathbf{Diff_{Cooling}}$ (%) of ICA against diversity factor ($\boldsymbol{\theta}$) for interior case

η	Fitted equations
1/5	$\text{Diff}_{\text{Cooling}} = 0.64\theta + 0.03 + \varepsilon, \varepsilon \sim \text{N}(0,0.05), R^2 = 0.71$
2/5	$\text{Diff}_{\text{Cooling}} = 0.70\theta + 0.01 + \varepsilon, \varepsilon \sim \text{N}(0,0.05), R^2 = 0.74$
3/5	$\text{Diff}_{\text{Cooling}} = 0.58\theta + 0.13 + \varepsilon, \varepsilon \sim \text{N}(0,0.06), R^2 = 0.75$
4/5	$\text{Diff}_{\text{Cooling}} = 0.59\theta + 0.11 + \varepsilon, \varepsilon \sim \text{N}(0,0.06), R^2 = 0.71$

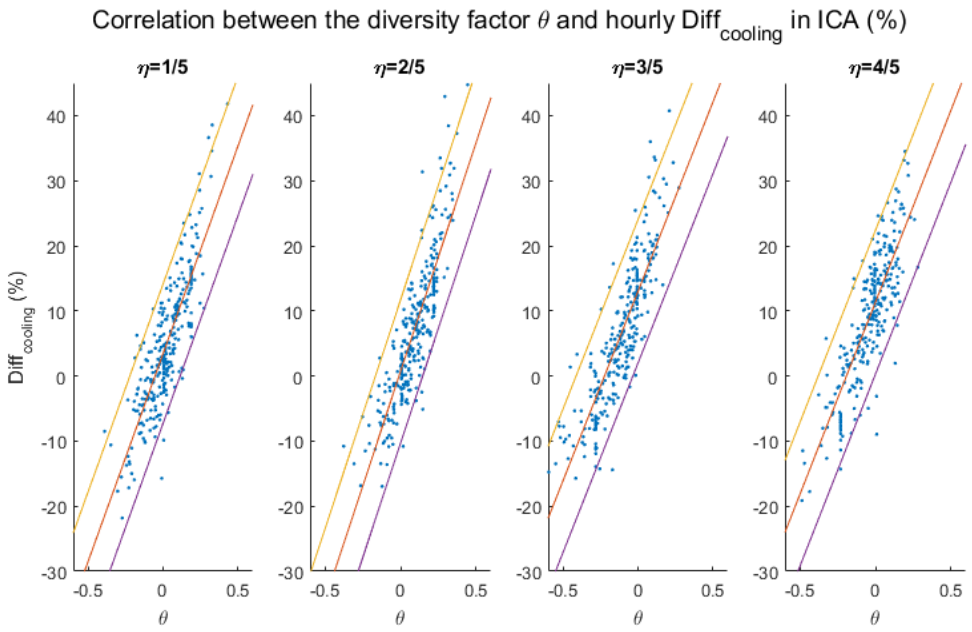

Figure 0.48 **$\mathbf{Diff_{Cooling}}$** (%) of ICA as function of diversity for interior case

The abovementioned cooling energy is for hourly intervals. This needs to repeated daily and monthly intervals. The dataset of daily $Diff_{Cooling}$ for the core zone contains 105 datapoints for the five alignment cases. Figure 0.49 depicts the distribution of daily $Diff_{Cooling}$ for the core zone as a whole. The result presents the daily cooling predicted by the EnergyPlus model is on average 16 Wh/m2 smaller than the outcomes of co-simulation model, which means that it underpredicts the real cooling energy on a daily basis by about 7% of the predicted cooling.

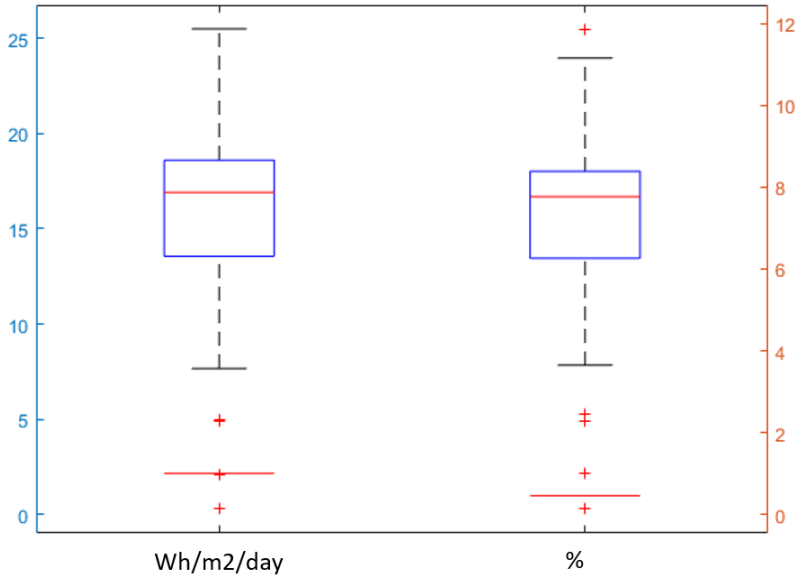

Figure 0.49 Distribution of daily $\mathbf{Diff_{Cooling}}$ for interior case

Figure 0.50 displays the comparison of monthly delivered cooling energy between the EnergyPlus model and the co-simulation model. The left figure depicts the predicted delivered cooling energy per square meter, the yellow bars are the outcomes of EnergyPlus model while the blue bars are the results of co-simulation model. We can see the $\mathrm{Diff_{Cooling}}$ are more noticeable when the misalignment is present in the thermal zone. The right figure shows the percentage of monthly $\mathrm{Diff_{Cooling}}$. The result presents that $\mathrm{Diff_{Cooling}}$ can reach to 8% when we include a detailed HVAC system with imperfect control in Model-3 with an alignment factor at 1; and the $\mathrm{Diff_{Cooling}}$ further increases by 5-6% for the cases with an alignment factor at 1/5, 2/5, 3/5, and 4/5. It confirms that misalignment impacts noticeably on the prediction of delivered cooling energy.

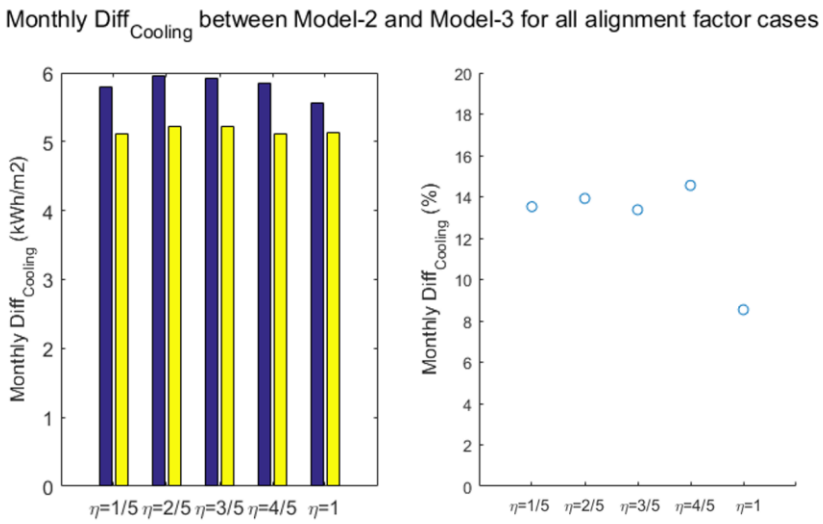

Figure 0.50 Comparison between Model-2 and Model-3 in monthly cooling energy for interior case

1.18.7 Impact on air flowrate

The difference of flowrate is presented as a percentage calculated by the equation introduced in Chapter 4 for the fixed daily occupancy schedules. The dataset contains 294 datapoints for alignment factor 1, and 1,176 datapoints for alignment factor as 1/5, 2/5, 3/5, and 4/5. Figure 0.51 shows the hourly $\text{Diff}_{\text{Flow}}$ between Model-2 and Model-3. The $\text{Diff}_{\text{Flow}}$ in Figure 0.51 is for the total supply air flowrate of the VAV box. The left figure shows that $\text{Diff}_{\text{Flow}}$ has a narrow range mainly from 3% to 9% with a mean value at 5.3%, which follows a logistic distribution: $L(0.053,0.005)$. It illustrates that the EnergyPlus model slightly underestimates the supply air flowrate when no misalignment occurs for interior case. his is mainly caused by the imperfect control in the real control system. The right figure in Figure 0.51 shows the distribution of $\text{Diff}_{\text{Flow}}$ for alignment factor 1/5, 2/5, 3/5, and 4/5. By performing a logistic distribution fitting, we obtain: $Diff_{flow,\eta\neq1} \sim Logistic(0.035,0.044)$ with a mean value at 3.3%. However, the

distribution of the $\mathrm{Diff}_{\mathrm{Flow},\eta\neq1}$ is much wider than that for no-misaligned case, which again confirms that misalignment impacts significantly on the flowrate prediction.

We plot the distribution of $\mathrm{Diff}_{\mathrm{Flow}}$ for the four alignment factor cases and perform distribution fittings, the results shown as Table 0.15.

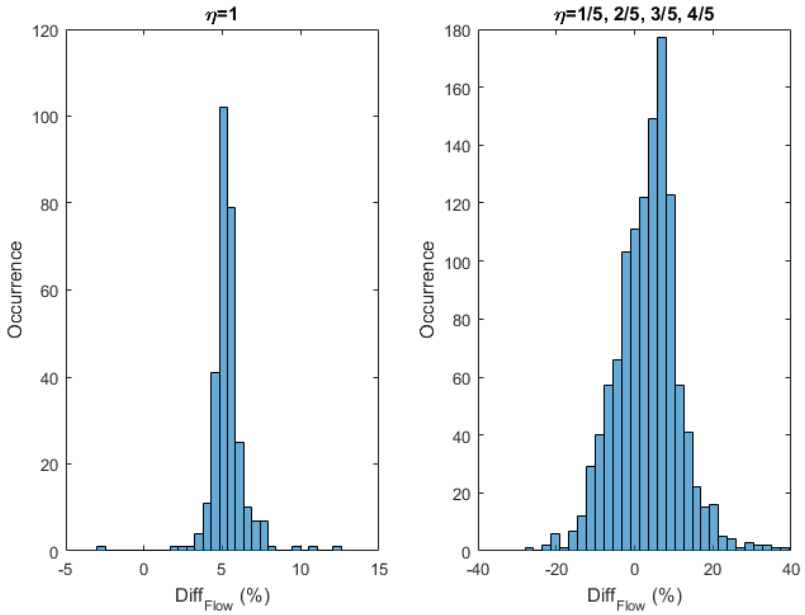

Figure 0.51 Distribution of $\mathbf{Diff_{Flow}}$ between the predictions of Model-2 and Model-3 for interior case

Table 0.15 Fitted distributions of $\mathbf{Diff_{Flow}}$ for interior case

$\eta = 1/5$	$\eta = 2/5$	$\eta = 3/5$	$\eta = 4/5$
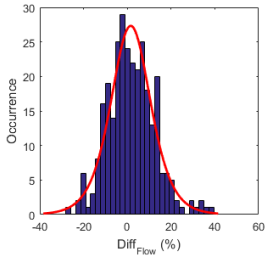	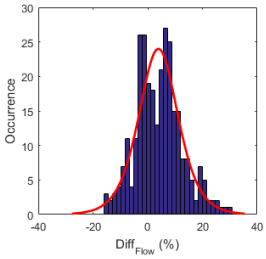	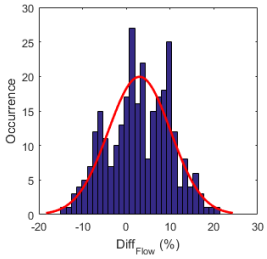	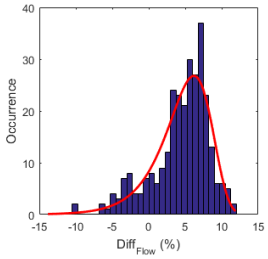
$L(0.016,0.060)$	$L(0.039,0.048)$	$N(0.03,0.071)$	$EV(0.062,0.030)$

To investigate the impact of diversity factor on the supply air flowrate, we plot the correlation between the diversity factor and the $\text{Diff}_{\text{Flow}}$ for each alignment factor case. Based on the knowledge we learned from the single façade case, we derive the linear correlation between the diversity factors against the $\text{Diff}_{\text{Flow}}$ of ICA, as shown in Figure 0.52. The band between the yellow and purple lines has a width of 4 standard deviations. The fitted linear equations are shown in Table 0.16.

Table 0.16 Fitted linear equations of the $\mathbf{Diff_{Flow}}$ (%) of ICA against diversity factor ($\boldsymbol{\theta}$) for interior case

η	Fitted equations
1/5	$\text{Diff}_{\text{Flow}} = 0.91\theta + \varepsilon, \varepsilon \sim \text{N}(0,0.07), R^2 = 0.75$
2/5	$\text{Diff}_{\text{Flow}} = 1.03\theta - 0.03 + \varepsilon, \varepsilon \sim \text{N}(0,0.07), R^2 = 0.78$
3/5	$\text{Diff}_{\text{Flow}} = 0.84\theta + 0.14 + \varepsilon, \varepsilon \sim \text{N}(0,0.07), R^2 = 0.79$
4/5	$\text{Diff}_{\text{Flow}} = 0.84\theta + 0.13 + \varepsilon, \varepsilon \sim \text{N}(0,0.07), R^2 = 0.73$

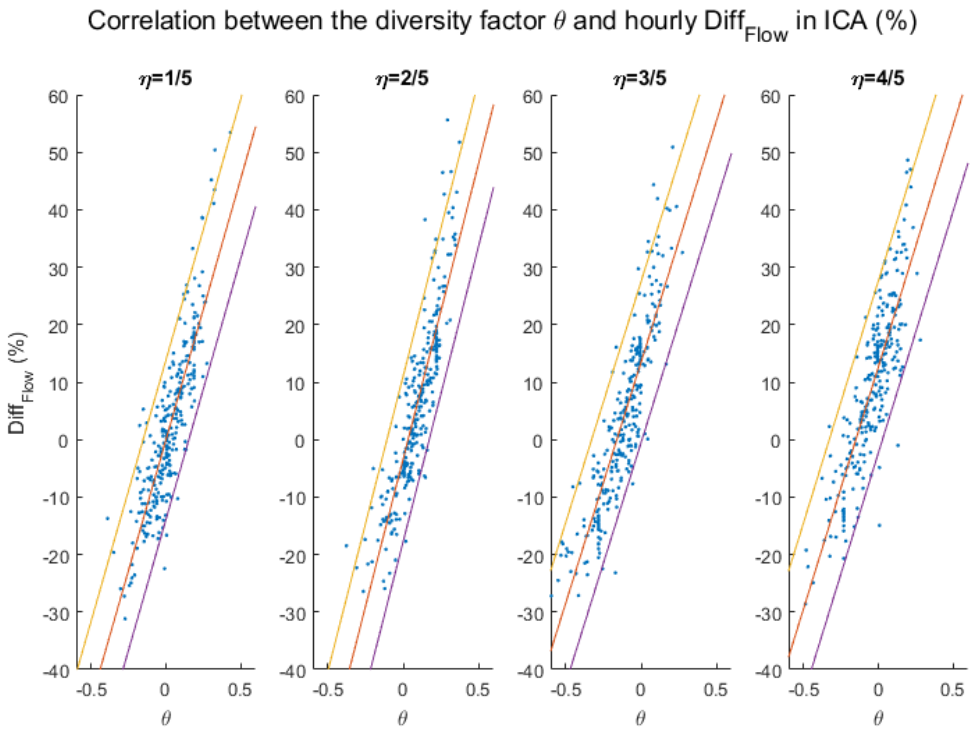

Figure 0.52 Correlation between the diversity factor ($\boldsymbol{\theta}$) and hourly $\mathbf{Diff_{Flow}}$ (%) of ICA for interior case

1.19 Multi-functional case

1.19.1 Model configurations

The cases studied thus far in this chapter consider the impact of façade exposures of the zone where all spaces in the zone of interest share the same building function. In this section, we evaluate the impact of multi building functions, translated into usage diversity, on the simulation outcomes of the different models. The zone of interest is the south perimeter zone, which is the same area we studied in the single façade case. The sub-zone partitions representing different values of the alignment factor are chosen in the same way as the configurations in the single external façade study. The meeting rooms are relocated from the north perimeter zone to the south perimeter zone. To generate the stochastic occupant presence in the meeting area, we establish the concept of meeting cell as the atomic unit of the meeting area. Each meeting cell represents a meeting room of 35 m^2, and only meetings are assumed to be held in a meeting cell. The area of each building function varies based on the alignment factor, Table 0.17 shows the space area of each building functions and its corresponding alignment factors. The idea behind this alignment variety is to partition the zone is spaces of two types, either office or meeting, each with their function specific usage.

Table 0.17 Space area of each building function with alignment factors

	Alignment factor (η)				
	1/5	2/5	3/5	4/5	1
Office (m^2)	35	70	105	140	175
Meeting Space (m^2)	140	105	70	35	0

The temperature sensor is assumed to be installed in the office area whereas the meeting area is assumed as the ICA. The basic control strategies and setpoints of the HVAC system are kept as same as before, i.e. in Chapter 4.

1.19.2 Occupancy profile and diversity factor

As mentioned in Chapter 2, the stochastic nature of occupant presence, lighting and plug load usage consequence is an important consideration in our assessment. We use Occupant Simulator to generate the occupant presence schedules for both office area and meeting area.

For the office area usage profile, the approach introduced in the previous cases is reused here. The occupant presence schedule in the office area is thus generated based on the reference value (18.58m^2/person) specified by ASHRAE. The mean profile of the lighting and appliance usage and the correlation between the occupant presence and the lighting/appliances operations derived from Wang's (2016) on-site measurement. For the meeting area usage profile, the basic assumptions for each meeting cell in Occupant Simulator are shown in Table 0.18. The probability value is predetermined by Occupant Simulator based on its collected measured data.

Table 0.18 Assumptions of the occupant presence in meeting cells

Day of Week: Monday to Friday					
	Max	Min		Max	Min
Meeting per day	*6*	*2*	People per meeting	*8*	*2*
Duration		30 min	60 min	90 min	120 min
Probability (%)		*12*	*72*	*12*	*4*

The plug and lighting loads in each meeting cell are assumed to depend on the occupant presence obeying the rules below (AZcentral, 2019) (EnergyUseCalculator, 2020):

Table 0.19 Assumptions of the lighting and plug usage in meeting cells

	Power density	Unoccupied	Occupied
Lighting	10.76/m2	5%	< 4 people, 50% ≥ 4 people, 100%
Plugs	10.76/m2	5%	100W + 30W/person

Figure 0.53 shows the occupancy variations in the south perimeter zone from June 1st to July 31st. The left figure shows the result for the multi-functional case, while the right figure shows the result of the office-only case. According to the simulation outcomes, the occupancy shows larger variations for multi-function than office-only, and this pattern gets more pronounced with increasing meeting cells.

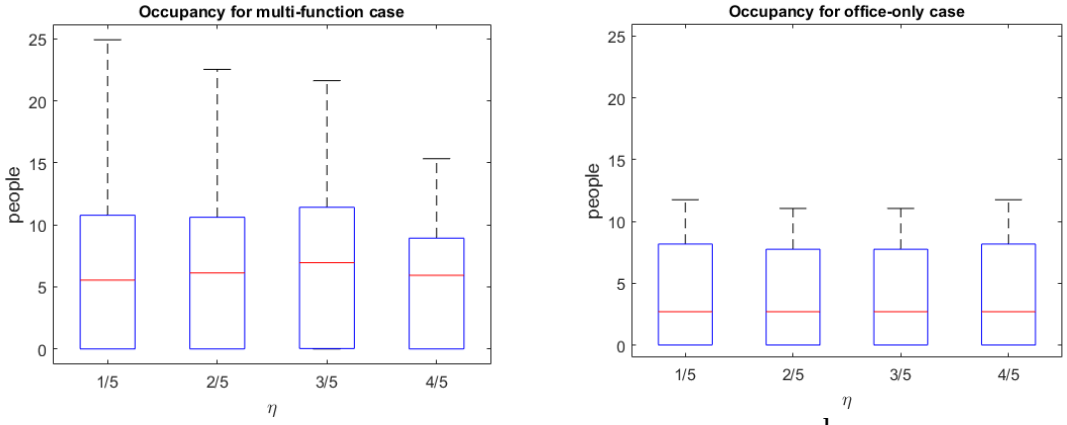

Figure 0.53 Variations of occupant presence during occupied hours (a: multi-function; b: office only)

Since the occupancy profile during the weekends and after work hours has very limited fluctuation, we select 4,160 working hours from the 8,760 hours in total to calculate the corresponding hourly diversity factors (θ) for each case. Figure 0.54 depicts the

distribution of the hourly diversity factor for different alignment values. the range of the diversity factor is extremely large compared to the office-only case. θ greater than 0 indicates occupancy has a more intensive usage in the DCA than that in the ICA, whereas θ less than 0 means the ICA is used more intensively than the DCA. And the larger the absolute value of the θ is, the larger this difference in usage is. According to the knowledge we obtained from the preliminary study, it is anticipated that the hours with large diversity factor introduce temperature controllability and hence discomfort issues into certain spaces.

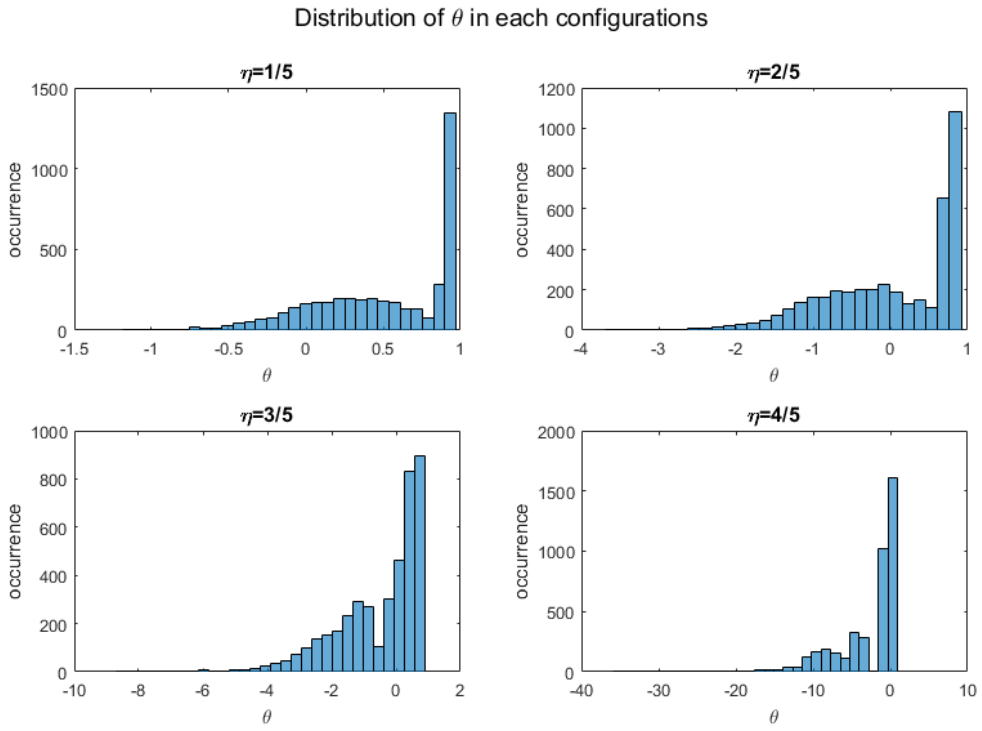

Figure 0.54 Distributions of diversity factor (***θ***) in the multi-functional case

To analyze the impacts of the usage diversity on space condition and energy consumptions, we utilize the sub-zone level occupancy profiles as input file in the three models as usual: the aggregated EnergyPlus model (Model-1), the sub-divided EnergyPlus model (Model-2), and the co-simulation model (Model-3). Since Model-1 does not

distinguish the ICA from the DCA, the two occupancy profiles are combined together and used to calculate the weighted average value as the zone level usage profile. The simulation period is from 6/24 to 7/31 and the predicted outcomes for July are used to conduct the following analysis.

1.19.3 Model-1 vs Model-2

In this section, we compare the auto-sizing results generated by the EnergyPlus function in Model-1 and Model-2. Figure 0.55a shows the design airflow sizes of the VAV box for the core zone delivered by Model-1 and Model-2. The maximum difference is about 5%. Figure 0.55b depicts the correlation between the alignment factor and the ratio of design size of DCA to the design size of the overall south perimeter zone. The results illustrate that the two models provide similar auto-sizing results and the relative design size of the virtual VAV boxes at the sub-zone level can be derived by applying the alignment factor to the overall design size. These results conform to what was found in the other cases. This guarantees that there is good enough sizing equivalence between Model-1 and Model-2 and that a comparison of predicted values of both models is meaningful.

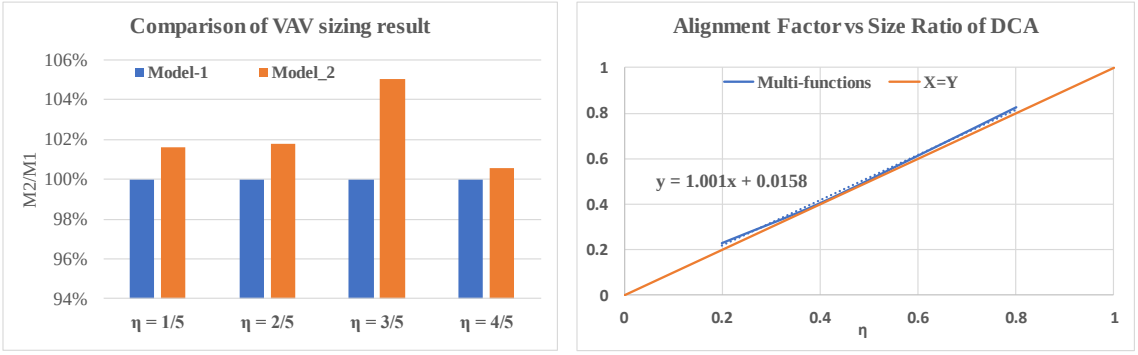

a b

Figure 0.55 Comparison of the auto sizing result between Model-1 and Model-2 for multi-functional case

Figure 0.56 shows the differences (Diff) of the hourly outcomes in the south perimeter zone between Model-1 and Model-2 for the five alignment factors, including room air temperature (RT) of ICA, supply air flowrate (AF), delivered cooling (Q), and fan power (FP). The comparison depicts that increasing the resolution of EnergyPlus model from zone level to sub-zone level has only a slight impact on the simulation outcomes for the thermal zone. The mean value of the differences in predicted outcome is close to zero, but many outliers exist, especially in the result of supply air flowrate and delivered cooling energy. However, the outliers have apparently little impact on the monthly result as the differences are no larger than 3% shown in Figure 0.57.

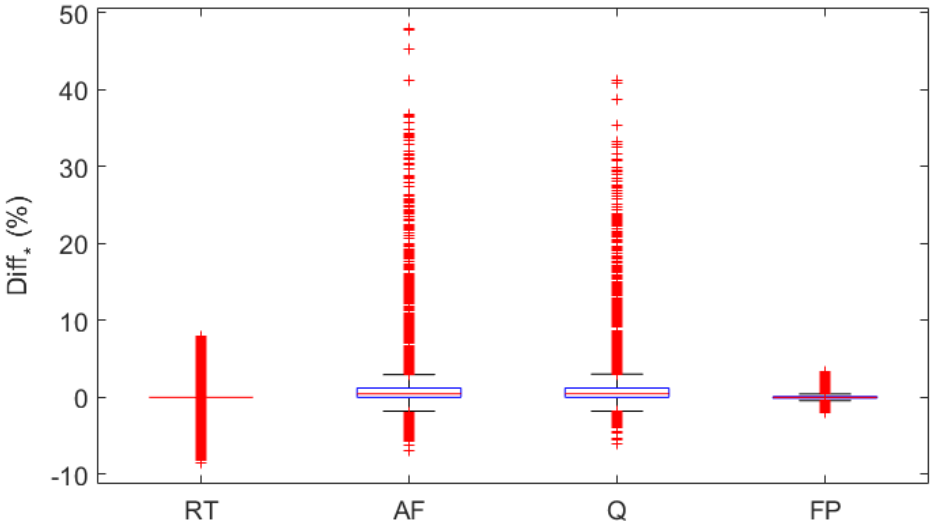

Figure 0.56 Comparison between Model-1 and Model-2 for multi-functional case

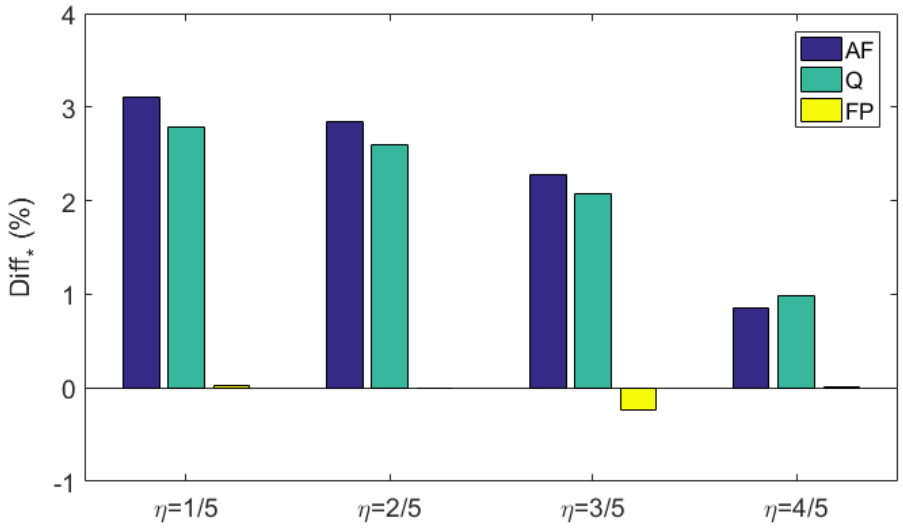

Figure 0.57 Differences of monthly predictions between Model-1 and Model-2 for multi-functional case

1.19.4 Data pre-processing

The first and the last operating hour of HVAC system is the daily occurrence of a control transition, i.e. when the HVAC system switches its operation status. The controlled variable in the actual HVAC system is the supply air flowrate. Because of the ducting system and the imperfect control, it inevitably leads to differences in the prediction of the supply air flowrate, which has the dominant effect on space air temperature, delivered cooling, and fan power consumption. To eliminate the impact of the transition period, we remove the datapoints measured in the first and the last operating hour of each day from the dataset to conduct the following curve fitting analysis.

1.19.5 Impact on space air temperature

The differences in the predicted space air temperature of the office area (the DCA) and the meeting area (the ICA) in each alignment case are presented. The differences in

temperature are calculated by using the outcome of Model-3 minus the result of Model-2 with the measurement unit degree Celsius. Figure 0.58 shows the histogram of the differences between Model-2 and Model-3 in the predicted hourly space air temperature. The dataset includes 1,176 occupied hour data for the multi-functional case with the different alignment factors. The left figure shows that the two models predict similar space air temperatures in DCA. The right figure shows noticeable differences in predicted air temperature in ICA ranging from -3°C to 1.5°C.

By performing an Inverse Gaussian distribution fitting, we obtain $Diff_{T,ICA} \sim IG((1.7,9.4)$. Comparing the result of the office only cases, the result illustrates that in reality the limited controllability of HVAC system may not meet the space requirement when multi building function are served by the same terminal unit.

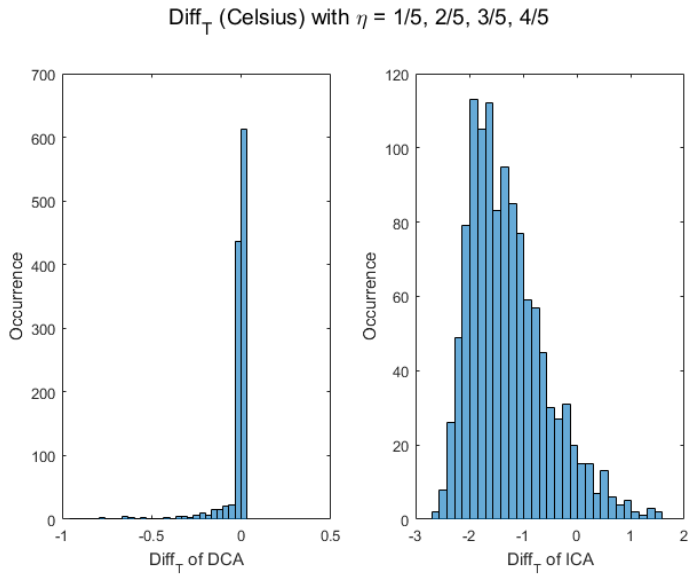

Figure 0.58 $\mathbf{Diff_T}$ between Model-2 and Model-3 predictions for multi-functional case (taken over all alignment and diversity cases)

Table 0.20 shows the distribution of Diff_T for each alignment factor; and gives the distribution fitting coefficients.

Table 0.20 Fitted distributions of $\mathbf{Diff_T}$ for multi-functional case

$\eta = 1/5$	$\eta = 2/5$	$\eta = 3/5$	$\eta = 4/5$
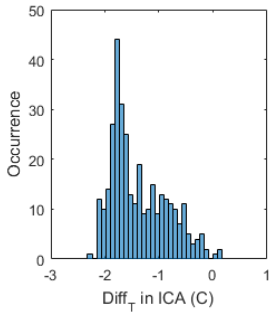	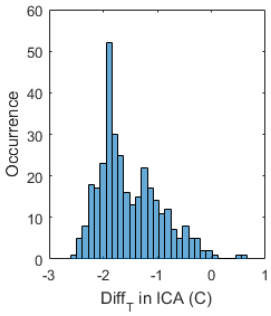	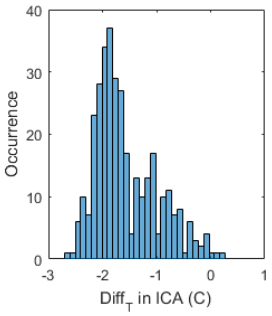	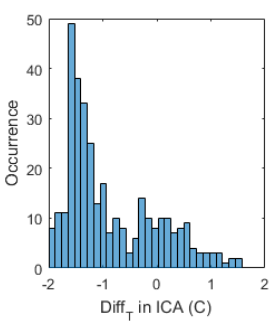
$InvGauss$ $(1.2,5.6,Shift(-2.6))$	$InvGauss$ $(1.5,9.6,Shift(-3))$	$InvGauss$ $(1.5,9.2,Shift(-3))$	$InvGauss$ $(1.3,2.6,Shift(-2.2))$

In trying to derive the correlation between the diversity factor and the Diff_T, it is found that the office area and the meeting area have very different usage patterns. Based on the distribution of the diversity factor, there are many hours with a diversity factor close to 1, which means the ICA is unoccupied. In this situation, the load in ICA is determined by the external load instead of the internal load, and the space air temperature is not only related to the external condition but also the thermal resistance of the building, which make the realized space air temperature unstable during the entire occupied hours. Figure 0.59 shows the Diff_T for every occupied hour of day, where each curve represents the Model-3 prediction for all possible values of η and θ. Therefore, the correlation between the diversity factor and Diff_T is weak, as shown in Figure 0.60. In this situation, the HVAC system lost its control in the ICA.

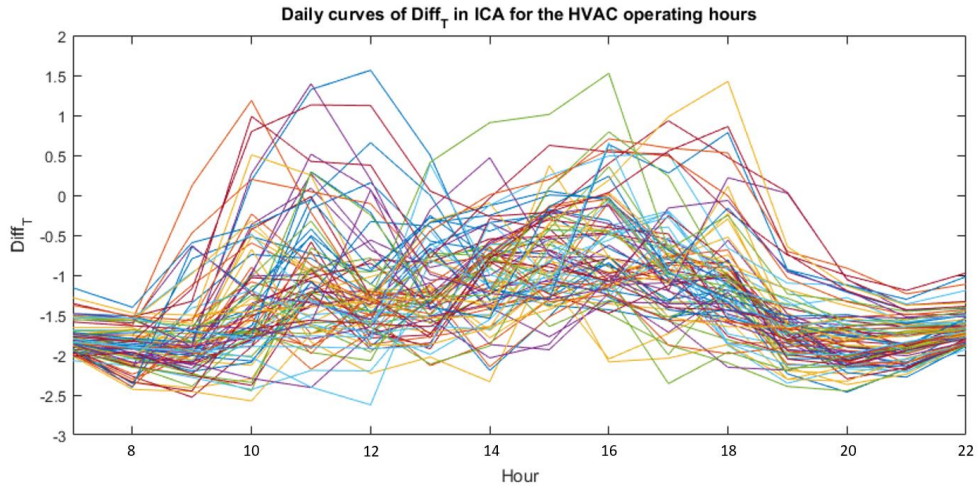

Figure 0.59 $\mathbf{Diff_T}$ during working hours in ICA for multi-functional case (sampled over $\boldsymbol{\eta}$ and $\boldsymbol{\theta}$ values)

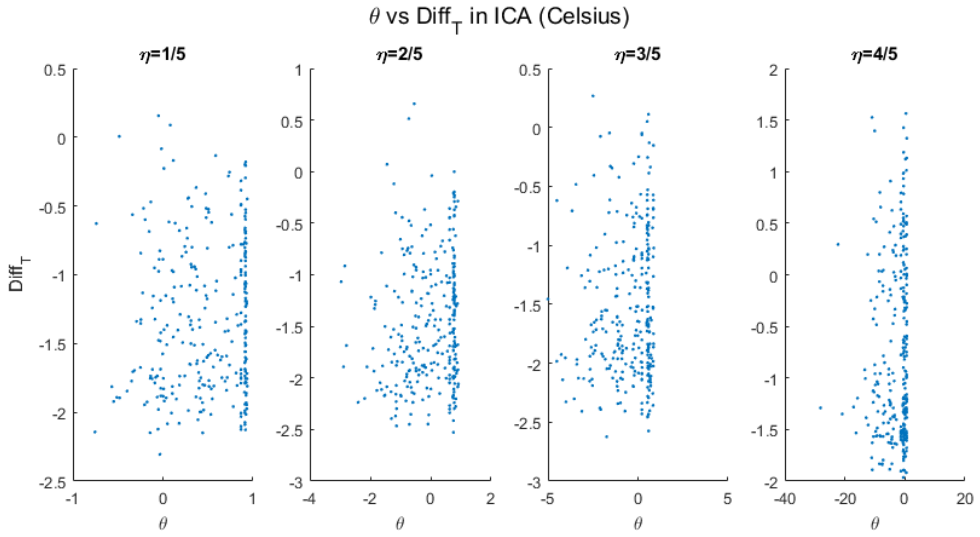

Figure 0.60 Diversity factor versus $\mathbf{Diff_T}$ for multi-functional case

Using the predicted space air temperature, the number of unmet hours during the occupied period (weekday from 8 am to 9 pm) in July is calculated to evaluate thermal comfort: an hour will be counted as unmet if the space air temperature is outside of the setpoint plus or minus 1℃. The dataset includes 294 occupied hours in July for all considered alignment factors (1/5, 2/5, 3/5, and 4/5) and the resulting number of unmet hours in July for each alignment factor case is shown in Figure 0.61. We can see that

Model-2 and Model-3 have similar predictions of unmet hours for the DCA. In the ICA EnergyPlus underestimates the unmet hours, which indicates that the space may experience severe discomfort issue which is undetected by Model-2. This is because, in reality the HVAC system operates with limited controllability.

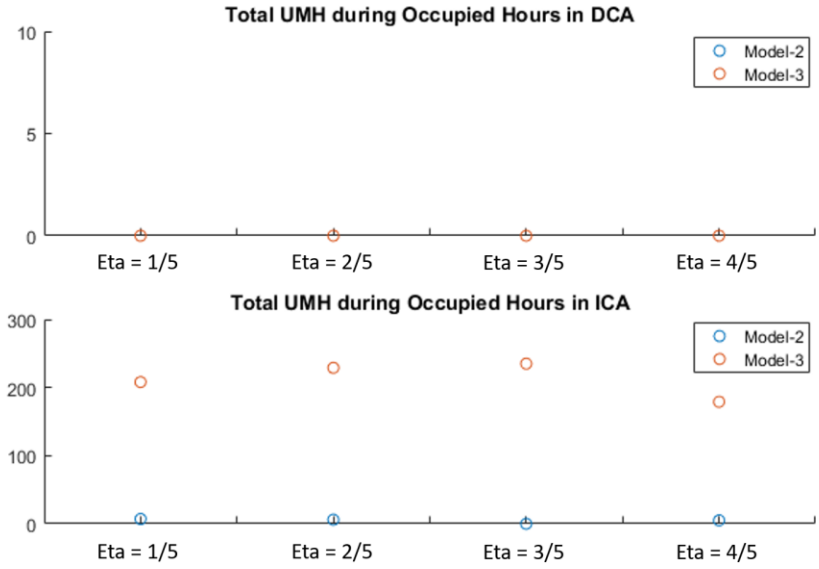

Figure 0.61 Outcomes of unmet hours from Model-2 and Model-3 for multi-functional case

1.19.6 Impact on delivered cooling energy

The calculation of the hourly $\text{Diff}_{\text{Cooling}}$ between the outcomes of Model-2 and Model-3 are based on the equations shown in Chapter 4. The dataset contains 1,176 datapoints for the $\text{Diff}_{\text{Cooling}}$ of DCA, and the same amount of datapoints for the $\text{Diff}_{\text{Cooling}}$ of ICA. The left figure in Figure 0.62 depicts the distribution of $\text{Diff}_{\text{Cooling}}$ of DCA; and the right one presents the distribution of $\text{Diff}_{\text{Cooling}}$ of ICA. The result shows that the hourly $\text{Diff}_{\text{Cooling}}$ in DCA is roughly from -20% to 10% with the mean value at 0, however,

the hourly $\text{Diff}_{\text{Cooling}}$ in ICA has a much wider distribution with a positive mean value. Based on the result, the $\text{Diff}_{\text{Cooling}}$ in ICA can reach up to 150% which indicates that the system in Model-3 supplies more than 2 times as many cooling as Model-2 predicts. In other words, at the hourly interval, EnergyPlus (Model-2) significantly underestimates the cooling consumptions in the ICA. As this is at the short interval (hourly) this is hardly a significant finding.

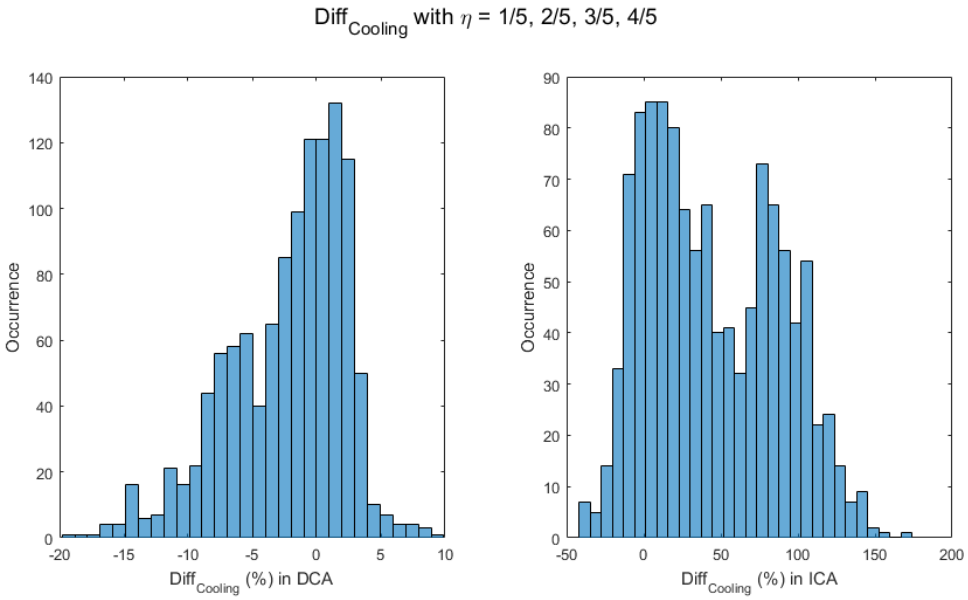

Figure 0.62 Hourly **$\text{Diff}_{\text{Cooling}}$** between Model-2 and Model-3 predictions for multi-functional case

Based on the distribution of diversity factor and the result of space air temperature, it proves hard to link the $\text{Diff}_{\text{Cooling}}$ distribution with the diversity factor in the multi-functional case. Therefore, we plot the correlation between the Diff_{T} against the $\text{Diff}_{\text{Cooling}}$ for each alignment factor, as shown in Figure 0.63. Table 0.21 shows the fitted polynomial coefficients and the fitting R^2 for each misalignment factor.

Table 0.21 Fitted polynomial equations of hourly $\mathbf{Diff_{Cooling}}$ (%) of ICA against $\mathbf{Diff_T}$ for multi-functional case

η	Fitted polynomial coefficients	R^2
1/5	(0.0383, 0.388, 0.1469, -0.0542)	0.7755
2/5	(-0.0419, 0.1223, -0.0671, -0.1113)	0. 8086
3/5	(0.0628, 0.4745, 0.2667, -0.0457)	0.7639
4/5	(0.0691, 0.1623, -0.4525, -0.0738)	0. 7877

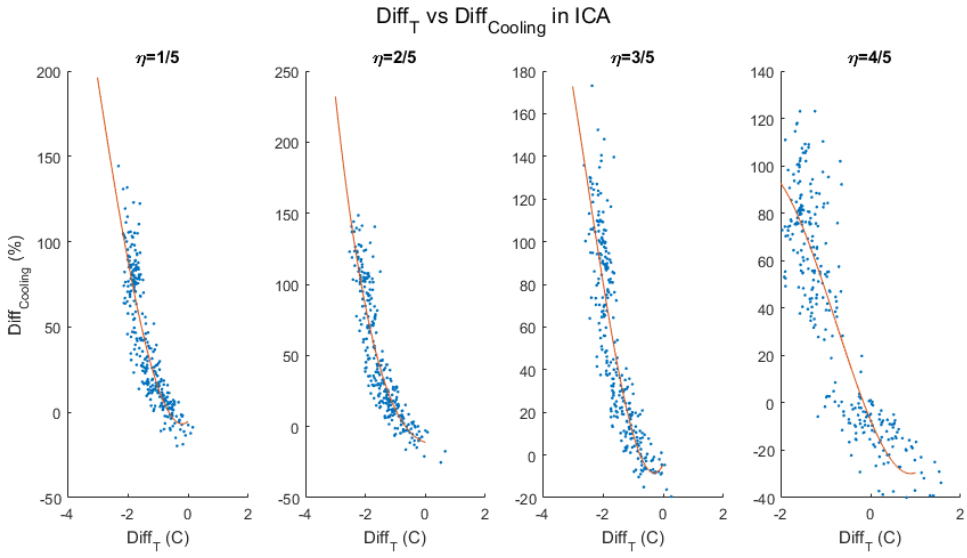

Figure 0.63 Correlation between hourly $\mathbf{Diff_T}$ and $\mathbf{Diff_{Cooling}}$ for multi-functional case

The above analysis is for hourly predictions. An analysis for daily and monthly outcomes is conducted next. The dataset of daily $\text{Diff}_{\text{Cooling}}$ of the entire south zone contains 84 datapoints for the four alignment factors. Figure 0.64 shows the distribution of daily $\text{Diff}_{\text{Cooling}}$ for the overall south perimeter zone. The result depicts the daily cooling predicted by the EnergyPlus model is on average 32.5 Wh/m2 smaller than the outcomes of the co-simulation model, or about 13% of the cooling predicted by the EnergyPlus model.

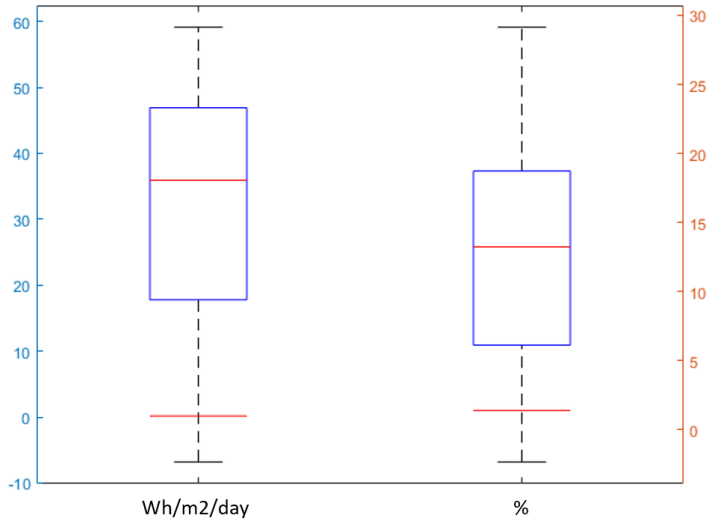

Figure 0.64 Distribution of daily $\mathbf{Diff_{Cooling}}$ for multi-functional case

Figure 0.65 displays the comparison of monthly delivered cooling energy between the EnergyPlus model and the co-simulation model. The left figure depicts the predicted delivered cooling energy per square meter, the yellow bar is the outcomes of EnergyPlus model while the blue bar is the result of co-simulation model. We can see the $\mathrm{Diff_{Cooling}}$ are more noticeable when the misalignment is present in the thermal zone. The right figure shows the percentage of monthly $\mathrm{Diff_{Cooling}}$. The result presents that $\mathrm{Diff_{Cooling}}$ can reach to 8% when we include a detailed HVAC system with imperfect control in Model-3 with an alignment factor at 1; and the $\mathrm{Diff_{Cooling}}$ increases along with the increase of the meeting area. The $\mathrm{Diff_{Cooling}}$ can reach up to 25% when the alignment factor equals 1/5. It confirms that misalignment impacts noticeably on the prediction of delivered cooling energy and that multi-functional space with different occupancy patterns exacerbates the impact.

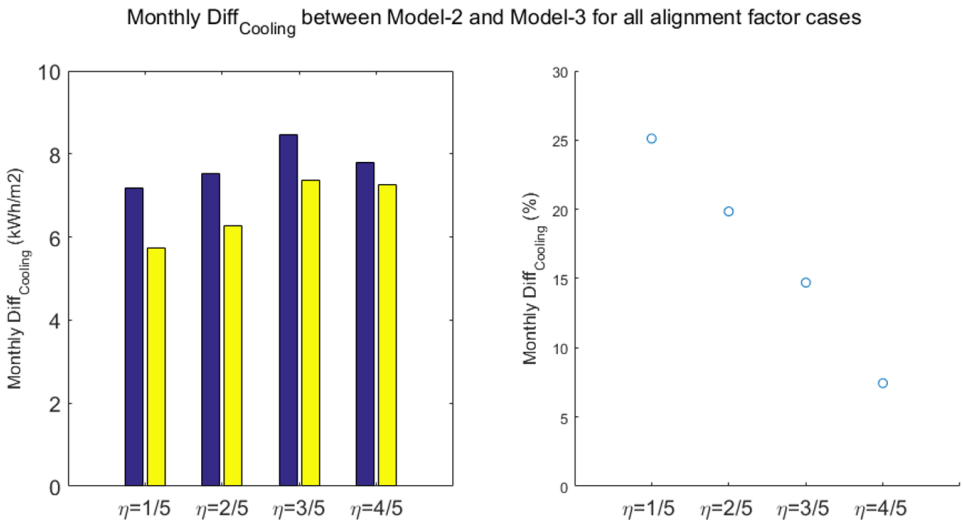

Figure 0.65 Monthly $\mathbf{Diff_{Cooling}}$ between Model-2 and Model-3 for multi-functional case

1.19.7 Impact on air flowrate

The difference of flowrate is presented as a percentage calculated by the equations introduced in Chapter 4. The hourly cooling discrepancies between the outcomes of Model-2 and Model-3 are determined from a dataset contains 1,176 predictions (datapoints) for the hourly $\mathrm{Diff_{Flow}}$ of DCA, and the same amount of datapoints for the $\mathrm{Diff_{Flow}}$ of ICA. The left figure in Figure 0.66 depicts the distribution of $\mathrm{Diff_{Flow}}$ of DCA; and the right one presents the distribution of $\mathrm{Diff_{Flow}}$ of ICA. The result shows that the $\mathrm{Diff_{Flow}}$ in DCA is mainly from -20% to 20% with the mean value at -1%, however, the hourly $\mathrm{Diff_{Flow}}$ in ICA have a much wider distribution with a positive mean value. Based on the result, the $\mathrm{Diff_{Flow}}$ in ICA can reach up to 200% which indicates that the system in Model-3 supplies 3 times as much air as Model-2. In other words, EnergyPlus (Model-2) significantly underestimates the air supply to the ICA taken over all possible alignment factor and diversity factor cases.

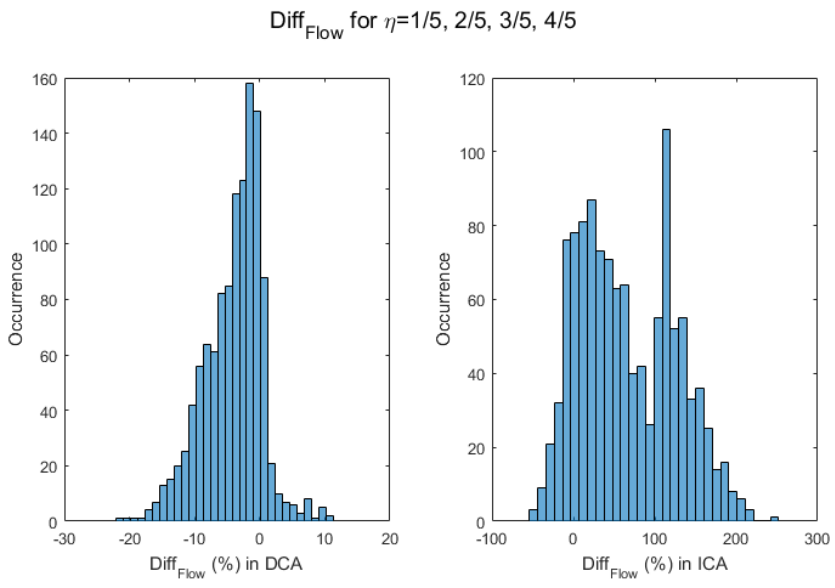

Figure 0.66 **Diff$_{Flow}$** between Model-2 and Model-3 predictions for multi-functional case

Since both DCA and ICA are served by one VAV terminal box, we plot the Diff$_{Flow}$ for the VAV terminal box, shown in Figure 0.67. By performing an Inverse Gaussian distribution fitting, obtaining $Diff_{flow} \sim IG(0.61, 3.03, Shift(-0.36))$.

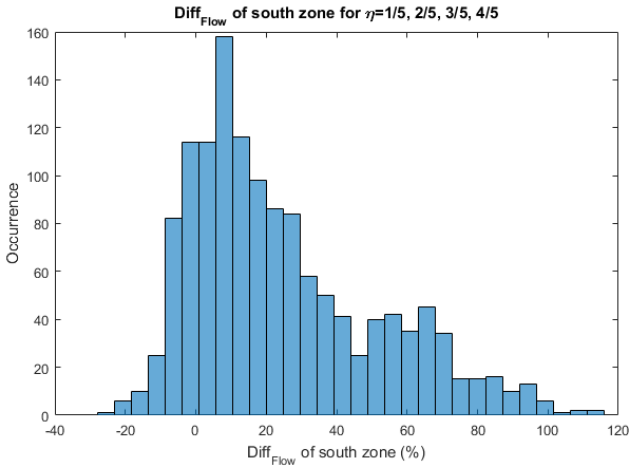

Figure 0.67 **Diff$_{Flow}$** of combined DCA-ICA for multi-functional case

Figure 0.68 diagrams the correlation between $\mathrm{Diff_T}$ and $\mathrm{Diff_{Flow}}$ for each alignment case. Table 0.22 shows the fitted polynomial coefficients and the fitting R^2 for each alignment factor.

Table 0.22 Fitted linear equations of hourly $\mathbf{Diff_{Flow}}$ (%) against $\mathbf{Diff_T}$ for multi-functional case

η	Fitted polynomial coefficients	R^2
1/5	(0.0079, 0.4064, 0.0896, -0.0625)	0.8417
2/5	(-0.0794, 0.1184, -0.1356, -0.1198)	0. 8661
3/5	(0.0420, 0.5192, 0.2323, -0.0537)	0. 8310
4/5	(0.0595, 0.2082, -0.5476, -0.0932)	0. 8513

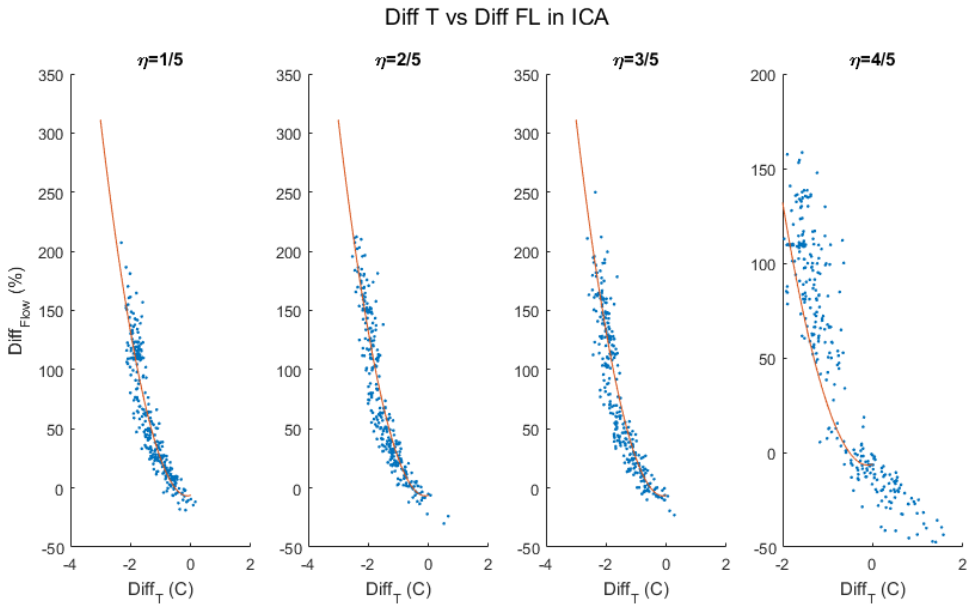

Figure 0.68 Correlation between $\mathbf{Diff_{Flow}}$ (%) against $\mathbf{Diff_T}$ for multi-functional case

EXPLORATION OF MFU CHARACTERIZATION

1.20 From Diff to MFU

In Chapter 5, we focused on the differences of the quantities of interest based on the comparison between the simulation outcomes from EnergyPlus and the co-simulation model in fully specified building cases. The noticeable differences provide statistical evidence to prove the inadequacy of the plain EnergyPlus model. Undoubtedly, various factors such as damper leakage, unexpected duct resistance, improper equipment sizing, sensor drift and failure, imprecise control, ageing and degradation, and HVAC system hardware faults can potentially contribute to the discrepancy between predicted and observed system. In this study, they are not considered. Instead only the model discrepancy is considered with quantified differences that are characterized by the alignment factor and the occupant load diversity factor. This characterization illustrates that these two factors are two contributors to the MFU in the low fidelity model. As explained earlier, the characterization of the discrepancy of the low fidelity model in terms of differences in outcomes when compared to a high fidelity model is one thing but the translation into a MFU that can now be embedded in the low fidelity model is quite another thing.

A typical model form uncertainty quantification (UQ) based on a high-fidelity model contains steps as follows.

Step 1: select the low fidelity model for a specific purpose

Step 2: develop the high-fidelity variant for the same purpose, while assuming that which model inadequacy has only a second order effect on the outcomes under study (if

the simplifying assumptions in the low fidelity make it totally inadequate for the stated purpose one should come to other conclusions that to chase MFU)

Step 3: identify the model inadequacy based on the Diff result of model comparisons;

Step 4: perform UQ by developing a statistical model that characterizes the Diff term through correlations with the input parameters or additional (internal) parameters;

Step 5: embed the sources of uncertainty associated these model parameters in the low fidelity model

Step 6: Run the low fidelity model as s stochastic simulation with the uncertainty terms from step 5 thus propagating uncertainty in predicted outcomes

Full development of MFU for misalignment and occupant diversity is not in the scope of this study because it requires intrusive software modifications in EnergyPlus in step 5 and 6. Moreover, step 4 requires full mastery of the internal software of EnergyPlus, understanding its causal links and underlying physical equations. To do this effectively, a software's hierarchical structure is commonly used to break down a complex system into subsystems with the aim to locate the submodules that should be targeted in step 4. This is further explained in Sun's work (Sun Y. , 2014).

EnergyPlus, as an integration of simulation routines for loads, systems, and plants, is a complex ensemble of software modules that work together to calculate the final outcomes. Each module performs a specific function that simulates a few physical processes. Some of the modules are relatively independent whereas other modules are

deeply interacting with other modules. Figure 0.1 shows the internal elements in EnergyPlus. The integrated solution manager is the central element in EnergyPlus where all the elements are integrated and controlled to connect the supply and demand sides. The ideal temperature control, which assumes that the space air temperature is always maintained at the setpoint, is one of the basic assumptions in EnergyPlus which is used to calculate the thermal load to link the supply and demand side. To quantify the deficiency of the ideal temperature control, we need to dissect this core element to allocate the source of uncertainties in the correct location (step 4).

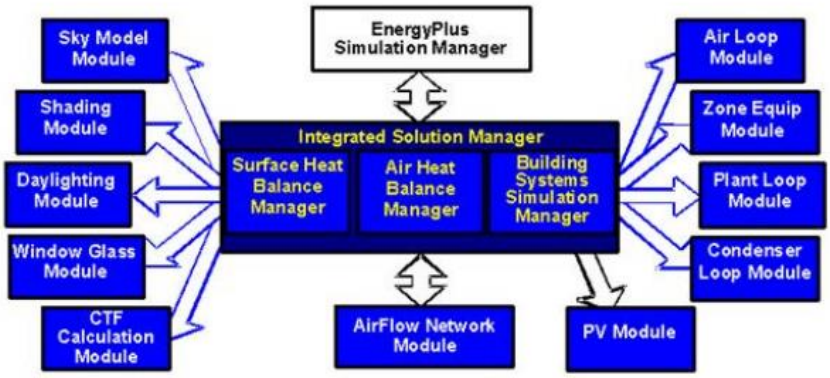

Figure 0.1 Internal elements in EnergyPlus

Although it is hard to conduct characterization and quantification of MFU modules in EnergyPlus, we can still use the Diff we obtained from the case studies to implement the post corrections to the outcomes of EnergyPlus model based on the alignment factor and the diversity factor. The post correction with the Diff from the case studies will give the modeler a sense of the prediction errors when compared with reality. But only 4 case studies have been performed with some sub variants which are typically not enough to generate a universally applicable MFU that can be represented in EnergyPlus. But one

could expect that if we limit the use of EnergyPlus to the configurations considered in this thesis, the effort could make sense to quantify MFU under these constraints, using η and θ as the main correlations. This is indeed the target in the remainder of this chapter. This is motivated by the need to explore how further investigation in embedding MFU related to misalignment in basic EnergyPlus could be handled. We will limit the treatment to predicting fan power as this illustrates the general procedure, while focusing on step 4 which is usually the hardest part.

1.21 Examples of model form uncertainty quantification

1.21.1 Single external façade case

Recall that we already identify the $\mathrm{Diff_{Flow}}$ based on the alignment factor as well as the diversity factor in the single façade case. When it comes to the comparison of fan power, EnergyPlus results show significant difference to the co-simulation model results. There are threefold causes for the $\mathrm{Diff_{FP}}$: first, EnergyPlus implements a pre-defined polynomial curve to link the fan power part load ratio (f_{pl}) with the flow fraction (f_{flow}) which is introduced in Section 3.2.1; second, EnergyPlus adopts a default efficiency factor without considering the fluctuations of fan power efficiency which varies along with the damper position and fan speed; last but not least, EnergyPlus introduces bias on the flowrate predictions because of the ideal temperature control by the idealized HVAC model.

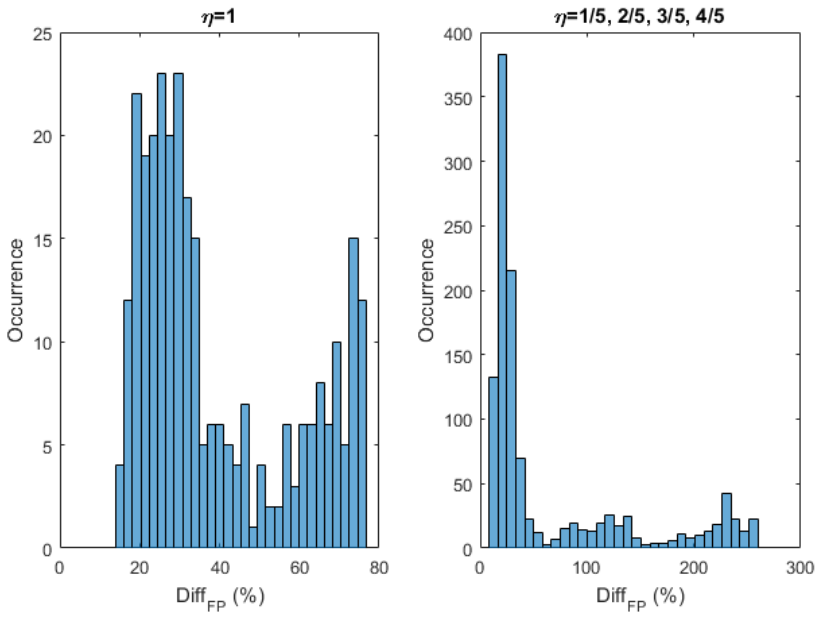

Figure 0.2 Distribution of $\mathbf{Diff_{FP}}$ between the prediction of Model-2 and Model-3 for single façade case

Figure 0.2 depicts that the $Diff_{FP}$ between the routine EnergyPlus and the high-fidelity model are widely distributed. In order to quantify MFU caused by the inadequacy of EnergyPlus in predicting fan power consumption, we need to map the results of high-fidelity model "improvements" to existing parameters in EnergyPlus.

In this situation, we develop a three-step statistical approach to quantify the discrepancies. Firstly, we compensate the supply air flowrate predicted by the original EnergyPlus model with a residual estimated by the linear fitting curves and calculate the adjusted flowrate ratio (relative to the design flowrate) of the EnergyPlus model. In the second step, we perform least square polynomial curve fittings to the $Diff_{FP}$ (as a percentage) against the adjusted flowrate ratio for each alignment case. Figure 0.3 shows the correlations between the $Diff_{FP}$ against the adjusted flowrate ratio. It depicts that the $Diff_{FP}$ are more noticeable at lower flowrate than that at higher flowrate. And the pattern

is exacerbated when misalignment is present in the systems. Table 0.1 shows the fitted polynomial coefficients and the fitting R^2 for each misalignment scenarios.

Table 0.1 Polynomial Fitting curves for single façade case

η	Fitted polynomial coefficients	R^2
1/5	(-9.2216, 28.1663, -26.1662, 7.8341)	0.9970
2/5	(-4.3852, 20.3391, -22.4387, 7.4396)	0.9971
3/5	(-7.0346, 24.1226, -23.7396, 7.3684)	0. 9985
4/5	(-2.9324, 17.7118, -20.6884, 6.9802)	0. 9977
1	(3.7765, -6.6771, 2.3395, 0.5315)	0.9804

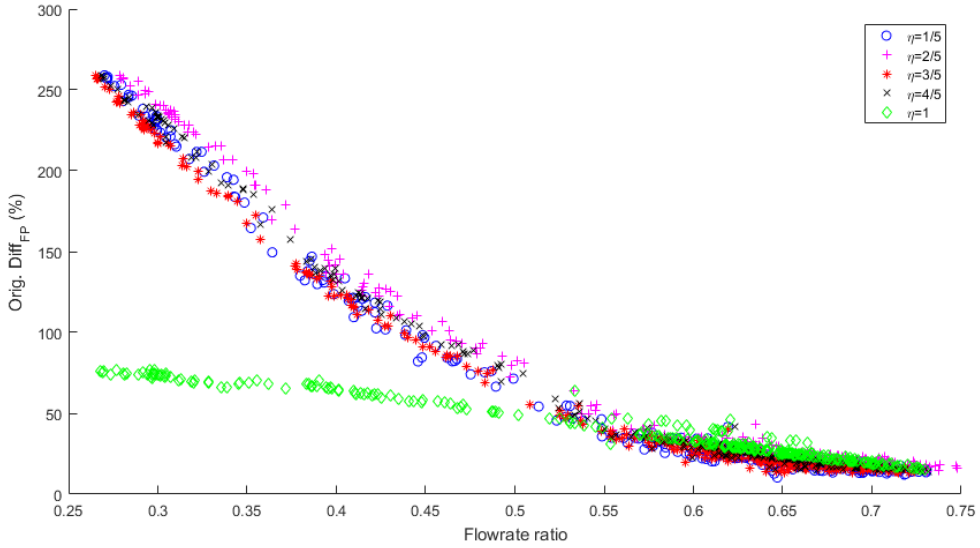

Figure 0.3 Correlations between $\mathbf{Diff_{FP}}$ against flowrate ratio for single façade case

In the last step, we compensate the fan power results in the EnergyPlus model by using the statistical curve fits and evaluate the residuals (the discrepancy between Modelica results and the fitted values). Figure 0.4 diagrams the comparison of the $Diff_{FP}$ with and without the compensation and Figure 0.5 depicts the distributions of the residues of fan power after the curve adjustment. We observe the hourly $Diff_{FP}$ reduces significantly by

using the adjusted fan power results instead of the original outcomes of EnergyPlus model. To evaluate the overall performance of the statistical model that approves the fitted coefficients, we compare the NMBE of the fan power consumption with/without curve adjustment for the five alignment cases, and the results are shown in Table 0.2.

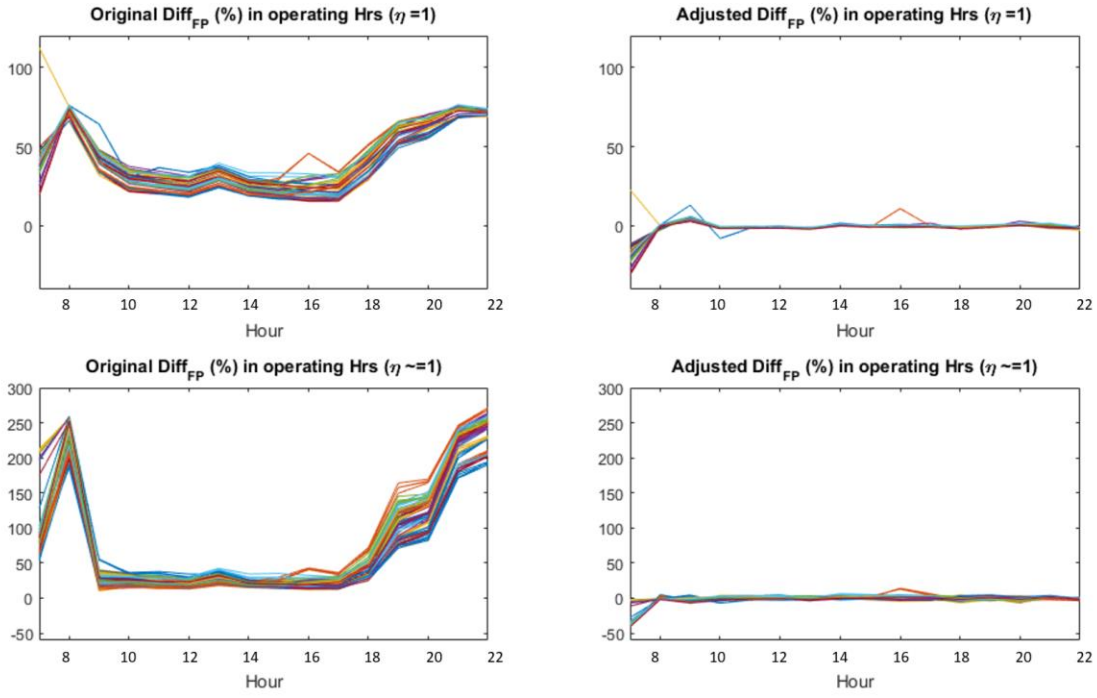

Figure 0.4 Comparison of the daily curve of $\mathbf{Diff_{FP}}$ before and after the curve fittings for single façade case

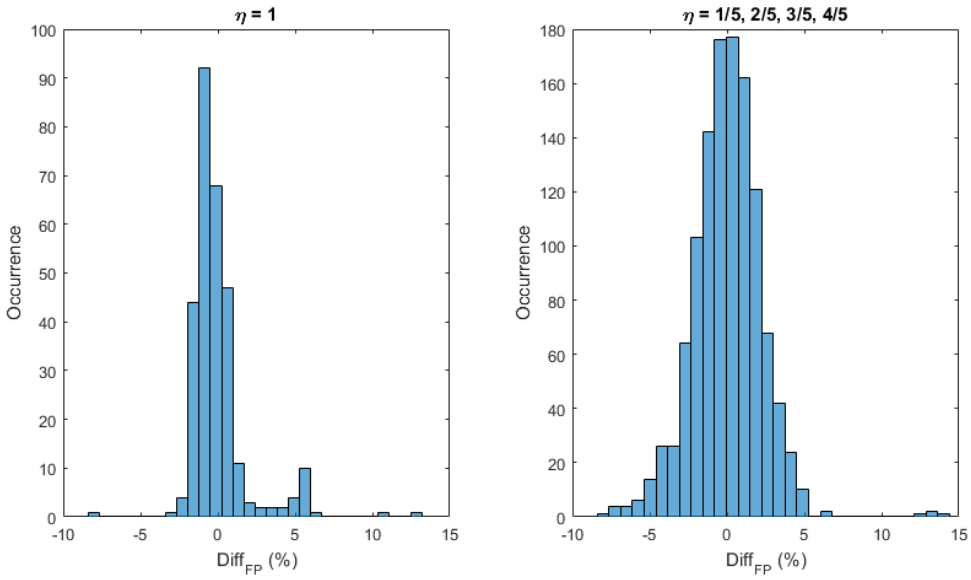

Figure 0.5 Distribution of residuals between the predictions of Modelica and adjusted EnergyPlus fan power model for single façade case

Table 0.2 NMBE of fan power results for single façade case

	η = 1/5	η = 2/5	η = 3/5	η = 4/5	η = 1
Original NMBE	31%	33%	31%	31%	25%
Adjusted NMBE	-2%	-2%	-2%	-2%	-1%

We also calculate the $Diff_{FP}$ in monthly interval, as shown in Figure 0.6. The result shows that the $Diff_{FP}$ between Model-2 and Model-3 increases when the misalignment is introduced in the model. Whereas the adjusted fan power model can significantly reduce the $Diff_{FP}$ in monthly interval. The residual of the monthly fan power consumption drops to -2% from 45%.

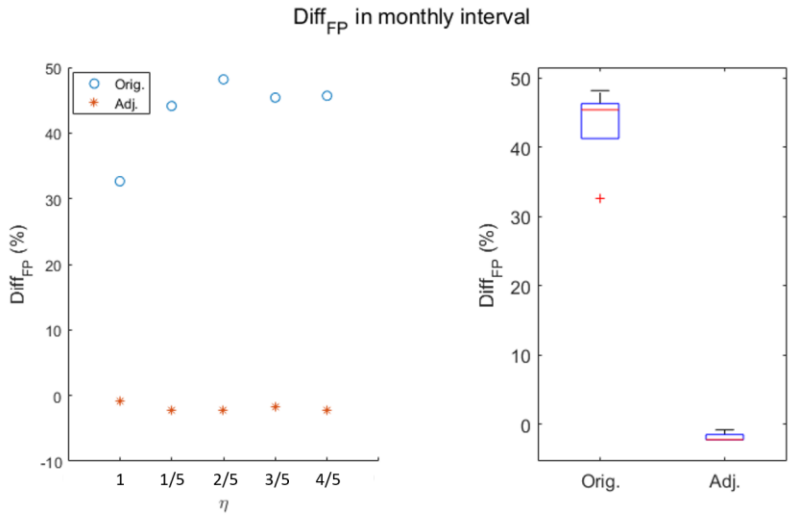

Figure 0.6 Comparison of the monthly **Diff$_{FP}$** for single façade case

1.21.2 Two external façades case

Figure 0.7 depicts that the Diff$_{FP}$ between the outcomes from the routine EnergyPlus and the high-fidelity model are widely distributed. We follow the approach introduced in the single façade study to characterize the Diff$_{FP}$.

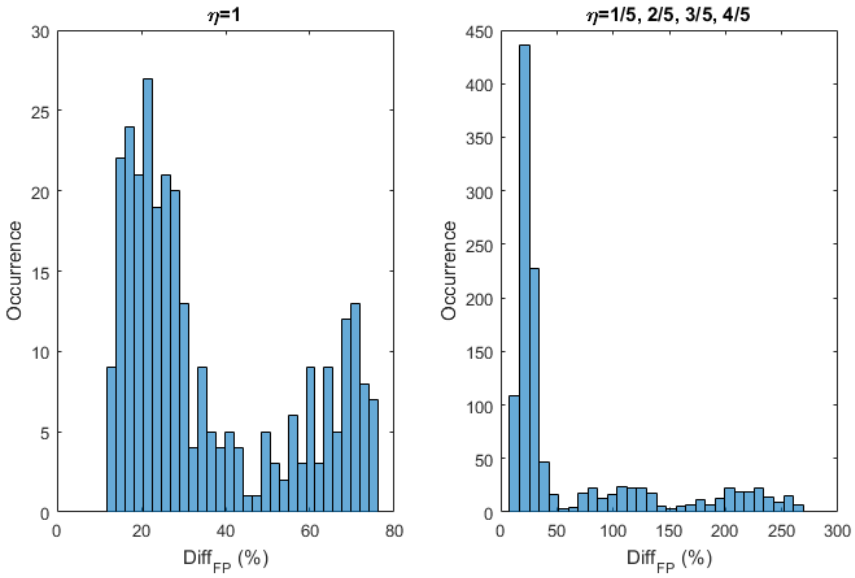

Figure 0.7 Distribution of **Diff$_{FP}$** between the predictions of Model-2 and Model-3 for two façades case

Figure 0.8 shows the correlations between the original Diff_{FP} against the adjusted airflow ratio. It depicts that the Diff_{FP} are large with small flowrate than that with large flowrate. And the pattern is more noticeable when misalignment is embedded in the systems. Table 0.3 shows the fitted polynomial coefficients and the fitting R^2 for each alignment case.

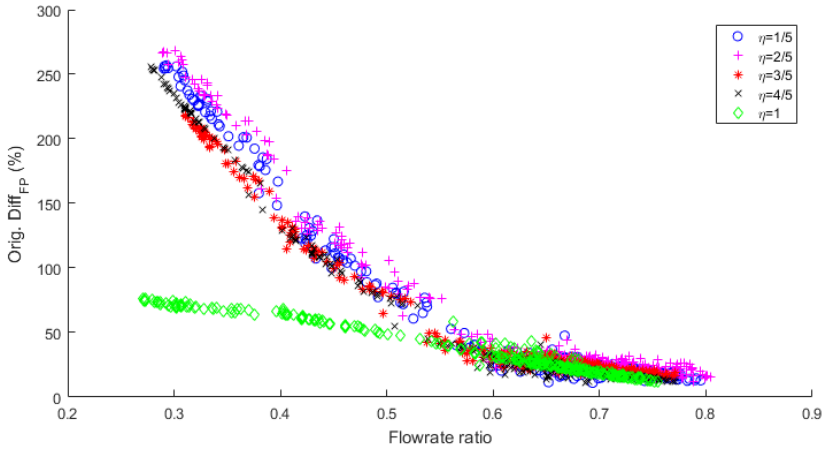

Figure 0.8 Correlations between $\mathbf{Diff_{FP}}$ against flowrate ratio for two façades case

Table 0.3 Polynomial fitting curves for two façades case

η	Fitted polynomial coefficients	R^2
1/5	(-7.9203, 26.0711, -25.4756, 7.9652)	0. 9934
2/5	(-6.2059, 23.5427, -24.3953, 7.8917)	0. 9925
3/5	(-10.6033, 29.9464, -26.9434, 8.0387)	0. 9945
4/5	(-7.1450, 24.2897, -23.9941, 7.5084)	0.9966
1	(4.2839, -7.5294, 2.8153, 0.4401)	0. 9812

We compensate the fan power results of the routine EnergyPlus model by using the statistical curve fittings and evaluate the residuals (the discrepancy between Modelica results and the updated EnergyPlus fan power results). Figure 0.9 shows the comparison of the hourly Diff_{FP} with and without the compensation. Figure 0.10 diagrams the distributions of the updated Diff_{FP}. We observe the hourly Diff_{FP} reduces significantly by

using the adjusted fan power results instead of the outcomes from the routine EnergyPlus model. To evaluate the overall performance of the statistical model that approves the fitted coefficients, we calculate the NMBE for the five alignment factor cases, and the results are shown in Table 0.4.

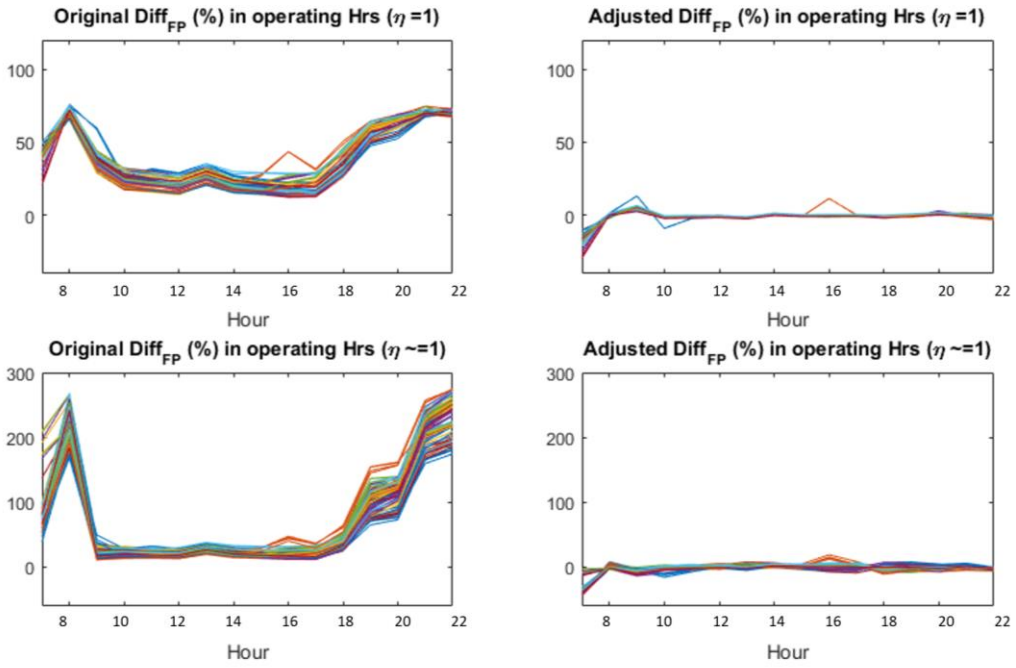

Figure 0.9 Comparison of the daily curve of $\mathbf{Diff_{FP}}$ before and after the curve fittings for two façades case

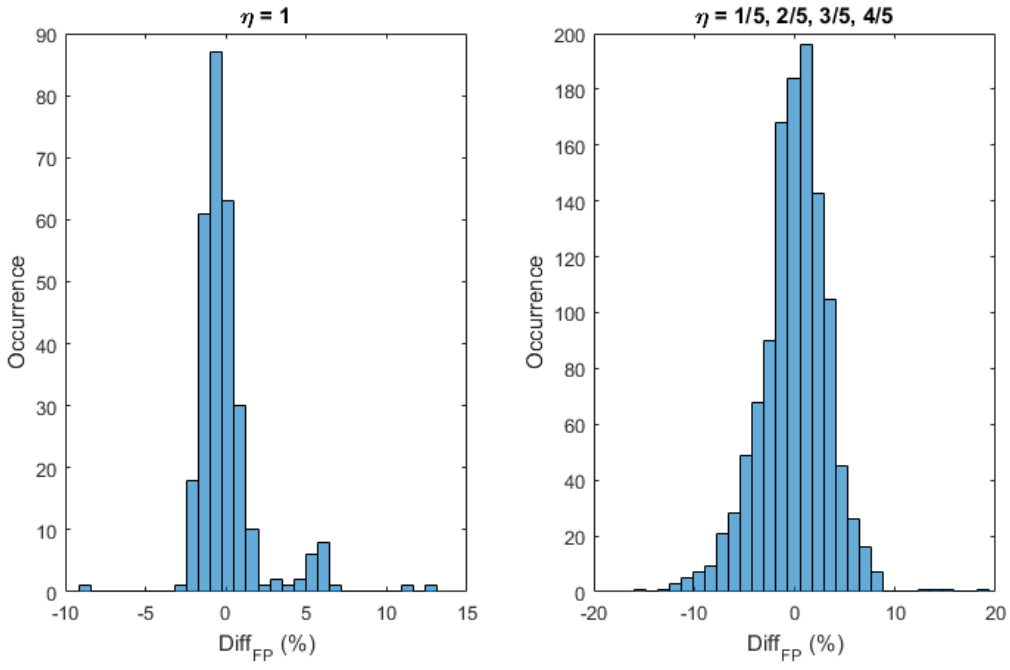

Figure 0.10 Distribution of residuals between the predictions of Modelica and adjusted EnergyPlus fan power model for two façades case

Table 0.4 NMBE of fan power results for two façades case

	η = 1/5	η = 2/5	η = 3/5	η = 4/5	η = 1
Original NMBE	30%	32%	31%	29%	23%
Adjusted NMBE	-3%	-3%	-2%	-2%	-1%

We also calculate the $Diff_{FP}$ in monthly interval, as shown in Figure 0.11. The result shows that the $Diff_{FP}$ between Model-2 and Model-3 increases when the misalignment is introduced in the model whereas the adjusted fan power model can significantly reduce the $Diff_{FP}$ in monthly interval. The residual of the monthly fan power consumption drops to -2% from 42%.

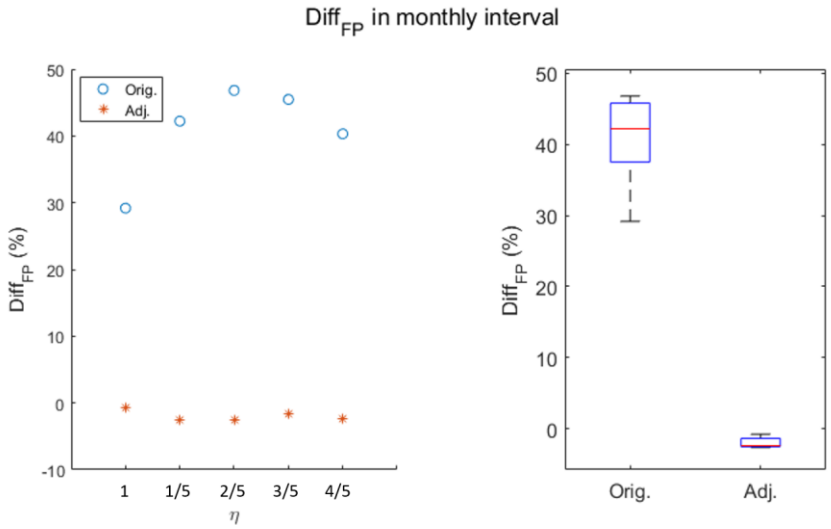

Figure 0.11 Comparison of the monthly $\mathbf{Diff_{FP}}$ for two façades case

1.21.3 Interior case

Figure 0.12 shows the correlations between the adjusted airflow ratio and the original $Diff_{FP}$ as a percentage. It depicts that the $Diff_{FP}$ is large with small flowrate than that with large flowrate. And the pattern is more noticeable when misalignment is introduced in the systems. Table 0.5 shows the fitted polynomial coefficients and the fitting R^2 for each alignment factor.

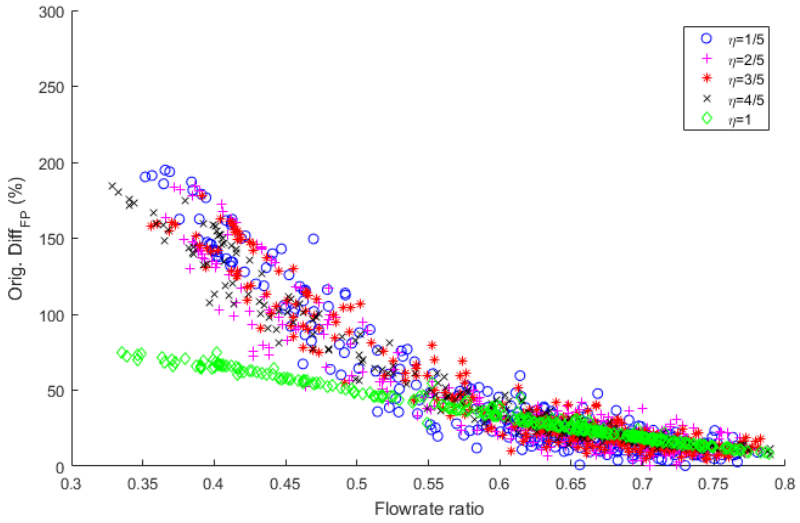

Figure 0.12 Correlations between $\mathbf{Diff_{FP}}$ against flowrate ratio for interior case

Table 0.5 Polynomial fitting curves for interior case

η	Fitted polynomial coefficients	R^2
1/5	(-9.3981, 29.6754, -27.6688, 8.1727)	0. 9349
2/5	(-17.9593, 43.8790, -36.1395, 10.1448)	0. 9237
3/5	(5.2060, 1.8625, -11.1765, 5.2713)	0. 9512
4/5	(-4.3311, 17.1315, -18.7814, 6.4094)	0.9727
1	(3.4843, -5.5906, 1.3474, 0.7926)	0. 9857

We compensate the fan power results of the routine EnergyPlus model by using the statistical curve fittings and evaluate the residuals (the discrepancy between Modelica results and updated EnergyPlus fan power results). Figure 0.13 shows the comparison of the hourly $Diff_{FP}$ with and without the compensation. Figure 0.14 depicts the distributions of the updated $Diff_{FP}$. We observe the hourly $Diff_{FP}$ reduces significantly by using the adjusted fan power results instead of the outcomes from the routine EnergyPlus model. To evaluate the overall performance of the statistical model that approves the fitted coefficients, we calculate the NMBE for the five alignment factor cases, and the results are shown in Table 0.6.

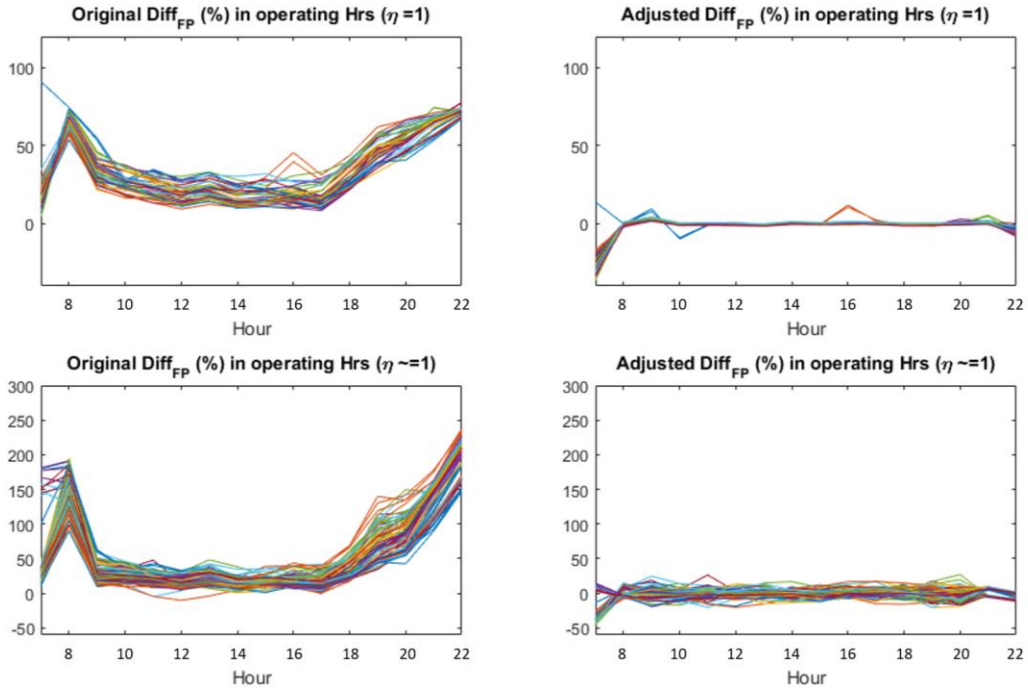

Figure 0.13 Comparison of the daily curve of **Diff$_{FP}$** before and after the curve fittings for interior case

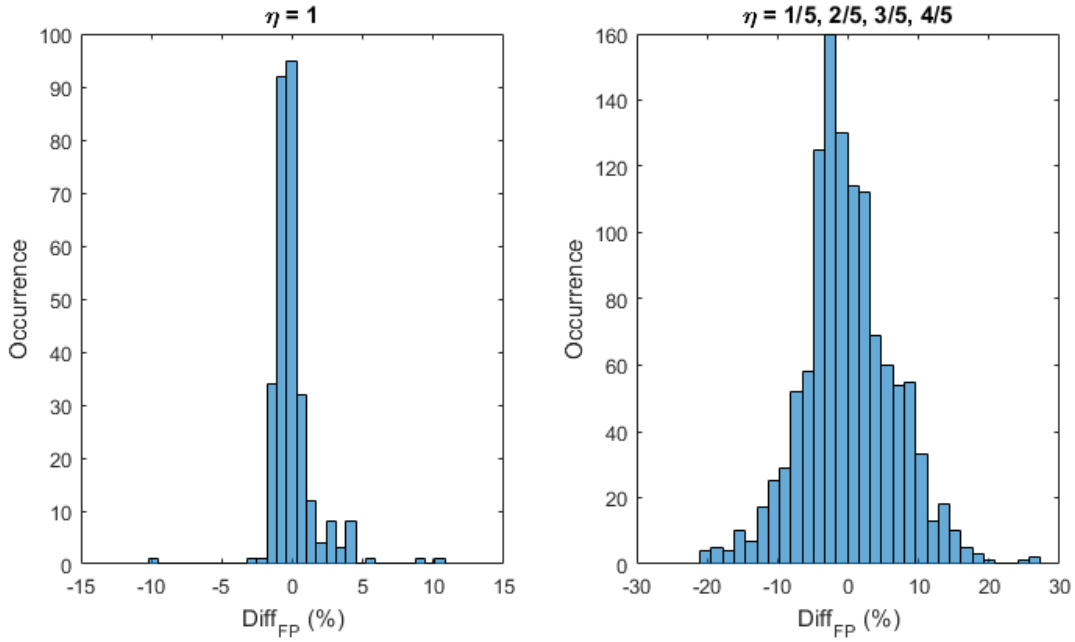

Figure 0.14 Distribution of residuals between the predictions of Modelica and adjusted EnergyPlus fan power model for interior case

Table 0.6 NMBE of fan power results for interior case

	η = 1/5	η = 2/5	η = 3/5	η = 4/5	η = 1
Original NMBE	26%	26%	26%	28%	22%
Adjusted NMBE	-2%	-3%	-2%	-2%	-1%

We also calculate the $Diff_{FP}$ in monthly interval, as shown in Figure 0.20. The result shows that the $Diff_{FP}$ between Model-2 and Model-3 increases when the misalignment is introduced in the model whereas the adjusted fan power model can significantly reduce the $Diff_{FP}$ in monthly interval. The residual of the monthly fan power consumption drops to -2% from 42%.

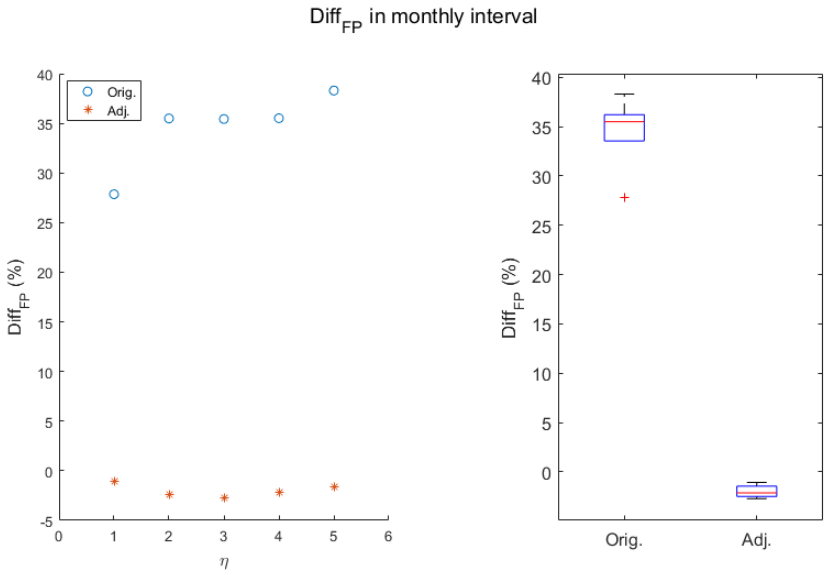

Figure 0.15 Comparison of the monthly **$Diff_{FP}$** for interior case

1.21.4 Multi-functional case

Figure 0.16 shows that $Diff_{FP}$ between Model-2 and Model-3 are widely distributed. The approach introduced in the single façade case is used again to evaluate the results. The only difference in this case is we use the $Diff_T$ instead of the diversity factor to compensate the prediction of supply air flowrate.

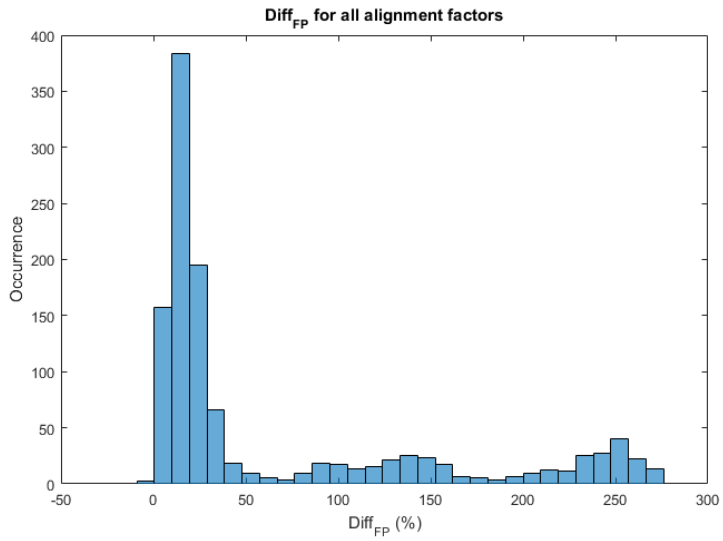

Figure 0.16 Distribution of **$\mathbf{Diff_{FP}}$** between the predictions of Model-2 and Model-3 for multi-functional case

Figure 0.17 shows the correlations between the adjusted airflow ratio and the original $Diff_{FP}$ as a percentage. It depicts that the $Diff_{FP}$ are large with small flowrate than that with large flowrate. Table 0.7 shows the fitted polynomial coefficients and the fitting R^2 for each alignment case.

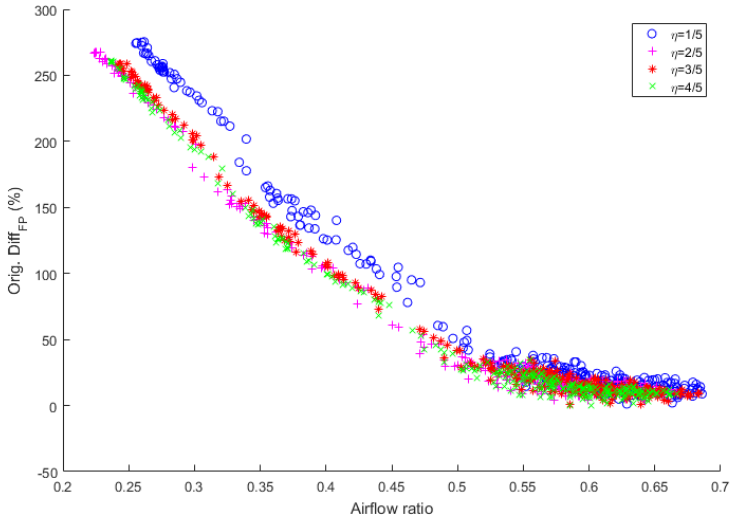

Figure 0.17 Correlations between **$\mathbf{Diff_{FP}}$** against flowrate ratio for multi-functional case

Table 0.7 Polynomial fitting curves for multi-functional case

Eta	Fitted polynomial coefficients	R^2
1/5	(11.2575, -0.4556, -13.7049, 6.1331)	0. 9949
2/5	(5.5148, 8.2316, -16.7450, 6.0164)	0. 9963
3/5	(1.1961, 13.8550, -19.3404, 6.4910)	0. 9968
4/5	(4.3383, 10.0561, -17.7871, 6.2197)	0.9967

We compensate the fan power results of the routine EnergyPlus model by using the statistical curve fittings and evaluate the residuals (the discrepancy between Modelica results and updated EnergyPlus fan power results). Figure 0.18 diagrams the comparison of the hourly $Diff_{FP}$ with and without the compensation. Figure 0.19 depicts the distributions of the updated $Diff_{FP}$. We observe the hourly $Diff_{FP}$ reduces significantly by using the adjusted fan power results instead of the outcomes from the routine EnergyPlus model. To evaluate the overall performance of the statistical model that approves the fitted coefficients, we calculate the NMBE for the five alignment factor cases, and the results are shown in Table 0.8.

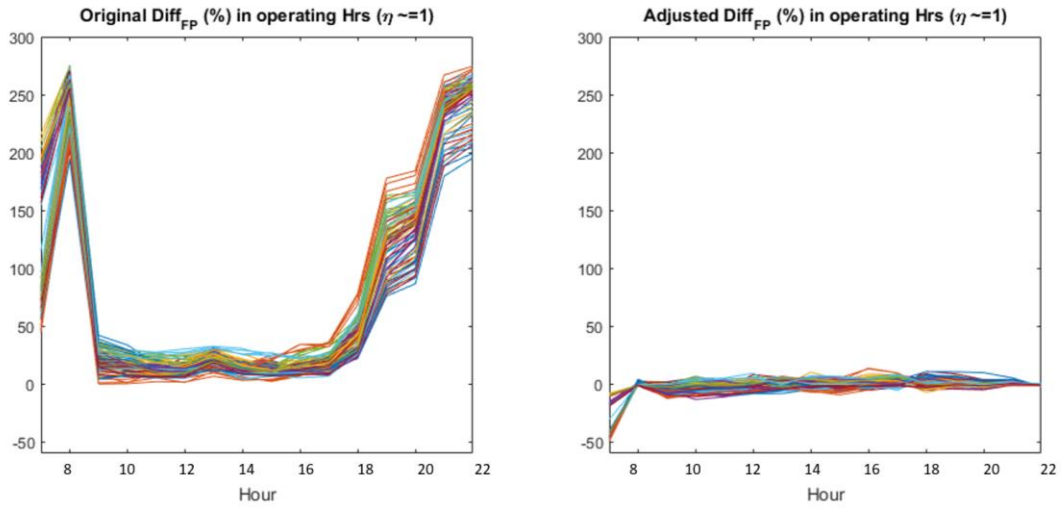

Figure 0.18 Comparison of the daily curve of $\mathbf{Diff_{FP}}$ before and after the curve fittings for multi-functional case

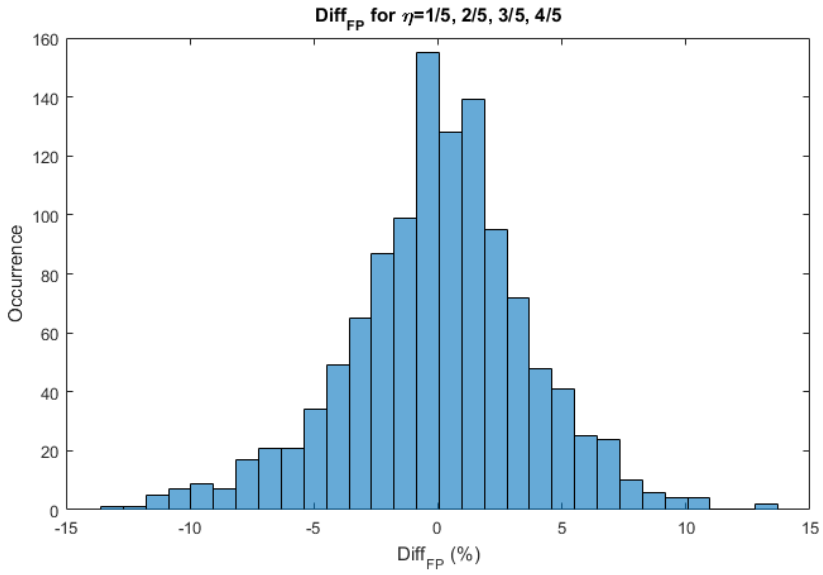

Figure 0.19 Distribution of residuals between the predictions of Modelica and adjusted EnergyPlus fan power model for multi-functional case

Table 0.8 NMBE of fan power results for multi-functional case

	η = 1/5	η = 2/5	η = 3/5	η = 4/5
Original NMBE	31%	30%	29%	28%
Adjusted NMBE	-2%	-3%	-3%	-2%

We also calculate the $Diff_{FP}$ in monthly interval, shown in Figure 0.20. The result shows that the $Diff_{FP}$ between Model-2 and Model-3 increases when the misalignment is introduced in the model whereas the adjusted fan power model can significantly reduce the $Diff_{FP}$ in monthly interval. The residual of the monthly fan power consumption drops from 42% to -2%.

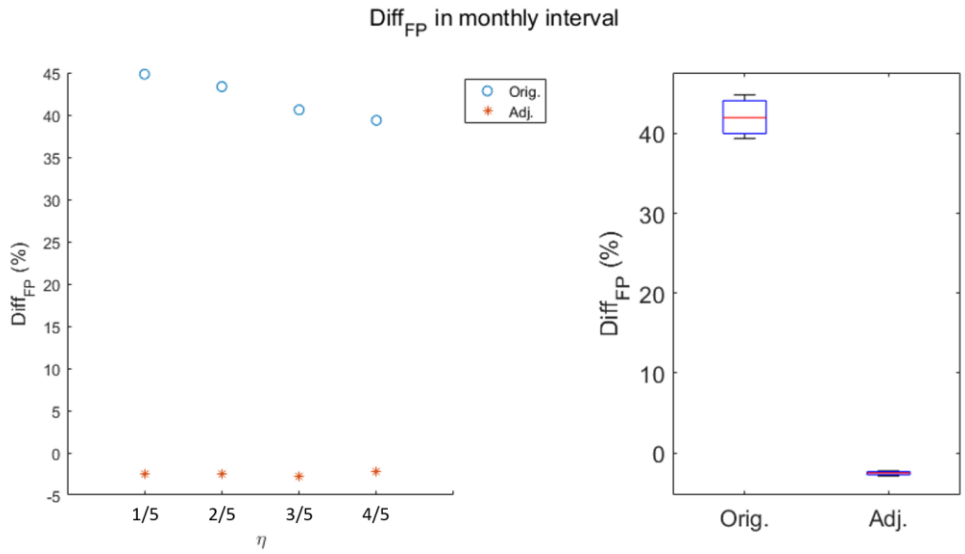

Figure 0.20 Comparison of the monthly $\mathbf{Diff_{FP}}$ for multi-functional case

The lesson from these four case studies is that the method we use to quantify the MFU of fan power by using a polynomial fit seems to apply to buildings served by VAV systems associated with similar fan performance and control sequence.

We can furthermore conclude that the introduction of the low fidelity model with embedded MFU (in the form of the fan power curve) makes the low fidelity model reasonably accurate for misalignment cases. This is an example where the MFU embeds a stochastic term in the low fidelity model that produces a distribution rather than a deterministic outcome, where the distribution shifts close to the true outcome.

Adjusting the fan power through an embedded MFU is relatively through the fact that the EnergyPlus module is easily accessible and has exposed parameters. For other quantities of interest this may prove to be much harder because (a) the model is more complex and has more interactions with other modules, and (b) the needed parameters are not exposed which forces an intrusive coding of MFU inside the existing software.

CONCLUSION AND FUTURE WORK

1.22 Summary and conclusions

Building energy simulation is widely adopted to evaluate building performance but certain deficiencies in the practice of building energy modeling persist. This has been recognized as a main contributor to the performance gap between predicted and actual building performance. Various researches have proved that uncertainty analysis is an effective approach to investigate the building performance gap. Based on prior uncertainty quantification studies, there is evidence that the uncertainties related to the modeling of HVAC systems are not well enough understood. This thesis focuses on one limitation of HVAC system modeling that is routinely done in current building simulation practice. It concerns the proper capture of its controllability in diverse spatial configurations and under varying occupancy usage. These two important factors are combined in this study to analyze the impacts on the accuracy of predictions of routine building energy models.

The two factors are introduced in Chapter 2: the alignment factor defines the area of directly controlled space temperature in relation to non-sensed spaces where the space temperature cannot be directly controlled. This reflects the relationship between spatial configuration and HVAC controllability. The second factor, occupant spatial load diversity, expresses the variability of occupancy related load profiles in each sub zone space. Combined with spatial alignment, load diversity plays an important role in HVAC control. In current studies, the combination of both influences is largely ignored in the standard EnergyPlus models.

In Chapter 3, we discuss the framework and approach to investigate the inadequacy of EnergyPlus by integrating a building energy heat transfer model with a deep HVAC system model.

Chapter 4 shows the deterministic results with a specified spatial configuration in three fixed usage diversity levels. We find the level of misalignment affects the simulation outcomes, and occupant load diversity exacerbates the impact of misalignment.

Chapter 5 presents the uncertainty analysis to quantify the model form uncertainty from the idealized temperature control of the EnergyPlus representation of VAV system considering stochastic usage patterns of occupants combined with five different alignment cases in three spatial configurations. An approach is presented to derive sub-zone level occupant usage profiles from zone level information.

Based upon the quantification of the differences between low and high fidelity predictions, we generate significant knowledge to the understanding of the origins of building energy model deficiency generated by idealization assumptions about temperature control. They are detailed below:

1. The idealized temperature control in EnergyPlus ignores the gap between thermal load and delivered energy. In fact, the point of linkage between building and HVAC system is the sensed space condition instead of the thermal load. The, in reality, limited sensing and controllability by the HVAC system leads to the discrepancies between the thermal load and the delivered energy.
2. The impact of ideal temperature control on the simulation outcomes (in particular space air temperature, delivered energy, and supply air flowrate) is

exacerbated along with increasing occupant usage diversity, especially at the hourly scale. Severe discomfort issues may arise in the indirectly controlled area. However, the negative impact of idealized temperature control in the low fidelity model is less severe at the monthly interval because of the stochastic nature of occupant usage. At the monthly aggregated level, only the mean occupancy plays a significant role.

3. According to a previous study conducted by Wang (2016), the monthly average unaccounted cooling energy consumption in office building in Atlanta is in the range from -5% to 35% with a mean value of 12%. This thesis shows that the unexplained energy consumption (by the routine EnergyPlus model) in the month of July is on average 11.7% based on the weighted average result from the case studies. Of course, we have no knowledge what percentage of floor area of the buildings in Wang's study suffer from some form of misalignment and occupant diversity. If we assume this to 30%, this study would explain $0.3 \times 11.7 = 3.5\%$ or roughly 1/3 of the reported average discrepancy in Wang' study. This study only discusses the impact of ideal temperature control to the unexplained cooling consumption, whereas the total unexplained HVAC related energy consumption contains many additional factors, not examined in this thesis.
4. In this thesis, we develop the spatial diversity factor to reflect the occupant usage and attempt to correlate the discrepancies in low fidelity outcomes with the diversity factors in each alignment case. The basic assumption is that the occupancy related load plays the dominant role in the space thermal load.

However, the results show that the correlation between diversity factor and outcome discrepancies becomes weak in some situation when the external load dominates the space overall thermal load.

5. Buildings may experience discomfort issue and unexpected energy consumption when the HVAC system operates in the normal condition without hardware faults. In the case studies we found that the discomfort issue and unexpected energy consumption become severe when: 1) the terminal box serves a multi-spaced area with complex external boundary conditions; 2) the service area of a terminal box contains different building functions with diverse usage patterns. Although these two situations can be avoided by the thoughtful HVAC design, however, they are still possible to occur after interior renovation or tenant replacement. In these cases, the requirement of space condition may not be satisfied while the HVAC system keeps working in a fault-free condition. The root cause of overuse of energy and discomfort should therefore be labeled as a "design fault" rather than a control or hardware fault as we witness frequently in practice.

1.23 Recommendations for Future Study

The ultimate goal of this thesis is to explain and further quantify the origins of the energy performance gap related to the HVAC systems, improving the speculative verification against an anecdotal study presented above. To better support the modeler and HVAC designers in many types of decision-making process, we recommend future studies on the following issues:

First, the findings should be generalized, i.e. for building function, weather condition, etc. This thesis considers the commercial office building with only office and meeting space as its organizational needs. Further studies should introduce more building types with multiple space functions, such as hospital, hotel, school, etc. Furthermore, HVAC system type is another important factor. This study is conducted solely for a VAV system with a particular ducting system and control consequence. Further study could explore more HVAC system types to evaluate the role of HVAC idealizations in low fidelity models and quantify the differences with higher fidelity models. The resulting sets of quantified uncertainties may then be categorized per building function, HVAC system type, climate zone etc.

Further studies should also include real buildings with actual measured data. We argue that the "spatial-HVAC mismatch" and occupant usage diversity are two major causes for the model form uncertainties in a low resolution model with idealized temperature control. However, the current study only compares the major outcomes of interest between three simulation models without backup from actual measured data. To complete the uncertainty quantification steps, the quantified uncertainties should be validated by using the measured data of actual buildings.

This study has not embarked on the natural extension into the characterization and quantification of model form uncertainty (MFU) modules that could be embedded, by intrusive software modifications, in the low fidelity model to generate uncertainty in the predicted outcomes. Chapter 6 has shown the possible direction towards this on the example of a fan power curve module. Future work should generalize this and introduce additional MFU modules in the low fidelity models. This would make sense if the

generation of uncertainty in the low fidelity prediction has equal value for decision making as the use of the higher fidelity model. However, this study reveals that it is very hard to embed the source of uncertainties and add the MFU modules into the low fidelity model. It looks like we are facing a bifurcation that: either keep adding MFU to current low-fidelity or making the higher fidelity model the new standard. The tough choice is the challenge for the developer community. Based on the purpose of the simulation and the required granularity of the simulation output, the choice may be different to researchers or practitioners. This should ultimately be based on a cost benefit analysis of building energy simulation, which is a fruitful direction for further research by any means.

Another promising perspective is that the approach introduced in this study can be used to quantify other origins of HVAC related uncertainties. The Modelica HVAC system model, as a system component model, provides the flexibility to establish the implicit parameters in the HVAC components which are not exposed in the EnergyPlus model. The bottom up method could provide a promising way to fully understand the origins of HVAC related uncertainties.

Apart from a focus on HVAC uncertainty quantification, the approach introduced in this thesis can be used as an effective supplementary to fault detection and diagnosis (FDD). As the most popular fault detection and diagnosis method, the data-driven method identifies the operation faults by distinguishing abnormal measured data. However, the FDD method may experience failures if the abnormal space condition cannot be observed due to the sensor's location. In this situation, the co-simulation approach becomes a solid model-based method to learn the root causes of the "ghost faults" and evaluate its impact on energy efficiencies.

REFERENCES

Abushakra, B., Sreshthaputra, A., Haberl, J. S., & Claridge, D. E. (2001). *Compilation of Diversity Factors and Schedules for Energy and Cooling Load Calculations, ASHRAE Research Project 1093-RP, Final Report.* Energy System Laboratory, Texas A&M University.

Ahn, K.-U., Kim, D.-W., Park, C.-S., & Wilde, P. d. (2017). Predictability of occupant presence and performance gap in building energy simulation. *Applied Energy*, 1639–1652.

American Society of Heating, R. a. (2013). *Handbook -- Fundamentals.* Atlanta.

Augenbroe, G., Zhang, Y., Khazaii, J., Su, H., Sun, Y., Lee, B. D., & Wu, C. J. (2013). Implications of the uncoupling of building and HVAC simulation in the presence of parameter uncertainties. *13th Conference of International Building Performance Simulation Association.* Chambery, France.

AZcentral. (2019). Retrieved from Electrical Usage of an LED TV Vs. Projector: https://yourbusiness.azcentral.com/electrical-usage-led-tv-vs-projector-11455.html

Bordass, B., Cohen, R., Standeven, M., & Leaman, A. (2001). Assessing building performance in use 3: energy performance of the Probe buildings. *Building Research & Information*, 114-128.

Breesch, H., & Janssens, A. (2010). Performance evaluation of passive cooling in office buildings based on uncertainty and sensitivity analysis. *Solar Energy*, 1453–1467.

Chen, Y., Hong, T., Luo, & Xuan. (2018). An Agent-Based Stochastic Occupancy Simulator. *Build Simulation*, 11: 37-49.

Cheng, Q., Wang, S., Yan, C., & Xiao, F. (2017). Probabilistic approach for uncertainty-based optimal design of chiller plants in buildings. *Applied Energy*, 1613-1624.

Davis III, J. A., & Nutter, D. W. (2010). Occupancy diversity factors for common university building types. *Energy and Buildings*, 1543-1551.

de Wilde, P. (2014). The gap between predicted and measured energy performance of buildings: A framework for investigation. *Automation in Construction*, 40-49.

de Wilde, P., Tian, W., & Augenbroe, G. (2011). Longitudinal prediction of the operational energy use of buildings. *Building and Environment*, 1670-1680.

De Wit, M. S. (2001). Uncertainty in Predictions of Thermal Comfort in Builidngs (Doctroal Dissertation).

de Wit, S., & Augenbroe, G. (2002). Analysis of uncertainty in building design evaluations and its implications. *Energy and Buildings*, 951–958.

Deru, M., Field, K., Studer, D., Benne, K., Griffith, B., Torcellini, P., . . . Crawley, D. (2011). *U.S. Department of Energy Commercial Reference Building Models of the National Building Stock.* NREL.

DoE. (2017). *EnergyPlus™ Version 8.8.0 Documentation -- Engineering Reference.*

Eguaras-Martínez, M., Vidaurre-Arbizu, M., & Martín-Gómez, C. (2014). Simulation and evaluation of Building Information Modeling in a real pilot site. *Applied Energy*, 475–484.

EIA. (2017). *International Energy Outlook 2016.* U.S. Energy Information Administration.

EIA. (2018). *How much energy is consumed in U.S. residential and commercial buildings?* Retrieved from https://www.eia.gov/tools/faqs/faq.php?id=86&t=1

Elmqvist, H., Mattsson, S. E., & Otter, M. (1998). MODELICA — THE NEW OBJECT-ORIENTED MODELING LANGUAGE. *The 12th European Simulation Multiconference.* Manchester, UK.

EnergyUseCalculator. (2020). Retrieved from Electricity usage of a Laptop, Notebook or Netbook: http://energyusecalculator.com/electricity_laptop.htm

Gang, W., Augenbroe, G., Wang, S., Fan, C., Xiao, & Fu. (2016). An uncertainty-based design optimization method for district cooling systems. *Energy*, 516-527.

Gang, W., Wang, S., Shan, K., & Gao, D. (2015). Impacts of cooling load calculation uncertainties on the design optimization of building cooling systems. *Energy and Buildings*, 1-9.

Hopfe, C. J., & Hensen, J. L. (2011). Uncertainty analysis in building performance simulation for design support. *Energy and Buildings*, 2798–2805.

Huang, P., & Huang, G. (2017). Investigation of maximum cooling loss uncertainty in piping network using Bayesian Markov Chain Monte Carlo method. *Energy Procedia*, 258–263.

Huang, P., Huang, G., & Wang, Y. (2015). HVAC system design under peak load prediction uncertainty using multiple-criterion decision making technique. *Energy and Buildings*, 26-36.

IEA. (2019). *Energy Efficiency: Buildings*. Retrieved from International Energy agency: https://www.iea.org/topics/energyefficiency/buildings/

ISO. (2008). *ISO 13790:2008 ENERGY PERFORMANCE OF BUILDINGS -- CALCULATION OF ENERGY USE FOR SPACE HEATING AND COOLING*. ISO.

Kim, J.-H., Augenbroe, G., & Suh, H.-S. (2013). COMPARATIVE STUDY OF THE LEED AND ISO-CEN BUILDING ENERGY PERFORMANCE RATING METHODS. *13th Conference of International Building Performance Simulation Association*, (pp. 3104-3111). Chambery, France.

LBNL. (2019). *Modelica Buildings Library*. Retrieved from Modelica Buildings Library: https://simulationresearch.lbl.gov/modelica/

Lee, B. D., Sun, Y., Augenbroe, G., & Paredis, C. J. (2013). Towards better prediction of building performance: a workbench to analyze uncertainty in building simulation. *Building Simulation 2013*, (pp. 1231-1238). Chambéry, France.

Li, H., Li, X., & Qi, M. (2014). Field testing of natural ventilation in college student dormitories (Beijing, China). *Building and Environment*, 36-43.

Luo, X., Lam, K. P., Chen, Y., & Hong, T. (2017). Performance evaluation of an agent-based occupancy simulation model. *Building and Environment*, 42-53.

Macdonald, I. A. (2002). Quantifying the Effects of Uncertainty in Building Simulation (Doctoral Dissertation).

Macdonald, I., & Strachan, P. (2001). Practical application of uncertainty analysis. *Energy and Buildings*, 219-227.

Menezes, C., Cripps, A., Bouchlaghem, D., & Buswell, R. (2012). Predicted vs. actual energy performance of non-domestic buildings: using post-occupancy evaluation data to reduce the performance gap. *Applied Energy*, 355–364.

Modelica. (2019, April 2). Retrieved from Wikipedia: https://en.wikipedia.org/wiki/Modelica

Moon, H. J. (2005). Assessing Mold Risks in Buildings under Uncertainty (Doctoral Dissertation).

Morgan, M. G. (2009). *Best Practice Approaches for Characterizing, Communicating and Incorporating Scientific Uncertainty in Climate Decision Making:*. DIANE Publishing.

Oberkampf, W. L., & Roy, C. J. (2010). *Verification and validation in scientific computing.* Cambridge University Press.

Silva, A. S., & Ghisi, E. (2014). Uncertainty analysis of user behaviour and physical parameters in residential building performance simulation. *Energy and Buildings*, 381-391.

Smith, A., Luck, R., & Mago, P. J. (2010). Analysis of a combined cooling, heating, and power system model under different operating strategies with input and model data uncertainty. *Energy and Buildings*, 2231–2240.

Sun, K., Hong, T., & Kim, J.-H. (2017). A Simulation Framework for Quantifying the Influence of Occupant Behavior on Savings of Energy Efficiency Measures. *15th International Building Performance Simulation Association Conference*, (pp. 536-544). San Francisco, CA, USA.

Sun, Y. (2014). Closing the Building Energy Performance Gap by Improving Our Predictions (Doctoral Dissertation).

Sun, Y., Gu, L., Wu, C. J., & Augenbroe, G. (2014). Exploring HVAC system sizing under uncertainty. *Energy and Buildings*, 243–252.

Sun, Y., Heo, Y., Tan, M., Xie, H., Wu, C. J., & Augenbroe, G. (2014). Uncertainty quantification of microclimate variables in building energy models. *Journal of Building Performance Simulation*, 17-32.

Sun, Y., Su, H., Wu, C. J., & Augenbroe, G. (2015). Quantification of model form uncertainty in the calculation of solar diffuse irradiation on inclined surfaces for building energy simulation. *Journal of Building Performance Simulation*, 253-265.

Tian, W., Heo, Y., Wilde, P. d., Li, Z., Yan, D., Park, C. S., . . . Augenbroe, G. (2018). A review of uncertainty analysis in building energy assessment. *Renewable and Sustainable Energy Reviews*, 285-301.

Turner, C. (2006). *LEED building performance in the Cascadia Region: a post occupancy evaluation report.* Cascadia Region Green Building Council.

Turner, C., & Franke, M. (2008). *Energy Performance of LEED® for New Construction Buildings.* New Buildings Institute.

UN. (2018). *Global status report 2017.* UN Environment.

WALKER, W., HARREMO€EES, P., ROTMANS, J., SLUIJS, J. V., ASSELT, M. V., JANSSEN, P., & KRAUSS, M. K. (2003). Defining Uncertainty A Conceptual Basis for Uncertainty Management in Model-Based Decision Support. *Integrated Assessment*, 5-17.

Wang, C., Yan, D., & Jiang, Y. (2011). A novel approach for building occupancy simulation. *Building Simulation*, 149-167.

Wang, L., Mathew, P., & Pang, X. (2012). Uncertainties in energy consumption introduced by building operations and weather for a medium-size office building. *Energy and Buildings*, 152–158.

Wang, Q. (2016). Accuracy, Validity and Relevance of Probabilistic Building Energy Models (Doctoral Dissertation).

Ward, R., Choudhary, R., Heo, Y., & Aston, J. (2019). A data-centric bottom-up model for generation of stochastic internal load profiles based on spaceuse type. *Journal of Building Performance Simulation*, 620–636.

Ward, R., Choudhary, R., Heo, Y., & Rysanek, A. (2016). Exploring the impact of different parameterisations of occupant-related internal loads in building energy simulation. *Energy and Buildings*, 92–105.

Wetter, M. (2009). Modelica-based modelling and simulation to support research and development in building energy and control systems. *Journal of Building Performance Simulation*, 1143-161.

Wetter, M., & Nouidui, T. S. (2016). *Building Controls Virtual Test Bed User Manual Version 1.6.0.* Berkeley: Lawrance Berkeley National Laboratory.

Wit, S. d., & Augenbroe, G. (2002). Analysis of uncertainty in building design evaluations and its implications. *Energy and Buildings*, 951-958.

Yan, B., Li, X., Malkawi, A. M., & Augenbroe, G. (2017). Quantifying uncertainty in outdoor air flow control and its impacts on building performance simulation and fault detection. *Energy and Buildings*, 115-128.

Yang, Z., & Becerik-Gerber, B. (2014). The coupled effects of personalized occupancy profile based HVAC schedules and room reassignment on building energy use. *Energy and Buildings*, 113-122.

Yu, Y., Woradechjumroen, D., & Yu, D. (2014). A review of fault detection and diagnosis methodologies on air-handling units. *Energy and Buildings*, 550–562.

Zhang, Q., Yan, D., An, J., Hong, T., Tian, W., & Sun, K. (2017). Spatial distribution of internal heat gains: A probabilistic representation and evaluation of its influence on cooling equipment sizing in large office buildings. *Energy and Buildings*, 407–416.

Zhang, Y., Bai, X., Mills, F. P., & Pezzey, J. C. (2018). Rethinking the role of occupant behavior in building energy performance: A review. *Energy and Buildings*, 279-294.

Zou, P. X., Xu, X., Sanjayan, J., & Wang, J. (2018). Review of 10 years research on building energy performance gap: Life-cycle and stakeholder perspectives. *Energy & Buildings*, 165-181.